

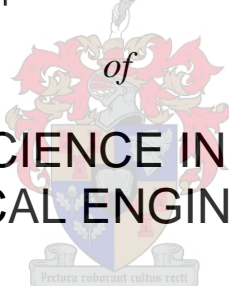
A NOVEL APPROACH TO SOLVENT SCREENING FOR POST- COMBUSTION CARBON DIOXIDE CAPTURE WITH CHEMICAL ABSORPTION

by

Frederik Jacobus Gideon Retief

Thesis presented in partial fulfillment
of the requirements for the Degree

of
MASTER OF SCIENCE IN ENGINEERING
(CHEMICAL ENGINEERING)



in the Faculty of Engineering
at Stellenbosch University

Supervisor
Prof. J.H. Knoetze

March 2012

Declaration

By submitting this thesis electronically, I declare that the entirety of the work contained therein is my own, original work, that I am the sole author thereof (save to the extent of explicitly otherwise stated), that reproduction and publication thereof by Stellenbosch University will not infringe any third party rights and that I have not previously in its entirety or in part submitted it for obtaining any qualification.

Signature

Date

Copyright © 2012 Stellenbosch University

All rights reserved

Abstract

Carbon dioxide (CO₂) is classified as the main greenhouse gas (GHG) contributing to global warming. Estimates by the Intergovernmental Panel on Climate Change (IPCC) suggest that CO₂ emissions must be reduced by between 50 to 85% by 2050 to avoid irreversible impacts. Carbon capture and storage (CCS) strategies can be applied to de-carbonize the emissions from fossil-fueled power plants. Compared to other CCS techniques, post-combustion capture (PCC) is most likely to be implemented effectively as a retrofit option to existing power plants. At present however CCS is not yet commercially viable. The main challenge with CCS is to reduce the inherent energy penalty of the CO₂ separation stage on the host plant.

Seventy-five to eighty percent of the total cost of CCS is associated with the separation stage. There are several technologies available for separating CO₂ from power plant flue gas streams. Reactive absorption with aqueous amine solutions has the ability to treat low concentration, low pressure and large flux flue gas streams in industrial-scale applications. It is most likely to be the first technology employed commercially in the implementation of CCS. The energy required for solvent regeneration however, is high for the standard solvent used in reactive absorption processes, i.e. MEA. This leads to a reduction in thermal efficiency of the host plant of up to 15%. Alternative solvent formulations are being evaluated in an attempt to reduce the energy intensity of the regeneration process.

The main objective of this study was to establish a novel, simplified thermodynamic method for solvent screening. Partial solubility parameters (PSPs) were identified as the potential basis for such a method. The major limitation of this approach is that the model doesn't account for effects from chemical reaction(s) between materials, e.g. CO₂ reacting with aqueous alkanolamine solutions; considering only the effects from dissolution. The EquiSolv software system was developed based on PSP theory. The Hansen 3-set PSP approach was used to describe the equilibrium behaviour of CO₂ absorbing in task specific solvents. The Hansen theory was expanded to a 4-set approach to account for contributions from electrostatic interactions between materials. The EquiSolv program was used successfully to screen large sets of solvent data (up to 400 million formulations) in the search for suitable alternative solvent formulations for CO₂ absorption.

The secondary objective of this study was to evaluate the ability of the proposed PSP model to accurately predict suitable alternative solvents for CO₂ absorption through preliminary experimental work. A series of CO₂ absorption experiments were conducted to evaluate the absorption performance of predicted alternative solvent formulations. The predicted alternative solvent formulations exhibited a significant improvement in absorption performance (up to a 97% increase in the measured absorption capacity) compared to conventional solvent formulations. Statistical analysis of the experimental results has shown that there is a statistically significant concordant relationship between the predicted and measured rankings for the absorption performance of the predicted solvent formulations. Based on this it was concluded that PSP theory can be used to accurately predict the equilibrium behaviour of CO₂ absorbing in task specific solvents.

Recently ionic liquids (ILs) have been identified as potential alternatives to alkanolamine solutions conventionally used for CO₂ absorption. Absorption experiments were conducted as a preliminary assessment of the absorption performance of ILs. Results have shown ILs to have significantly improved performance compared to conventional alkanolamine solvents; up to a 96% increase in the measured absorption capacity compared to conventional solvents. Future work should focus on developing task specific ionic liquids (TSILs) in an attempt to reduce the energy intensity of solvent regeneration in CO₂ absorption processes.

Opsomming

Koolsuurgas (CO_2) word geklassifiseer as die vernaamste kweekhuis gas (GHG) wat bydra to globale verwarming. Beramings deur die Interregeringspaneel oor Klimaatsverandering (IPKV) toon aan dat CO_2 emissies teen 2050 verminder moet word met tussen 50 en 85% om onomkeerbare invloede te vermy. Verskeie koolstof opvangs en bergings (KOB) strategieë kan toegepas word ten einde die koolstof dioksied konsentrasie in die emissies van kragstasies wat fossielbrandstowwe gebruik, te verminder. Naverbranding opvangs (NVO) is die mees aangewese KOB tegniek wat effektief toegepas kan word op bestaande kragstasies. Tans is KOB egter nog nie kommersieël lewensvatbaar nie. Die hoof uitdaging wat KOB in die gesig staar is om die energie boete inherent aan die CO_2 skeidingstap te verminder.

Tussen vyf-en-sewentig en tagtig persent van die totale koste van KOB is gekoppel aan die skeidingstap. Daar is verskeie metodes beskikbaar vir die skeiding van CO_2 uit die uitlaatgasse van kragstasies. Reaktiewe absorpsie met waterige oplossings van amiene kan gebruik word om lae konsentrasie, lae druk en hoë vloeitlaatgasstrome in industriële toepassings te behandel. Dit is hoogs waarskynlik die eerste tegnologie wat kommersieël aangewend sal word in die toepassing van KOB. Die oplosmiddel wat normalweg vir reaktiewe absorpsie gebruik word (d.w.s. MEA) benodig egter 'n groot hoeveelheid energie vir regenerasie. Dit lei tot 'n afname in die termiese doeltreffendheid van die voeder aanleg van tot 15%. Alternatiewe oplosmiddelstelsels word tans ondersoek in 'n poging om die energie intensiteit van die regenerasieproses te verminder.

Die hoof doelwit van hierdie studie was om 'n nuwe, ongekompliseerde termodinamiese metode te vestig vir die keuring van alternatiewe oplosmiddels. Parsiële oplosbaarheidsparameters (POPs) is geïdentifiseer as 'n moontlike grondslag vir so 'n metode. Die model beskryf egter slegs die ontbindings gedrag van materiale. Die effekte van chemiese reaksie(s) tussen materiale, bv. die tussen CO_2 en waterige oplossings van alkanolamiene, word nie in ag geneem nie. Die POP teorie het gedien as grondslag vir die ontwerp van die EquiSolv sagteware stelsel. Die Hansen stel van drie POPs is gebruik om die ewewigsgedrag te beskryf van CO_2 wat absorbeer in doelgerig-ontwerpte oplosmiddels. Die Hansen teorie is verder uitgebrei na 'n stel van vier POPs om die bydrae van elektrostatiese

wisselwerking tussen materiale in ag te neem. Die EquiSolv program is verskeie kere met groot sukses gebruik vir die sifting van groot stelle data (soveel as 400 miljoen formulasies) in die soektog na alternatiewe oplosmiddels vir CO₂ absorpsie.

Die sekondêre doelwit van die studie was om die vermoë van die voorgestelde POP model om geskikte alternatiewe oplosmiddels vir CO₂ absorpsie akkuraat te voorspel, te ondersoek deur voorlopige eksperimentele werk. 'n Reeks CO₂ absorpsie eksperimente is gedoen ten einde die absorpsie werkverrigting van die voorspelde alternatiewe oplosmiddels te ondersoek. 'n Verbetering in absorpsie werkverrigting van tot 97% is gevind vir die voorspelde oplosmiddels vergeleke met die van oplosmiddels wat tipies in die industrie gebruik word. Statistiese ontleding van die eksperimentele resultate het getoon dat daar 'n beduidende ooreenstemming tussen die voorspelde en gemete rangskikking van die voorspelde oplosmiddels se werkverrigting bestaan. Dus kan POP teorie gebruik word om die absorpsie van CO₂ in doelgerig-ontwerpte oplosmiddels akkuraat te beskryf.

Ioniese vloeistowwe (IVs) is onlangs geïdentifiseer as moontlike alternatiewe oplosmiddels vir die alkanolamien oplossings wat normaalweg gebruik word vir CO₂ absorpsie. Absorpsie eksperimente is gedoen ten einde 'n voorlopige raming van die absorpsie werkverrigting van IVs te bekom. Daar is bevind dat IVs 'n beduidende verbetering in werkverrigting toon in vergelyking met die alkanolamien oplosmiddels wat normaalweg gebruik word. 'n Verbetering in absorpsie werkverrigting van tot 96% is gevind vir die voorspelde IV-bevattende oplosmiddels vergeleke met die van oplosmiddels wat tipies in die industrie gebruik word. Die fokus van toekomstige navorsing moet val op die ontwikkeling van doelgemaakte ioniese vloeistowwe (DGIVs) in 'n poging om die energie intensiteit van oplosmiddel regenerasie in CO₂ absorpsie prosesse te verminder.

Acknowledgements

To my grandparents: Thank you for your wisdom and motivation to persevere and strive to become the best I possibly can.

To my parents: Thank you for your continued motivation, guidance and support, both emotional and financial, throughout my life. Thank you for inspiring me to live to my full potential.

To Prof. Hansie Knoetze: Thank you for your guidance, advice and financial support throughout the project.

To Dr. Deon de-wet Roos: Thank you for your insight and guidance in the initial phases of the project.

To Dr. Catherine Esterhuysen: Thank you for your guidance and advice on quantum chemical calculations and chemical modeling.

To Mr Anton Cordier and Mr Alvin Petersen: Thank you for helping with tools and equipment when necessary.

To Dr. Charles Hansen and Prof. Steven Abbott: Thank you for your advice and guidance on partial solubility parameter theory and the HSPiP program.

To Dr. Lidia Auret: Thank you for your advice and guidance on statistical hypothesis testing.

To my friends, Aldrich and Carli: Thank you for your continued interest, confidence and support in my work.

Table of Contents

| | |
|--|-------|
| Declaration..... | i |
| Abstract | ii |
| Opsomming..... | iv |
| Acknowledgements | vi |
| Table of Contents | vii |
| List of Figures | xiv |
| List of Tables | xx |
| Nomenclature | xxiii |
| General Symbols..... | xxiii |
| Greek Symbols | xxiv |
| Subscripts..... | xxiv |
| Superscripts | xxvi |
| 1. Introduction | 1 |
| 2. Literature Study | 7 |
| 2.1. Introduction..... | 7 |
| 2.2. Carbon Dioxide Abatement Strategies..... | 7 |
| 2.3. Carbon Capture and Storage (CCS) | 8 |
| 2.3.1. CO ₂ Capture/Extraction (Stage 1)..... | 9 |
| 2.3.1.1. Post-Combustion Capture Process | 9 |
| 2.3.1.2. Pre-Combustion Capture Process..... | 10 |
| 2.3.1.3. Oxy-Fuel Combustion Capture Process..... | 11 |
| 2.3.1.4. Novel Technology: Chemical-looping Combustion Capture | 12 |
| 2.3.1.5. In Summary | 13 |

| | | |
|----------|--|----|
| 2.3.2. | CO ₂ Transport and Storage (Stages 2 and 3)..... | 15 |
| 2.4. | Post-Combustion CO ₂ Capture | 15 |
| 2.4.1. | CO ₂ Separation Technologies..... | 16 |
| 2.4.1.1. | Adsorption..... | 16 |
| 2.4.1.2. | Cryogenics Separation | 16 |
| 2.4.1.3. | Membrane-based Separation | 16 |
| 2.4.1.4. | Physical Absorption | 17 |
| 2.4.1.5. | Chemical Absorption..... | 17 |
| 2.4.1.6. | In Summary | 17 |
| 2.4.2. | Post-Combustion CO ₂ Capture with Chemical Absorption | 18 |
| 2.4.2.1. | Preparation of the Flue Gas | 18 |
| 2.4.2.2. | Process Description | 19 |
| 2.4.3. | Process Modeling and Simulation..... | 20 |
| 2.4.3.1. | Model Complexity | 20 |
| 2.4.3.2. | Basic Model Theory | 22 |
| 2.4.3.3. | Current Modeling Research Status..... | 23 |
| 2.4.4. | Solvents and Solvent Selection | 24 |
| 2.4.4.1. | Amine-based Solvents | 25 |
| 2.4.4.2. | Ammonia..... | 26 |
| 2.4.4.3. | Piperazine..... | 27 |
| 2.4.4.4. | Amino Acid and Amine Amino Acid Salts..... | 27 |
| 2.4.4.5. | In Summary | 28 |
| 2.4.5. | Process Intensification..... | 29 |
| 2.4.6. | International PCC Research Programmes and Pilot Plant Projects..... | 30 |
| 2.4.6.1. | The Luminant Carbon Management Programme..... | 30 |
| 2.4.6.2. | The International Test Centre (ITC) for CO ₂ Capture | 31 |

| | | |
|----------|---|----|
| 2.4.6.3. | The CASTOR Project | 31 |
| 2.4.6.4. | The iCap Project..... | 32 |
| 2.4.6.5. | The CAPRICE Project | 33 |
| 2.4.6.6. | The CESAR Project | 33 |
| 2.4.6.7. | The joint UK-China Near Zero Emissions Coal (NSEC) Initiative | 33 |
| 2.4.6.8. | The Cooperative Research Centre for Greenhouse Gas Technologies (CO2CRC) | 33 |
| 2.4.6.9. | Studies at Mitsubishi Heavy Industries, Hiroshima R&D Centre, Japan | 34 |
| 2.4.7. | Retrofitting Post-Combustion CO ₂ Capture Units to Existing Coal-fired Power Plants..... | 34 |
| 2.5. | CA-PCC: Challenges and Possibilities in the Future | 39 |
| 2.5.1. | Solvents | 39 |
| 2.5.1.1. | Ionic Liquids (ILs) | 40 |
| 2.5.2. | Pilot Plants | 41 |
| 2.5.3. | Modeling and Process Simulation..... | 42 |
| 2.5.4. | Reduced Energy Consumption..... | 42 |
| 2.5.4.1. | Through Alternative Solvent Selection | 42 |
| 2.5.4.2. | Through Heat Integration | 46 |
| 2.5.5. | Simultaneous Separation of SO _x and NO _x | 46 |
| 2.6. | Conclusions..... | 47 |
| 3. | CO ₂ Solubility: Theoretical Modeling..... | 48 |
| 3.1. | Introduction..... | 48 |
| 3.2. | Hypothesis..... | 49 |
| 3.3. | Partial Solubility Parameters (PSPs): A Novel Method for Solvent Screening/Selection..... | 49 |
| 3.3.1. | Background | 49 |
| 3.3.2. | Hansen Solubility Parameters (HSPs) | 51 |
| 3.3.2.1. | Basic Modeling Theory..... | 51 |
| 3.3.2.2. | Optimizing Solvent Designs..... | 54 |

| | | |
|----------|---|-----|
| 3.3.2.3. | Temperature and Pressure Dependencies of HSPs | 55 |
| 3.3.2.4. | Hansen Solubility Parameters in Practice (HSPiP) Software Package..... | 56 |
| 3.3.3. | Expanding the HSP Theory: Considering the Effect of Electrostatic Bond Energies | 61 |
| 3.4. | The EquiSolv Analysis Package | 66 |
| 3.4.1. | Analyzing Alternative Solvent Blend Formulations | 69 |
| 3.4.2. | Calculating the Solvent Relative Energy Differences (REDs)..... | 70 |
| 3.4.3. | Performing Quick Blend Calculations | 71 |
| 3.4.4. | Estimating Electrostatic (Ionic) Bond Solubility Parameters | 73 |
| 3.5. | Conclusions..... | 73 |
| 4. | Experimental: Design, Materials & Methods | 75 |
| 4.1. | Experimental Design | 75 |
| 4.1.1. | Equipment Design and Setup..... | 75 |
| 4.1.1.1. | Temperature Control and Data Recording..... | 78 |
| 4.1.1.2. | Pressure Control and Data Recording..... | 79 |
| 4.1.2. | Experimental Plan | 80 |
| 4.1.2.1. | Reference Samples | 81 |
| 4.1.2.2. | Hypothesis Test Samples | 81 |
| 4.1.2.3. | Ionic Liquid (IL) Test Samples | 82 |
| 4.2. | Data Analysis | 82 |
| 4.3. | Experimental Setup Maintenance and Safety | 85 |
| 4.4. | Materials Used..... | 85 |
| 5. | Results & Discussion: Modeling..... | 86 |
| 5.1. | Estimating the Electrostatic (Ionic) Bond HSP Values..... | 86 |
| 5.2. | Calculating the Solvent RED Values w.r.t. a Particular Target Solute | 90 |
| 5.3. | Searching for Solvent Blend Formulations w.r.t. a Particular Target Solute | 93 |
| 5.4. | Using the EquiSolv Quick Blend Calculator | 101 |

| | | |
|----------|--|-----|
| 6. | Results & Discussion: Experimental..... | 105 |
| 6.1. | Reference Solvent Sample Results..... | 106 |
| 6.2. | Hypothesis Test Results | 113 |
| 6.3. | Ionic Liquid CO ₂ Absorption Results..... | 124 |
| 6.4. | Pressure Test Results | 134 |
| 7. | Conclusions | 137 |
| 7.1. | Modeling CO ₂ Solubility | 137 |
| 7.2. | CO ₂ Absorption Experiments..... | 139 |
| 8. | Recommendations..... | 142 |
| 8.1. | Future Work on CO ₂ Solubility Modeling | 142 |
| 8.2. | Future Experimental Work and Model Validation..... | 143 |
| | References | 144 |
| | Appendix A: EquiSolv Fundamentals..... | 155 |
| A.1. | Introduction..... | 155 |
| A.2. | Solvent Blend Calculations: Matrix Manipulation | 155 |
| A.2.1. | Two-Component Blends | 157 |
| A.2.1.1. | Linear Calculation Method..... | 157 |
| A.2.1.2. | Square Calculation Method..... | 160 |
| A.2.2. | Three-Component Blends..... | 161 |
| A.2.2.1. | Linear Calculation Method..... | 161 |
| A.2.2.2. | Square Calculation Method..... | 164 |
| A.2.3. | Four-Component Blends..... | 164 |
| A.2.3.1. | Linear Calculation Method..... | 164 |
| A.2.3.2. | Square Calculation Method..... | 167 |
| A.3. | Solvent Blend Calculations: Gauss-Seidel Iteration | 167 |
| A.3.1. | Two-Component Blends | 169 |

| | | |
|--------|---|-----|
| A.3.2. | Three-Component Blends..... | 170 |
| A.3.3. | Four-Component Blends..... | 170 |
| | Appendix B: Modeling Data | 171 |
| | Appendix C: Experimental Procedure..... | 182 |
| C.1. | Absorbent Sample Preparation | 183 |
| C.2. | Preparing the Experimental Environment..... | 183 |
| C.3. | Setting the Experimental Conditions | 184 |
| C.4. | Performing an Experimental Run..... | 184 |
| C.5. | Experimental Data Acquisition | 184 |
| C.6. | Equilibrium Absorbent Sampling for GC analysis | 185 |
| C.7. | System Cleanup and Preparation for the next Experimental Run..... | 185 |
| | Appendix D: Experimental Run Data Sheet | 186 |
| | Appendix E: Experimental Data..... | 187 |
| | Appendix F: Sample Calculations | 188 |
| | Appendix G: Equipment Calibration Data..... | 192 |
| G.1. | Pressure Transmitter Calibration Data..... | 192 |
| G.2. | Temperature Transmitter Calibration Data..... | 193 |
| G.3. | System Pressure Test Data | 194 |
| | Appendix H: EquiSolv User Manual | 198 |
| H.1. | Getting Started | 198 |
| H.2. | Importing and Exporting Solvent Data..... | 199 |
| H.3. | Browsing and Querying Data..... | 204 |
| H.4. | Performing Calculations | 208 |
| H.4.1. | Estimating Solvent Ionic Bond Energies | 208 |
| H.4.2. | Calculating the Relative Energy Differences (REDs) | 212 |
| H.4.3. | Using the Solvent Blend Optimizer | 215 |

| | | |
|-------------|---|-----|
| H.4.4. | Using the Quick Blend Calculator | 220 |
| H.4.4.1. | Estimating the Solvent Blend Composition and HSPs..... | 220 |
| H.4.4.2. | Estimating the Solvent Blend HSPs for a Specified Composition | 224 |
| H.5. | Pulling Solvent Data and Calculation Reports | 225 |
| H.6. | Clearing Solvent Data..... | 225 |
| Appendix I: | MATLAB Code for Statistic Tests..... | 227 |

List of Figures

| | |
|--|----|
| Figure 1.1 – The forecasted global energy demand supply share by fuel type (Redrawn from (Aboudheir & ElMoudir, 2009)). | 2 |
| Figure 1.2 – Block flow diagram of the thesis structure. | 6 |
| Figure 2.1 – The three basic stages of the CCS process. | 8 |
| Figure 2.2 – A block flow diagram of an oxy-fuel carbon capture process (Redrawn from (Feron & Hendriks, 2005)). | 9 |
| Figure 2.3 – A block flow diagram for a pre-combustion carbon capture process (Redrawn from (Feron & Hendriks, 2005)). | 10 |
| Figure 2.4 – A block flow diagram of an oxy-fuel carbon capture process (Redrawn from (Feron & Hendriks, 2005)). | 11 |
| Figure 2.5 – A schematic of a typical chemical-looping combustion (CLC) capture process (Redrawn from (Rydén & Lyngfelt, 2006)). | 12 |
| Figure 2.6 – Schematic diagram of the integration of a flue gas treatment process to a coal-fired power plant (Redrawn from (Thitakamol et al., 2007)). | 18 |
| Figure 2.7 – Process flow diagram for a post-combustion CO ₂ capture process by chemical absorption (Redrawn from (IPCC, 2005)). | 19 |
| Figure 2.8 – Schematic depicting the varying levels of reactive absorption model complexity (Redrawn from (Kenig et al., 2001)). | 21 |
| Figure 2.9 – Schematic depicting the vapour-liquid bulk phase, films and contact interface for reactive absorption modeling (Redrawn from (Noeres et al., 2003)). | 23 |
| Figure 2.10 – A schematic depicting a first law energy analysis of a power cycle without (upper) and with (lower) a retrofitted capture unit (Redrawn from (Lucquiaud & Gibbins, 2010)). | 35 |
| Figure 2.11 – Schematic of a single-reheat steam cycle configuration without a CO ₂ capture unit (Redrawn from (Lucquiaud & Gibbins, 2010)). | 36 |
| Figure 2.12 – Schematic of a single-reheat steam cycle configuration with steam extraction for CO ₂ capture and low-grade heat recovery (Redrawn from (Lucquiaud & Gibbins, 2010)). | 37 |
| Figure 2.13 – Schematic depicting the relationships of selected process parameters on the net power output of the host plant (Redrawn from (Oexmann & Kather, 2010)). | 45 |
| Figure 3.1 – Rendering and description of a typical HSP solubility sphere (generated using the HSPiP software package). | 54 |

| | |
|---|----|
| Figure 3.2 – (a) Screenshot of the 3D HSPiP solvent-solute analysis (with CO ₂ selected as the target solute), (b) Screenshot of three section views of the analysis..... | 57 |
| Figure 3.3 – Screenshot of the 3D HSPiP solvent-solute analysis (with CO ₂ selected as the target solute) showing a rotated view of the solvent distribution. | 58 |
| Figure 3.4 – Screenshot of the HSPiP DIY solvent property calculator results for Benzimidazole..... | 60 |
| Figure 3.5 – Rendering of an isolated molecule structure for a typical ionic liquid ([bmim][PF ₆]) (drawn using the ACD/ChemSketch Freeware package)..... | 62 |
| Figure 3.6 – Screenshot of the results obtained for an optimized ionic pair ([bmim][PF ₆]). | 63 |
| Figure 3.7 – A block flow diagram of the proposed solvent screening software system analysis. | 68 |
| Figure 3.8 – Screenshot of the setup window for analyzing alternative solvent blends..... | 70 |
| Figure 3.9 – Screenshot of the setup window for calculating the solvent relative energy differences (REDs). | 71 |
| Figure 3.10 – Screenshot of the setup window for quick blend calculations (estimating both the blend composition and HSPs). | 72 |
| Figure 3.11 – Screenshot of the setup window for quick blend calculations (estimating both the blend composition and HSPs). | 72 |
| Figure 3.12 – Screenshot of the setup window used for estimating the ionic bond energy parameters (δ) of selected solvents. | 73 |
| Figure 4.1 – Schematic of the experimental setup design..... | 76 |
| Figure 4.2 – Experimental setup with descriptions. | 76 |
| Figure 4.3 – Temperature-controlled environment of the experimental setup with descriptions..... | 77 |
| Figure 4.4 – Equilibrium cell with descriptions of the various design details. | 78 |
| Figure 4.5 – Reducer fitting that was made to connect a luer lock needle to the pressure transmitter. ... | 79 |
| Figure 4.6 – Screenshot of the Picolog® data acquisition software used to monitor and record the temperature and pressure of the system..... | 80 |
| Figure 5.1 – (a) Screenshot of the 3D HSPiP solvent-solute analysis of the solvents with RED values between 0 and 1 (with CO ₂ selected as the target solute), (b) Screenshot of the planar analysis of the 3D rendering. | 92 |
| Figure 5.2 – A block flow diagram of the original iterative algorithm used by the EquiSolv solvent optimizer for Gauss-Seidel iteration..... | 96 |
| Figure 5.3 – A block flow diagram of the updated iterative algorithm. | 99 |

| | |
|---|-----|
| Figure 6.1 – A cropped section view of the P-v-t graph for Run 1 (30wt% MEA (aq) exposed for 50000s). | 107 |
| Figure 6.2 – P-v-t graph for Run 2 (the repeated experimental run for 30wt% MEA (aq) exposed for 2000s). | 109 |
| Figure 6.3 – P-v-t graph for Run 3 (30wt% K ₂ CO ₃ (aq) exposed for 2000s). | 110 |
| Figure 6.4 – P-v-t graph for Run 4 (the repeated experimental run for 30wt% K ₂ CO ₃ (aq) exposed for 2000s). | 111 |
| Figure 6.5 – P-v-t graph for Run 5 (an aqueous solution of 22.1wt% K ₂ CO ₃ and 13.8wt% Piperazine (PZ) exposed for 2000s). | 112 |
| Figure 6.6 – P-v-t graph for Run 6 (an aqueous solution of 83.39vol% Trioctylamine and 9.34vol% Monoethanolamine (MEA) exposed for 2000s). | 114 |
| Figure 6.7 – P-v-t graph for Run 7 (an aqueous solution of 28.13vol% Auramine and 55.45vol% Hexylamine exposed for 2000s). | 116 |
| Figure 6.8 – P-v-t graph for Run 8 (an aqueous solution of 50.06vol% Tryptamine and 29.62vol% Diisobutylamine exposed for 2000s). | 117 |
| Figure 6.9 – P-v-t graph for Run 9 (an aqueous solution of 33.45vol% sec-Butylamine and 43.09vol% Auramine exposed for 2000s). | 118 |
| Figure 6.10 – P-v-t graph for Run 10 (an aqueous solution of 9.02vol% Hexylamine and 67.99vol% 2,4-Dichlorobenzylamine exposed for 2000s). | 119 |
| Figure 6.11 – P-v-t graph for Run 11 (an aqueous solution of 55.97vol% Di-p-Tolylamine and 7.23vol% Dimethyl ethanolamine (DMEA) exposed for 2000s). | 120 |
| Figure 6.12 – Comparison of the solvent rich loadings for the six randomly selected solvent formulations to the loadings measured for the three reference solvent blends. | 123 |
| Figure 6.13 – P-v-t graph for Run 12 (60wt% [bmim][PF ₆] (aq) exposed for 2000s). | 124 |
| Figure 6.14 – P-v-t graph for Run 13 (60wt% [bmim][BF ₄] (aq) exposed for 2000s). | 125 |
| Figure 6.15 – P-v-t graph for Run 14 (60wt% [omim][PF ₆] (aq) exposed for 2000s). | 126 |
| Figure 6.16 – P-v-t graph for Run 15 (a solution of 88.45vol% Diisobutylamine and 11.55vol% [omim][PF ₆] exposed for 2000s). | 128 |
| Figure 6.17 – P-v-t graph for Run 16 (a solution of 88.12vol% Diisobutylamine and 11.88vol% [bmim][PF ₆] exposed for 2000s). | 129 |
| Figure 6.18 – P-v-t graph for Run 17 (a solution of 60.11vol% 2,4-Dichlorobenzylamine and 39.89vol% [omim][PF ₆] exposed for 2000s). | 130 |

| | |
|---|-----|
| Figure 6.19 – P-v-t graph for Run 18 (a solution of 78vol% Monoethanolamine (MEA) and 22vol% [bmim][BF ₄] exposed for 2000s). | 131 |
| Figure 6.20 – Comparison of the solvent rich loadings for the seven IL solvent blends to the loadings measured for the three reference solvent blends. | 133 |
| Figure 6.21 – P-v-t data obtained for one of the pressure test runs (negative force exerted). | 134 |
| Figure 6.22 – P-v-t graph for Run 19 (the third experimental run for 30wt% MEA (aq) exposed for 2000s). | 135 |
| Figure 6.23 – P-v-t graph for Run 20 (the fourth experimental run for 30wt% MEA (aq) exposed for 2000s). | 136 |
| Figure A.1 – A block flow diagram of the algorithm used by the EquiSolv solvent optimizer for matrix manipulation calculations..... | 156 |
| Figure A.2 – A block flow diagram of the iterative algorithm used by the EquiSolv solvent optimizer for Gauss-Seidel iteration..... | 168 |
| Figure C.1 – Schematic of the experimental setup design. | 182 |
| Figure G.1 – Calibration certificate for the pressure transmitter. | 192 |
| Figure G.2 – P-v-t graph for Pressure Test Run 1 (Positive Force Exerted)..... | 194 |
| Figure G.3 – P-v-t graph for Pressure Test Run 2 (Positive Force Exerted)..... | 195 |
| Figure G.4 – P-v-t graph for Pressure Test Run 3 (Positive Force Exerted)..... | 195 |
| Figure G.5 – P-v-t graph for Pressure Test Run 4 (Negative Force Exerted)..... | 196 |
| Figure G.6 – P-v-t graph for Pressure Test Run 5 (Negative Force Exerted)..... | 196 |
| Figure G.7 – P-v-t graph for Pressure Test Run 6 (Negative Force Exerted)..... | 197 |
| Figure H.1 – Screenshot of the EquiSolv logon screen. | 198 |
| Figure H.2 – Screenshot of the EquiSolv main screen. | 199 |
| Figure H.3 – A screenshot of the Import/Export dropdown menu option. | 201 |
| Figure H.4 – Screenshot of the solvent data import screen. | 202 |
| Figure H.5 – Screenshot of the import file lookup and selection screen..... | 202 |
| Figure H.6 – Screenshot of the import screen upon completion of a successful solvent (and solute) data import run..... | 203 |
| Figure H.7 – Screenshot of the data export screen..... | 204 |
| Figure H.8 – Screenshot of the Browse dropdown menu option..... | 206 |
| Figure H.9 – Screenshot of a browse window for a selected set of solvent data. | 206 |
| Figure H.10 – Screenshot of the individual record browse window for a selected solvent. | 207 |

| | |
|---|-----|
| Figure H.11 – Screenshot of the query function provided from the browse window. | 207 |
| Figure H.12 – Screenshot of the Calculate dropdown menu option. | 208 |
| Figure H.13 – Screenshot of the setup window used for estimating the ionic bond energy parameters (δ) of selected solvents. | 209 |
| Figure H.14 – Screenshot of the setup window for estimating the ionic bond energies upon completion of a successful calculation run. | 210 |
| Figure H.15 – Screenshot of a browse window for a set of solvents selected for estimating the ionic bond energies. | 211 |
| Figure H.16 – Screenshot of a browse window indicating that the ionic bond energy estimation have been reversed. | 211 |
| Figure H.17 – Screenshot of the setup window for calculating the solvent relative energy differences (REDs). | 213 |
| Figure H.18 – Screenshot of the solute lookup and selection window for the RED calculations. | 213 |
| Figure H.19 – Screenshot of the RED calculation setup window with the target solute selected and ready for calculation. | 214 |
| Figure H.20 – Screenshot of the setup window for calculation the solvent REDs upon completion of a successful calculation run. | 214 |
| Figure H.21 – Screenshot of a browse window for the consolidated solvent RED results. | 215 |
| Figure H.22 – Screenshot of the setup window for analyzing alternative solvent blends. | 217 |
| Figure H.23 – Screenshot of the solvent list lookup and selection window. | 217 |
| Figure H.24 – Screenshot of the solvent optimizer window set up and prepared for a calculation run. | 218 |
| Figure H.25 – Screenshot of the solvent optimizer setup window upon completion of a successful calculation run. | 218 |
| Figure H.26 – Screenshot of the blend analysis error report window. | 219 |
| Figure H.27 – Screenshot of the calculated alternative blends browse window. | 219 |
| Figure H.28 – Screenshot of the setup window for quick blend calculations (estimating both the blend composition and HSPs). | 221 |
| Figure H.29 – Screenshot of the solvent list lookup and selection window. | 222 |
| Figure H.30 – Screenshot of the solvent lookup and selection window. | 222 |
| Figure H.31 – Screenshot of the quick blend calculator setup window prepared and ready for a calculation run. | 223 |

Figure H.32 – Screenshot of the quick blend calculator setup window upon completion of a successful calculation run..... 223

Figure H.33 – Screenshot of the setup window for quick blend calculations (estimating the blend HSPs for a specified composition). 224

Figure H.34 – Screenshot of the Reports drop down menu option. 225

Figure H.35 – Screenshot of the Utilities/Clear Records drop down menu option..... 226

List of Tables

| | |
|--|-----|
| Table 1.1 – Summary of the suitability of separation technologies to feed gas streams (Redrawn from (Wong et al., 2002)). | 3 |
| Table 2.1 – Summary of the major advantages and disadvantages of the various separation processes discussed. | 14 |
| Table 2.2 – Typical operating conditions for amines used in CO ₂ capture processes (Redrawn from (Kohl. & Nielsen, 1997)). | 25 |
| Table 2.3 – Summary of major advantages and disadvantages of the various chemical solvents discussed. | 29 |
| Table 2.4 – Summary of the individual contributions to the overall reboiler heat duty at the reference desorber pressure for a generic high- and low heat of absorption solvent (Redrawn from (Oexmann & Kather, 2010)). | 44 |
| Table 3.1 – Summary of the derivative equations for the temperature and pressure effects on HSPs (Hansen, 2007). | 55 |
| Table 3.2 – Summary of the solubility parameter data and molar volumes for the ionic liquids studied by Abbott et al. (2010). | 64 |
| Table 4.1 – A summary of the randomly selected blend formulations predicted by the EquiSolv model that will be used to test the null hypothesis formulated for the study. | 81 |
| Table 4.2 – A summary of the randomly selected amine-IL blend formulations predicted by the EquiSolv model. | 82 |
| Table 4.3 – A summary of the chemicals acquired for the experimental work planned. | 85 |
| Table 5.1 – Summary of the accuracy gained by using a larger quantum chemical basis set, expressed as a percentage value. | 89 |
| Table 5.2 – Summary of the δI and cl values calculated for the set of ILs considered. | 90 |
| Table 5.3 – Summary of the error made by assuming a constant value of 0.001 for cl for each of the ILs considered. | 90 |
| Table 5.4 – Summary of the solvents found with a calculated RED value between 0 and 1. | 91 |
| Table 5.5 – Summary of the six blend formulations random selected from the EquiSolv solvent optimizer predictions. | 94 |
| Table 5.6 – Summary of the six blend formulations randomly selected normalized to a sum of volume fractions equal to 1. | 100 |

| | |
|--|-----|
| Table 5.7 – Summary of the six blend formulations randomly selected balanced with water to a sum of volume fractions equal to 1..... | 100 |
| Table 5.8 – Results for converting the conventional 30wt% MEA solution composition to volume percentage contributions. | 101 |
| Table 5.9 – Summary of HSP values calculated for the conventional 30wt% MEA solution using the quick blend calculator..... | 102 |
| Table 5.10 – Summary of the quick blend calculator predictions for the conventional 30wt% MEA solution at 60 and 110°C..... | 103 |
| Table 6.1 – Summary of the solvent formulations randomly selected for synthesis and experimental testing..... | 113 |
| Table 6.2 – Summary of the CO ₂ absorption capacities (rich loadings) experimentally measured for the six randomly selected blend formulations..... | 121 |
| Table 6.3 – Summary of the MATLAB results obtained for the Kendall coefficient of concordance statistical test conducted for the results of the experimental hypothesis test results..... | 121 |
| Table 6.4 – Summary of the four IL-based solvent formulations randomly selected for synthesis and experimental testing. | 127 |
| Table 6.5 – Summary of the CO ₂ absorption capacities experimentally measured for the four amine-IL blend formulations..... | 131 |
| Table 6.6 – Summary of the results obtained for the Kendall coefficient of concordance statistical test conducted for the results of the combined experimental hypothesis test results..... | 132 |
| Table B.1 – Summary of the molecular mechanics (MM+) calculation results for the ionic bond energies of the 74 selected ionic liquids..... | 171 |
| Table B.2 – Summary of the molecular mechanics (MM+) calculation results for the ionic bond energies of the 74 selected ionic liquids (continued)..... | 172 |
| Table B.3 – Summary of the semi-empirical (AM1) calculation results for the ionic bond energies of the 74 selected ionic liquids..... | 173 |
| Table B.4 – Summary of the Ab-Initio calculation results using a minimal basis set (STO-3G) geometry optimization for the ionic bond energies of the 74 selected ionic liquids. | 174 |
| Table B.5 – Summary of the Ab-Initio calculation results using a small basis set (3-21G) geometry optimization with MP2 correction for the ionic bond energies of the 74 selected ionic liquids..... | 175 |
| Table B.6 – Summary of the RED values calculated for the collective list of solvents analyzed in the EquiSolv package..... | 176 |

| | |
|--|-----|
| Table B.7 – Summary of the RED values calculated for the collective list of solvents analyzed in the EquiSolv package (continued)..... | 177 |
| Table B.8 – Summary of the RED values calculated for the collective list of solvents analyzed in the EquiSolv package (continued)..... | 178 |
| Table B.9 – Summary of the RED values calculated for the collective list of solvents analyzed in the EquiSolv package (continued)..... | 179 |
| Table B.10 – Summary of the RED values calculated for the collective list of solvents analyzed in the EquiSolv package (continued)..... | 180 |
| Table B.11 – Summary of the blend formulations randomly selected from the solvent optimizer predictions (with the six blend formulations selected for synthesis highlighted in red). | 181 |
| Table E.1 – Summary of the experimental data for the six solvent formulations synthesized. | 187 |
| Table G.1 – Calibration data entered into the DMS for the pressure transmitter..... | 193 |
| Table G.2 – Calibration data entered into the DMS for the temperature controller and recorder..... | 193 |
| Table H.1 – Description of the CSV file column layout required for importing solvent data into the EquiSolv database. | 200 |
| Table H.2 – Description of the CSV file column layout required for importing solute data into the EquiSolv database. | 200 |

Nomenclature

General Symbols

| Symbol | Description | Units |
|--------|---|------------------------------------|
| W | Mechanical work | J |
| LHV | Fuel energy input based on low heating value | kJ/mol |
| q or Q | Heat requirement | J |
| m | Mass flow rate | kg/s |
| c | Specific heat capacity | kJ/kg.K |
| M | Molar weight | g/mol |
| p | Partial pressure | Pa or bar |
| T | Temperature | K |
| R | Universal gas constant | J/mol.K |
| P | Pressure | Pa or bar |
| V | Volume | m ³ or cm ³ |
| E | Bond energy | J/mol or kcal/mol |
| RI | Refractive index | |
| DM | Dipole moment | Debyes |
| Ra | Distance between the solubility parameters of two materials | MPa ^{0.5} |
| Ro | Solute interaction radius | MPa ^{0.5} |
| RED | Relative energy difference | |
| x | Volume percentage contribution | vol% |
| C | Coefficient of interaction | |
| m | Mass | kg or g |
| a | PR-EoS attractive parameter | J.m ³ /mol ² |
| b | PR-EoS covolume | m ³ /mol |
| n | Molar amount | mol |
| l | Solvent loading | mol CO ₂ /mol solvent |
| Det | Matrix determinant | |

Greek Symbols

| Symbol | Description | Units |
|----------------|---|--|
| η | Power cycle efficiency | % |
| $\Delta\alpha$ | Difference in CO ₂ loading between the rich and lean streams | mol CO ₂ /mol solvent |
| Δ | Difference | |
| δ | Solubility parameter | MPa ^{0.5} |
| α | Isobaric coefficient of thermal expansion | |
| β | Isothermal compressibility | |
| ρ | Density | kg/m ³ or g/cm ³ |
| κ | PR-EoS constant from Pitzer acentric factor contributions | |
| ω | Pitzer acentric factor | |
| $\alpha(T)$ | PR-EoS temperature dependent variable | |
| ε | Error | % |

Subscripts

| Symbol | Description |
|--------|---|
| A | Boiler ancillary power or solvent contributions |
| abs | Absorption |
| An | Anion |
| B | Solute contributions |
| C | Steam cycle condenser |
| c | Critical |
| Calc | Calculated |
| CAP | Retrofitted CCS capture |
| Cat | Cation |
| cell | Equilibrium cell |
| D | Dispersion interaction forces |
| eq | Equilibrium state |

| | |
|-----------|--|
| exc | Excess |
| feed | Feed point conditions |
| H | Hydrogen bond interaction forces |
| HI | Hydrogen bond-Ionic force interactions |
| HT | True hydrogen bond interaction force contributions |
| I | Ionic interaction forces |
| i | Element considered |
| ini | Initial state |
| j | State considered (initial or equilibrium) |
| liq | Stream liquid fraction |
| m | Molar |
| mix | Solvent mixture |
| Mol | Molecule |
| p | At constant pressure |
| P | Polar interaction forces |
| Pred | Predicted |
| r | Reduced |
| reb | Reboiler |
| ref | Reference standard |
| rich | Rich conditions |
| sample | Solvent considered |
| sens | Sensible heat |
| sol | Solution |
| solv | Solvent |
| steam | Stream steam fraction |
| T | Mechanical work output |
| TS or tar | Target solute |
| v or vap | Vaporization |
| void | Atmospheric void inside the equilibrium cell |

Superscripts

| Symbol | Description |
|--------|-------------------------------------|
| * | Equilibrium state conditions |
| R | Including a retrofitted CCS process |
| s | Dynamic state conditions |

1. Introduction

The International Energy Agency (IEA) classified greenhouse gas (GHG) emissions released into the atmosphere as a primary contributor to global warming and climate change (IEA, 2007). Carbon dioxide (CO₂), methane (CH₄), nitrous oxide (N₂O), sulphur hexafluoride (SF₆), perfluorocarbons (PFCs) and hydrofluorocarbons (HFCs) have been identified as the main greenhouse gases (GHGs) produced by anthropogenic (human) activity (Aboudheir & ElMoudir, 2009). Mathews (2007) proposed a set of seven initiatives to curb global warming through reduced net global GHG emissions into the atmosphere:

1. Enforce a global regime that puts an effective price on carbon; forcing major economic entities to consider the cost of emitting carbon and how these costs can be mitigated through reduced emissions.
2. Establish a global monitoring system for measuring net GHG emissions.
3. Compensate developing tropical countries, should they preserve rainforests to act as major carbon sinks.
4. Enforce the dismantling of newly created trade barriers hindering the global trade in biofuels.
5. Promote the transition from fossil fuels to renewable energy to reduce the global energy intensity.
6. Recycle carbon revenues earned to promote the use of renewable energy sources in developing countries.
7. Enforce a moratorium on the construction of new coal-fired power plants and the reduction of CO₂ emissions from existing plants.

Although CO₂ has a smaller impact potential compared to other GHGs, it is considered to be the primary GHG contributor by more than 65% based on the vast amounts emitted into the atmosphere (Yamasaki, 2003). Current estimates suggest that net global CO₂ emissions will have to be reduced by 70% by 2050 to avoid serious negative, irreversible impacts on the environment (Mathews, 2007). Parallel to this, net global CO₂ emissions are expected to increase over the same period of time, with fossil fuel (e.g. oil and coal) remaining a significant source of energy for the global economy for several decades (IEA, 2009). Figure 1.1 shows forecasts by the IEA for the global energy supply share of various energy sources.

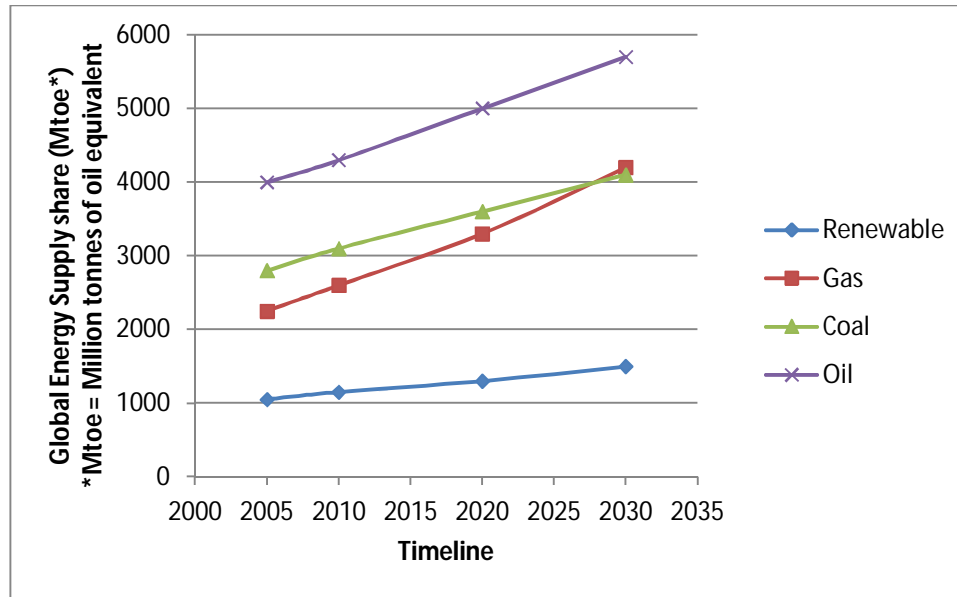


Figure 1.1 – The forecasted global energy demand supply share by fuel type (Redrawn from (Aboudheir & ElMoudir, 2009)).

Significant changes to reduce net global CO₂ emissions must be implemented by 2020 if dangerous climate change with serious negative impacts on human activity is to be avoided (Mathews, 2007). Possible CO₂ abatement strategies include reducing energy intensity (improving process efficiencies), reducing carbon intensity (making the transition from fossil fuel to renewable energy), and enhanced CO₂ sequestration. CO₂ sequestration provides a mid- to long-term solution to mitigate negative environmental impacts while allowing the continued use of fossil fuel until renewable energy technologies mature (Yang et al., 2008). Globally, fossil-fueled power plants generate the largest amount of CO₂ emissions, accounting for 33-40% of the total net emissions (Stewart & Hessami, 2005). Riahi *et al.* (2004) concluded that carbon capture and storage (CCS) is an obvious priority candidate for long-term technology policies and enhanced research and development (R&D) efforts to reduce CO₂ emissions from fossil fuel power plants.

CCS consists of three basic stages, i.e. (a) extraction and capture of the CO₂, (b) transportation and (c) storage (Wang et al., 2010). Extraction and capture of CO₂ can be realized by three major approaches: pre-combustion carbon capture, oxy-fuel processes and post-combustion carbon capture (Yang et al., 2008). Only post-combustion capture (PCC) can effectively address the emissions of existing fossil-fueled

power plants. Both pre-combustion capture and oxy-fuel processes can only be implemented in newly constructed power plants, causing a delayed impact of CCS on the reduction of CO₂ emissions (Feron, 2010).

Post-combustion extraction is comprised of two main steps: first an energy conversion step in which power is produced, followed by a CO₂ separation process from which a concentrated stream of CO₂ is produced (Feron & Hendriks, 2005). It offers the advantage that the technology can be implemented as a retrofit option to existing plants without radical changes. This advantage comes at the expense of the thermal efficiency of the power generation process, with an energy penalty between 25 and 30% of the total steam produced by the plant (Elwell & Grant, 2006). The separation process is energy intensive and largely determines the cost of the CCS process, representing about 75-80% of the total process cost (Davison, 2007). A number of separation technologies are available for extraction of CO₂ with PCC (Wang et al., 2010). These include: (a) adsorption, (b) cryogenics separation, (c) membrane-based separation, (d) physical absorption and (e) chemical absorption. Table 1.1 shows the suitability of the alternative separation technologies to feed gas streams. Among these alternatives, chemical absorption with aqueous organic solvent solutions (e.g. alkanolamines) was demonstrated as one of the most mature and least expensive technologies to be applied to fossil-fueled power plants (Erga et al., 1995).

Table 1.1 – Summary of the suitability of separation technologies to feed gas streams (Redrawn from (Wong et al., 2002)).

| Separation Technology | Flue Gas CO₂ Concentration [vol%] | Feed Gas Pressure [MPa] | Operating Temperature [°C] |
|------------------------------|---|--------------------------------|-----------------------------------|
| Adsorption | > 30 | Moderate | Low to moderate |
| Cryogenic | > 50 | Moderate | Low |
| Membrane | > 15 | > 0.7 | Feed temperature |
| Absorption | | | |
| Physical | > 20 | > 2 | 50 |
| Chemical | > 3 | > 0.1 | Low - 10 |

In designing the separation process, the primary concern is that the sweetened (extracted) gas meets the required CO₂ purity specifications for the storage process. Second to this, the objective is to select the solvent such that the process equipment size is optimized and the plant operating cost is minimized. Factors that need to be considered in the process of solvent selection include (Mofarahi et al., 2008):

1. Is it possible to reduce the solvent circulation rate by selecting it such that the solvent can be used at higher concentration and/or acid gas (CO₂) loading?
2. Is it possible to minimize the reboiler/condenser size and duty by selecting a solvent that requires a lower circulation rate, and/or has lower heats of reaction with CO₂ (i.e. reduced energy requirement for solvent regeneration)?
3. Is there any possibility of corrosion problems with the selected solvent?

Between 50 and 70% of the initial capital investment for a CO₂ recovery plant is directly associated with the magnitude of the solvent circulation rate. A further 10 to 20% is dependent on the solvent regeneration energy requirement (Astarita et al., 1983). Solvent selection can greatly reduce both the solvent circulation rate and regeneration energy requirement. Hence, the choice of solvent (or combination of solvents) can have a significant impact on the overall costs associated with a CO₂ recovery plant (Mofarahi et al., 2008).

Aqueous alkanolamine solutions, e.g. aqueous monoethanolamine (MEA), have been shown to be industrially effective for capturing CO₂. There are several serious drawbacks however, inherently connected to these solutions, e.g. (Yu et al., 2006):

1. Concurrent losses of volatile amines and the uptake of water into the sweetened gas stream cause intensive energy consumption;
2. Increased operating costs as a result of the intensive energy consumption mentioned above;
3. Corrosion problems.

It is paramount to find a new kind of sequestering agent that can overcome these problems (Rogers & Seddon, 2002). In this regard, ionic liquids (ILs) offer a unique set of characteristics such as negligible vapour pressure, high thermal stability, excellent solvent power, and the ability to be easily structurally modified to obtain a set of desired physical properties (Bates et al., 2002). ILs have been identified as a versatile alternative to the conventional organic solvents used in reactions, separation processes, material engineering, and other industries. There is little research however, dedicated to the solubility and phase equilibria of ILs used for chemical capture of CO₂ from gas streams (Yu et al., 2006).

Partial solubility parameters offer a simple method of predicting the solubility and phase equilibria behaviour of one material in another. Parameters such as the Hansen solubility parameters (HSPs) evaluate the differences between the various bonding energies of the different materials. By minimizing these differences the dissolution energy requirement is reduced and the materials become more soluble in each other. The only drawback of the HSPs is that they do not account for electrostatic (ionic) bond energies – the primary bond energy present in IL solutions. The key research questions for this study include:

1. Can the Hansen solubility parameters (HSPs) accurately predict the solubility behaviour of CO₂ in certain task specific design solvents?
2. Is it possible to expand the model theory to include contributions from electrostatic (ionic) bond energies?
3. If the answer to the above question is yes, can the model be designed such that it is possible to select specific cation/anion pairs for solvent formulation analysis?
4. Is there any improvements/advantages in using ILs rather than aqueous alkanolamines solutions (e.g. MEA) to chemically absorb CO₂?

The research plan for this study is divided into three key stages: (i) develop a simplified thermodynamic model for solvent selection based on the Hansen partial solubility parameters, (ii) use the model to predict alternative solvent blend formulations for use in the chemical absorption of CO₂, and (iii) test the model hypothesis through random sample testing of the model predictions. A block flow diagram of the basic structure of the thesis is shown in Figure 1.2.

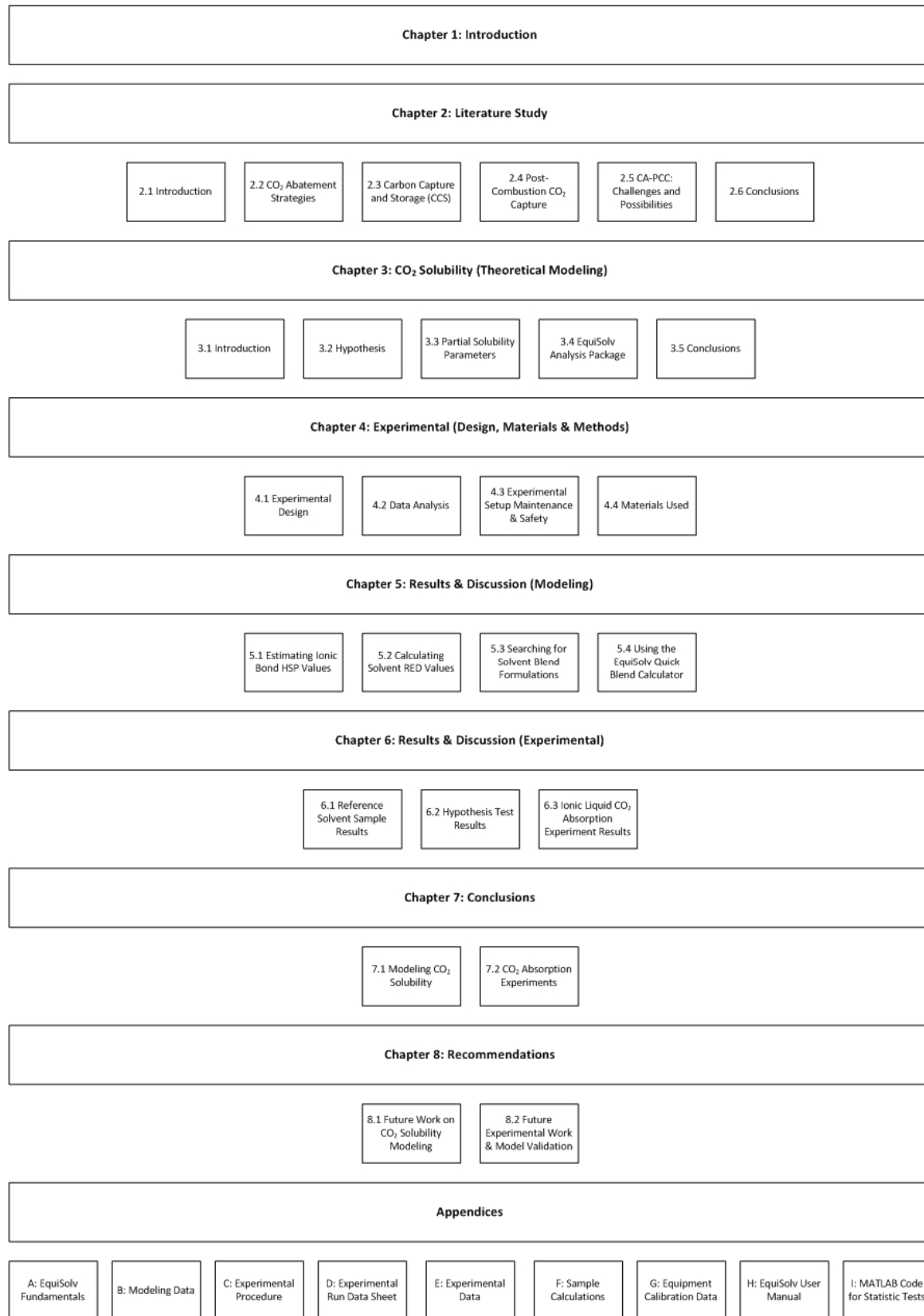


Figure 1.2 – Block flow diagram of the thesis structure.

2. Literature Study

2.1. Introduction

The rapid increase in global population in the 20th century has caused an exponential growth in energy consumption. It is estimated that the global energy demand will increase by 57% from 2004 to 2030 (IEA, 2007). Currently more than 85% of the global energy demand is supplied by fossil fuels (Carapellucci & Milazzo, 2003). It is forecasted that fossil fuel, primarily coal, will remain a significant source of energy for the global economy for decades to come; the net carbon dioxide (CO₂) emissions from large emerging economies increasing over the same period of time (IEA, 2009). Considering the time period from pre-industrialization around 1860 to 1958, global concentrations of CO₂ in the atmosphere increased from 280 parts per million by volume (ppmv) to approximately 316 ppmv; rapidly increasing to approximately 369 ppmv today (UNEP, 2005). It is estimated that this value will increase to 750 ppmv by 2100 considering the current global situation (Wang et al., 2010). It is clear that the net global CO₂ emissions must be significantly reduced if dangerous climate change is to be avoided. Ultimately the net global CO₂ emissions will have to be reduced to near zero levels for a significant period of time (CCC, 2008).

2.2. Carbon Dioxide Abatement Strategies

Three options are available to reduce the net global CO₂ emissions into the atmosphere, i.e. to reduce energy intensity, reduce carbon intensity, and enhance CO₂ sequestration (Yang et al., 2008). The first option emphasizes the efficient use of energy. It is paramount that investments be made towards developing more efficient processing techniques to reduce the overall energy demand (Nyquist & Ruys, 2009). The second option requires switching from fossil to non-fossil fuels, e.g. hydrogen, biofuels and renewable energy. The third option focuses on developing technologies to capture CO₂ emissions and successfully sequester them for a period of time. This provides a mid- to long-term CO₂ mitigation solution and allows the continued use of fossil fuel energy until technologies for option two mature (Herzog & Drake, 1996).

2.3. Carbon Capture and Storage (CCS)

It is widely recognized that capture and geological storage of CO₂ (CCS) as abatement strategy is a promising option that could significantly contribute to the reduction of net global CO₂ emissions, next to other options such as, energy efficiency improvements, the use of renewable and/or nuclear energy and switching from coal to gas firing (Feron, 2010). It is estimated that the CCS approach would entail an interim energy target of 240 GW of the total installed CCS capacity by 2030, assuming a long-term atmospheric CO₂ concentration target of 450 ppm CO₂eq (IEA, 2009). Power generation from fossil fuel-fired power plants (i.e. coal and natural gas) is recognized as the single largest source of anthropogenic CO₂ emissions (Freund, 2003). Applying CCS technology to fossil fuel-fired power plants offers great potential to store the CO₂ emissions generated by these plants for many years (Feron, 2010).

CCS is defined as a “process consisting of the separation of CO₂ from industrial and energy-related sources, transport to a storage location and long-term isolation from the atmosphere” (IPCC, 2005). From this it can be deduced that CCS consists of three fundamental stages (Figure 2.1):

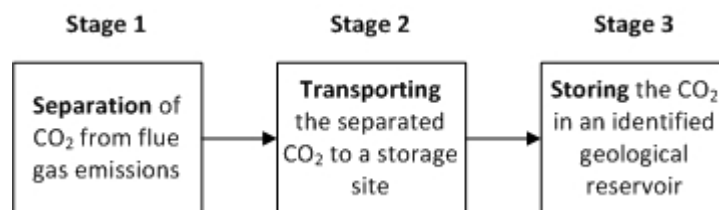


Figure 2.1 – The three basic stages of the CCS process.

The CO₂ is extracted, or separated, at some point in the energy conversion process, depending on the energy conversion technology used, where after it is prepared for transportation to and storage in a suitable geological reservoir for a significant period of time. CCS offers the potential to either limit or altogether avoid the release of CO₂ emissions from combustion processes into the atmosphere. This approach to CO₂ abatement allows the continued use of fossil fuels (e.g. coal, gas and oil), while significantly reducing the net CO₂ emissions into the atmosphere (Feron & Hendriks, 2005).

For the extraction or separation stage (Stage 1), there are three major approaches for separating, or capturing, the CO₂ emissions: post-combustion capture, pre-combustion combustion capture, and oxy-fuel combustion capture (Wang et al., 2010). Typically, power stations emit large quantities of CO₂ in diluted streams into the atmosphere. The CO₂ is separated from these diluted streams, concentrated to a near pure CO₂ product stream, and compressed typically to an absolute pressure of 100 bars to prepare the product for transportation and storage (Feron & Hendriks, 2005).

2.3.1. CO₂ Capture/Extraction (Stage 1)

2.3.1.1. Post-Combustion Capture Process

In the post-combustion capture (PCC) approach, the CO₂ is extracted from a dilute CO₂ flue gas stream (3-20%) at low pressure (typically 1 bar) (Feron & Hendriks, 2005). The primary separation task here is to remove the CO₂ from a NO_x and SO₂-containing gas mixture (Yang et al., 2008). The process consists of two main stages: an energy conversion stage and a subsequent CO₂ separation stage (Figure 2.2).

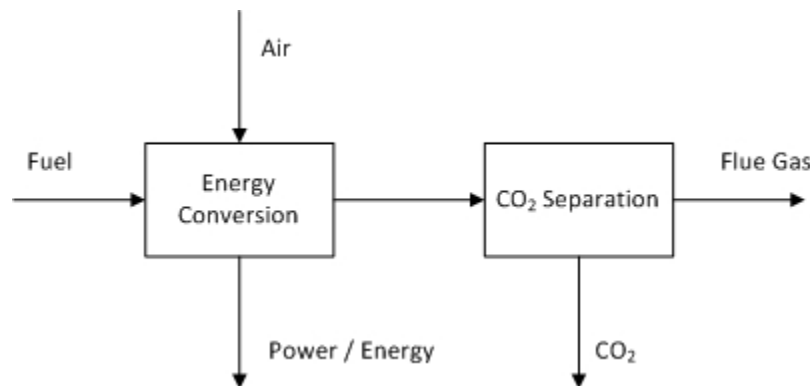


Figure 2.2 – A block flow diagram of an oxy-fuel carbon capture process (Redrawn from (Feron & Hendriks, 2005)).

Typically a chemical absorption process is used to extract the CO₂. This technique has been used to extract CO₂ in the natural gas industry for over 60 years. When implemented at fossil-fueled power plants however, the separation stage would consume one-quarter to one-third of the total steam produced by the plant, reducing the generation capacity of the plant by the same amount (Yang et al., 2008). Furthermore the carbon footprint of the host plant is increased by up to 60%. In 2000, the

National Energy Technology Laboratory (NETL) estimated that implementing PCC would increase the cost of electricity production by as much as 70% (Elwell & Grant, 2006). The challenge is to develop a separation process capable of delivering a near pure extracted CO₂ product stream at an acceptable energy penalty and cost (both capital and operating) (Feron & Hendriks, 2005).

2.3.1.2. Pre-Combustion Capture Process

In a pre-combustion carbon capture process the fuel first reacts with air or oxygen at high pressure (15–40 bar) to produce a gas mixture of predominantly H₂ and moderate CO₂ content (15-40%) (Aboudheir & ElMoudir, 2009). For natural gas this is achieved through a reforming process, and for coal it is done through gasification and a subsequent shift-reaction. The high pressure of the gas mixture product stream facilitates the extraction of CO₂ (Feron & Hendriks, 2005). The CO₂/H₂ product stream is sent to a separation stage where the CO₂ is separated from the conversion product stream. Several techniques are available for separating the CO₂ from the conversion product stream, e.g. pressure swing adsorption (PSA), physical absorption or chemical absorption. These techniques are discussed in detail in Section 2.4.1. The H₂ is sent to an energy conversion stage and burnt as fuel in a gas turbine, with a subsequent heat recovery and steam generation process (Yang et al., 2008). A block flow diagram of the process is shown in Figure 2.3.

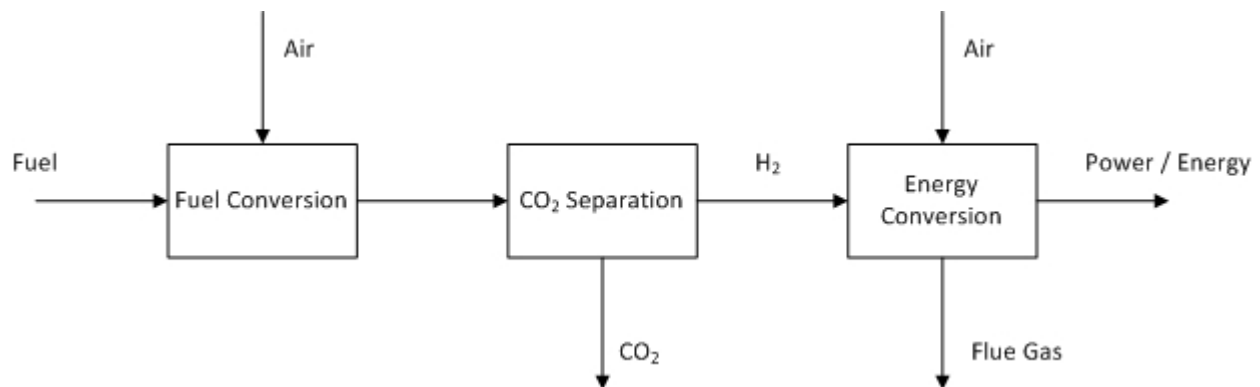


Figure 2.3 – A block flow diagram for a pre-combustion carbon capture process (Redrawn from (Feron & Hendriks, 2005)).

It is suggested that pre-combustion capture provides the greatest potential for high efficiency energy conversion. This is attributed to the fact that the H₂ intermediate product can be converted into power

at high efficiency through gas turbine combined cycles (GCC) using existing technology or through fuel cells in the future (Feron, 2010). It is estimated that implementing pre-combustion capture would increase the cost of electricity production by 25% (Yang et al., 2008).

2.3.1.3. Oxy-Fuel Combustion Capture Process

The oxy-fuel, also called oxy-firing, combustion capture technique introduces an air separation stage to the process. Pure oxygen (O_2) is separated from air and sent to the energy conversion stage, combined with partially recycled flue gas of concentrated CO_2 . This is done to control the furnace temperature (Yang et al., 2008). Combustion takes place in an O_2/CO_2 mixture environment to yield a high-purity CO_2 flue gas stream (Feron & Hendriks, 2005). A block flow diagram of the oxy-fuel combustion process is shown (Figure 2.4).

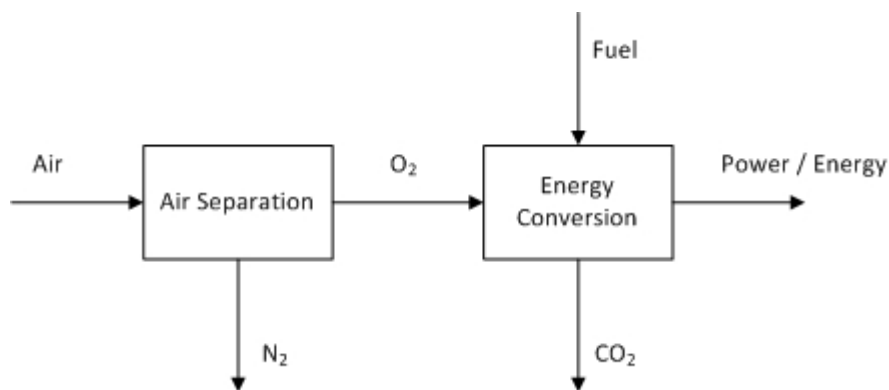


Figure 2.4 – A block flow diagram of an oxy-fuel carbon capture process (Redrawn from (Feron & Hendriks, 2005)).

A major advantage of the oxy-fuel technique is that the flue gas stream is free of nitrogen components. Particulate matter and sulfur compounds are removed from the flue gas to yield a product stream consisting of approximately 90% CO_2 by volume on a dry basis. This is sufficiently pure that further separation of CO_2 is not necessary. The primary advantage of the oxy-fuel technique is the elimination of NO_x control equipment as well as the CO_2 separation stage. This results in a reduction of the capital cost. A major disadvantage to the technique is the corrosion of equipment as a result of increased SO_2 concentrations in the flue gas stream (Yang et al., 2008). The operating and capital costs of this technology would be comparable to that of post-combustion capture processes. The oxygen separation

unit would consume between 23% and 37% of the host plant's total electricity output (Elwell & Grant, 2006).

2.3.1.4. Novel Technology: Chemical-looping Combustion

The chemical-looping combustion (CLC), also referred to as unmixed combustion, process is a new approach to heat and power production with inherent CO₂ capture. The process avoids direct contact between the fuel and the combustion air (Rydén & Lyngfelt, 2006). An oxygen carrier is utilized to extract oxygen from the air and supply it to the fuel. Typical carriers are small particles of metal oxides such as Fe₂O₃ (hematite), NiO (nickel oxide), CuO (copper oxide) or Mn₂O₃ (manganese oxide) (Yang et al., 2008). A basic CLC process is shown in Figure 2.5:

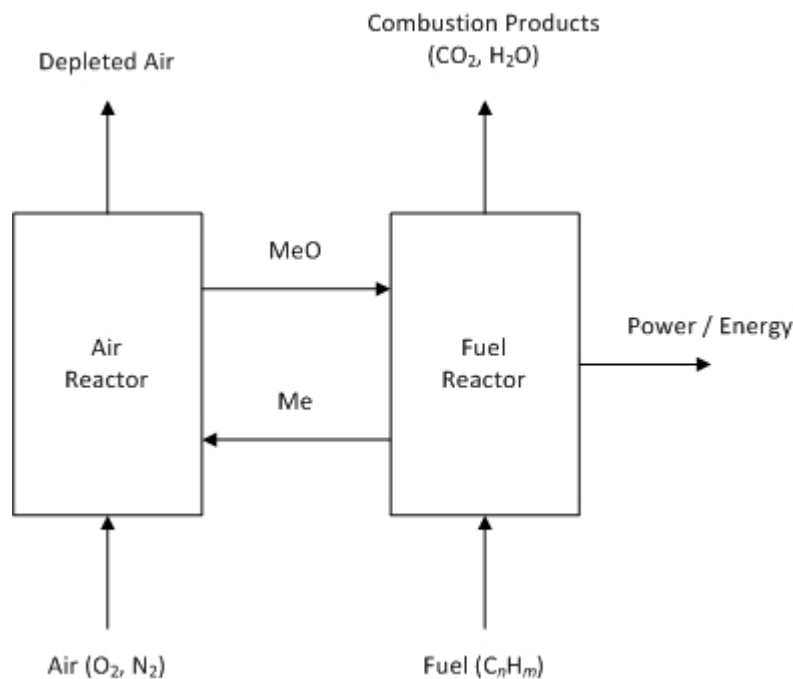
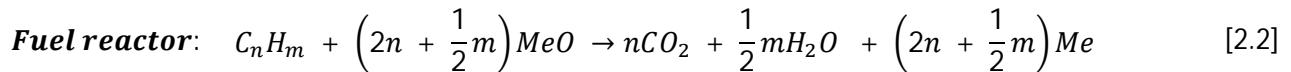
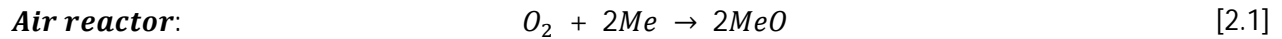


Figure 2.5 – A schematic of a typical chemical-looping combustion (CLC) capture process (Redrawn from (Rydén & Lyngfelt, 2006)).

The CLC process comprises two reactors: one for the air and one for the fuel. In the air reactor, the oxygen carrier (denoted as Me) reacts with air to form an oxidized product according to reaction [2.1].

The oxidized product (denoted as MeO) is carried over to the fuel reactor where it is reduced by the fuel to its initial state according to reaction [2.2]. The fuel is oxidized to produce a gas mixture product of CO₂ and water vapour (H₂O) (Rydén & Lyngfelt, 2006).



Reaction [2.1] is highly exothermic. Depending on the selection of fuel and oxygen carrier combination, reaction [2.2] can be either endothermic or slightly exothermic. The CLC process offers several advantages over the conventional combustion processes discussed earlier. Flue gas from the air reactor consists mainly of nitrogen (N₂) and, if air is used in surplus, some oxygen (O₂); both harmless elements to the environment. Furthermore, in a well-configured process, the thermal formation of nitrogen oxides (NO_x) is avoided as the regeneration of the oxygen carrier occurs without flame contact and at moderate temperatures (Rydén & Lyngfelt, 2006). The major advantage of the CLC process however, is that the flue gas from the fuel reactor consists of CO₂ and water vapour (H₂O). Hence only a condenser is needed to remove the water vapour and deliver a near pure CO₂ product stream. This significantly reduces the energy penalty and costs of the CO₂ extraction stage.

2.3.1.5. In Summary

Post-combustion capture is the capture process most-likely to first be implemented in industry since it is the only option that can be retrofitted to existing power plants without major modifications to process equipment. Nevertheless, a comparison of the major advantages and disadvantages of the discussed capture processes are summarized in Table 2.1

Table 2.1 – Summary of the major advantages and disadvantages of the various separation processes discussed.

| Capture Process | Advantages | Disadvantages |
|-------------------------------------|---|--|
| Post-Combustion Capture | <ul style="list-style-type: none"> • Offers flexibility, i.e. the host plant can continue to function even if the capture process is shut down; • Produce a relatively pure CO₂ product stream; • Requires minimal modifications when retrofitted to existing power plants. | <ul style="list-style-type: none"> • Significant higher performance or circulation volume required for high capture levels due to low CO₂ partial pressure in the flue gas; • Low pressure CO₂ product stream require compression for transport and storage. |
| Pre-Combustion Capture | <ul style="list-style-type: none"> • Produce high purity CO₂ product stream at elevated pressures, reducing capture costs; • Produces low NO_x and SO_x emissions; • Main product is syngas, useable in commercial products and applications; • Wide range of fuels can be used as feedstock. | <ul style="list-style-type: none"> • Feed fuel must be converted to syngas first; • Gas turbines, heaters and boilers must be modified for hydrogen firing; • Requires major modifications when retrofitted to existing power plants; • Applicable mainly to new power plants. |
| Oxy-Fuel Combustion Capture | <ul style="list-style-type: none"> • Produce a high purity CO₂ product stream; • Exhaust gas free of nitrogen components, eliminating the need for NO_x control equipment and a CO₂ separation step; • Significant reduction in size and capital cost of all plant equipment; • Minor modifications required when retrofitted to existing power plants. | <ul style="list-style-type: none"> • High capital cost and significant energy requirement inherent to cryogenic air separation processes; • Flue gas recycling required to moderate flame temperatures; • Equipment corrosion due to increased SO₂ concentrations in the exhaust gas stream. |
| Chemical-Looping Combustion Capture | <ul style="list-style-type: none"> • Inherent CO₂ capture (avoids significant energy penalty on host plant); • Harmless exhaust gas product stream from air reactor (mainly N₂); • No formation of thermal NO_x components. | <ul style="list-style-type: none"> • Transport of oxygen carrier required; • Cyclone required to separate particles from hot air; • Coking; • Applicable mainly to new power plants. |

2.3.2. CO₂ Transport and Storage (Stages 2 and 3)

The extracted CO₂ is compressed and transported to sites identified for storage. A transportation system (e.g. via a pipeline or transported by ship) is implemented to link the CO₂ emitting point source with the identified CO₂ storage site (Feron & Hendriks, 2005). Storage of the extracted CO₂ emissions is subject to certain key design criteria (Herzog et al., 2000):

1. The stored CO₂ should remain isolated from the atmosphere for a suitably long period of time, i.e. the storage period should be prolonged;
2. Cost of storing the CO₂ (including transportation costs) should be minimized;
3. Risk of any type of accident should be eliminated;
4. The impact of the storage process on the environment should be minimized;
5. In no way should the process violate any national or international legislation.

A number of possible approaches to transportation and storage of extracted CO₂ is discussed by Retief (2009) and Gertenbach (2009).

2.4. Post-Combustion CO₂ Capture

Post-combustion capture (PCC) technology allows the continued use of existing combustion processes without major changes to them. This advantage makes PCC easier and cheaper to implement as a retrofit option compared to pre-combustion capture, oxy-fuel capture and CLC capture technologies (Wang et al., 2010). The advantage comes at the expense of the power generation process efficiency, with an energy penalty between 25 and 30% of the total plant steam production (Elwell & Grant, 2006). The separation, or capture, stage represents about 75-80% of the total cost involved with CCS (Davison, 2007). Hence the majority of the research focuses on optimizing this stage. The separation technologies available for PCC include: (a) adsorption, (b) cryogenics separation, (c) membrane separation, (d) physical absorption and (e) chemical absorption.

2.4.1. CO₂ Separation Technologies

2.4.1.1. Adsorption

Adsorption separation technology is based on the physical attraction between the gas components and active sites on a solid surface (Mofarahi et al., 2008). The adsorbent (solid material) is regenerated either by the application of heat (temperature swing adsorption, TSA) or by the reduction of pressure (pressure swing adsorption, PSA) (Wang et al., 2010). Both TSA and PSA are commercially available technologies used in the production of H₂, large-scale separation of O₂ and the removal of CO₂ from natural gas streams. The low adsorption capacity of most common available adsorbents (e.g. activated carbon, alumina and zeolites) may pose significant challenges for the application of adsorption in large-scale power plant flue gas treatment processes (Mofarahi et al., 2008). Furthermore the low selectivity of most adsorbents requires high CO₂ concentration flue gas streams (Zhao et al., 2007).

2.4.1.2. Cryogenics Separation

In this process, CO₂ is condensed at cryogenic temperature to separate it from other gases. This is achieved by lowering the temperature and raising the total system pressure to equilibrium conditions. The triple point for CO₂ is at a temperature of -56.6°C and a pressure of 5.18 bar abs. At temperatures and pressures above the triple point it is possible to extract CO₂ in pure form by partially liquefying the mixture of CO₂ and other inert gases. A subsequent distillation stage could be added if a very pure CO₂ product stream is required (Mofarahi et al., 2008). This technique is capable of delivering a high purity CO₂ product stream. It is typically used for treating flue gas streams that already have high concentrations of CO₂ (typically > 50%) considering the costs of refrigeration (Wang et al., 2010).

2.4.1.3. Membrane-based Separation

In membrane-based separation processes, selectivity is provided by the membranes themselves (Wang et al., 2010). Differences in physical or chemical properties of gas components cause some gas molecules to permeate faster through the membrane than other (Chakma, 1995). The driving force for the permeation is the difference in partial pressure of gas components on either side of the membrane (Wang et al., 2010). A major obstacle with membrane-based separation is the cost of compression and heat exchange required to obtain a high-pressure feed. Furthermore, the selectivity of the separation process is low and thus the purity of the CO₂ product stream is low (Saha & Chakma, 1992). The

presence of fly ash and trace components such as SO_x , NO_x , HCl, and HF in the flue gas stream also hold complications (Mofarahi et al., 2008). Typically membranes can't achieve high degrees of separation, calling for multiple stages and/or recycle streams to be included; resulting in increased process complexity, energy consumption and costs (Chapel & Mariz, 1999).

2.4.1.4. Physical Absorption

CO_2 can be physically absorbed into a solvent according to Henry's law. Hence, physical absorption processes are more applicable for treating flue gas streams with high partial pressure of acid gas (CO_2) (Mofarahi et al., 2008). Solvent regeneration can be achieved by raising the temperature, reducing the pressure or both. As such, the main energy requirement originates from compression of the flue gas stream (Wang et al., 2010). As a result, physical absorption is not economical for treating flue gas streams with CO_2 partial pressures below 15vol% (Chakravati et al., 2001). Furthermore, since solvent regeneration usually takes place at atmospheric pressure, the process would require extensive energy consumption for solvent circulation (Sada et al., 1992).

2.4.1.5. Chemical Absorption

In chemical absorption processes CO_2 reacts with a treating (or chemical) solvent. The reaction forms a weakly bonded intermediate compound that can be regenerated through the application of heat to produce the original treating solvent and a CO_2 product stream (IPCC, 2005). Chemical solvents are typically used for treating flue gas streams with low concentrations of CO_2 (Mofarahi et al., 2008). The selectivity of chemical absorption processes is relatively high, capable of producing a relatively pure CO_2 product stream (> 90% CO_2) (Wang et al., 2010). These factors make chemical absorption the favorite separation process for treating thermal power plant flue gas streams (Wilson et al., 1992). A detailed discussion on post-combustion CO_2 capture with chemical absorption is given in Section 2.6.2.

2.4.1.6. In Summary

Flue gas streams from thermal power plants have very low CO_2 partial pressures. These streams are typically available at or near atmospheric pressure with CO_2 concentrations of 3 – 13vol% (Mofarahi et al., 2008). Wong et al. (2002) summarized the suitability of the above discussed separation technologies

to flue gas stream feed conditions (see Table 1.1 in Chapter 1). From this it is clear that chemical absorption is the best option for treating flue gas streams from thermal power plants.

2.4.2. Post-Combustion CO₂ Capture with Chemical Absorption

2.4.2.1. Preparation of the Flue Gas

Particulate matter (PM) and other acid gases (i.e. SO_x and NO_x) must be removed prior to CO₂ absorption as they have a negative effect on the performance of the system by forming heat stable salts with the aqueous alkanolamine solvents typically used. Monoethanolamine (MEA) is the most commonly used solvent (Thitakamol et al., 2007). A schematic diagram of a typical post-combustion flue gas treatment process is shown in Figure 2.6.

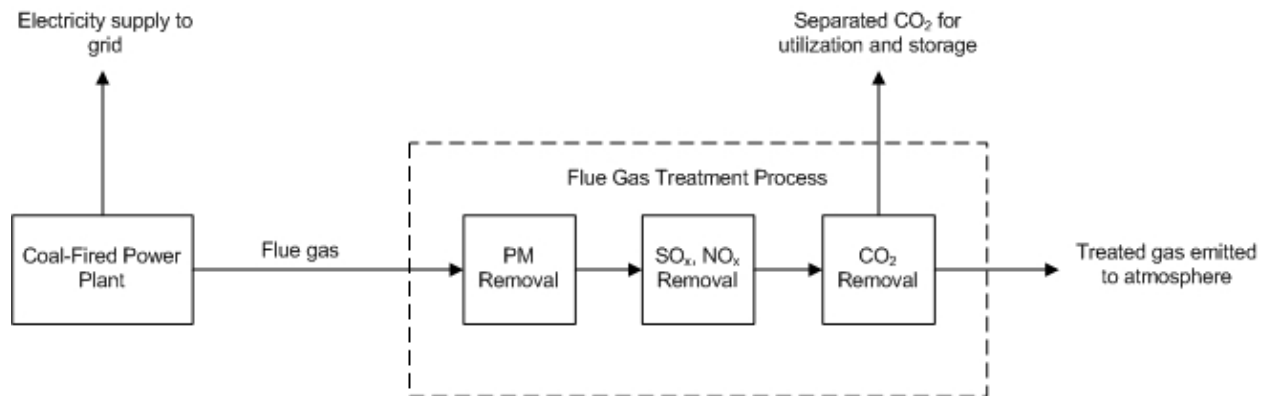


Figure 2.6 – Schematic diagram of the integration of a flue gas treatment process to a coal-fired power plant (Redrawn from (Thitakamol et al., 2007)).

Particulate matter such as fly ash would cause foaming in the absorber and solvent regeneration columns, decreasing the performance of the system. PM is removed from the flue gas either by electrostatic precipitators (ESP) or bag house filters (Thitakamol et al., 2007). Davidson (2007) recommended SO₂ concentrations in the CO₂ absorber feed gas to be less than 10 ppm. SO₂ is usually removed from the flue gas using a Flue Gas Desulphurization (FGD) unit. NO_x gases are removed either through Selective Catalytic Reduction (SCR), Selective Noncatalytic Reduction (SNCR) or low NO_x burners. Furthermore, the presence of oxygen increases the possibility of corrosion in the columns

(Davidson, 2007). Oxygen concentrations of less than 1 ppm are recommended when using MEA without corrosion inhibitors (IEA, 1993).

2.4.2.2. Process Description

A process flow diagram (PFD) of a conventional chemical absorption post-combustion CO₂ capture (CA-PCC) process is shown in Figure 2.7. The flue gas fed to the absorber column is cooled with water in a direct contact cooler (DCC) to between 45 and 50°C (Rao et al., 2004). This is to improve the absorption of CO₂ and minimize solvent losses due to evaporation. The addition of water also saturates the flue gas fed to the absorber, helping with the process water balance (Wang et al., 2010).

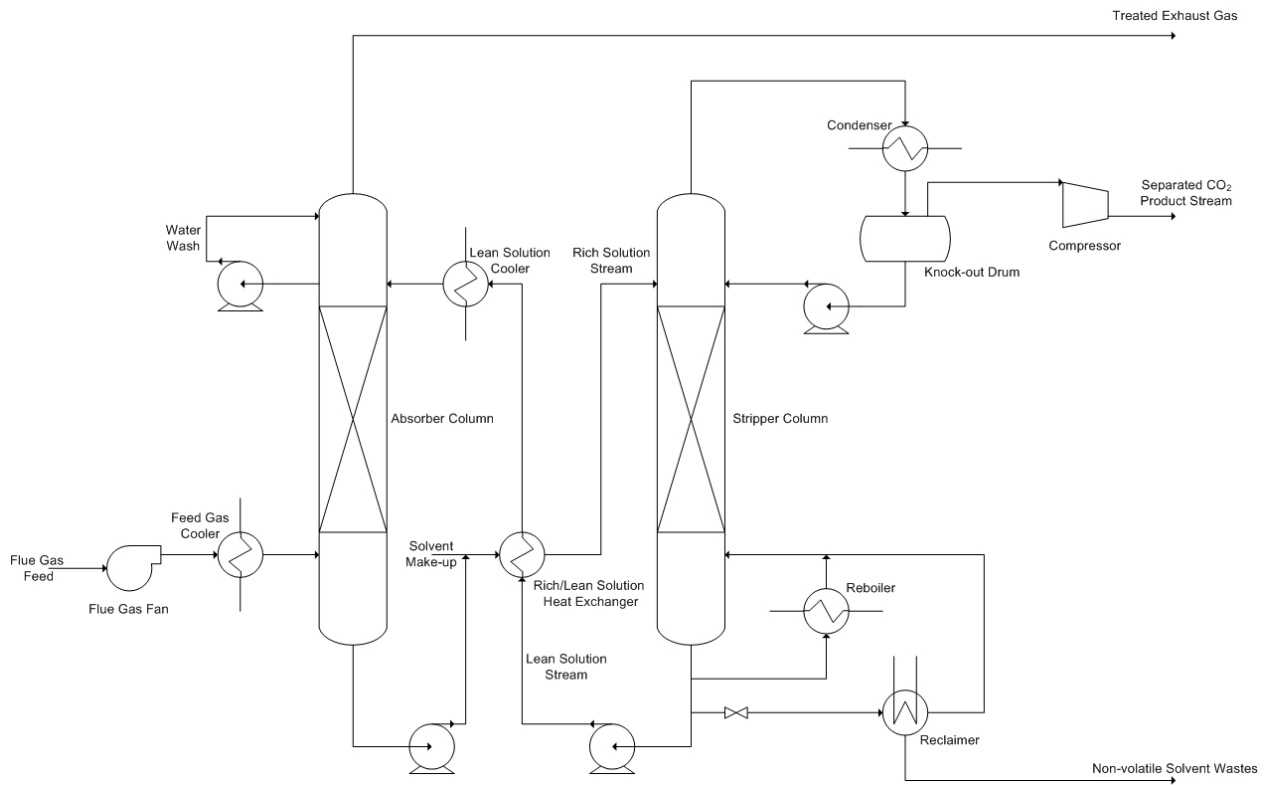


Figure 2.7 – Process flow diagram for a post-combustion CO₂ capture process by chemical absorption (Redrawn from (IPCC, 2005)).

The cooled flue gas is fed to the absorber column and contacted counter-currently with the lean (or regenerated) solvent (typically with CO₂ loading of 0.1-0.2 mol CO₂/mol MEA) yielding a rich solvent

stream of about 0.4-0.5 mol CO₂/mol MEA loading (Freguia & Rochelle, 2003). The scrubbed (treated) flue gas is water washed at the top of the absorber column and vented to the atmosphere.

The lean solvent is fed to the top of the absorber, typically at a temperature of 40°C. Heat of absorption is released as CO₂ is absorbed into the liquid phase, gradually increasing the temperature of the lean solvent (Notz et al., 2010). The temperature inside the absorber is typically between 40 and 60°C (Wang et al., 2010). The rich solvent (containing the absorbed CO₂) is collected at the bottom of the absorber and sent to the desorber column where it is regenerated at elevated temperature and pressure. The rich solvent is preheated in a rich-lean solvent heat exchanger before it enters the desorber column. The cross-flow rich-lean heat exchanger is typically designed to achieve a temperature difference of 10K or less on the hot side (Notz et al., 2010). The preheated rich solvent is fed to the top of the desorber column where CO₂ is released from the solvent at elevated temperatures (100-120°C) and slightly higher than atmospheric pressure (1.5-2 bar), causing a shift of the equilibrium isotherm to lower loadings. The heat required for regeneration is supplied via a reboiler at the bottom of the desorber. This is the major energy penalty of the absorption-desorption process (Wang et al., 2010). Since amines have comparably low vapour pressures, the steam generated in the reboiler consists primarily of water. This reduces the partial pressure of CO₂ in the desorber column, favoring the desorption process. Condensation of the steam provides the energy and desorption enthalpy required to raise the temperature of the rich solvent and reflux up to the desorption temperature. Remaining steam at the top of the desorber is passed through a condenser, separating the CO₂ from the water. The CO₂ is compressed for transport and sent for storage (Notz et al., 2010). The regenerated lean solvent is pumped back to the absorber column via the rich-lean heat exchanger to lower its temperature. Part of the bottoms product from the desorber column is passed through a reclaimer unit to evaporate the solvent. The evaporated solvent is returned to the system and the remaining non-volatile solvent wastes are purged (Wang et al., 2010).

2.4.3. Process Modeling and Simulation

2.4.3.1. Model Complexity

Two approaches are commonly used to represent mass transfer in modeling absorber and/or desorber columns, i.e. equilibrium-based and rate-based (Wang et al., 2010). The equilibrium-based approach

assumes a theoretical stage in which the gas and liquid phases attain a state of equilibrium. The performance of each stage is adjusted according to a tray efficiency correction factor (Schneider et al., 1999). Equilibrium-based models are usually sufficient to describe non-reactive systems. However, a state of equilibrium is rarely attained with the chemical reactions involved in reactive absorption. Hence, a rate-based approach is more applicable to describe the chemical absorption process. The rate-based approach takes into account the actual rates of multi-component mass and heat transfer, as well as the various chemical reactions (Noeres et al., 2003). Figure 2.8 shows the differences in varying levels of reactive absorption model complexity.

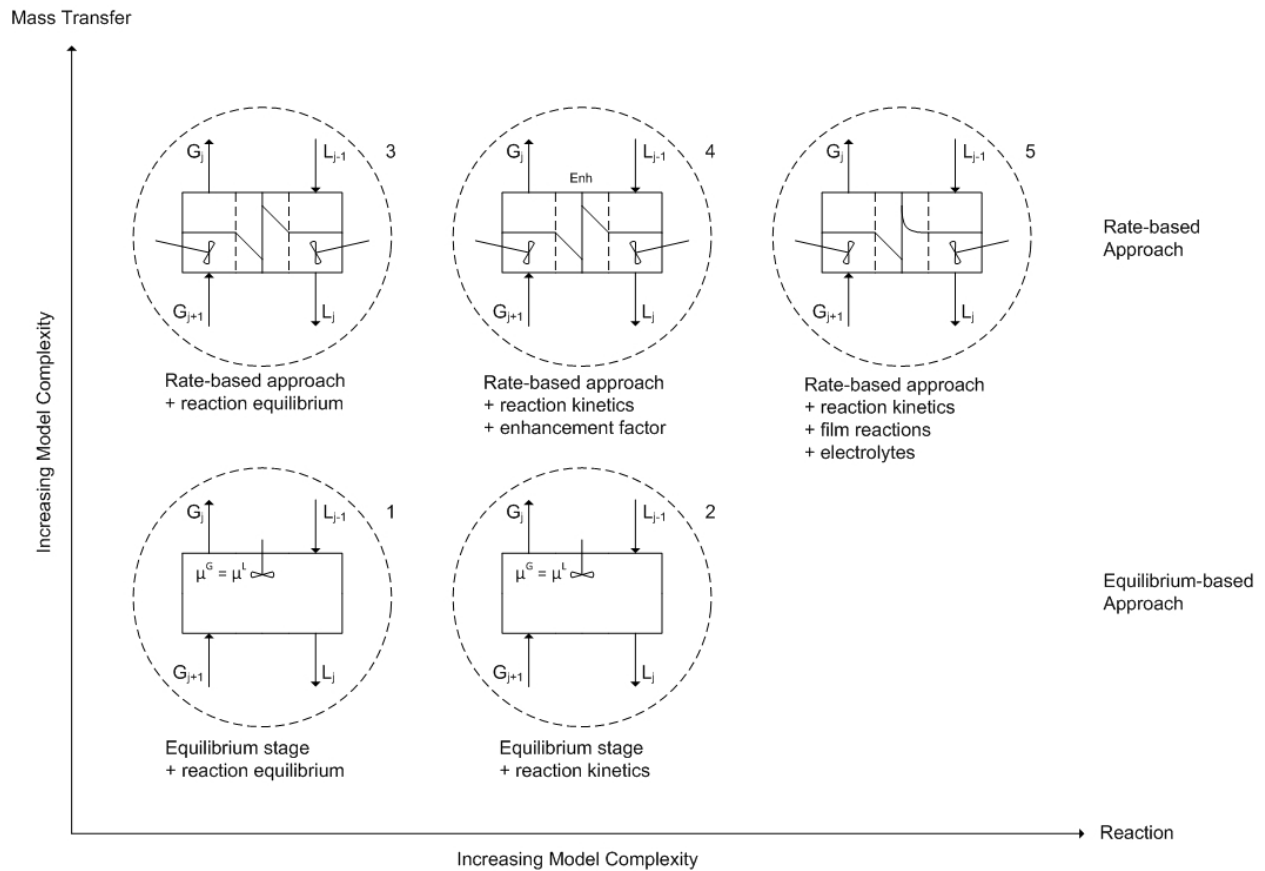


Figure 2.8 – Schematic depicting the varying levels of reactive absorption model complexity (Redrawn from (Kenig et al., 2001)).

Model 1 in Figure 2.8 describes the packed column as containing different equilibrium stages. Model 2 offers increased accuracy by considering the bulk phase reaction kinetics. Models 3, 4 and 5 all take into

account the mass transfer rate, classifying these models as rate-based models. The mass transfer across the gas-liquid interface is described using two-film theory (see Section 2.4.3.2). At its lowest level of model complexity (i.e. Model 3 in Figure 2.8), the chemical reactions are assumed to be at a state of equilibrium. This model can only be accurate when the reaction rate between CO₂ and the solvent is very fast (Wang et al., 2010). An enhancement factor is included in Model 4 to estimate the actual absorption rates. This factor however, is strictly only valid for pseudo first-order reaction kinetics between the gas and liquid phase (Kucka et al., 2003). The model assumes chemical reactions to be completed in the liquid film, with chemical equilibrium remaining in the bulk fluid. At the highest level of complexity (i.e. Model 5 in Figure 2.8), the model takes into account mass transfer resistances, electrolyte thermodynamics, the various chemical reactions as well as different column configurations (Wang et al., 2010). Furthermore, the model considers the acceleration of mass transfer as a result of reactions occurring in the liquid film (Kucka et al., 2003).

2.4.3.2. Basic Model Theory

In developing a mathematical model to accurately describe the reactive absorption process, it is paramount to take into account the column hydraulics, mass transfer resistances and the various chemical reactions occurring. Figure 2.9 is a schematic representation of the gas-liquid bulk phase and film interactions at the interface. From this it is clear that the model assumes ideally mixed gas (vapour) and liquid bulk phases and two film regions adjacent to the interface (Wang et al., 2010). Furthermore, the model assumes heat and mass transfer resistances to be limited to the laminar film regions. Penetration theory assumes that every element on the surface of the liquid phase is exposed to the vapour phase for the same period of time before being replaced by liquid of the bulk composition. This exposure time embrace all effects of the hydrodynamic properties of the system, and is used to define the effect of these properties on the mass transfer coefficient (Danckwerts, 1970).

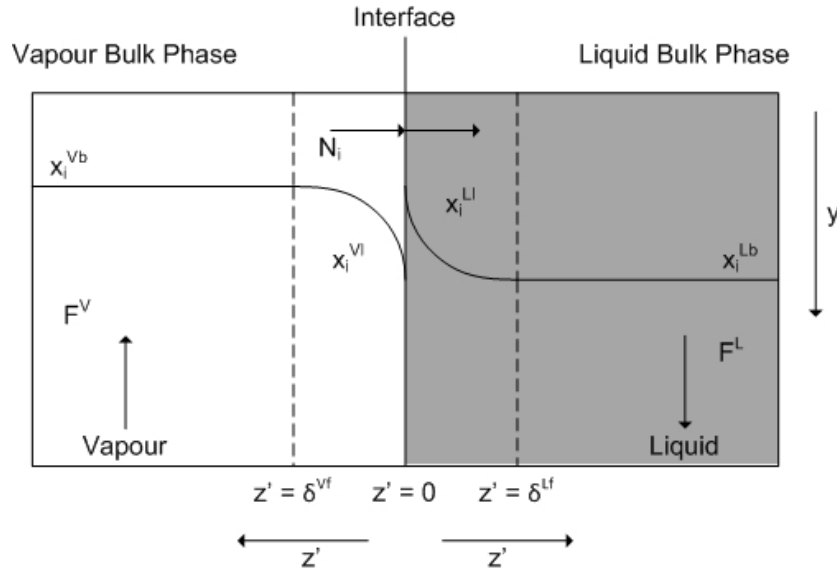


Figure 2.9 – Schematic depicting the vapour-liquid bulk phase, films and contact interface for reactive absorption modeling (Redrawn from (Noeres *et al.*, 2003)).

2.4.3.3. Current Modeling Research Status

Lawal *et al.* (2009a) recently proposed a dynamic rigorous model for describing the reactive absorption process in the absorber column. The model assumes rate-based mass transfer, with chemical reactions at a state of equilibrium (i.e. Model 3 in Figure 2.8). Results predict that the column performance can be maintained during partly loaded operation through maintaining the ratio of lean solvent and flue gas flowrates to the column (Wang *et al.*, 2010). This is strictly valid for the operating region of the column. The dynamic model developed by Kvamsdal *et al.* (2009) also assumes rate-based mass transfer, but takes into account the effect of chemical reaction by including an enhancement factor (i.e. Model 4 in Figure 2.8). The model was used to investigate the two transient operation scenarios, i.e. start-up and load reduction (Wang *et al.*, 2010). Lawal *et al.* (2009b) proposed a dynamic model for the desorber column, similar to the one proposed for the absorber column (i.e. Model 3 in Figure 2.8). The model was used to investigate the impact of the reboiler duty on CO₂ loadings in the lean solvent at the bottom of the desorber column (Wang *et al.*, 2010). Ziaii *et al.* (2009) also modeled the desorber column dynamically assuming rate-based mass transfer and chemical reactions at equilibrium (i.e. Model 3 in Figure 2.8), and used this model to minimize the energy requirement of the desorber column.

The limitation of the research projects discussed above however is that they all consider the absorber and desorber columns in isolation from each other, neglecting the possible interaction between them when operating together as a process (Wang et al., 2010). Recently, Lawal *et al.* (2010) used the gPROMS advanced process modeling package to develop dynamic models (Model 3 in Figure 2.8) for both the absorber and desorber columns, linking the models with a recycle (including heat exchanger). The model was used to investigate the possible disturbances resulting from integrated operation of the absorber-desorber process with a power generation plant. Results showed the significance of appropriate water balance in the absorber column. All of the above models were developed based on two-film theory (Wang et al., 2010).

2.4.4. Solvents and Solvent Selection

In designing a reactive absorption process, one of the main objectives is to select a solvent that will optimize the equipment size and minimize the plant operating costs. Factors to be considered in selecting a solvent include (Mofarahi et al., 2008):

1. Can the solvent circulation rate be reduced through selecting a solvent that may be used at higher concentration and/or acid gas loading levels?
2. Can using a solvent that requires a lower circulation rate, and/or has lower heats of reaction with CO₂ minimize the desorber column reboiler/condenser size and duty?
3. Is there any possibility of corrosion problems?

Astarita *et al.* (1983) suggests that between 50 and 70% of the initial investment for a reactive absorption plant is directly associated with the magnitude of the solvent circulation rate. Another 10-20% of the investment is dependent on the solvent regeneration energy requirement. Furthermore, approximately 70% of the plant operating costs results from solvent regeneration. Hence it is clear that proper solvent selection can have a significant impact on the overall costs associated with the reactive absorption process. Davidson (2007) described the ideal solvent as one possessing the following qualities:

- High reactivity w.r.t. CO₂ – reducing the absorber column height and/or solvent circulation rate;
- Low regeneration cost (low heat of reaction with CO₂);
- High absorption capacity;

- High thermal stability as well as reduced solvent degradation, leading to reduced solvent waste;
- Low environmental impact;
- Low production cost.

2.4.4.1. Amine-based Solvents

Amines have been used as solvents in the treatment of industrial gas streams for approximately 75 years; alkanolamines being the most popular group. Depending on the degree of substitution of the nitrogen atom, amines are classified as primary, secondary or tertiary amines (Wang et al., 2010). Singh *et al.* (2007, 2008 & 2009) have shown the position of different functional groups in the structure of various amine-based solvents to have a significant effect on the activity and CO₂ absorption capacity of the solvent. Primary and secondary amines usually react rapidly with CO₂ to form carbamates. Tertiary amines however do not have a hydrogen atom attached to the nitrogen atom; facilitating a hydrolysis reaction with CO₂ to form bicarbonates (Wang et al., 2010). The formation of bicarbonates allows for higher CO₂ loadings (Chakraborty et al., 1986). The reduced heat of reaction involved with bicarbonate formation often lead to tertiary amines (e.g. MDEA) being used in blends with primary or secondary amines to reduce solvent regeneration costs (Vaidya & Kenig, 2007). Amines most commonly used in CO₂ capture processes include: monoethanolamine (MEA), methyldiethanolamine (MDEA), 2-Amino-2-methylpropanol (AMP), Piperazine (PIPA), diglycolamine (DGA), diethanolamine (DEA), and diisopropanolamine (DIPA) (Shao & Stangeland, 2009). Typical operating conditions for some of the commonly used amines are summarized in Table 2.2.

Table 2.2 – Typical operating conditions for amines used in CO₂ capture processes (Redrawn from (Kohl. & Nielsen, 1997)).

| Amine | MEA | DEA | DGA | MDEA |
|---|----------|----------|----------|-----------|
| Solution Concentration [wt%] | 15-30 | 25-35 | 50-70 | 20-50 |
| Maximum Concentration [wt%] | 30 | 50 | 70 | 50 |
| Temperature [°C] | 25-127 | 25-127 | 25-127 | 25-127 |
| Acid Gas Loading [mol CO ₂ /mol amine] | 0.3-0.35 | 0.3-0.35 | 0.3-0.35 | Unlimited |

An aqueous solution of MEA (30wt%) is often regarded as the solvent of choice in early large-scale applications of chemical absorption post-combustion CO₂ capture from coal-fired power plants (Oexmann & Kather, 2010). MEA is a relatively cheap solvent capable of capturing CO₂ in low partial

pressures (Wang et al., 2010). Problems encountered in using MEA include: (a) solvent degradation, (b) intensive solvent regeneration energy requirements, and (c) corrosion. Shao and Stangeland (2009) discussed three different mechanisms for amine degradation:

- Oxidative degradation (primarily occurring in the absorber column);
- Thermal degradation (primarily occurring in the desorber column);
- Atmospheric degradation (amines emitted to the atmosphere that degrades).

There are a number of degradation products from each of the different degradation mechanisms. The products formed however are not only dependent on the degradation mechanism, but also on the type of amine(s) used and the residence times of the CO₂ capture process. For MEA, there are four main carboxylic acid degradation products (i.e. formate, glycolate, oxalate and acetate). Significant quantities of nitrites, nitrates and ethylenediamine were also found (Davidson, 2007). Studies by Davis and Rochelle (2009) focused on thermal degradation of MEA at typical operating conditions for the desorber column. At a temperature of 135°C they found the solvent degradation rate to be 2.5-6% per week. They concluded that thermal degradation of MEA solvent is significantly reduced at temperatures below 110°C.

MEA is classified as one of the most corrosive amines used for CO₂ capture. Oxygen contained in the flue gas from fossil-fueled power plants reacts with MEA to form heat stable, corrosive amine salts (Shao & Stangeland, 2009). Factors that influence amine corrosion rates include: CO₂ loading, amine type and concentration, operating temperature, solution velocity and degradation products formed (Davidson, 2007).

2.4.4.2. Ammonia

Ammonia has been identified as a possible alternative solvent to MEA. Ammonia is a relatively cheap, commercially available solvent with a relatively high CO₂ absorption capacity. It has a low heat of reaction with CO₂, reducing regeneration energy requirements, and it is less corrosive than MEA (Wang et al., 2010). The solvent is stable with lower susceptibility to degradation compared with MEA. Although the solvent itself is harmless to the environment, the technology is immature and NH₃ emissions to the environment pose a possible environmental risk. Alstom developed the chilled

ammonia process (CAP) in which the separation process is driven by chilled ammonium bicarbonate (Shao & Stangeland, 2009). At low temperatures and above certain CO₂ loading levels, carbonate salts will precipitate and form a solid phase dispersed in the liquid solvent (Raynal et al., 20011). The absorber column is operated at low temperatures to minimize solvent losses (ammonia has a relatively high volatility compared to MEA). The flue gas is cooled to 0-20°C (preferably 0-10°C) before it enters the absorber and is contacted with the lean solvent (typically 28wt% ammonia with a CO₂ loading of 0.25-0.67 mol CO₂/mol ammonia and water). The CO₂ rich stream is typically a slurry containing solid ammonium bicarbonate formed in the absorption process (Darde et al., 2010). The desorber is typically operated at temperatures between 50 and 200°C (preferable between 50 and 150°C), and pressures between 2 and 136 atm, producing a high pressure CO₂ rich product stream. Solvent regeneration energy requirements are significantly reduced (by more than a factor of 2) compared with conventional MEA absorption processes ((Wang et al., 2010); (Raynal et al., 20011)).

2.4.4.3. Piperazine

Commercial processes such as Benfield and Catacarb use aqueous solutions of potassium carbonate (K₂CO₃) (typically 20 to 30wt%) for CO₂ removal from gas streams. Slow absorption rates and low selectivity limit the performance of these processes when integrated with coal-fired power plants (Oexmann et al., 2008). Piperazine (PZ) promoted K₂CO₃ has been shown to exhibit a comparably fast CO₂ absorption rate with that of the conventional 30wt% aqueous MEA solution. The significantly lower heat of absorption of the blended solvent could translate to between 29 and 33% regeneration energy savings compared to MEA processes (Davidson, 2007). Another promising alternative is concentrated aqueous piperazine. Industrial studies have shown that, with a CO₂ absorption rate significantly faster than MEA, as well as negligible thermal degradation (up to temperatures of 150°C); PZ could reduce regeneration energy requirements by as much as 20% (Freeman et al., 2010).

2.4.4.4. Amino Acid and Amine Amino Acid Salts

Amino acid salts, as well as amine amino acid salts, have been identified as potential alternatives to amine solvent solutions conventionally used for CO₂ absorption (Aronu et al., 2010). The primary advantage of these salts is that they are classified as so-called “green” chemicals, i.e. they have no detrimental effect on the environment (Aronu et al., 2011). The argument for amino acid salts is further

strengthened by the fact that these salts are naturally present in the environment (Knuutila et al., 2011). Furthermore, the ionic state of amino acid- and amine amino acid-based solvents result in a reduced solvent volatility (Kumar et al., 2003). Also, amino acid salt solutions have the same functional group as that of alkanolamine solutions. Hence their reactivity, as well as CO₂ absorption capacity, is comparable to aqueous alkanolamine solutions (Van Holst et al., 2009). In addition, amine amino acid salt solvents have been shown to have the potential to reduce energy requirements compared to MEA or amino acid salt solutions (Aronu et al., 2009). However, concerns have been raised regarding the potentially high energy requirement for solvent regeneration (Knuutila et al., 2011).

2.4.4.5. In Summary

The ideal chemical solvent for CO₂ absorption should adhere to certain criteria, including (Davidson, 2007):

- High reactivity w.r.t. CO₂, reducing equipment size and solvent circulation rates;
- Low solvent regeneration cost requirements;
- High CO₂ absorption capacity;
- High thermal stability and reduced susceptibility towards solvent degradation;
- Low environmental impact;
- Low solvent cost, i.e. relatively cheap and commercially available.

A summary of the major advantages and disadvantages of the chemical solvents discussed is presented in Table 2.3 w.r.t the criteria specified above.

Table 2.3 – Summary of major advantages and disadvantages of the various chemical solvents discussed.

| Chemical Solvent | Advantages | Disadvantages |
|--|---|---|
| Amine-Based Solvents | <ul style="list-style-type: none"> • Commercially available and proven technology; • Relatively high capacity for CO₂ capture; • Relatively cheap and commercially available. | <ul style="list-style-type: none"> • High susceptibility for solvent degradation; • High energy requirements for solvent regeneration; • Equipment corrosion; • Formation of heat stable salts. |
| Ammonia | <ul style="list-style-type: none"> • Relatively cheap and commercially available; • Relatively high CO₂ absorption capacity; • Low energy requirements for solvent regeneration; • Less tendency for equipment corrosion; • Less susceptibility to solvent degradation. | <ul style="list-style-type: none"> • High volatility; • Toxic emissions; • Additional handling required when ammonium bicarbonate precipitates as solid at low absorber temperatures. |
| Piperazine or Piperazine-Promoted Solvents | <ul style="list-style-type: none"> • Fast CO₂ absorption rate; • Negligible thermal degradation; • Reduced solvent regeneration energy requirements. | <ul style="list-style-type: none"> • More expensive than conventional alkanolamine solvents; • Reduced CO₂ absorption capacity. |
| Amino Acid or Amine Amino Acid Salts | <ul style="list-style-type: none"> • Fast reaction kinetics; • High achievable cyclic loadings; • “Green”, naturally occurring solvents; • Reduced solvent volatility; • Good stability towards oxygen. | <ul style="list-style-type: none"> • Potentially high energy requirements for solvent regeneration; • Additional handling required for solid and liquid byproducts. |

2.4.5. Process Intensification

The objective of process intensification (PI) is to dramatically reduce the volume of a processing plant without compromising its production rate. This can be achieved by reducing the volume of individual process elements and, if possible, combining process functions in multi-functional modules. The benefits of PI include (Wang et al., 2010):

1. Substantial reductions in piping and structural support costs, resulting in reduced capital costs;
2. Reduced process inventories, leading to improved inherent safety if toxic or flammable material is handled;

3. Significant reductions in plant residence times (seconds rather than hours);
4. Improved heat/mass transfer coefficients could lead to reduced thermodynamically parasitic differences in temperature and/or concentrations – improving the thermodynamic efficiency of the process;
5. Possible improved compatibility with the environment.

Recent studies by Lin and Liu (2007) and Cheng and Tan (2009) have shown that PI has the potential to significantly reduce the size of CO₂ capture plants, reducing both capital and operating costs. Solution viscosity and corrosion potential limits the concentration of MEA solvent in conventional CO₂ capture processes to 30wt% (Wang et al., 2010). Through PI, stronger solutions of MEA (in the range 50-100wt%) can be used to achieve significant improvements in absorption capacities (Jassim et al., 2009).

2.4.6. International PCC Research Programmes and Pilot Plant Projects

To date there are no full-scale post-combustion CO₂ capture processes treating flue gas from fossil-fueled power plants. A publicly funded demonstration project of such a process operated feasibly at full scale is required to initiate the commercialization of CCS. The European Union (EU) is planning to build 12 such demonstration projects by 2015 (Shao & Stangeland, 2009). An overview is given below on some of the important CCS research projects currently piloted (Wang et al., 2010):

2.4.6.1. The Luminant Carbon Management Programme

The Luminant carbon management programme aims to investigate the technical obstacles involved with the deployment of a chemical absorption post-combustion CO₂ separation process; integrating the design of the separation process with aquifer storage/enhanced oil recovery (EOR) processes. The project is conducted by the Department of Chemical Engineering at the University of Texas. The pilot plant is comprised of two identical packed columns. Both the absorber and desorber columns have an internal diameter of 0.427 m and a total column height of 11 m. Random, as well as structured packing were investigated for both columns. The plant is capable of processing approximately 3 tonnes of CO₂ per day (Dugas, 2006). Studies linked to the pilot plant include (Wang et al., 2010):

- CO₂ reaction kinetics and solubility measurements;
- Degradation of solvents;

- Modeling the reactive absorption process;
- And pilot plant testing.

The project was also used to investigate the possibility of K_2CO_3 and/or piperazine-promoted K_2CO_3 as alternative solvent to MEA. It was shown that piperazine-promoted K_2CO_3 could significantly reduce the solvent regeneration energy requirements compared with the conventional MEA solvent.

2.4.6.2. The International Test Centre (ITC) for CO₂ Capture

The ITC is a collaboration project between a consortium of government and industrial partners, and the University of Regina (Canada). The objective of the project is to investigate and develop novel cost effective CO₂ capture technologies. The project is comprised of several bench-scale CO₂ separation units, as well as a multi-purpose pilot plant unit. The pilot plant unit is capable of processing approximately 1 tonne of CO₂ per day. The absorber column has an internal diameter of 0.3 m and a total column height of 10 m. The facility was used to perform numerous studies (Wang et al., 2010):

- Aboudheir *et al.* (2003) studied the reaction kinetics of CO₂ absorbed in high CO₂-loaded, concentrated aqueous MEA solutions;
- Edali *et al.* (2009) studied the kinetics of reactive CO₂ absorption in blended solvents of MEA and MDEA;
- Idem *et al.* (2006) compared the CO₂ capture performance of aqueous MEA and blended MEA/MDEA solutions at the facility to that of the Boundary Dam CO₂ capture demonstration project;
- Uyanga and Idem (2007) studied the degradation of MEA solvent in the presence of SO₂ and oxygen;
- And Kittel *et al.* (2009) studied the corrosion potential of MEA.

2.4.6.3. The CASTOR Project

This European Commission-funded collaboration between 11 European countries is aimed at developing technologies to capture and store 10% of the net CO₂ emissions in Europe. The project is an industrial demonstration unit with a specific goal to reduce the cost of CO₂ capture by 30-50% (De Marignan, 2008). Initiated in February 2004, the project ran for a period of 4 years. Major stakeholders include 16

industrial companies (such as Dong Energy, Vattenfall, Repsol, Statoil, Alstom power, RWE, etc.) and 12 research institutes (such as the IFP, BGRM, Imperial College, etc.). A mini plant comprised of an absorber (4m high) and desorber (2.5m high) column, both with an internal diameter of 0.125m, was first built at the University of Stuttgart (Wang et al., 2010). This was followed by an industrial-scale power plant (absorber column diameter: 1.1m and total column height: 34.5 m) capable of processing approximately 24 tonnes of CO₂ per day, installed at the Dong Energy power plant in Esbjerg, Denmark in March 2006 (Knudsen et al., 2008). Studies primarily focused on solvent selection as well as solvent degradation (Notz et al., 2010). Results have shown that it is possible to achieve up to 90% CO₂ capture levels with continuous operation of the post-combustion CO₂ capture plant (Wang et al., 2010). The energy requirement for solvent regeneration was found to be approximately 3.7 GJ/ton-CO₂, and the MEA consumption was found to be 1.4 kg/ton-CO₂ (Pires et al., 2011).

2.4.6.4. The iCap Project

iCap is a 4-year collaboration project between 8 research and technical development providers, 6 power generation companies, the Australian Research Institute and a Chinese University (Wang et al., 2010). Supported by the European Commission, the project started on January 1, 2010 with the objective of developing novel CO₂ capture technologies that will enable highly efficient and cost effective fossil-fueled power generation at near zero emissions. Specific targets include reducing the process energy penalty by 40-50%, as well as reducing the associated CO₂ avoidance cost to €15/tonne CO₂. Objectives for the iCap project include (iCap, 2010):

- Developing new solvents that will allow a significantly reduced solvent circulation rate;
- Developing simultaneous SO₂ and CO₂ capture units;
- Developing new high selectivity/high permeability membranes;
- Developing novel coal and gas-based power cycles, allowing high pressure post-combustion CO₂ capture that will significantly reduce capture costs;
- Implementing the developed technologies in both retrofit and greenfield power plants.

2.4.6.5. The CAPRICE Project

The EU-funded CAPRICE project was started on January 1, 2007 and ran for two years. CAPRICE is an acronym for CO₂ capture using Amine Process International Cooperation and Exchange. The aim of the project is to gather information and research findings on amine-based CO₂ capture processes from non-European Carbon Sequestration Leadership Forum (CSLF) countries; comparing findings from projects such as CASTOR with that of the ITC at the University of Regina (Canada). Stakeholders involved include 10 research institutes (such as the University of Regina, ITC, IFP, Trondheim University, etc.) and 3 power generation companies (i.e. E-ON, Dong Energy and Vattenfall) (Wang et al., 2010).

2.4.6.6. The CESAR Project

CESAR is a 4-year project funded by the EU under the Seventh Framework Programme (FP7). Launched in 2008, the aim of the project is to develop novel low-cost post-combustion CO₂ capture technology and/or solvents to be implemented in new power plants as well as capture processes retrofitted to existing power plants. The primary objective of the project is to reduce the cost of CO₂ capture to €15/tonne CO₂. The consortium is comprised of 3 research institutes, 3 universities, 1 commercial solvent supplier, 1 membrane producer, 3 equipment suppliers, 2 oil and gas companies and 6 power generation companies (Wang et al., 2010).

2.4.6.7. The joint UK-China Near Zero Emissions Coal (NZEK) Initiative

Started in 2007, the NZEK initiative is a consortium involving 28 industrial and academic partners from the UK and China that ran for a period of two years. The objectives of the project include: (a) the exchange of knowledge and capacity building, (b) future technology perspectives, (c) case studies on post-combustion CO₂ capture, (d) CO₂ storage potential, and (e) CO₂ capture policy assessment (Wang et al., 2010); (NZEK, 2009).

2.4.6.8. The Cooperative Research Centre for Greenhouse Gas Technologies (CO2CRC)

The CO2CRC project focuses on three main CCS research fields, i.e. CO₂ capture research, CO₂ storage research, and demonstration and pilot plant projects. The project was initiated in July 2003 with an

expected duration of 7 years; recently extended to a period of 12 years. Participants of the project are primarily from Australia and New Zealand. The facility includes an absorber column (with a total column height of 28m) capable of processing 50 tonnes of CO₂ per day. Research involving CO₂CRC, Loy Yang Power, International Power and Australia's Commonwealth Scientific and Industrial Research Organization (CSIRO) is aimed at reducing CO₂ emissions from brown coal fueled power plants. Novel solvents such as BASF PuraTreat™ are investigated at industrial scale (Wang et al., 2010).

2.4.6.9. Studies at Mitsubishi Heavy Industries, Hiroshima R&D Centre, Japan

Mitsubishi Heavy Industries (MHI) and the Kansai Electric Power Company (KEPCO) have been conducting research on the development of post-combustion CO₂ capture processes since 1990. To date MHI has deployed four industrial post-combustion CO₂ capture plants for treating flue gas from natural gas fired power plants, operating in Malaysia, Japan and two locations in India (the latter having a capacity of 450 tonnes CO₂/day) (Wang et al., 2010). A 10-tonne CO₂/day pilot plant was recently used to demonstrate the applicability of the process in the treatment of flue gas streams from coal-fired power plants (Davidson, 2007). At present, studies at MHI are aimed at resolving issues identified in the deployment of post-combustion CO₂ capture processes, including: (a) reducing the process energy requirements, (b) improving the process compatibility with the environment, and (c) minimizing the process energy penalty on the host power generation plant (Kishimoto et al., 2009).

2.4.7. Retrofitting Post-Combustion CO₂ Capture Units to Existing Coal-fired Power Plants

It is paramount that future fossil-fueled power plants be designed to be CO₂ capture ready (CCR). This will ensure that these plants can be effectively retrofitted with CO₂ capture without any unnecessary difficulties. Post-combustion CO₂ capture is an 'end of pipe solution' and the only feasible possibility in the deployment of CCS within existing fossil-fueled power plants. The feasibility of retrofitting capture however is subject to numerous technical and economic factors, mostly site specific, including: (a) access to a CO₂ storage site, (b) space available on site for additional capture equipment, (c) the remaining life expectancy of the plant, (d) the performance of existing pollution control equipment, and (e) the nature of the electricity and carbon markets in which the plant is operated (Lucquiaud & Gibbins, 2010). The power cycle of capture ready plants are designed to accommodate a possible future CO₂

capture unit retrofit. The power cycles of existing plants were never designed to be able to handle such a retrofit, resulting in significant energy penalties. Hence, in considering CO₂ capture retrofits, it is vital to perform a proper thermodynamic analysis of the entire process.

In the case of retrofitting CO₂ capture to existing power plants, steam is taken from the steam cycle to provide the heat required for solvent regeneration in the desorber column; reducing the power output of the steam cycle. This reduction translates to a thermal energy penalty of 25-30% of the power output capacity of the host plant (Elwell & Grant, 2006). The extent to which non-site-specific factors affects the economics of CO₂ retrofits have raised concern. Lucquiaud and Gibbins (2010) have conducted a thermodynamic analysis to investigate the effect of the host plant efficiency on the energy penalty for post-combustion CO₂ capture. The analysis was done for both older sub-critical boiler technology, as well as later supercritical steam plants. An overall energy balance for a coal-fired power plant without, and with retrofitted CO₂ capture is shown in Figure 2.10.

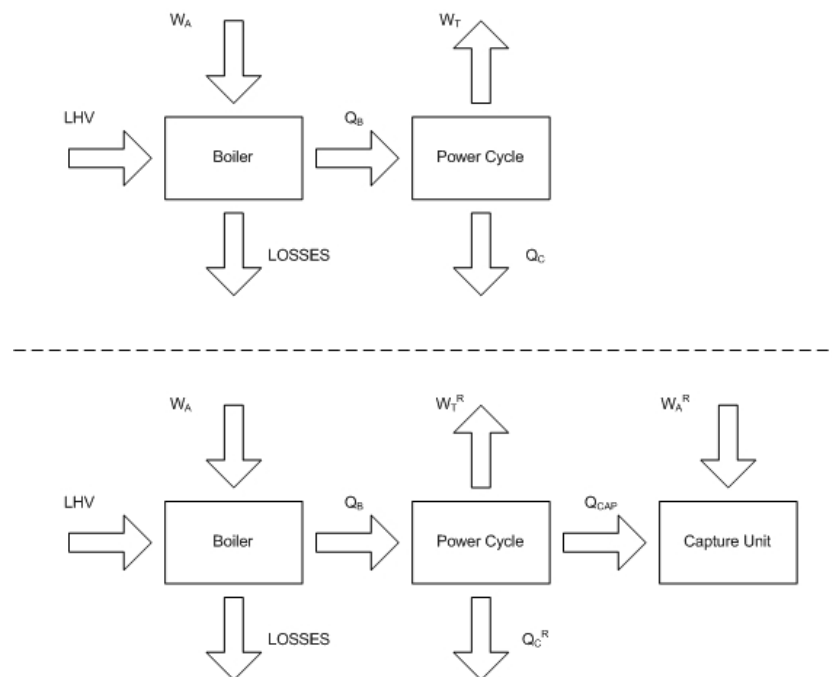


Figure 2.10 – A schematic depicting a first law energy analysis of a power cycle without (upper) and with (lower) a retrofitted capture unit (Redrawn from (Lucquiaud & Gibbins, 2010)).

For an existing power plant without CO₂ capture (upper part of Figure 2.10) it is seen that there are two sources of energy to the boiler, i.e. the total calorific value of the fuel (LHV) and ancillary power supplied to the boiler machinery (W_A). Upon combustion of the fuel, an amount of heat (Q_B) is supplied from the boiler to the power cycle. Energy losses from the boiler (LOSSES) comprise primarily stack and heat losses from the boiler and pipework. The heat supplied to the power cycle is used to generate mechanical work (W_T), and heat (Q_C) is rejected through condensation. Assuming negligible losses, the sum of W_T and Q_C will be equal to Q_B . When the plant is retrofitted with CO₂ capture, additional heat (Q_{CAP}) is taken from the power cycle and supplied to the capture unit. This is the net heat required for solvent regeneration. Ancillary power (W_A^R) is supplied for ancillary capture machinery (Lucquiaud & Gibbins, 2010). Detailed typical power plant steam cycle configurations without and with retrofitted CO₂ capture are shown in Figures 2.11 and 2.12 respectively.

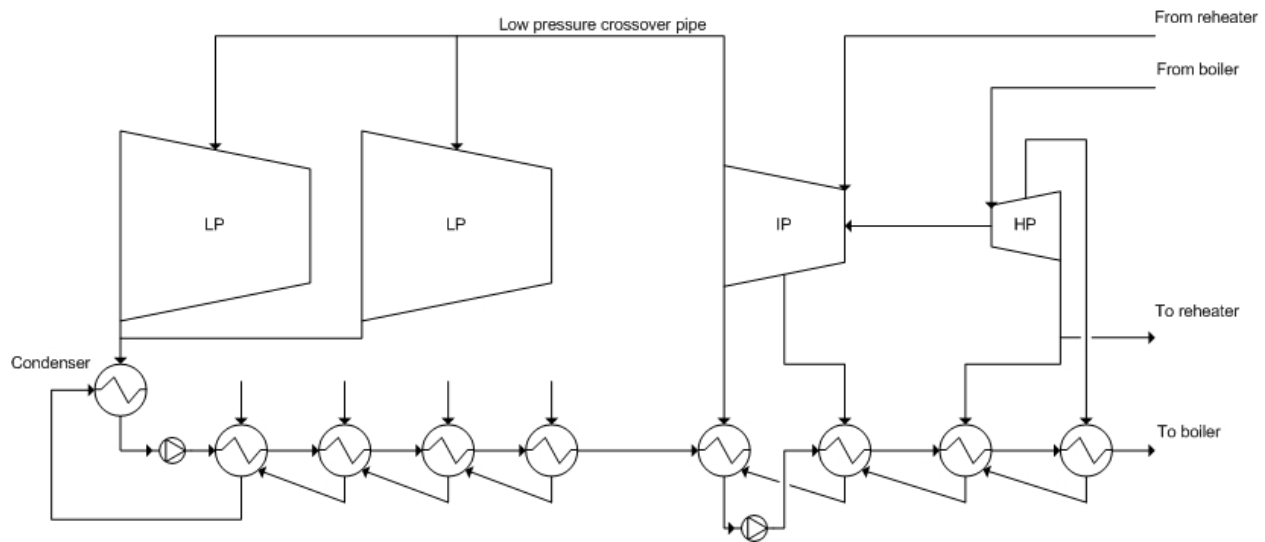


Figure 2.11 – Schematic of a single-reheat steam cycle configuration without a CO₂ capture unit (Redrawn from (Lucquiaud & Gibbins, 2010)).

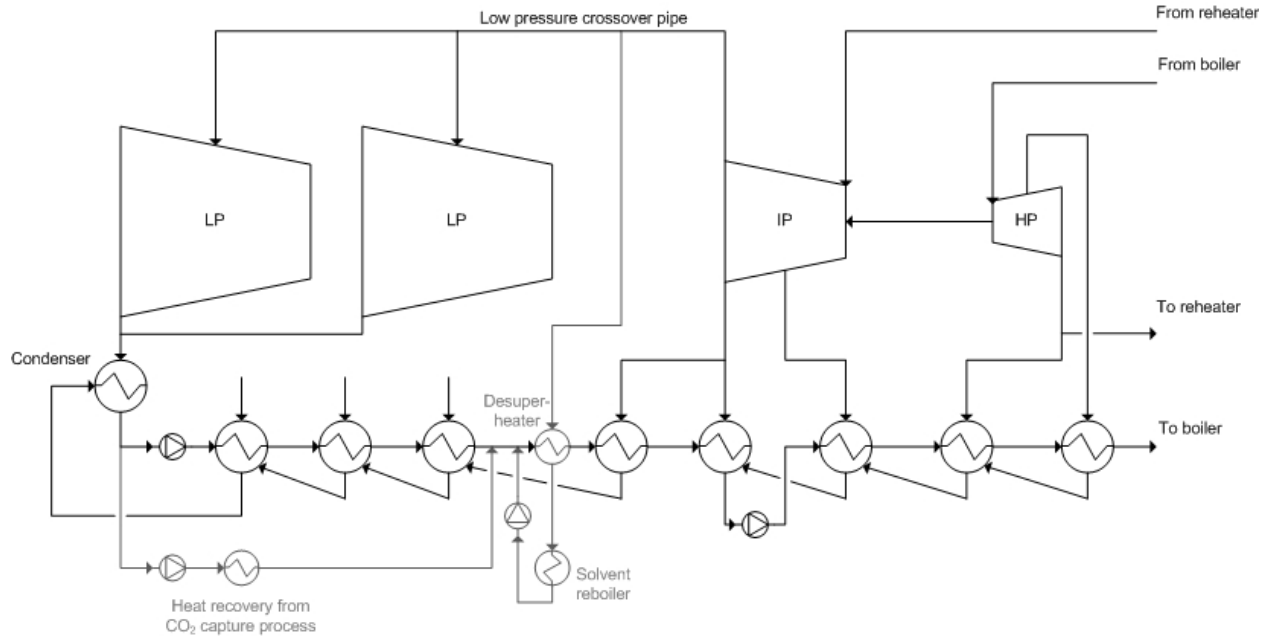


Figure 2.12 – Schematic of a single-reheat steam cycle configuration with steam extraction for CO₂ capture and low-grade heat recovery (Redrawn from (Lucquiaud & Gibbins, 2010)).

If CO₂ capture is retrofitted, the energy required for solvent regeneration is supplied by extracting and condensing steam from the low pressure crossover pipe between the intermediate pressure (IP) and low pressure (LP) turbines (Figure 2.12). The extracted steam is sent through a heat exchanger to recover remaining super heat available for water heating. From there the steam is sent to the capture unit where its latent heat is used to regenerate the solvent. Condensate from the desorber column reboiler is returned to the power cycle. It enters the cycle after the LP feed water heater sequence. Residual heat is recovered from the purified CO₂ stream leaving the desorber column, as well as the CO₂ compressor intercoolers. This is used for condensate heating instead of extracting more steam from the steam cycle. Lucquiaud and Gibbins (2010) expressed the efficiency of the power cycle without and with capture as follow (Eqns. 2.4.7.1 and 2.4.7.2 respectively):

$$\eta = \frac{W_T - W_A}{LHV} \quad [2.4.7.1]$$

$$\eta^R = \frac{W_T^R - W_A - W_A^R}{LHV} \quad [2.4.7.2]$$

Where η is the power cycle efficiency without CCS based on fuel low heating value, W_T is the mechanical work output without CCS, W_A is the boiler ancillary power, LHV is the fuel energy input based on low heating value, η^R is the power cycle efficiency with CCS based on fuel low heating value, W_T^R is the mechanical work output with CCS and W_A^R is the ancillary power for CCS. From this, the energy efficiency penalty on the power cycle for retrofitting CO₂ capture can be expressed as follow:

$$\eta - \eta^R = \frac{W_T + W_T^R + W_A^R}{LHV} \quad [2.4.7.3]$$

Equation 2.4.7.3 can be written in terms of mechanical work losses resulting from steam extraction to give (Lucquiaud & Gibbins, 2010):

$$\eta - \eta^R = \frac{Q_{CAP} + \dot{m}_c [(h_{steam}^R - h_{steam}) - (h_{liq}^R - h_{liq})] - (\dot{m}_c - \dot{m}_c^R)(h_{steam}^R - h_{liq}^R) + W_A^R}{LHV} \quad [2.4.7.4]$$

Where the subscript R designates retrofitted CCS, \dot{m}_c is the steam cycle condenser mass flow rate without CCS, h_{steam} is the stagnation enthalpy per unit mass of steam at the LP turbine outlet and h_{liq} is the stagnation enthalpy per unit mass of condensate at the condenser outlet. In their comparison of sub- and supercritical plants, Lucquiaud and Gibbins (2009) only considered the effect of site-specific factors inherently related to the steam conditions, i.e.:

- Calorific values and quantities of CO₂ produced per unit of heat are assumed to be identical;
- Assuming identical amounts of heat (Q_B) transferred to the power cycle;
- Assuming identical fuel specific emissions;
- Assuming identical ambient conditions, cooling systems and LP turbine exit dryness fractions;
- Assuming identical steam extraction pressures and low-grade heat used for condensate heating;
- Assuming identical capture unit design and operation.

From this, they concluded that the difference in energy efficiency penalty of retrofitted capture is a function only of the condenser mass flow rate without capture (\dot{m}_C), and the steam and condensate enthalpies with capture (h_{steam}^R and h_{liq}^R). It was also concluded that the plant steam conditions have no significant effect on the energy efficiency penalty of the retrofitted capture process. Furthermore, Lucquiaud and Gibbins (2009) have shown that the CO₂ abatement cost (cost per tonne of CO₂ required to justify retrofitted capture) is similar for both less efficient sub-critical as well as more efficient supercritical units, assuming identical capture equipment characteristics. This translates to a wider variety of existing power plants being potentially suitable candidates for retrofitted CO₂ capture. Finkenrath (2011) has found the overnight costs of power plants with retrofitted CO₂ capture to be USD 3800 per kW across capture routes. This is approximately 74% higher than reference costs found for power plants without CO₂ capture. The average cost of CO₂ avoidance for pulverized coal-feed power plants was found to be about USD 55 per tonne of CO₂.

2.5. CA-PCC: Challenges and Possibilities in the Future

2.5.1. Solvents

As discussed in Section 2.4.4.1, the solvent most commonly used in reactive CO₂ absorption processes (i.e. MEA) has several drawbacks, including: (a) low CO₂ loading capacity, (b) solvent degradation as a result of SO₂ and O₂ in the flue gas, (c) high corrosion potential, and (d) intensive solvent regeneration energy requirements (Resnik et al., 2004). Furthermore, amine-based solvents have the tendency to react with CO₂. This is problematic as it could result in the accumulation of byproducts in the system. Suitable alternative solvents should be designed to absorb the CO₂ gas, and not react with it to form byproducts. Future work in developing alternative solvents should aim to (Wang et al., 2010):

- Reduce the solvent-solute reaction potential;
- Reduce solvent regeneration energy requirements;
- Improve environmental compatibility;
- Reduce the solvent degradation and corrosion potential;
- Combine all the above characteristics in a single solvent.

Progress in the development of alternative solvents includes: ammonia (Darde et al., 2010); (Raynal et al., 20011), piperazine promoted K_2CO_3 (Cullinane & Rochelle, 2005); (Oexmann et al., 2008), concentrated aqueous piperazine (Freeman et al., 2010), and alkanolamines blended enzymes (Wang et al., 2010). Recently, ionic liquids (ILs) have started to receive a lot of attention as potential alternative solvents (Wappel et al., 2009); (Feng et al., 2010); (Yu et al., 2006); (Shiflett & Yokozeki, 2005); (Llovel et al., 2010); (Mattedi et al., 2011); (Cabaco et al., 2011).

2.5.1.1. Ionic Liquids (ILs)

ILs are organic salts with a melting temperature below the boiling point of water (100°C) (Wasserscheid & Welton, 2008). The major advantage is that, based on the selection of cation, anion or other substituents, ILs can easily be structurally modified to obtain a set of desired physical properties (Yu et al., 2006). This translates to untold different possible structures and physical properties (Wappel et al., 2009). Anderson *et al.* (2007) estimates the number of possible alternative ILs at room temperature (RTILs) to be in the order of 10^{18} . Hence, ILs can be seen as 'designer solvents' with an almost limitless potential of solvent capabilities. Using *in situ* attenuated total reflection infrared (ATR-IR) spectroscopy and quantum chemical molecular simulation, studies on CO_2 solubility in imidazolium-based ILs revealed that the interactions with CO_2 are dominated by the anion. The interactions between the solvent and CO_2 were identified to be weak Lewis acid-base or electrostatic interactions (Fernandes et al., 2011). Other advantages of ILs include (Yu et al., 2006): (a) high thermal stability, (b) nonflammability, (c) excellent solvent potential and (d) negligible vapour pressure. The negligible vapour pressure means that there would be no contamination of the separated gas product stream, and solvent losses due to evaporation would be effectively circumvented. Furthermore, ILs are reversible absorbents. The dissolved CO_2 can easily be recovered from the solvent by increasing the temperature; reversing the initial absorption reaction (Wappel et al., 2009). Hence, the energy requirements for solvent regeneration and CO_2 recovery (i.e. the stripping process) is essentially the energy input to the desorber required to reverse the absorption reaction.

Studies of the solubility and phase behaviour of CO_2 in a variety of ILs (i.e. imidazolium-based, phosphonium-based and pyridinium-based ILs) have shown insignificant CO_2 solubilities at room temperature and pressure (typically around $0.02 \text{ mol } CO_2/\text{mol IL}$) (Yu et al., 2006); (Scovazzo et al.,

2004); (Baltus et al., 2004); (Husson-Borg et al., 2003). This can be explained by the high heat of absorption, as none of the ILs were task specifically designed for CO₂ capture. With conventional off-the-shelf ILs the absorption of CO₂ is driven purely by physical dissolution. Task specific ILs (TSILs) have the potential to capture larger quantities of CO₂, exploiting chemical reactions with CO₂ induced by structurally manipulated solvent constituents (Wappel et al., 2009). Vega *et al.* (2010) have identified 6 barriers in the commercialization of ionic liquids as solvents:

1. Extended research into process engineering – To date IL studies have been performed at laboratory scale and under conditions that are not representative of full scale industrial applications;
2. Environmental, health and safety impact concerns – The environmental impact of every newly developed IL must be investigated individually;
3. Economic benefit analysis;
4. Extended research into the fundamental understanding of the compositional structure-performance relationship of ILs;
5. Increased production of ILs – At present ILs are produced in small quantities for lab-scale research at very high costs;
6. Improved institutional awareness – Industry has been slow to recognize the potential economic value of ILs.

Despite the technical and economic barriers involved, Wappel *et al.* (2009) concluded that ILs are a promising alternative for solvent selection in reactive absorption post-combustion CO₂ capture processes.

2.5.2. Pilot Plants

In Section 2.4.6 a number of pilot plant studies currently underway were discussed. All of these projects however are below the 10MWe scale. Proper analysis of the effect of CCS energy requirements would necessitate a demonstration project at a scale of 100s of MWe. The investment required for a project of this magnitude would easily run into billions of dollars (Wang et al., 2010). Public funding is required to stimulate commercial interest in CCS projects. The EU has allocated 300 million carbon credits from its emission trading scheme (ETS) to promote and fund the development of CCS demonstration projects

and innovative renewable energy projects. This translates to billions of Euros of public funding (Shao & Stangeland, 2009).

2.5.3. Modeling and Process Simulation

To date almost all of the dynamic models developed (see Section 2.4.3) were validated based on steady state data. In order to obtain a fundamental understanding of the operation and control of the reactive absorption process, it is paramount that these models be validated for the transient (or dynamic) state as well. Limiting experimental transient data available for CO₂ capture processes currently prevents this. Furthermore, all of the current models were developed by experts in the field of modeling and simulation. It is vital that these tools be converted to commercial, easy-to-use packages (Wang et al., 2010). It has also become important to incorporate a model for solvent selection with the model describing the reactive absorption process. This would make it possible to assess the complete effect of different solvents of the performance of the capture process.

2.5.4. Reduced Energy Consumption

2.5.4.1. Through Alternative Solvent Selection

Chemical absorption processes consume large quantities of energy, i.e. heat needed for solvent regeneration, as well as auxiliary power required for pumps, blowers and CO₂ compression. Optimizing design and operating conditions for a given solvent could reduce the energy consumption by up to 10% (Freguia & Rochelle, 2003). Darde *et al.* (2010) suggests that alternative solvents have the potential to reduce energy consumption by 30% or more. The majority of studies searching for more efficient solvents focus exclusively on alternatives with a heat of absorption lower than that of MEA. These studies neglect the effect of sensible heat (required to raise the temperature of the rich solution to the temperature of the solvent reboiler) and the heat of evaporation of the water vapour fraction in the stripping steam at the top of the desorber on the overall reboiler heat duty. The heat required to regenerate the solvent is the sum of these three terms (Oexmann & Kather, 2010):

$$q_{reb} = q_{sens} + q_{vap,H_2O} + q_{abs,CO_2} \quad [2.5.4.1]$$

Where q_{sens} is the sensible heat required to raise the temperature of the solvent from the temperature downstream of the rich-lean heat exchanger to the temperature of the reboiler, q_{vap,H_2O} is the heat of evaporation required to produce the fraction of stripping steam in the reboiler that does not condense inside the column and is ultimately condensed in the overhead product condenser, and q_{abs,CO_2} is the overall heat required to desorb the CO_2 captured in the solution. In developing alternative solvents, it is vital to consider the effect of all three these terms on the overall reboiler heat duty. By considering one of the terms in isolation, e.g. the heat of absorption (q_{abs,CO_2}), the effect of their interdependencies as well as their combined dependence on process parameters is neglected. Previous studies have pointed out this mistaken belief that a low heat of absorption is directly equal to a low overall solvent regeneration heat duty (Oexmann & Kather, 2010); (Tobiesen & Svendsen, 2006); (Oyenekan, 2007); (Oyenekan & Rochelle, 2007). From Eqn. 2.5.4.1, considering that equilibrium is usually not reached in large scale applications and neglecting flashing of the rich solution at the inlet of the desorber column, the weight specific overall reboiler heat duty can be expressed as follow (Oexmann & Kather, 2010):

$$q_{reb} \cong \frac{\overbrace{c_p(T_{reb} - T_{feed}) \cdot M_{sol}}^{q_{sens}}}{\Delta\alpha \cdot M_{CO_2} \cdot x_{solv}} + \frac{\overbrace{\Delta h_{vap,H_2O} \cdot p_{H_2O}}^{q_{vap,H_2O}}}{p_{CO_2} \cdot M_{CO_2}} + \frac{\overbrace{\Delta h_{abs,CO_2}}^{q_{abs,CO_2}}}{M_{CO_2}} \quad [2.5.4.2]$$

Where c_p is the molar specific heat of the solution, T_{reb} and T_{feed} are the temperatures inside the reboiler and at the reboiler inlet respectively, M_{sol} and M_{CO_2} are the molar weights of the solution and CO_2 respectively, $\Delta\alpha$ is the difference in CO_2 loading between the absorber outlet (rich stream) and inlet (lean stream), x_{solv} is the molar fraction of solvent in the solution, $\Delta h_{vap,H_2O}$ is the heat of evaporation of water, p_{H_2O} and p_{CO_2} are the partial pressures of water vapour and CO_2 in the gas phase at the desorber outlet respectively and $\Delta h_{abs,CO_2}$ is the heat of absorption for the solvent. The majority of studies focus on finding alternative solvents with a low heat of absorption ($\Delta h_{abs,CO_2}$ in Eqn. 2.5.4.2), neglecting the effect of the rest of the terms on the overall reboiler heat duty (q_{reb}). Studies by Oexmann and Kather (2010) have shown that the ratio p_{H_2O}/p_{CO_2} is a function of the heat of absorption. Through simplified thermodynamic analysis, it can be shown that (Oexmann & Kather, 2010):

$$\frac{p_{H_2O}^S}{p_{CO_2}^*} = \frac{p_{H_2O,ref}^S}{p_{CO_2,ref}^*} \exp\left(\left[\frac{T - T_{ref}}{RTT_{ref}}\right] [|\Delta h_{vap,H_2O}| - |\Delta h_{abs,CO_2}|]\right) \quad [2.5.4.3]$$

Equations 2.5.4.2 and 2.5.4.3 can be used to analyze the performance of aqueous solvents in reactive absorption post-combustion CO₂ capture processes. Such a case study was presented by Oexmann and Kather (2009) for two competing hypothetical solvents. Assumptions for the case study include:

- The heat of absorption of Solvent A is twice that of the heat of evaporation;
- The heat of absorption of Solvent B is half that of the heat of evaporation;
- Both solvents have the same working capacity (i.e. the quantity of CO₂ absorbed by the solvent in the absorber column) and specific heat capacity;
- The hot end temperature difference of the rich-lean heat exchanger is kept constant;
- The ratio of p_{H_2O}/p_{CO_2} at the rich end of the desorber (inlet) is chosen such that both solvents have the same overall reboiler heat duty at the desorber reference pressure.

A summary of the contributions to the overall reboiler heat duty for a generic high and low heat of absorption solvent comparison is shown in Table 2.4.

Table 2.4 – Summary of the individual contributions to the overall reboiler heat duty at the reference desorber pressure for a generic high- and low heat of absorption solvent (Redrawn from (Oexmann & Kather, 2010)).

| | Solvent A | Solvent B |
|---|------------------|------------------|
| $\Delta h_{abs,CO_2}/\Delta h_{vap,H_2O}$ | 2 | 0.5 |
| $q_{abs,CO_2}/q_{reb,ref}$ | 50.0% | 12.5% |
| $q_{sens}/q_{reb,ref}$ | 15.0% | 15.0% |
| $q_{vap,H_2O}/q_{reb,ref}$ | 35.0% | 72.5% |

With q_{sens} and q_{abs,CO_2} constant, the overall reboiler heat duty depends on q_{vap,H_2O} only. Assuming a constant heat of evaporation of water ($\Delta h_{vap,H_2O}$), it can be shown that the ratio of p_{H_2O}/p_{CO_2} is directly proportional to the ratio of water vapour pressure and CO₂ equilibrium partial pressure (Oexmann & Kather, 2010):

$$q_{vap,H_2O} = f\left(\frac{p_{H_2O}}{p_{CO_2}}\right) \propto \frac{p_{H_2O}^s}{p_{CO_2}^*} = f(T_{reb}, \Delta h_{abs,CO_2}) \quad [2.5.4.4]$$

From this it is clear that the ratio of p_{H_2O}/p_{CO_2} is a function of the heat of absorption ($\Delta h_{abs,CO_2}$). The relations of process parameters (both positive and negative) with respect to the net power output of the power cycle are summarized in Figure 2.13. The detailed derivations and assumptions of the simplified analysis are given by Oexmann and Kather (2010).

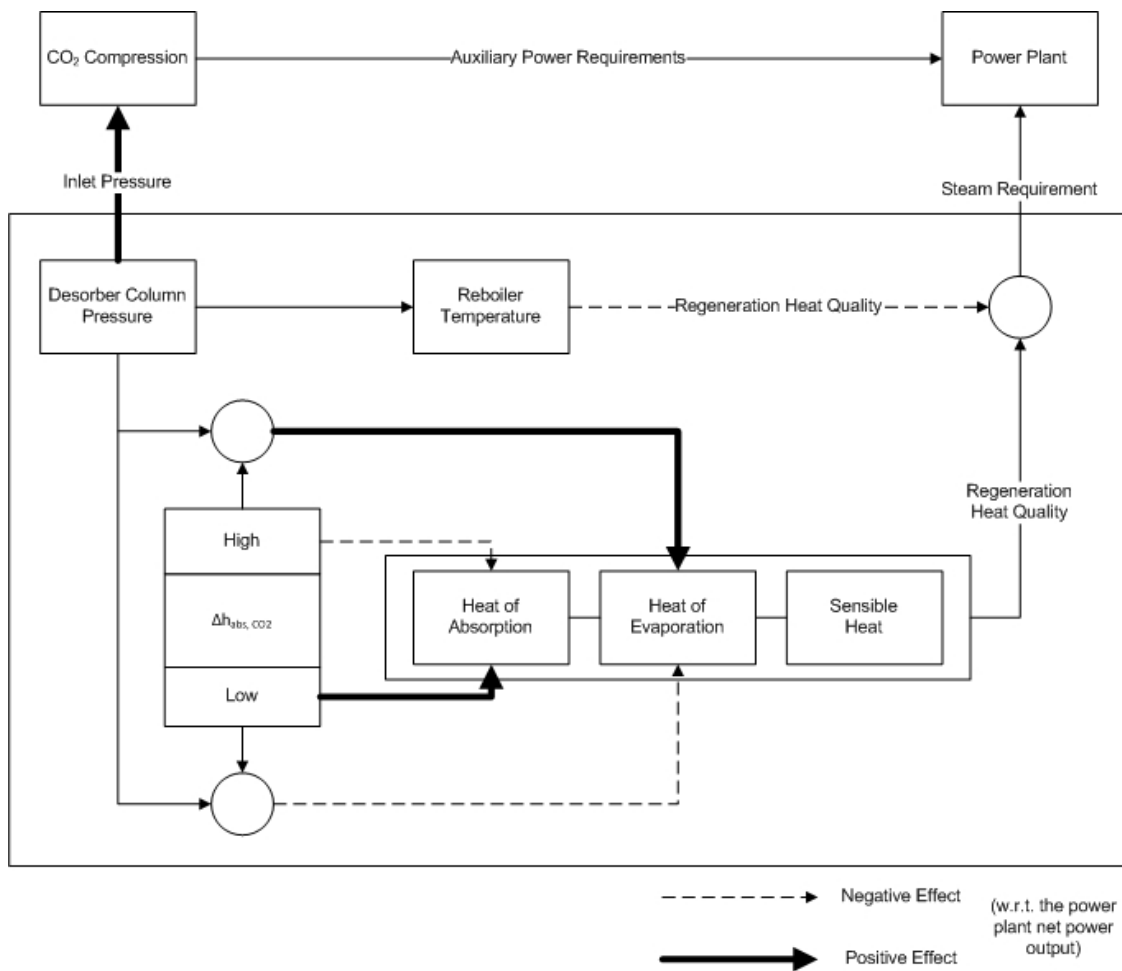


Figure 2.13 – Schematic depicting the relationships of selected process parameters on the net power output of the host plant (Redrawn from (Oexmann & Kather, 2010)).

For example, from Figure 2.13 it is clear that a higher heat of absorption will necessitate a higher quality steam, increasing the energy penalty and reducing the net power output of the power cycle. From this analysis it is clear that focusing exclusively on solvents with a low heat of absorption is not sufficient in quantifying the energy performance of alternative solvents (Oexmann & Kather, 2010). It is important to consider all contributions to the overall regeneration heat duty and evaluate the performance of the solvent accordingly.

2.5.4.2. Through Heat Integration

Proper analysis of the temperature profile inside the absorber column could greatly assist in reducing the energy consumption of the CO₂ capture unit. Studies by Freguia and Rochelle (2003) have shown an insignificant temperature bulge inside the absorber for MEA solvent and 3vol% CO₂ in the flue gas. The temperature bulge was found to be significant if the CO₂ concentration in the flue gas is increased to 10vol%. Intercooling can be used to redistribute heat from the middle section of the absorber to the reboiler of the desorber. For the case of 10vol% CO₂ in the flue gas it was shown that intercooling could reduce the reboiler heat duty by 3.8% (Wang et al., 2010). Studies by Lucquiaud and Gibbins (2009) suggest that the energy consumption can further be reduced through improved integration between the CO₂ capture unit and the power cycle.

2.5.5. Simultaneous Separation of SO_x and NO_x

Studies performed by Resnik *et al.* (2004) investigated the use of an ammonia solvent to extract CO₂, SO₂ and NO_x components simultaneously from the flue gas. Benefits of such a process would include: (a) reduced capital cost and process complexity, (b) ammonia has an increased CO₂ loading capacity compared to conventional MEA solvents (almost 3 times as much) and (c) preliminary tests have shown an up to 64% reduction in solvent regeneration energy requirements (Wang et al., 2010). Further work is needed to investigate and assess the performance of different solvents in such a simultaneous removal process.

2.6. Conclusions

Post-combustion capture (PCC) with chemical absorption is likely to be the first CCS technology that will be deployed. It is the only CCS option that can be retrofitted to existing fossil-fueled power plants without major modifications. At present there are no full-scale operated chemical absorption post-combustion CO₂ capture (CA-PCC) demonstration projects treating flue gas from fossil-fuel power plants. Public funding is vital to stimulate the interest in commercializing CCS. Further work is needed to improve the capture efficiency and reduce the energy requirements of the capture unit. Future efforts should focus on the development of alternative solvents with reduced energy requirements for solvent regeneration. At present there are no simple, easy-to-use methods to screen solvents for CO₂ absorption processes. There is a desperate need for a simplified, easy-to-use model to describe the equilibrium behaviour of CO₂-absorbing solvents. The model should be capable of screening through large sets of solvent data in the search for the optimal solvent for CO₂ absorption processes. The model should be based on thermodynamically sound principles to accurately quantify the energy performance of the solvents evaluated. The end goal of the research should be to develop a model that could be integrated with the reactive absorption process models. This will allow real-time assessment of the energy performance of various solvents in reactive absorption processes. Proper process heat integration should also be considered in future process design and optimization efforts.

3. CO₂ Solubility: Theoretical Modeling

3.1. Introduction

Classical models used to predict the equilibrium behaviour of chemicals are based on complex thermodynamic correlations. Models typically used include: cubic equations of state (EoS), activity coefficient models, group contribution methods, quantum chemistry calculations, statistical mechanics, lattice model, various versions of the Statistical Associating Fluid Theory (SAFT), etc. (Vega et al., 2008).

There are several drawbacks to using these models:

- Due to the complexity of these models, they can typically only be used by experts in the field of modeling;
- The models require an extensive knowledge of the thermodynamic properties of the chemicals to be modeled;
- The models typically require time-consuming system specific data set regression;
- Most of these models will fail to describe the physico-chemical properties of non-ideal systems (e.g. solutions containing ionic liquids or water) (Vega et al., 2008).

Although these models are extremely powerful in predicting vapour-liquid and liquid-liquid equilibrium (VLE and LLE respectively), there is an urgent need for a simplified screening model to predict the equilibrium solubility behaviour of chemicals. The model should adhere to certain design criteria:

- The model theory should be easy to understand and apply;
- The model should circumvent the need for extensive chemical property data;
- The model should be able to screen large sets of solvent data in a timely manner;
- The model should have the potential to be applied to complex non-ideal systems (e.g. systems containing ionic liquids).

Partial solubility parameters such as the Hansen Solubility Parameters (HSPs) show great potential to be implemented in such a simplified thermodynamic screening model.

3.2. Hypothesis

The null hypothesis (H_0) and alternative hypothesis (H_1) for this study is formulated as follow:

H₀: Partial solubility parameters cannot be used to accurately describe the equilibrium behaviour of carbon dioxide (CO_2) reactively absorbing into task specific designed solvents.

H₁: It is possible to use partial solubility parameters to predict the equilibrium behaviour of CO_2 reactively absorbing into task specific designed solvents.

The research plan is designed to test the null hypothesis through random sampling. The hypothesis will be accepted or rejected based on the test statistics results computed for the sample data.

3.3. Partial Solubility Parameters (PSPs): A Novel Method for Solvent Screening/Selection

3.3.1. Background

Solubility parameters (δ) can be used to predict the degree of interaction between materials. Solubility parameters provide a numerical estimate of the internal energy characteristics (i.e. the energy required to create a hole in the solvent and break up the solute) as well as the interactive energy between materials (Abbott et al., 2010). Materials with similar solubility parameters are likely to be miscible in each other. Hildebrand originally characterized these interactions based on the cohesive energy density (Lee & Lee, 2005):

$$\delta = \sqrt{\frac{\Delta H_v - RT}{V_m}} \quad [3.1]$$

Where δ is the Hildebrand solubility parameter, ΔH_v is the enthalpy of evaporation (at 298 K), R is the universal gas constant and V_m is the molar volume. The units of solubility parameters are $[\text{J}/\text{cm}^3]^{0.5}$ or

[MPa]^{0.5}. Older papers may express the units as [cal/cm³]^{0.5}. The following relation can be used to convert between the different unit types:

$$1 [\text{cal}/\text{cm}^3]^{0.5} = 2.046 [\text{MPa}]^{0.5}$$

Multiply these values by a factor of 2.046 to convert to the new units. One energy value, such as the Hildebrand solubility parameter, would be sufficient to predict these interactions if the system contained only materials that are all of the same general type. The majority of systems however contain materials of more than one general type. Without partitioning the interaction energy, the predictive power of solubility parameters would be limited. For most systems there are four main forms of interaction energy that need to be considered (Abbott et al., 2010):

- Dispersion forces (atomic) – typically van der Waals interactions between almost all molecules;
- Polar forces (molecular) – so called “positive attracts negative” electrical interactions due to dipole moments;
- Hydrogen bond forces (molecular) – a type of polar force, considered as a form of electron exchange;
- Ionic forces – the electrostatic forces that keep inorganic crystals together.

At least two of these energies (i.e. dispersion and polar forces) are required to accurately describe the molecular interactions between materials. Including a third parameter (i.e. hydrogen bond forces), Hansen developed a set of partitioned solubility parameters capable of predicting the thermodynamic interactions of all systems except those containing strong ionic interactions. The Hansen solubility parameters offer certain advantages compared with other parameter approaches:

- HSPs have been tested and proven in industry for more than 40 years (Hansen, 2007);
- An existing database containing HSP values for more than 10000 chemicals (Abbott et al., 2010);
- Hansen developed the HSPiP software package for analyzing and determining HSPs;
- The HSP theory has the potential to be easily expanded to account for ionic bond interactions;
- The theory is easy to understand and apply.

Based on this, the Hansen solubility parameter approach was chosen as basis for this study. A detailed description of the Hansen solubility parameters is given in Section 3.3.2. The primary limitation of HSPs is that it ignores the effect of electrostatic molecular interactions. These interactions are the dominant energy force present in systems containing inorganic compounds (e.g. ionic liquid solutions).

The principle limitation of the solubility parameter approach is that it is based on the idea of “like dissolves like”, i.e. it cannot account for negative deviations from Raoult’s law resulting from solvation or the formation of electron donor/acceptor complexes (Hansen, 2007). Numerous studies have focused on dividing the hydrogen bond parameter into donor/acceptor terms (i.e. Abraham parameters, COSMO-RS, MOSCED, UNIFAC, etc.) as to account for the formation of electron donor/acceptor complexes. Practical problems involved with partitioning the hydrogen bond into two such terms however have proven to be a major obstacle in the way forward. Solubility parameters should be used as a simplified screening method to predict the equilibrium solubility behaviour of materials.

3.3.2. Hansen Solubility Parameters (HSPs)

3.3.2.1. Basic Modeling Theory

HSPs are based on thermodynamics, i.e. whether something is fundamentally possible or not. Although HSPs were determined empirically, recent work by Panayiotou (2008) has shown that it is possible to derive HSPs from first principles. The basis for HSPs is that the total energy of vaporization consists of three individual parts, i.e. the dispersion cohesive energy (E_D), the polar cohesive energy (E_P), and the hydrogen bonding cohesive energy (E_H). The basic equation governing the assignment of HSPs is defined as follow (Hansen, 2007):

$$E = E_D + E_P + E_H \quad [3.2]$$

Dividing the terms of Eqn. 3.2 by the molar volume (V_m) as in Eqn. 3.3, gives the square of the total (or Hildebrand) solubility parameter as the sum of the squares of the Hansen partial solubility parameter components (Eqn. 3.4):

$$\frac{E}{V_m} = \frac{E_D}{V_m} + \frac{E_P}{V_m} + \frac{E_H}{V_m} \quad [3.3]$$

$$\delta^2 = \delta_D^2 + \delta_P^2 + \delta_H^2 \quad [3.4]$$

From Eqn. 3.4 it is clear that HSPs quantitatively account for the cohesion energy density. Materials with similar HSP values are expected to have a high affinity for each other. The partitioning of the cohesive energy density allows HSPs to account for polar interactions between materials as well, whereas the application of the Hildebrand solubility parameter is restricted to non-polar species. The dispersion and polar bond energy components can be determined empirically using Equations 3.5 and 3.6 respectively (Abbott et al., 2010):

$$\delta_D = \frac{RI - 0.784}{0.0395} \quad [3.5]$$

$$\delta_P = \frac{36.9 \times DM}{\sqrt{V_m}} \quad [3.6]$$

In Eqns. 3.5 and 3.6 RI is the refractive index, DM is the dipole moment and V_m is the molar volume. The hydrogen bond energy component is commonly calculated by subtracting the dispersion and polar energies of vaporization from the total energy of vaporization (i.e. the difference of the squares of δ , δ_D and δ_P). Group-contribution methods have started to be used more recently (Hansen, 2007). Although this method is more accurate than the original approach, it still leads to an overestimation of δ_H . In essence, the value calculated for δ_H is representative of the collective bond energies remaining (i.e. hydrogen bond interactions, electrostatic interactions, induced dipole and metallic interactions, etc.). This should be kept in mind when analyzing systems containing dominant molecular interactions other than dispersion and polar interactions.

Furthermore, Hansen proposed a so-called “solubility sphere” technique to visualize and evaluate the solubility behaviour between materials. The components of the HSPs can be seen as three coordinates

to be plotted in 3D. The plot can be used to visualize the approximate “distance” between materials. The HSP distance (R_a) between two materials is given by Hansen (2007) to be:

$$Ra^2 = 4(\delta_{D,A} - \delta_{D,B})^2 + (\delta_{P,A} - \delta_{P,B})^2 + (\delta_{H,A} - \delta_{H,B})^2 \quad [3.5]$$

Where the subscripts D, P and H indicate the respective HSP components, and the subscripts A and B indicate the solvent and solute respectively. This value can be used to determine the ratio of the distance of the solvent HSPs from the solute HSPs to the solute interaction radius. This ratio is known as the relative energy difference (or RED):

$$RED = \frac{Ra}{Ro} \quad [3.6]$$

Where Ro is the solute interaction radius. The interaction radius for CO_2 is $3.3 \text{ MPa}^{0.5}$ (Abbott et al., 2010). For a given solvent, a value of $RED < 1$ would indicate favorable solvent-solute interactions, i.e. a “good” solvent. A value of $RED \approx 1$ indicates a boundary condition between a “good” and “bad” solvent. Increasing values of RED above a value of 1 would represent progressively unfavorable solvent-solute interactions (i.e. progressively “worse” solvents). Figure 3.1 shows a rendering of a typical solubility sphere.

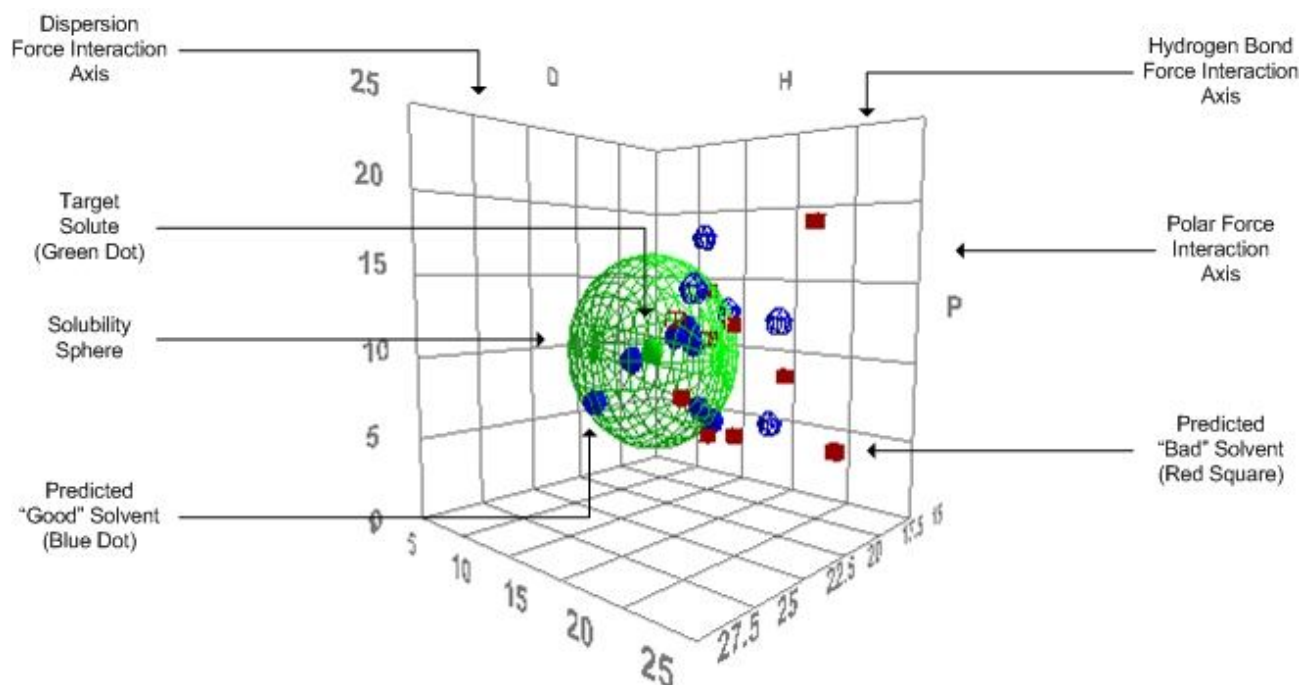


Figure 3.1 – Rendering and description of a typical HSP solubility sphere (generated using the HSPiP software package).

The solute HSPs (i.e. the coordinates to the green dot in Figure 3.1) is the target HSP values. The solute interaction radius is used to construct the solubility sphere around the solute HSP values (i.e. the meshed green sphere). Solvents with a RED value less than 1 (i.e. “good” solvents”) are indicated as blue dots located inside the solubility sphere. The red squares located outside of the sphere indicate the “bad” solvents.

3.3.2.2. Optimizing Solvent Designs

The HSPs can be used to quickly screen solvent formulations in search for a blend with HSP values similar to that of the target solute. The solvent blend HSP components can be calculated using a simple weighted volume average (Abbott et al., 2010):

$$\delta_{i,mix} = \sqrt{(x_1\delta_{i,1}^2 + x_2\delta_{i,2}^2 + \dots + x_n\delta_{i,n}^2)} \quad [3.7]$$

Where the subscript i denote the HSP component considered, the subscript mix denotes mixture and x is the individual material volume fractions. Although Eqn. 3.7 is based on a square-mixing algorithm, the weighted average can also be calculated using a linear mixing algorithm. The computational capacity of modern computers make it possible to apply Eqns. 3.5 to 3.7 to swiftly search through large sets of data for the solvent blend with the minimum RED value, i.e. the best possible solvent for the target solute.

3.3.2.3. Temperature and Pressure Dependencies of HSPs

The HSPs will vary with change in temperature and pressure. It is suggested that the hydrogen bond component (δ_H) is the most sensitive to a change in temperature. The number of hydrogen bonds weakened will increase with increasing temperature, causing the δ_H to decrease more rapidly with increasing temperature than the other HSP components. The temperature dependencies (derivative form) for each of the HSP components are summarized in Table 3.1 (Hansen, 2007):

Table 3.1 – Summary of the derivative equations for the temperature and pressure effects on HSPs (Hansen, 2007).

| | Temperature Increment | Pressure Increment | Eqn. |
|------------|---|--|---------------|
| δ_D | $\left(\frac{\partial\delta_D}{\partial T}\right)_P = -1.25\alpha\delta_D$ | $\left(\frac{\partial\delta_D}{\partial P}\right)_T = 1.25\beta\delta_D$ | [3.8]/[3.9] |
| δ_P | $\left(\frac{\partial\delta_P}{\partial T}\right)_P = -0.5\alpha\delta_P$ | $\left(\frac{\partial\delta_P}{\partial P}\right)_T = 0.5\beta\delta_P$ | [3.10]/[3.11] |
| δ_H | $\left(\frac{\partial\delta_H}{\partial T}\right)_P = -(1.32 \times 10^{-3} + 0.5\alpha)\delta_H$ | $\left(\frac{\partial\delta_H}{\partial P}\right)_T = \left(\frac{1.32 \times 10^{-3}\beta}{\alpha} + 0.5\beta\right)\delta_H$ | [3.12]/[3.13] |

An increase in temperature usually results in an increased rate of solubility/diffusion/permeation, as well as an increase in the size of solubility spheres. From Table 3.1 it is clear that the HSPs will decrease with an increase in temperature (Eqns. 3.8, 3.10 and 3.12 where α is the isobaric coefficient of thermal expansion). Also indicated in Table 3.1 are the pressure dependencies (derivative form) for each of the HSP components (Eqns. 3.9, 3.11 and 3.13 where β is the isothermal compressibility). It is clear that the HSPs will increase with an increase in pressure. These equations make it possible to study the effect of temperature and pressure on the molecular interactions between materials.

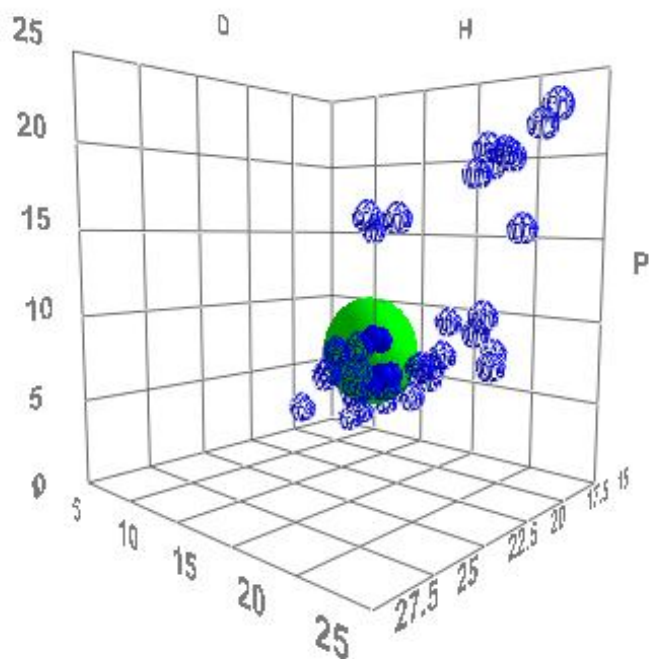
3.3.2.4. Hansen Solubility Parameters in Practice (HSPiP) Software Package

A major advantage of HSPs compared with other solubility parameter approaches is the availability of parameter specific analysis software as well as a large chemical dataset. Hansen, in collaboration with Prof. Steven Abbott and Dr. Hiroshi Yamamoto, developed the Hansen Solubility Parameters in Practice (HSPiP) software package as an easy-to-use, practical tool for analyzing the molecular interactions between materials.

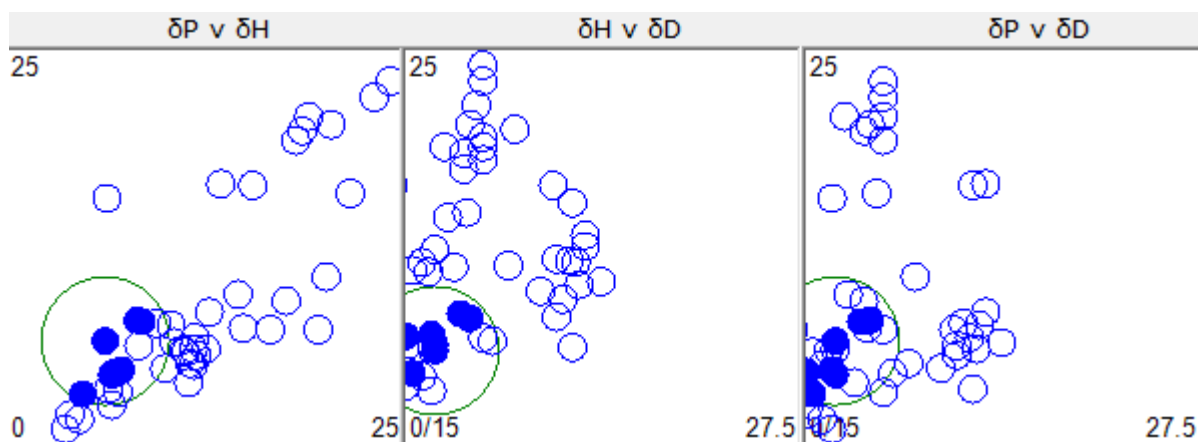
The software comes standard with a database containing HSP and other physical property data for approximately 10000 compounds. HSP values were experimentally determined for about 1200 of the chemicals; the remainder being obtained through predictions. The software offers several functions for analyzing and calculating HSP data, including (Hansen, 2011):

- The ability to calculate and visualize HSPs in 3D;
- A solvent blend optimizer capable of analyzing the effects of relative evaporation rates, activity coefficients and temperature;
- A polymer calculator;
- A diffusion modeler;
- A solvent GC and HPLC retention time predictor;
- And, a do-it-yourself (DIY) HSP calculator.

A detailed description of the software features as well as how to use it is given in the Hansen Solubility Parameters in Practice eBook (supplied with the software). A quick overview is given on the key features provided by the software, i.e. (a) the 3D visualizer, (b) the solvent blend optimizer, and (c) the DIY Y-MB (Yamamoto Molecule Breaker) HSP calculator. Figure 3.2 shows a visualization of typical solvent-solute molecular interactions.



(a)



(b)

Figure 3.2 – (a) Screenshot of the 3D HSPiP solvent-solute analysis (with CO₂ selected as the target solute), (b) Screenshot of three section views of the analysis.

The visualizations shown in Figure 3.2 were generated to show the interactions of 296 amine solvents with CO₂ selected as the target solute. As in Figure 3.1, the solute is shown as a green dot surrounded by

a green meshed sphere (i.e. the solubility sphere). The solvents are indicated as individual blue spheres. Solvents located inside the green meshed solubility sphere are classified as ideal solvents for absorbing the target solute (CO_2). The solvents are classified as increasingly “poorer” solvents with increasing distance from the centre of the solubility sphere. The 3D visualizer serves as an easy-to-use method to quickly eliminate numerous inferior solvents. Part (b) of Figure 3.2 shows three different section views of the 3D rendering shown in part (a). The 3D plot can be rotated to view specific solvent positions w.r.t. the selected solute (Figure 3.3).

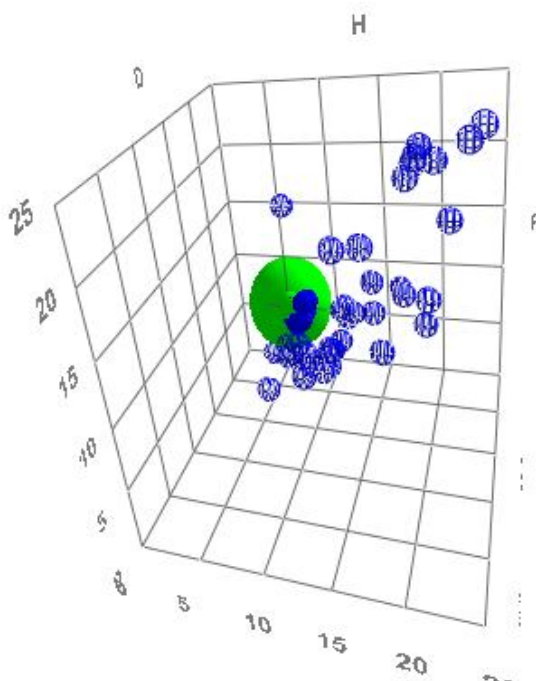


Figure 3.3 – Screenshot of the 3D HSPiP solvent-solute analysis (with CO_2 selected as the target solute) showing a rotated view of the solvent distribution.

The 3D visualizations can serve as preliminary screening method in the search for an optimal solvent. In addition to the 3D plot, a set of 2D plots (i.e. δ_P vs δ_H , δ_H vs δ_D and δ_P vs δ_D) is provided to analyze specific viewing angles of the solubility sphere. Solvents located far from the solubility sphere can quickly and easily be identified and removed from the analysis dataset.

The solvent optimizer offers a refined, calculated approach in the search for an optimal solvent. The optimizer can analyze a set of solvents for an optimal blend formulation (up to three components) w.r.t. the selected target solute. The blend is formulated such that the solvent RED is minimized. The optimizer calculates the volume percentage contribution for each of the formulated blend's constituents. The temperature can also be varied to study the effect of temperature changes on the molecular interactions between the solvent and solute. This makes it possible to screen solvent blends for specific operating conditions. There is however a limit on the calculation capacity of the solvent optimizer. For larger datasets, e.g. the 296 amines considered above, the optimizer is limited to a two-component blend formulation.

Another major feature of the HSPiP software is the do-it-yourself (DIY) HSP calculator. The calculator offers 6 approaches to calculate the HSP values for a given molecule (Abbott et al., 2010):

- Calculating the HSP component values from the input enthalpy, molar volume, refractive index and dipole moment (i.e. the "Numbers" method);
- Using the Stefanis-Panayiotou (S-P) group-contribution method to calculate the HSP component values by specifying the various molecule groups;
- Using the Van Krevelen method (similar to the S-P method);
- Calculating the component values using the Hoy group-contribution method (also similar to the S-P method);
- Using the neural network (NN) molecule breaking (MB) technique (i.e. the "Y-MB" method);
- Using an extended Y-MB approach specifically for calculating the HSP component values of polymers.

The so-called "Y-MB" method shows the most potential for future work in solubility parameter. The method, developed by Dr. Hiroshi Yamamoto, is based on a neural network algorithm for fitting the full set of available HSPs (i.e. the supplied set of 10000 chemicals). The DIY Y-MB calculator can import standard molecular structure data inputs (i.e. SMILES, .mol files, PDB and XYZ). The imported molecule structure is broken down into the main contributing groups and fitted to the neural network. Based on this, the Y-MB is able to calculate the HSP components values as well as several other physical properties. It is suggested that future versions of the Y-MB will be augmented via molecular orbital (MO) calculations (Abbott et al., 2010). The major drawback of the Y-MB is that, at present it is not able to

calculate HSP data for molecules comprised of two or more ions. A screenshot of a typical DIY Y-MB calculation is shown in Figure 3.4.

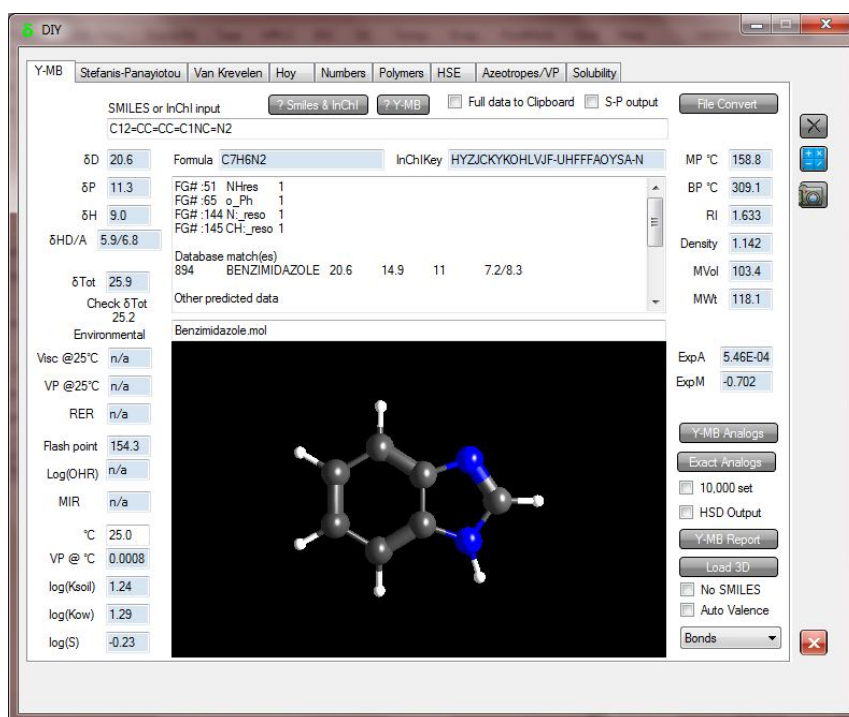


Figure 3.4 – Screenshot of the HSPiP DIY solvent property calculator results for Benzimidazole.

A .mol file of a Benzimidazole molecule was imported into the DIY Y-MB calculator. Figure 3.4 shows a 3D rendering of the imported molecule as well as the calculation results obtained for the molecule. Indicated in the top left-hand corner of the screen are the values calculated for the δ_D , δ_P , δ_H , and δ_{Tot} . The Y-MB module also calculates other important property data including the material viscosity, density, melting- and boiling points, molar- volume and weight, and the refractive index. These values are indicated in the top right-hand corner of the screen.

3.3.3. Expanding the HSP Theory: Considering the Effect of Electrostatic Bond Energies

The major limitation of the HSP approach is that it neglects the effect of electrostatic interactions between molecules. It is vital to be able to predict the thermodynamics of these interactions when considering systems containing strong ionic molecular interactions, e.g. systems containing ionic liquids (ILs). With the focus progressively shifting towards the use of ILs in solvent design for CO₂ capture, there is an urgent need to expand the solubility parameter theory to include an ionic bond component (δ_I).

$$\delta^2 = \delta_D^2 + \delta_P^2 + \delta_{HT}^2 + c_I \delta_I^2 \quad [3.14]$$

Where δ_{HT} is the true hydrogen bond component value and c_I is the coefficient of ionic interaction. Both of these terms are introduced to address the error made in calculating the hydrogen bond component (δ_H) (see Section 3.3.2.1). Typically, the value calculated for δ_H is representative of the collective bond energies remaining (see Section 3.3.2.1). For the purpose of this study it is assumed that the calculated hydrogen bond parameter is comprised of the true hydrogen and ionic interaction energies:

$$\delta_H = \delta_{HT} + \delta_I \quad [3.15]$$

The ionic bond energy parameter is defined as the square root of the ionic bond energy (E_I) divided by the molar volume of the molecule (V_m):

$$\delta_I^2 = \frac{E_I}{V_m} \quad [3.16]$$

Ionic bond interactions are expected to be the dominant forces present in ionic liquid solutions. Ionic liquids are typically comprised of a large organic cation and a smaller inorganic anion (Figure 3.5).

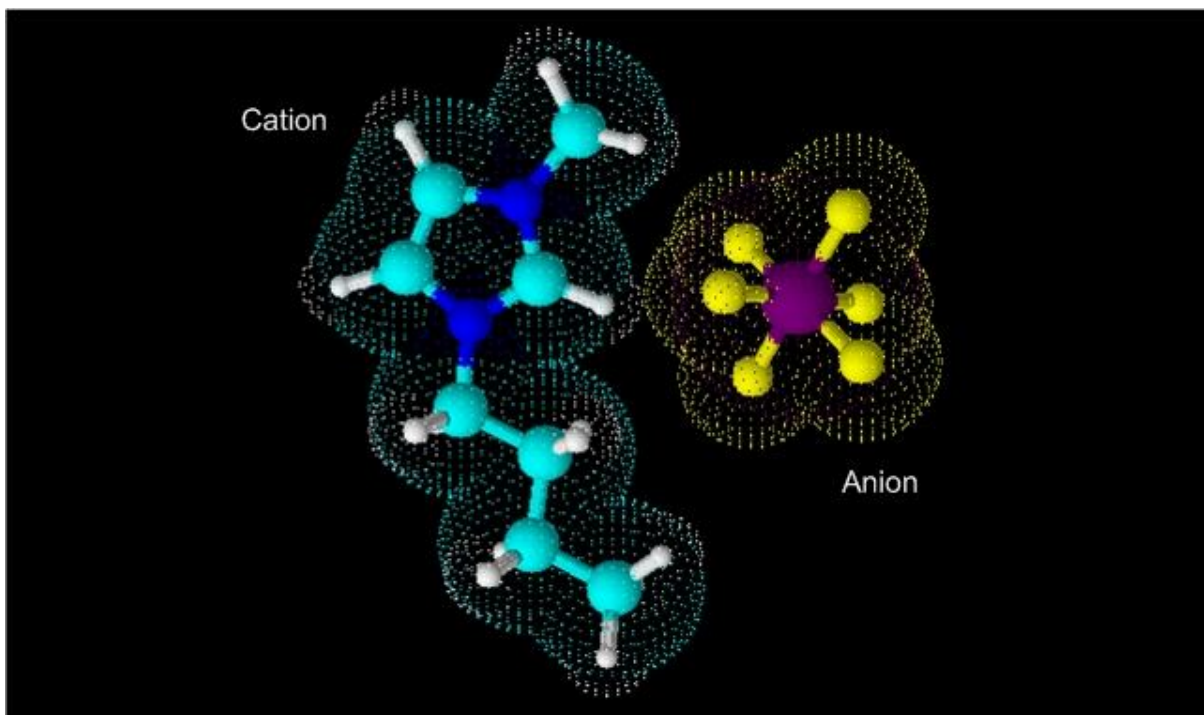


Figure 3.5 – Rendering of an isolated molecule structure for a typical ionic liquid ([bmim][PF₆]) (drawn using the ACD/ChemSketch Freeware package).

The ionic bond energy is the force that keeps the cation and anion together. This energy resulting from the electrostatic attraction between the cation and anion can be calculated using Equation 3.17:

$$E_I = E_{Mol} - E_{Cat} - E_{An} \quad [3.17]$$

Where E_{Mol} is the total equilibrium state energy of the molecule, E_{Cat} is the total equilibrium state energy of the cation, and E_{An} is the total equilibrium state energy of the anion. The individual energy values can be determined using a molecular orbital approach. Molecular mechanics (MM+), semi-empirical (AM1) as well as quantum chemical (Ab-Initio) calculations were used to quantify the ionic bond energies for a set of 74 ionic liquids. Minimal (STO-3G) and small (3-21G) basis sets were used for the Ab-Initio calculations. All calculations were done using the HyperChem software package (Figure 3.6).

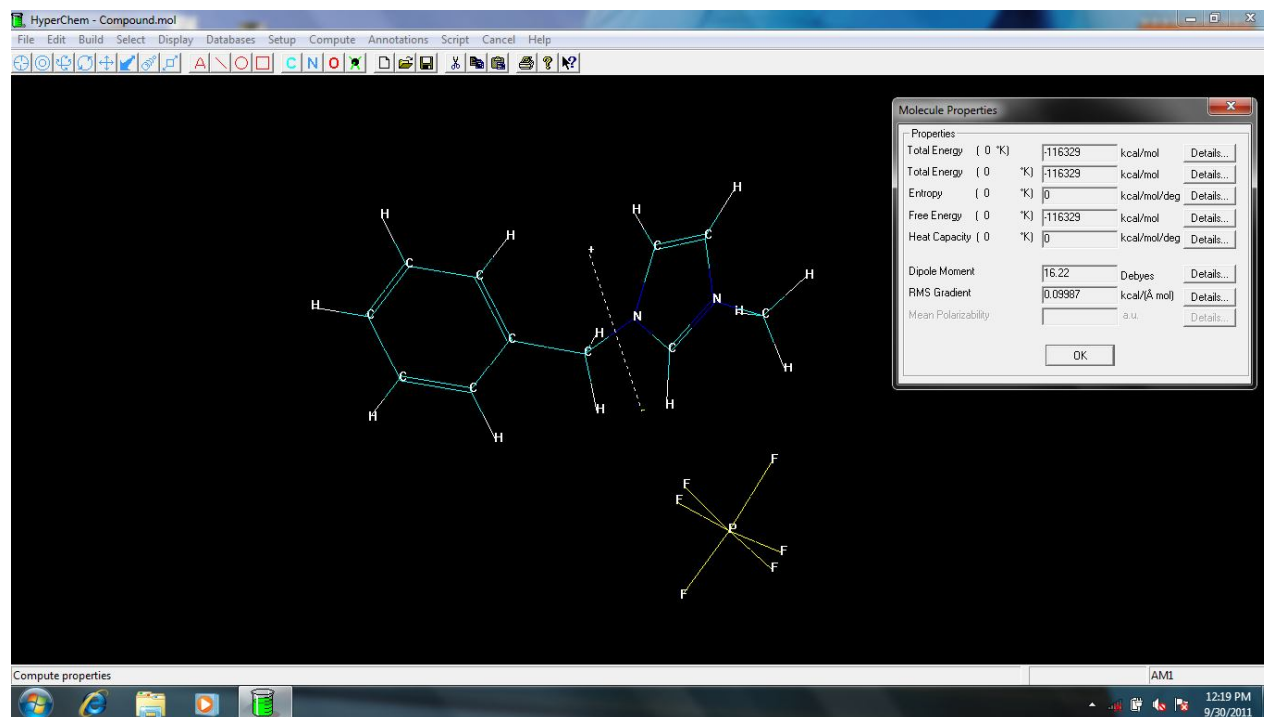


Figure 3.6 – Screenshot of the results obtained for an optimized ionic pair ([bmim][PF₆]).

Figure 3.6 shows the calculation results obtained for a [bmim][PF₆] molecule. It shows the optimized geometric layout of the cation and anion in three dimensions (3D). The value calculated for the minimum free energy of the optimized system is indicated in the “Molecule Properties” popup window in the top right-hand corner of the screen. Also indicated here is the dipole moment calculated for the material. This value is useful as it could be used in future calculations to quantify the polar bond energy component values of ILs (see Equation 3.6).

The Polak-Ribiere (conjugate gradient) algorithm was used for all of the calculations to optimize the structure geometry of the element considered. For each calculation the iteration loop was set to terminate at a RMS gradient less than 0.1 kcal/(Å mol) or after 5000 cycles, whichever occurs first. The RMS gradient is the total energy gradient calculated as a root mean square value. A value of 0 for the RMS gradient would indicate that the structure is at a local minimum or saddle point in the potential energy surface (HyperChem, 2011). Different initial spatial arrangements have to be investigated to determine whether the obtained minimum is local or global. For all of the materials considered, the

values obtained for the free energy was the same when calculated from different initial spatial arrangements. Results of the molecular mechanics, semi-empirical and quantum chemical calculations for the selected set of ionic liquids are summarized in Tables B.1 to B.5 (Appendix B).

At present there is very limited data available on the physical properties of ionic liquids. From Eqn. 3.16 it is clear that the molar volumes are required to calculate the δ_i parameters. The lack of this data in literature proves to be the main obstacle in quantifying the ionic bond energy parameter. Recent work by Abbott *et al.* (2011) determined the HSP component values for four key ionic liquids used in solvent design, i.e.:

- 1-butyl-3-methylimidazolium chloride ([bmim][Cl]);
- 1-butyl-3-methylimidazolium hexafluorophosphate ([bmim][PF₆]);
- 1-octyl-3-methylimidazolium hexafluorophosphate ([omim][PF₆]);
- 1-butyl-3-methylimidazolium tetrafluoroborate ([bmim][BF₄]).

The HSP component values assigned to each of these ILs by Abbott *et al.* (2011) as well as their molar volumes are summarized in Table 3.2. The molar volumes were used to determine the δ_i parameters from the ionic bond energies calculated for each of the ILs. The complete set of partitioned solubility parameters was used to calculate the respective coefficients of ionic interaction. The calculated δ_i values are also shown for each of the ILs.

Table 3.2 – Summary of the solubility parameter data and molar volumes for the ionic liquids studied by Abbott et al. (2010).

| Ionic Liquid | δ [MPa^{0.5}] | δ_D [MPa^{0.5}] | δ_P [MPa^{0.5}] | δ_H [MPa^{0.5}] | δ_i [MPa^{0.5}] | V_m [cm³/mol] |
|--------------------------|--|--|--|--|--|--|
| [bmim][Cl] | 35.0 | 19.1 | 20.7 | 20.7 | 48.6 | 175.0 |
| [bmim][PF ₆] | 29.3 | 21.0 | 17.2 | 10.9 | 47.2 | 207.6 |
| [omim][PF ₆] | 27.8 | 20.0 | 16.5 | 10.0 | 40.9 | 276.0 |
| [bmim][BF ₄] | 31.5 | 23.0 | 19.0 | 10.0 | 46.3 | 201.4 |

From Table 3.2 it is clear that the δ_i parameter is the dominating factor (at least double the value of the δ_D or δ_P parameters). Furthermore, it can be seen that the δ_i parameters are significantly larger than the δ_H parameters. Based on this, Eqn. 3.15 was rejected and Eqn. 3.14 revised:

$$\delta^2 = \delta_D^2 + \delta_P^2 + \delta_H^2 + c_I \delta_I^2 \quad [3.18]$$

Another obstacle faced when including a fourth parameter is visualizing the molecule data in a 4D viewing environment. The problem is calculating the distance (Ra) between the solvent and solute component values. The original algorithm (Eqn. 3.5) must be expanded to include the fourth parameter. Equation 3.19 is adapted from the difference equation proposed by Abbott *et al.* (2011) for a 4-set HSP parameter approach. :

$$Ra^2 = 4(\delta_{D,A} - \delta_{D,B})^2 + (\delta_{P,A} - \delta_{P,B})^2 + (\Delta\delta_{HI})^2 \quad [3.19]$$

Where $\Delta\delta_{HI}$ represents the collective difference between the hydrogen bond and ionic bond parameter values. This collective difference can be calculated using Eqn. 3.20 (Abbott et al., 2010):

$$(\Delta\delta_{HI})^2 = (\min X_1^2 + \min X_2^2) + \min \left[\sqrt{(X_1^2 + X_2^2)}, \sqrt{(S_1^2 + S_2^2)} \right] \quad [3.20]$$

Where:

$$\min X_1 = \min(\delta_{H,A}, \delta_{I,B}) \quad [3.21]$$

$$\min X_2 = \min(\delta_{H,B}, \delta_{I,A}) \quad [3.22]$$

$$X_1 = \delta_{H,A} - \delta_{I,B} \quad [3.23]$$

$$X_2 = \delta_{H,B} - \delta_{I,A} \quad [3.24]$$

$$S_1 = \delta_{H,A} - \delta_{H,B} \quad [3.25]$$

$$S_2 = \delta_{I,A} - \delta_{I,B} \quad [3.26]$$

Equation 3.20 was developed such that, if both δ_i values are 0, it reduces to the original 3D distance equation (Eqn. 3.5) (Abbott et al., 2010). Equipped with the above set of equations, the expanded HSP theory has the potential to predict the thermodynamic behaviour of almost any type of molecular interactions. However, future work is needed to determine the physical property data of ILs before the expanded theory can thoroughly be tested. Current efforts by Abbott *et al.* (2011) to assign HSP values to ILs suggests that this process could take up to 10 years.

3.4. The EquiSolv Analysis Package

The HSPiP software package developed by Hansen provides a set of practical tools for analyzing and predicting the molecular interactions between materials. The package does however have several limitations:

- It is only capable of analyzing one list of solvents at a time;
- The solvent optimizer is limited to analyzing solvent blend formulations for a maximum of three constituents;
- For larger datasets (> 200 solvents) the solvent optimizer is limited to two-component blend formulations;
- Specific blend formulations and/or compositions cannot be analyzed;
- All of the calculation tools are limited to the 3-set HSP theory.

The EquiSolv analysis package was developed to address the issues stated above. A block flow diagram of the system analysis is presented in Figure 3.7.

The EquiSolv program was developed using Clarion 6.3 (a SoftVelocity product). The software utilizes the TOPSPEED™ database driver supplied with the Clarion language. The database driver was chosen based on the following considerations:

- It is supplied as freeware when purchasing the Clarion developer language;
- At present it is one of the fastest and most reliable database drivers available;

- It is compiled into the software executable (.exe) as opposed to other drivers such as SQL which requires an additional database management system (e.g. SQL Server);
- As a result of the above processing is significantly improved, i.e. read-write procedures from and to the database is optimized, maximizing calculation speed and consequently minimizing calculation time;
- There is no limit on the size of the database; it is limited only by the availability of the resources of the computer on which it is run (e.g. memory, disk space, processing power, etc.).

Furthermore numerous keys can be assigned to each data table to allow the user to quickly, and easily sort data according to various parameters.

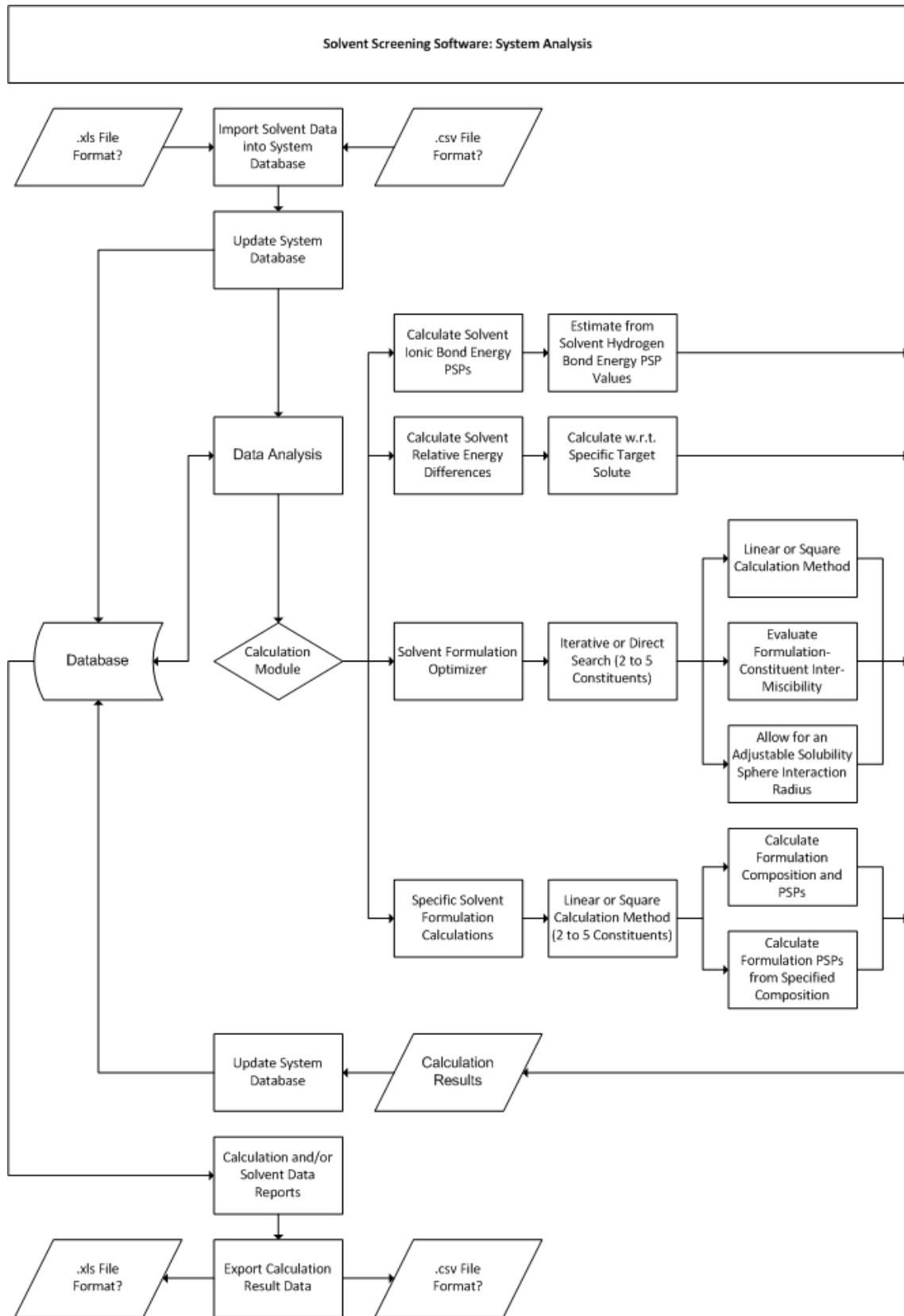


Figure 3.7 – A block flow diagram of the proposed solvent screening software system analysis.

The EquiSolv program was designed to import solvent data from CSV format files into the system database. The program offers four calculation modules for data analysis, i.e. calculating the ionic bond partial solubility parameters, calculating the solvent relative energy differences (REDs), a solvent formulation optimizer, and a quick blend calculator to evaluate specific solvent formulations. Structures were put in place to allow for up to five formulation constituents. However, due to the increasing complexity of the mathematics for each additional constituent the program currently allows only for up to four formulation constituents. The program was also designed to be able to evaluate the miscibility of the constituents of proposed solvent formulations in each other. This is essential to evaluate whether a proposed formulation can be synthesized to produce a homogenous solution. Furthermore, structures were put in place to allow the user to pull various reports on imported solvent data and/or calculation results. Also, the program was designed to allow the user to export results from calculations to CSV format files for further statistical analysis in e.g. Microsoft Excel.

A detailed discussion of the mathematical algorithms implemented in the EquiSolv program is given in Appendix A. Also, a user manual describing the step-by-step procedure for each module is given in Appendix H. A discussion on each of the four calculation modules is presented below.

3.4.1. Analyzing Alternative Solvent Blend Formulations

The EquiSolv program has the capability to import up to five solvent data lists and one solute data list from CSV format files. This allows the user to organize the data using Microsoft Excel before importing it into the EquiSolv database. The solvent optimizer can be used to search through the imported data to find the optimal blend formulation w.r.t. a target solute. The solvent optimizer has the potential to analyze blend formulations of up to four constituents (Figure 3.8). Furthermore, there is no limitation to the size of the respective solvent lists. In preliminary calculation runs, the EquiSolv program was able to analyze four-component blend formulations from a dataset containing approximately 400 million records. This is orders of magnitude more than what the HSPiP package is capable of achieving. The solvent optimizer also offers the option to use either Gauss-Seidel iteration or matrix manipulation in the search for optimal blend formulations. A detailed discussion of the calculation algorithms used by the solvent blend optimizer is given in Appendix A. Although matrix manipulation provides quicker convergence, Gauss-Seidel iteration is recommended for improved accuracy.

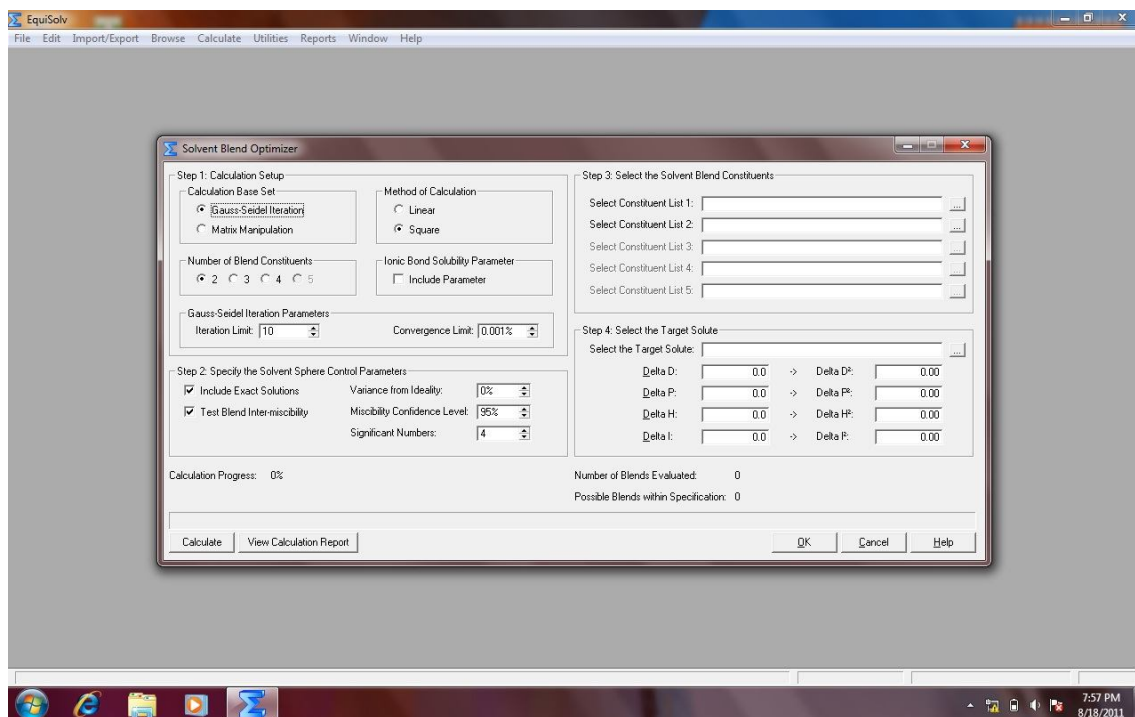


Figure 3.8 – Screenshot of the setup window for analyzing alternative solvent blends.

The solvent optimizer also offers the ability to specify the “variance from ideality”. This is the acceptable range of interaction from the target solute HSP component values, i.e. the solubility sphere. The optimizer also offers the option to test the miscibility of the blend constituents in each other. The solubility parameter data for each constituent is used to predict the probability of miscibility. Based on this, blend formulations can be rejected if the constituents are predicted to be immiscible.

3.4.2. Calculating the Solvent Relative Energy Differences (REDs)

Another key feature of the EquiSolv program is the ability to calculate and rank the solvent relative energy differences w.r.t. a target solute (Figure 3.9). The RED calculator offers the option to consolidate the individual solvent lists imported into a collective solvent data list. This makes it possible to rank the individual solvents according to ascending RED value. This feature can serve as preliminary screening method to identify and construct a list of optimal solvents for further analysis using the solvent blend optimizer.

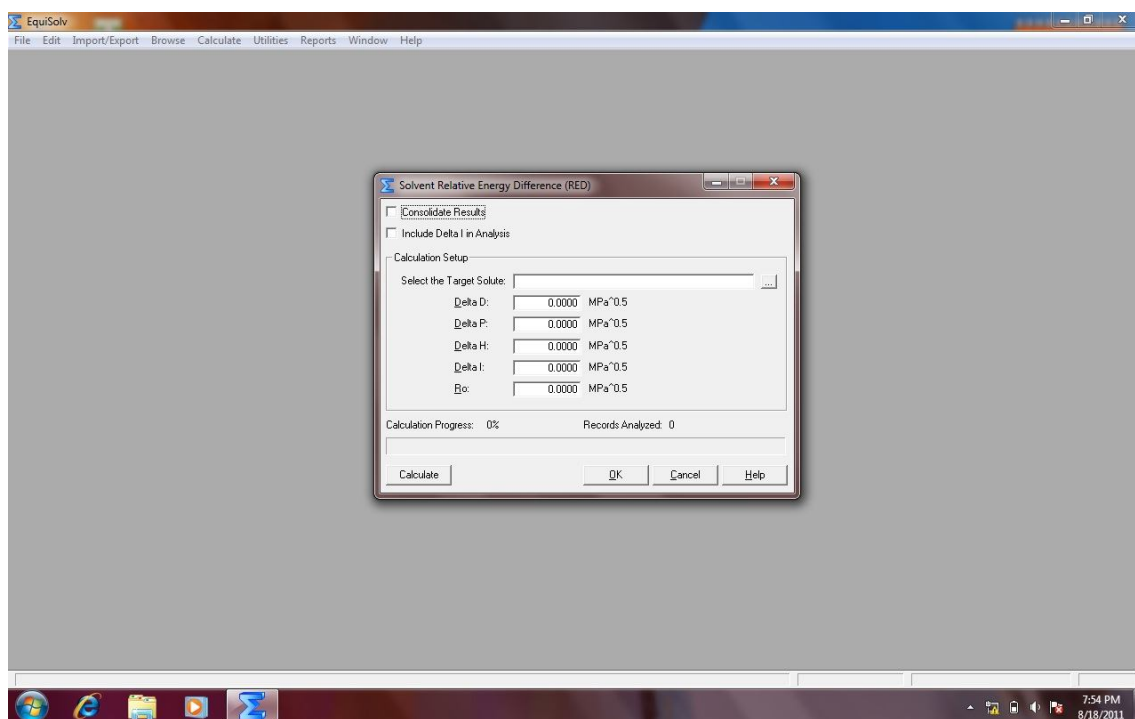


Figure 3.9 – Screenshot of the setup window for calculating the solvent relative energy differences (REDs).

3.4.3. Performing Quick Blend Calculations

In addition to the solvent blend optimizer, the EquiSolv package includes a quick blend calculator. The quick blend calculator offers two calculation options:

- To calculate the HSP values as well as the composition of a specific blend formulation w.r.t. a target solute (Figure 3.10);
- To calculate the HSP values of a blend formulation for a specific composition w.r.t. a target solute (Figure 3.11).

This feature makes it easy to quickly analyze and predict the molecular interactions of specific blend formulations, avoiding the need to scan through entire lists of solvent data. The quick blend calculator is based on Gauss-Seidel iteration rather than matrix manipulation.

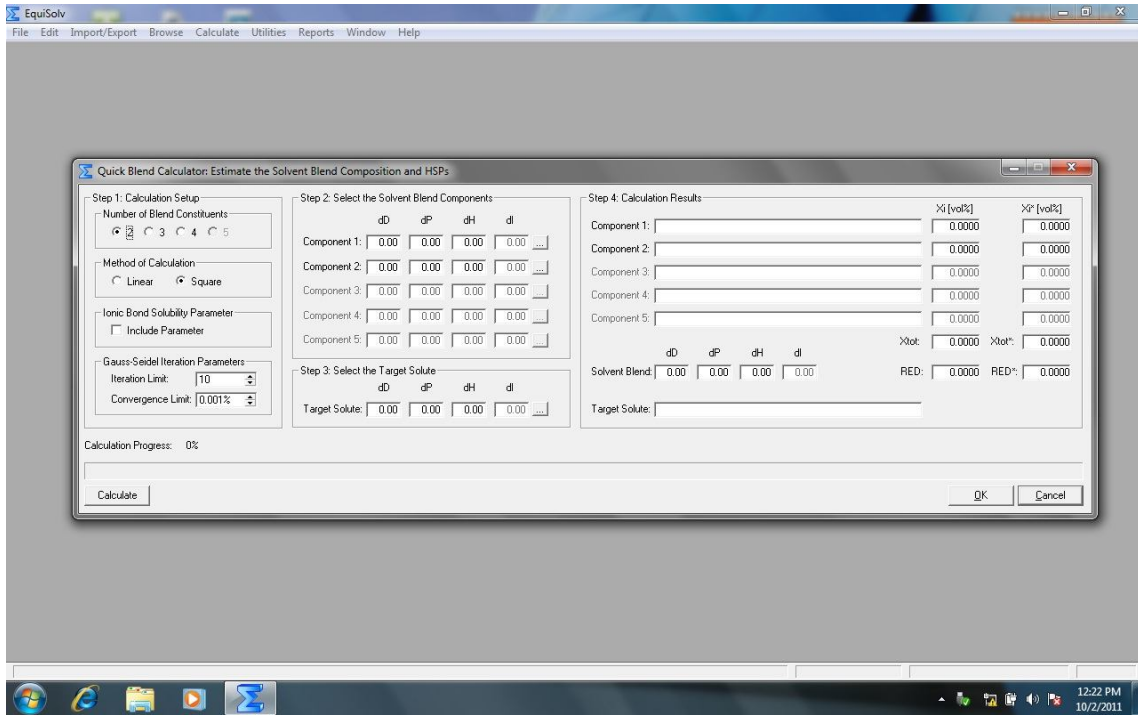


Figure 3.10 – Screenshot of the setup window for quick blend calculations (estimating both the blend composition and HSPs).

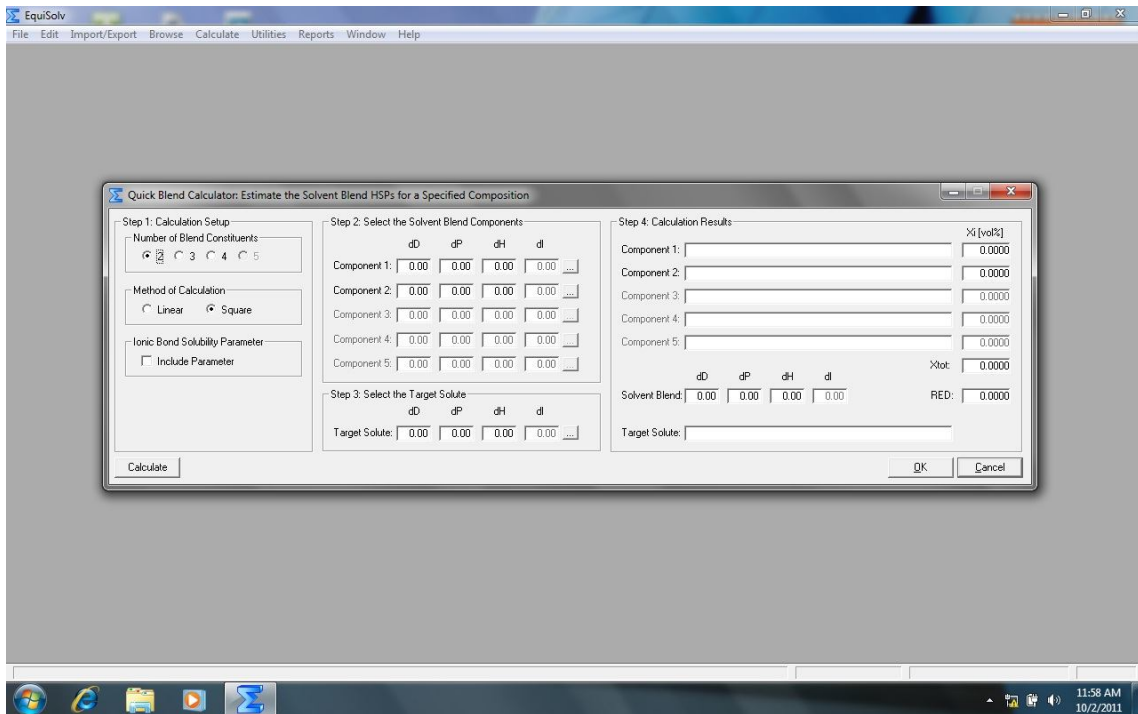


Figure 3.11 – Screenshot of the setup window for quick blend calculations (estimating both the blend composition and HSPs).

3.4.4. Estimating Electrostatic (Ionic) Bond Solubility Parameters

The proposed δ_i parameter theory is built into all of the analysis features of the EquiSolv package, i.e. the solvent blend optimizer, the RED calculator, as well as the quick blend calculator. Each of the analysis tools offers the option to include the proposed δ_i parameter. Furthermore, the EquiSolv program has the capability to estimate the value of this parameter from imported solvent data. The parameter is estimated as a fraction of the imported δ_H value (Figure 3.12). However, this feature is recommended only for solvents in which the ionic bond interactions are not the dominating force, i.e. it should not be used for solvents such as ionic liquids.

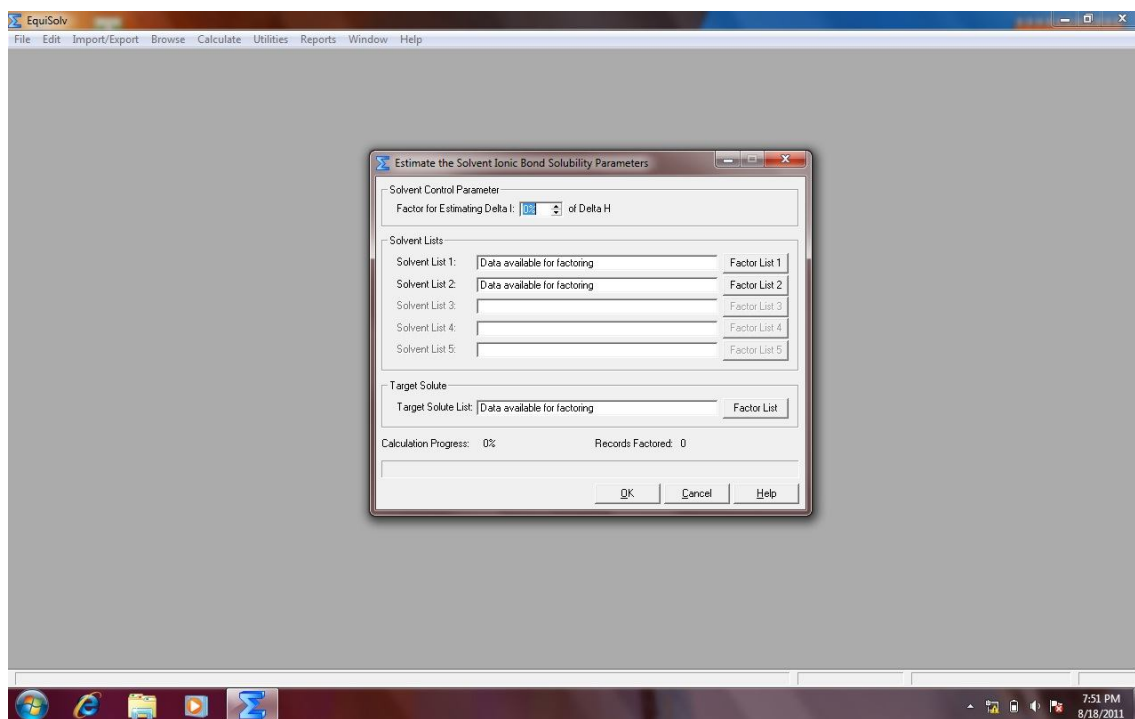


Figure 3.12 – Screenshot of the setup window used for estimating the ionic bond energy parameters (δ_i) of selected solvents.

3.5. Conclusions

The Hansen solubility parameter (HSP) approach has the potential to be used as screening method for solvent selection in the chemical absorption of CO_2 . The model is easy to understand and apply to almost any system. Furthermore, the HSP approach circumvents the need for extensive property data.

The theory is limited however as it cannot predict the thermodynamics of strong ionic molecular interactions (e.g. in ionic liquid solutions). It is proposed that the model theory be expanded to include a fourth (ionic bond energy) parameter (δ_i). The HSPiP analysis package provides a practical tool for analyzing and predicting the molecular interactions between materials. The package does however have several limitations. The EquiSolv program was developed to overcome the limitations of the HSPiP package. The program was shown to be able to screen large sets of data (up to 400 million records) in a timely manner. Further work is needed to quantify the physical properties of ionic liquids before the proposed theory expansion can be tested thoroughly. The EquiSolv program should also be upgraded to allow for temperature and pressure adjustments in the solvent screening process.

4. Experimental: Design, Materials & Methods

The experimental plan was designed to test the null hypothesis formulated for the research project, i.e. partial solubility parameters cannot be used to accurately describe the equilibrium behaviour of carbon dioxide (CO₂) reactively absorbing into task specific designed solvents. An experimental setup was designed and constructed for the solvent screening experiments required to validate (or reject) the blend formulation predictions made by the EquiSolv model.

4.1. Experimental Design

4.1.1. Equipment Design and Setup

The experimental design is based on the setups used by Retief (2009) and Wappel *et al.* (2009). The design is based on a volumetric method for gas absorption measurements. Volumetric techniques allow for the measurement of the equilibrium gas uptake as a function of pressure within a constant volume. A cubic equation of state (EoS) is applied to determine the amount of absorbate (solute) absorbed (see Section 4.2) (Gertenbach, 2009). A schematic of the experimental design is shown in Figure 4.1. The technique is comprised of an absorbent sample (of known volume) injected into a fixed volume, thermally stable absorbate gas atmosphere (i.e. the equilibrium cell in Figure 4.1). The equilibrium (absorption) cell is set inside of a temperature-controlled environment. The main sources of error for this technique include:

- Error made in determining the equilibrium cell volume;
- Error made in temperature and pressure measurements;
- Error made in determining the absorbent sample volume;
- Error made in using the EoS to calculate the amount of absorbate absorbed.

Photographs of the entire experimental setup as well as a close-up of the temperature controlled environment are shown in Figures 4.2 and 4.3 respectively.

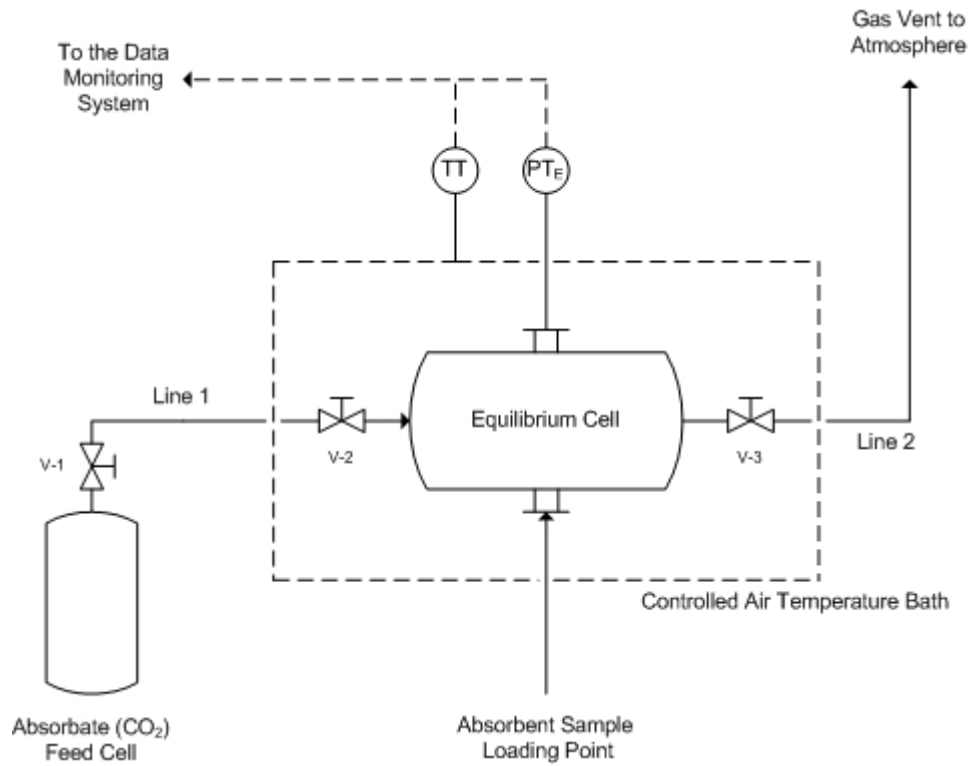


Figure 4.1 – Schematic of the experimental setup design.



Figure 4.2 – Experimental setup with descriptions.



Figure 4.3 – Temperature-controlled environment of the experimental setup with descriptions.

The absorption setup is designed to conduct solvent screening tests inside a variable pressure, thermally controlled environment. The setup is designed for low-pressure gas absorption experiments, as flue gas streams from fossil-fueled power plants are typically available at near atmospheric pressures. The equilibrium cell was constructed of glass to avoid the need for a prolonged design and construction process. The volume of the equilibrium cell was determined to be 25.87 ml. The cell was first weighed to determine the dry weight of the cell. Next, the cell was completely filled with water and weighed again. The weight of the water contained inside the cell was determined from the difference between the two readings. The volume of the water was then calculated using Equation. 4.2.1:

$$V_{cell} \cong V_{H_2O} = \frac{m_{H_2O}}{\rho_{H_2O}} \quad [4.2.1]$$

Where V_{cell} is the volume of the equilibrium cell, V_{H_2O} is the volume of the water contained inside the cell, m_{H_2O} is the mass of the water contained inside the cell, and ρ_{H_2O} is the density of the water at the ambient temperature and pressure.

The equilibrium cell was designed with two sampling points (Figure 4.4). Two gas chromatography (GC) septums were used to seal the sampling points. One of the sampling points was used for the pressure transmitter, while the other was used to inject the solvent samples into the absorbate atmosphere. The solvent samples were injected using a Hamilton gas-tight syringe (5 ml).

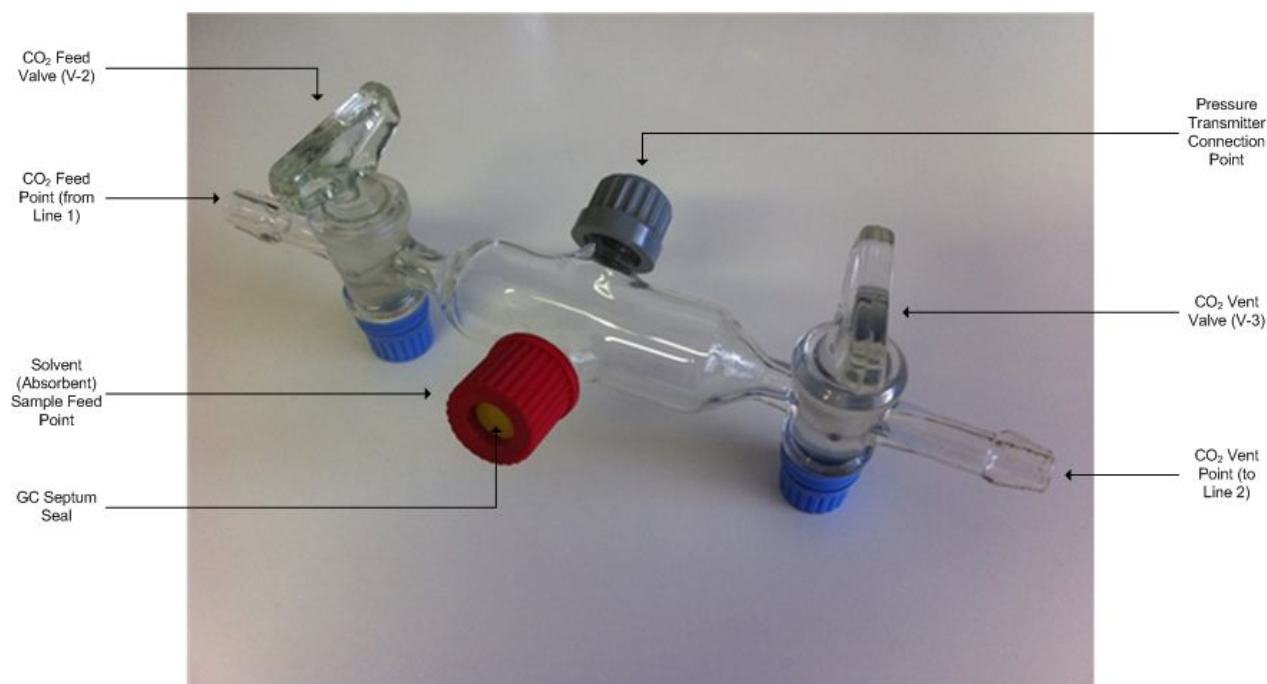


Figure 4.4 – Equilibrium cell with descriptions of the various design details.

4.1.1.1. Temperature Control and Data Recording

The temperature of the controlled environment for the absorption experiments must be maintained at 25°C. An indirect control and record technique was used to achieve this. Two temperature sensors, one for temperature control and the other for data recording, was connected to the data monitoring system (DMS) and used to monitor the system temperature. Both the sensors and DMS were supplied by Pico® Technology. Ordinary household light bulbs (100W) were used as heating elements. The controller was set to maintain the system temperature within a $\pm 1^\circ\text{C}$ deviation from the set point. Although Hansen partial solubility parameters are temperature sensitive, this deviation will not result in any significant changes in parameter values.

4.1.1.2. Pressure Control and Data Recording

A voltage-to-pressure pressure transmitter was connected to the DMS and used to monitor and record the pressure inside the equilibrium cell. A pressure transmitter with an effective measuring range of 0-1.6 bar absolute was acquired from Wika® Instruments. A reducer fitting was constructed to connect a SGE luer lock needle (50mm x 0.63mm) to the pressure transducer (¼" NPT thread) (Figure 4.5). The pressure transmitter was connected to the equilibrium cell by inserting the needle through one of the sampling point septums (Figure 4.4). The transmitter has a reported accuracy of 0.25%.

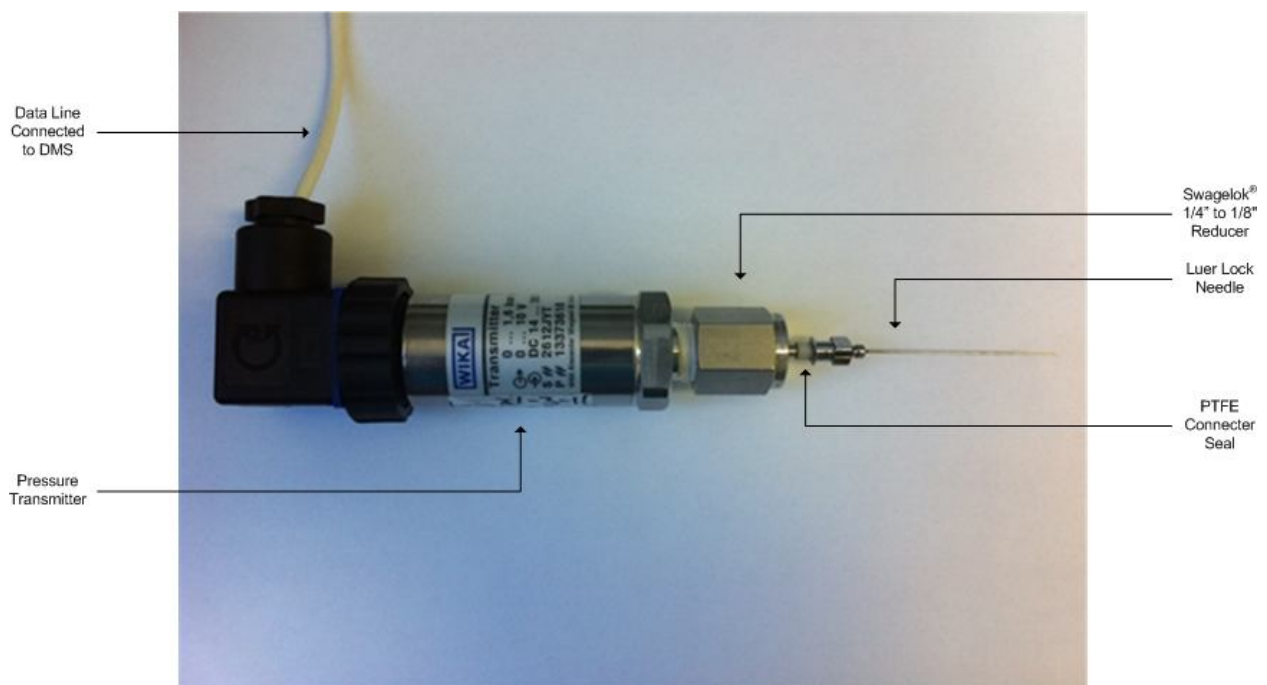


Figure 4.5 – Reducer fitting that was made to connect a luer lock needle to the pressure transmitter.

A screenshot of the Picolog® data acquisition software that was used to monitor and record the system temperature and pressure readings is shown in Figure 4.6. Indicated on the screen is the data reading sample number and the temperature and pressure readings.

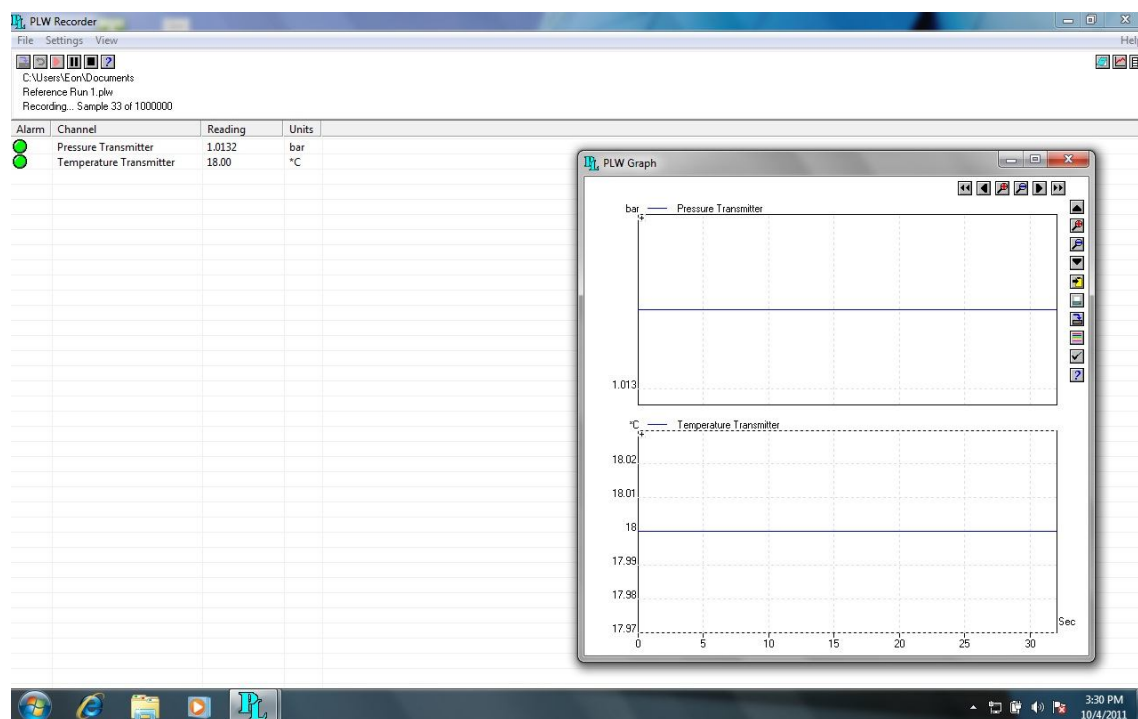


Figure 4.6 – Screenshot of the Picolog® data acquisition software used to monitor and record the temperature and pressure of the system.

Figure 4.6 also shows the “PLW Graph” popup window presenting the pressure versus time, and temperature versus time plots. These plots were continuously used throughout the experimental runs to monitor the system for sudden pressure and/or temperature fluxuations, especially during solvent injection.

4.1.2. Experimental Plan

The experimental plan is comprised of three key stages: (i) conduct a set of reference absorption experiments, (ii) conduct a set of random sampling experiments to test the null hypothesis formulated for the study, and (iii) conduct preliminary absorption experiments to investigate the performance of ionic liquids (ILs) as alternative solvents.

4.1.2.1. Reference Samples

There are three chemical blends commonly used in industry for separating CO₂ from gas streams. As their absorption capacities are available in literature, these blends were selected as reference samples.

The blends include:

- An aqueous solution of 30wt% MEA (the most commonly used solvent in post-combustion CO₂ separation process);
- An aqueous solution of 30wt% K₂CO₃ (Oexmann et al., 2008);
- An aqueous solution of 13.8wt% piperazine (PZ) promoted K₂CO₃ (22.1wt%) (Oexmann et al., 2008).

4.1.2.2. Hypothesis Test Samples

The EquiSolv solvent blend optimizer was used to predict a set of blend formulations for CO₂ absorption (see Chapter 5 for a summary of the model parameters specified for the calculation). Six blend formulations were randomly selected from the model results. The procedure for selecting the blend formulations was as follow:

- Randomly select two blend formulations, each with a predicted RED value close to zero;
- Randomly select two blend formulations, each with a predicted RED value close to 0.5;
- Randomly select two blend formulations, each with a predicted RED value close to 1.

The solvent formulations were randomly selected on the precondition that their respective constituents are commercially available. The blend formulations selected for experimental testing, including their respective RED values, are summarized in Table 4.1:

Table 4.1 – A summary of the randomly selected blend formulations predicted by the EquiSolv model that will be used to test the null hypothesis formulated for the study.

| Blend Number | Blend Constituent 1 | Blend Constituent 2 | Predicted Blend RED Value |
|--------------|---------------------|------------------------------|---------------------------|
| 1 | Di-p-Tolylamine | Dimethyl ethanolamine (DMEA) | 0.0019 |
| 2 | Trioctylamine | Monoethanolamine (MEA) | 0.0037 |
| 3 | sec-Butylamine | Auramine | 0.2179 |
| 4 | Tryptamine | Diisobutylamine | 0.2235 |
| 5 | Auramine | Hexylamine | 0.3257 |
| 6 | Hexylamine | 2,4-Dichlorobenzylamine | 0.8614 |

4.1.2.3. Ionic Liquid (IL) Test Samples

Three ionic liquids were identified for preliminary CO₂ absorption tests: 1-butyl-3-methylimidazolium hexafluorophosphate [bmim][PF₆], 1-butyl-3-methylimidazolium tetrafluoroborate [bmim][BF₄] and 1-octyl-3-methylimidazolium hexafluorophosphate [omim][PF₆]. For each IL, a 60wt% aqueous sample was synthesized and tested experimentally. Furthermore, the EquiSolv solvent optimizer was used to predict four amine-IL blends for absorbing CO₂ (Table 4.2).

Table 4.2 – A summary of the randomly selected amine-IL blend formulations predicted by the EquiSolv model.

| Blend Number | Blend Constituent 1 | Blend Constituent 2 | Predicted Blend RED Value |
|--------------|-------------------------|--------------------------|---------------------------|
| 1 | Diisobutylamine | [omim][PF ₆] | 0.0117 |
| 2 | Diisobutylamine | [bmim][PF ₆] | 0.0404 |
| 3 | 2,4-Dichlorobenzylamine | [omim][PF ₆] | 0.0544 |
| 4 | MEA | [bmim][BF ₄] | 6.9678 |

The set of amine-IL blend formulations serve a dual purpose: (i) to investigate the effect of ILs on the absorption capacity of amine-based blends, and (ii) to act as a supplementary set of blends in testing the research hypothesis. A detailed description of the experimental procedure is given in Appendix C. All solvent samples synthesized were mixed thoroughly to ensure the solutions to be as homogeneous as possible.

4.2. Data Analysis

The experimental data was analyzed to determine the amount of carbon dioxide (CO₂) gas absorbed by the absorbent for each experimental run. The process used to do this is similar to that discussed by Retief (2009) and is outlined below.

The first step is to determine the size of the absorbent sample loaded. For this study the absorbent sample size was specified to be 5ml for each sample analyzed. Next the void volume in the equilibrium cell is determined. This is the volume of vapour above the liquid sample loaded in the cell. The void volume is determined from Equation 4.2.2:

$$V_{void,i} = V_{cell} - V_{sample,i} \quad [4.2.1]$$

Where V_{void} is the void volume inside the equilibrium cell, V_{cell} is the total volume of the cell, V_{sample} is the volume of the absorbent sample injected into the cell, and the subscript i indicates the absorbent sample considered. The volume of the equilibrium cell was determined to be 25.87 ml (see Section 4.1). The initial and equilibrium state molar volumes of the absorbent are determined using the Peng-Robinson equation of state (PR-EOS):

$$P_{i,j} = \frac{RT}{(V_m)_{i,j} - b} - \frac{a\alpha(T)}{(V_m)_{i,j}^2 + 2b(V_m)_{i,j} - b^2} \quad [4.2.2]$$

Where:

$$a = \frac{0.45724R^2T_c^2}{P_c} \quad [4.2.3]$$

$$b = \frac{0.07780RT_c}{P_c} \quad [4.2.4]$$

$$\alpha(T) = [1 + \kappa(1 - \sqrt{T_r})]^2 \quad [4.2.5]$$

$$\kappa = 0.37464 + 1.54226\omega - 0.26992\omega^2 \quad [4.2.6]$$

Where P is the pressure inside the equilibrium cell, R is the universal gas constant, T is the temperature inside the cell, V_m is the molar volume of the absorbate, T_c and P_c are the critical temperature and pressure respectively, T_r is the reduced temperature, ω is the Pitzer acentric factor of the absorbate (i.e. CO_2), and the subscript j indicates the corresponding state (i.e. initial or equilibrium). The Pitzer acentric factor for CO_2 is 0.239 (Koretsky, 2004). The calculated initial and equilibrium state molar volumes are

used to determine the initial and equilibrium amounts of excess absorbent present in the cell respectively:

$$(n_{exc})_{i,ini} = \frac{V_{cell}}{(V_m)_{i,ini}} \quad [4.2.7]$$

$$(n_{exc})_{i,eq} = \frac{V_{void,i}}{(V_m)_{i,eq}} \quad [4.2.8]$$

Where n_{exc} is the excess absorbent present inside the cell, the subscript ini denotes the initial state and the subscript eq denotes the equilibrium state. With the amount of excess absorbent calculated for the initial and equilibrium states, the amount of gas absorbed by the absorbent for that experimental run is calculated as follow:

$$n_{abs,i} = |n_{ini,i} - n_{eq,i}| \quad [4.2.9]$$

From this, the rich loading of the absorbent sample (i.e. the maximum number of moles of CO₂ absorbed per mole of absorbent sample) is calculated as follow:

$$l_{rich,i} = \frac{n_{abs,i}}{n_{sample,i}} \quad [4.2.10]$$

Where l_{rich} is the rich loading, n_{abs} is the number of moles of CO₂ absorbed by the absorbent and n_{sample} is the number of moles of absorbent injected into the equilibrium cell. The number of moles of the absorbent was calculated using the weighted averages for the densities and molecular weights of the respective blend constituents. The rich loading of the various absorbent samples can be compared as it is dimensionless. Sample calculations based on Eqns. 4.2.1 to 4.2.10 are presented in Appendix F for one of the CO₂ absorption experiments conducted.

4.3. Experimental Setup Maintenance and Safety

All of the equipment used for experimental work was either new, or in excellent working order. Furthermore, the equipment was operated at low pressures (at or near atmospheric pressure). The gas regulator on the CO₂ feed cylinder was checked for leaks before commencing with experimental work. The temperature sensors were new and calibrated before commencing with experimental work (see Section G.2 of Appendix G for a summary of the temperature sensor calibration data). The pressure transmitter was new and calibrated by Wika® Instruments (see Section G.1 of Appendix G for the calibration certificate). The CO₂ vent line was extended out of the laboratory through a nearby window. In addition, ventilation by means of an extraction fan was permanently in operation. The prescribed PPE (i.e. safety glasses and latex gloves) were used.

4.4. Materials Used

High purity carbon dioxide gas (99.95%) from AirProducts was used as absorbate. A summary of the chemicals acquired for the experimental work, the quantity acquired, as well as the respective supplier is given in Table 4.3:

Table 4.3 – A summary of the chemicals acquired for the experimental work planned.

| Product | Purity | Quantity | Product Code | Supplier |
|---|--------|----------|---------------|----------------------|
| Piperazine | 99% | 100 g | P45907-100G | <i>Sigma-Aldrich</i> |
| Diisobutylamine | 99% | 250 ml | 135186-250ML | <i>Sigma-Aldrich</i> |
| 2,4-Dichlorobenzylamine | 98% | 25 g | D58406-25G | <i>Sigma-Aldrich</i> |
| Di-p-tolylamine | 97% | 5 g | 461083-5G | <i>Sigma-Aldrich</i> |
| sec-Butylamine | 99% | 100 ml | B89000-100ML | <i>Sigma-Aldrich</i> |
| Hexylamine | 99% | 100 ml | 219703-100ML | <i>Sigma-Aldrich</i> |
| Trioctylamine | n/a | 100 ml | 92830-100ML | <i>Sigma-Aldrich</i> |
| Ethanolamine (MEA) | 99% | 1 l | 110167-1L | <i>Sigma-Aldrich</i> |
| Potassium bicarbonate | n/a | 500 g | 60339-500G | <i>Sigma-Aldrich</i> |
| Tryptamine | 98% | 50 g | 193747-50G | <i>Sigma-Aldrich</i> |
| Auramine | n/a | 100 g | SAAR1202000DC | <i>Merck</i> |
| 2-(Dimethylamino)-ethanol (DMEA) | n/a | 100 ml | 8.03237.0100 | <i>Merck</i> |
| 1-Butyl-3-methylimidazolium tetrafluoroborate | n/a | 100 g | 711748-100G | <i>Sigma-Aldrich</i> |

5. Results & Discussion: Modeling

Three sets of solvents were identified for the purpose of this study: (i) a list of 296 amines obtained from the HSPiP database, (ii) the set of four ionic liquids recently presented by Abbott *et al.* (2011), and (iii) water. All of the simulations in the EquiSolv analysis package were done with CO₂ specified as the target solute. The dispersion, polar and hydrogen bond component values for CO₂ are 15.7 MPa^{0.5}, 6.3 MPa^{0.5} and 5.7 MPa^{0.5} respectively (Hansen, 2007). Material HSP values are typically presented in literature for a temperature and pressure of 25°C and 1 atm respectively. This temperature is significantly less than the operating temperatures typically found for CO₂ recovery processes, i.e. 60-70°C in the absorber column, and 110-120°C in the desorber column. Hence it is expected that predictions made based on HSP data obtained for operating temperature conditions would differ from predictions made based on the HSP data typically found in literature (i.e. at 25°C). Obtaining the HSP values for various temperature settings however proved to be a tedious and time-consuming process. Furthermore, the HSP values for the selected set of four ionic liquids are only available for a temperature of 25°C. Based on this, and considering the purpose of this study, it was decided to perform all simulations using the HSP values obtained for the default temperature and pressure conditions (i.e. 25°C and 1 atm). Future analysis however should be based on HSP data obtained for temperatures close to typical process operating conditions.

5.1. Estimating the Electrostatic (Ionic) Bond HSP Values

Ionic liquids (ILs) have recently started to be considered as a promising alternative to conventional alkanolamine solvents used for chemical CO₂ absorption processes. The dominating force in IL solutions is expected to be ionic molecular interactions. The respective IL ionic (electrostatic) bond energies are required to calculate the proposed ionic bond solubility parameter (δ_i). The ionic bond energies (E_i) for 74 commercially available ILs were quantified using quantum chemical calculations. The HyperChem program was used for all of the molecular orbital calculations. The ionic bond energy of each IL was quantified using four different algorithms. The algorithms, in ascending order of accuracy, are:

- Molecular mechanics (MM+);
- Semi-empirical calculations (AM1);

- Ab-Initio geometry optimization using a minimal basis set (STO-3G);
- Ab-Initio geometry optimization with a single point calculation using a small basis set including Møller-Plesset perturbation theory (3-21G + MP2).

Møller-Plesset perturbation theory provides improved accuracy of the total energy predicted by the standard Hartree-Fock approximation by considering specific electron-electron interactions between the cation and anion. The results for the cation, anion and component (i.e. entire IL molecule) molecular orbital calculations for the set of ionic liquids identified are summarized in Tables B.1 to B.5 (Appendix B). Typically an increase in the size of the quantum chemical base set applied translates to an increase in the accuracy of the calculation results. Increasing the size of the base set however also increases the calculation time. The medium base set (6-31G*) is the most commonly used in molecular orbital calculations. It usually provides the best tradeoff between accuracy and calculation time. Due to the time constraints of this study however, the minimum and small basis sets were chosen. Random sampling of the calculation results was done to investigate the accuracy gained by using a larger base set, i.e. applying the small basis set (3-21G) opposed to the minimal basis set (STO-3G). The accuracy gained was analyzed for cation, anion and component calculations. The results of the accuracy gain are summarized in Table 5.1. For the cation and anion calculations, the average gain in accuracy was found to be 1.144% and 1.880% respectively. The average gain in accuracy for the component calculations was found to be 4.867%. The average calculation time for all three component calculations (i.e. cation, anion and component) based on the minimal basis set approach was found to be about 8 hours. The average calculation time based on the small base set approach was found to be about 4 days. Based on this, the average gain in accuracy does not justify the increase in calculation time for any of the calculations. Hence the minimal basis set (STO-3G) was chosen as primary algorithm.

The lack of IL molar volume data in literature however prevented the δ_1 parameters from being calculated. Furthermore, to date there have been no efforts to quantify the HSP values of ILs except for that of Hansen and his team. Most studies only quantify the total (Hildebrand) solubility parameter values for the ILs they investigate. Marciniak (2010) recently presented the Hildebrand solubility parameter (δ) for 45 ILs. Recent work by Abbott *et al.* (2011) however quantified the Hildebrand solubility parameter, HSP component values and molar volumes for four ILs, including: 1-butyl-3-methylimidazolium chloride, 1-butyl-3-methylimidazolium hexafluorophosphate, 1-octyl-3-

methylimidazolium hexafluorophosphate and 1-butyl-3-methylimidazolium tetrafluoroborate. The molar volumes were used to calculate the δ_i parameters from the IL ionic bond energies calculated for each IL. For each IL, the collective set of partitioned solubility parameters was fitted to the proposed 4-set parameter model (Eqn. 3.18 in Section 3.3.3, Chapter 3). The results for the calculated δ_i parameters and respective model fitted coefficients of ionic interaction (c_i) are summarized in Table 5.2.

Table 5.1 – Summary of the accuracy gained by using a larger quantum chemical basis set, expressed as a percentage value.

| Ionic Liquid | Cation | | | Anion | | | Component | | |
|---|-----------------------------------|--|------------------------------|-----------------------------------|--|------------------------------|-----------------------------------|--|------------------------------|
| | E _{STO-3G} [kcal/mol] | E _{3-21G + MP2} [kcal/mol] | ΔE _{improve} [%] | E _{STO-3G} [kcal/mol] | E _{3-21G + MP2} [kcal/mol] | ΔE _{improve} [%] | E _{STO-3G} [kcal/mol] | E _{3-21G + MP2} [kcal/mol] | ΔE _{improve} [%] |
| 1,2,3-Trimethylimidazolium methyl sulfate | -212233.367 | -214574.655 | 1.103 | -456350.367 | -460489.463 | 0.907 | -668736.610 | -675150.555 | 0.959 |
| 1,2,3-Trimethylimidazolium trifluoromethanesulfonate | -212233.367 | -214574.655 | 1.103 | -593497.229 | -599138.964 | 0.951 | -805876.996 | -819234.007 | 1.657 |
| 1,2-Dimethyl-3-propylimidazolium bis(trifluoromethylsulfonyl)imide | -260656.064 | -263531.910 | 1.103 | -1128180.656 | -1138652.655 | 0.928 | -1388951.323 | -1402254.926 | 0.958 |
| 1,2-Dimethyl-3-propylimidazolium tris(trifluoromethylsulfonyl)methide | -260656.064 | -263531.910 | 1.103 | -1665187.797 | -1680512.734 | 0.920 | -1925912.978 | -1944200.126 | 0.950 |
| 1,3-Dimethylimidazolium methyl sulfate | -188013.718 | -191551.801 | 1.882 | -456350.367 | -460489.463 | 0.907 | -644504.390 | -650671.773 | 0.957 |
| 1-Allyl-3-methylimidazolium chloride | -235665.806 | -240120.527 | 1.890 | -285190.791 | -287053.451 | 0.653 | -520988.765 | -525414.544 | 0.849 |
| 1-Benzyl-3-methylimidazolium chloride | -330305.047 | -333991.402 | 1.116 | -285190.791 | -287053.451 | 0.653 | -615624.948 | -621113.319 | 0.892 |
| 1-Benzyl-3-methylimidazolium hexafluorophosphate | -330305.047 | -333991.402 | 1.116 | -580409.485 | -586215.710 | 1.000 | -910824.835 | -920281.477 | 1.038 |
| 1-Benzyl-3-methylimidazolium tetrafluoroborate | -330305.047 | -333991.402 | 1.116 | -261429.508 | -264518.720 | 1.182 | -591855.127 | -598592.651 | 1.138 |
| 1-Butyl-2,3-dimethylimidazolium chloride | -284865.802 | -288008.492 | 1.103 | -285190.791 | -287053.451 | 0.653 | -570181.262 | -575135.257 | 0.869 |
| 1-Butyl-2,3-dimethylimidazolium hexafluorophosphate | -284865.802 | -288008.492 | 1.103 | -580409.485 | -586215.710 | 1.000 | -865363.415 | -874314.880 | 1.034 |
| 1-Butyl-2,3-dimethylimidazolium tetrafluoroborate | -284865.802 | -288008.492 | 1.103 | -261429.508 | -264518.720 | 1.182 | -546394.680 | -550622.553 | 0.774 |
| 1-Butylpyridinium bromide | -250010.542 | -252774.518 | 1.106 | -1597261.406 | -1606525.405 | 0.580 | -1847430.093 | -1859396.704 | 0.648 |
| 1-Dodecyl-3-methylimidazolium iodide | -454321.540 | -459331.490 | 1.103 | -4301226.885 | -4322272.243 | 0.489 | -4755634.662 | -3902897.289 | 17.931 |
| 1-Ethyl-2,3-dimethylimidazolium chloride | -236445.892 | -239054.842 | 1.103 | -285190.791 | -287053.451 | 0.653 | -521762.328 | -526182.591 | 0.847 |
| 1-Ethyl-2,3-dimethylimidazolium ethyl sulfate | -236445.892 | -239054.842 | 1.103 | -480561.667 | -484969.245 | 0.917 | -717115.091 | -724105.362 | 0.975 |
| 1-Ethyl-2,3-dimethylimidazolium trifluoromethanesulfonate | -236444.774 | -239054.009 | 1.104 | -593497.229 | -599138.964 | 0.951 | -830046.772 | -838287.054 | 0.993 |
| 1-Ethyl-3-methylimidazolium acetate | -212226.661 | -214569.353 | 1.104 | -140592.467 | -93890.438 | 33.218 | -352956.950 | -356995.959 | 1.144 |
| 1-Ethyl-3-methylimidazolium bis(pentafluoroethylsulfonyl)imide | -212226.661 | -214569.353 | 1.104 | -1421211.134 | -1434996.329 | 0.970 | -1633546.449 | -1649652.467 | 0.986 |
| 1-Ethyl-3-methylimidazolium bis(trifluoromethylsulfonyl)imide | -212226.661 | -214569.353 | 1.104 | -1128180.656 | -1138652.655 | 0.928 | -1340526.904 | -1353275.982 | 0.951 |
| 1-Ethyl-3-methylimidazolium bromide | -212226.661 | -214569.353 | 1.104 | -1597261.406 | -1606525.405 | 0.580 | -1809639.308 | -1821167.006 | 0.637 |
| 1-Ethyl-3-methylimidazolium chloride | -212226.661 | -214569.353 | 1.104 | -285190.791 | -287053.451 | 0.653 | -497516.273 | -501709.214 | 0.843 |
| 1-Ethyl-3-methylimidazolium dicyanamide | -212226.661 | -214569.353 | 1.104 | -148016.490 | -149825.635 | 1.222 | -360365.543 | -364474.998 | 1.140 |
| 1-Ethyl-3-methylimidazolium ethyl sulfate | -212226.661 | -214569.353 | 1.104 | -480561.667 | -484969.245 | 0.917 | -692946.914 | -699617.609 | 0.963 |
| 1-Ethyl-3-methylimidazolium hexafluorophosphate | -212226.661 | -214569.353 | 1.104 | -580409.485 | -586215.710 | 1.000 | -792747.347 | -800859.581 | 1.023 |
| 1-Ethyl-3-methylimidazolium hydrogen sulfate | -212226.661 | -214569.353 | 1.104 | -432139.533 | -436014.012 | 0.897 | -644525.308 | -650654.357 | 0.951 |
| 1-Ethyl-3-methylimidazolium methanesulfonate | -212226.661 | -214569.353 | 1.104 | -410017.509 | -413601.105 | 0.874 | -622412.387 | -628270.326 | 0.941 |
| 1-Ethyl-3-methylimidazolium methyl sulfate | -212226.661 | -214569.353 | 1.104 | -456350.367 | -460489.463 | 0.907 | -668736.179 | -675139.029 | 0.957 |
| 1-Ethyl-3-methylimidazolium nitrate | -212226.661 | -214569.353 | 1.104 | -172545.703 | -174646.560 | 1.218 | -384882.912 | -389323.274 | 1.154 |
| 1-Ethyl-3-methylimidazolium tetrachloroaluminate | -212226.661 | -214569.353 | 1.104 | -1291236.008 | -1299339.681 | 0.628 | -1503531.589 | -1513984.507 | 0.695 |
| 1-Ethyl-3-methylimidazolium tetrafluoroborate | -212226.661 | -214569.353 | 1.104 | -261429.508 | -264518.720 | 1.182 | -473759.006 | -479172.308 | 1.143 |
| 1-Ethyl-3-methylimidazolium thiocyanate | -212226.661 | -214569.353 | 1.104 | -303824.303 | -306178.647 | 0.775 | -516141.716 | -520808.127 | 0.904 |
| 1-Ethyl-3-methylimidazolium tosylate | -212226.661 | -214569.353 | 1.104 | -552311.689 | -557513.863 | 0.942 | -764682.602 | -772187.590 | 0.981 |
| 1-Ethyl-3-methylimidazolium trifluoromethane | -212226.661 | -214569.353 | 1.104 | -593497.229 | -545839.014 | 8.030 | -805825.210 | -813788.882 | 0.988 |
| 1-Ethyl-3-methylimidazolium trifluoromethanesulfonate | -212226.661 | -214569.353 | 1.104 | -593497.229 | -599138.964 | 0.951 | -805830.765 | -813801.814 | 0.989 |
| 1-Hexyl-3-methylimidazolium chloride | -309064.714 | -312474.621 | 1.103 | -285190.791 | -287053.451 | 0.653 | -594354.167 | -599614.627 | 0.885 |
| 1-Hexyl-3-methylimidazolium hexafluorophosphate | -309064.714 | -312474.621 | 1.103 | -580409.485 | -586215.710 | 1.000 | -889584.725 | -592028.962 | 33.449 |
| 1-Hexyl-3-methylimidazolium tetrafluoroborate | -309064.714 | -312474.621 | 1.103 | -261429.508 | -264518.720 | 1.182 | -570597.092 | -453004.384 | 20.609 |
| 1-Hexyl-3-methylimidazolium trifluoromethanesulfonate | -309064.714 | -312474.621 | 1.103 | -593497.229 | -599138.964 | 0.951 | -902662.946 | -911689.193 | 1.000 |
| 1-Methyl-3-(3,3,4,4,5,5,6,6,7,7,8,8,8-tridecafluorooctyl)-imidazolium hexafluorophosphate | -1152482.221 | -1165419.960 | 1.123 | -580409.485 | -586215.710 | 1.000 | -1732978.659 | -210437.088 | 87.857 |
| Average Accuracy Gain | | | 1.144 | | | 1.880 | | | 4.867 |

Table 5.2 – Summary of the δ and c_i values calculated for the set of ILs considered.

| Ionic Liquid | δ [MPa ^{0.5}] | δ_D [MPa ^{0.5}] | δ_P [MPa ^{0.5}] | δ_H [MPa ^{0.5}] | δ_I [MPa ^{0.5}] | V_m [cm ³ /mol] | c_i |
|--------------------------|--------------------------------|----------------------------------|----------------------------------|----------------------------------|----------------------------------|------------------------------|----------|
| [bmim][Cl] | 35.0 | 19.1 | 20.7 | 20.7 | 48.6 | 175.0 | 0.001357 |
| [bmim][PF ₆] | 29.3 | 21.0 | 17.2 | 10.9 | 47.2 | 207.6 | 0.001273 |
| [omim][PF ₆] | 27.8 | 20.0 | 16.5 | 10.0 | 40.9 | 276.0 | 0.000353 |
| [bmim][BF ₄] | 31.5 | 23.0 | 19.0 | 10.0 | 46.3 | 201.4 | 0.001050 |
| | | | | | | Average: | 0.001009 |

From Table 5.2 it is clear that, for the set of ILs considered, the coefficient of ionic interaction (c_i) can be assumed a constant value of 0.001. This constant value was used to back-calculate the total (Hildebrand) solubility parameter (δ) for each of the ILs. The differences between the calculated and literature values of δ for each of the ILs are summarized in Table 5.3.

Table 5.3 – Summary of the error made by assuming a constant value of 0.001 for c_i for each of the ILs considered.

| | Literature | Calculated | Error |
|--------------------------|--------------------------------|--------------------------------|------------------|
| Ionic Liquid | δ [MPa ^{0.5}] | δ [MPa ^{0.5}] | ϵ_i [%] |
| [bmim][Cl] | 35.0 | 34.988 | 0.034 |
| [bmim][PF ₆] | 29.3 | 29.290 | 0.036 |
| [omim][PF ₆] | 27.8 | 27.819 | 0.070 |
| [bmim][BF ₄] | 31.5 | 31.498 | 0.005 |
| | | Average: | 0.036 |

For the set of ILs considered, the maximum error made by assuming a constant value of 0.001 for c_i was found to be 0.070%, with an average of 0.036%. This is significantly less than the 5% margin of error accepted for a 95% confidence level. Hence, the assumption of a constant value of 0.001 for c_i for this set of ILs is valid. Further work however is needed to quantify the molar volumes of ILs before the proposed model can be tested comprehensively.

5.2. Calculating the Solvent RED Values w.r.t. a Particular Target Solute

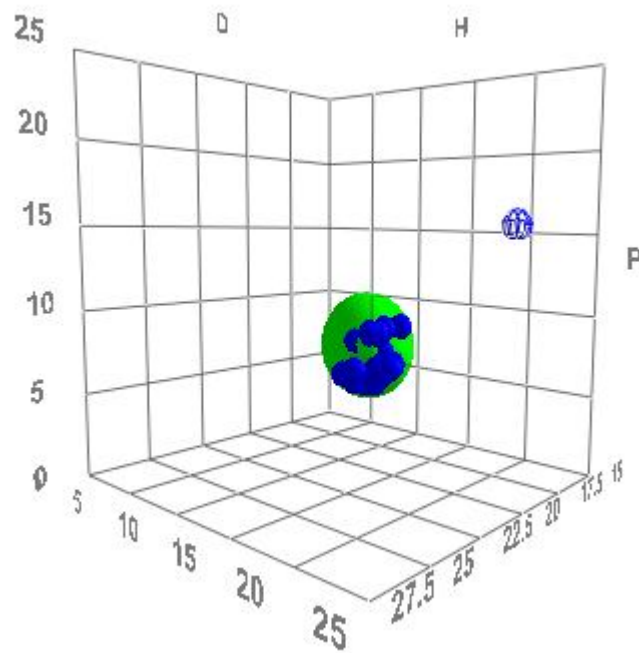
The EquiSolv program was used to calculate the REDs for the sets of solvents identified and rank them accordingly. RED results for the collective set of solvents (i.e. amines, ILs and water) are summarized in

Tables B.6 to B.10 (Appendix B). Solvents with an RED value between 0 and 1 are shown in Table 5.4. Also indicated in Table 5.4 is the RED value calculated for the alkanolamine conventionally used in chemical solvent solutions (i.e. monoethanolamine (MEA)).

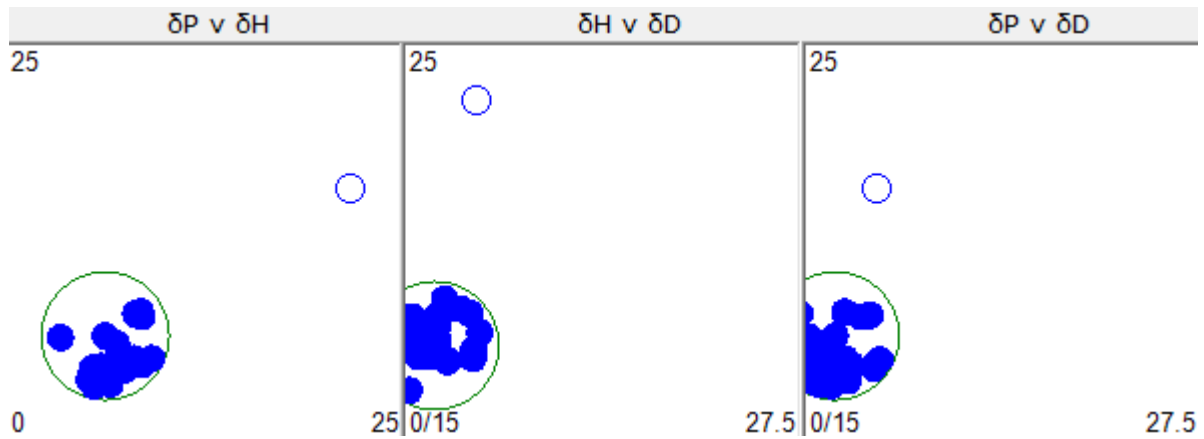
Table 5.4 – Summary of the solvents found with a calculated RED value between 0 and 1.

| Solvent Name | δ_D [MPa ^{0.5}] | δ_P [MPa ^{0.5}] | δ_H [MPa ^{0.5}] | δ_T [MPa ^{0.5}] | V_m [cm ³ /mol] | R_a [MPa ^{0.5}] | RED |
|--|----------------------------------|----------------------------------|----------------------------------|----------------------------------|------------------------------|-----------------------------|---------------|
| 1,1-Dimethylpropylamine | 15.1 | 5.8 | 6.4 | 0.0 | 114.3 | 1.4765 | 0.4474 |
| Pentylamine | 15.6 | 4.7 | 6.7 | 0.0 | 115.4 | 1.8974 | 0.5750 |
| Heptylamine | 15.7 | 4.4 | 6.4 | 0.0 | 148.4 | 2.0248 | 0.6136 |
| Diallyl Amine | 15.6 | 4.5 | 6.7 | 0.0 | 124.3 | 2.0688 | 0.6269 |
| 2-Ethylhexyl Amine | 15.7 | 4.2 | 6.1 | 0.0 | 163.3 | 2.1378 | 0.6478 |
| Methyl-Propylamine | 15.2 | 4.2 | 5.7 | 0.0 | 102.8 | 2.3259 | 0.7048 |
| Hexylamine | 15.8 | 4.0 | 6.1 | 0.0 | 132.1 | 2.3431 | 0.7100 |
| sec-Butylamine | 15.7 | 4.6 | 7.4 | 0.0 | 98.9 | 2.4042 | 0.7285 |
| (+)-sec-Butylamine | 15.7 | 4.6 | 7.4 | 0.0 | 98.9 | 2.4042 | 0.7285 |
| Methylethylamine | 15.0 | 4.4 | 6.2 | 0.0 | 85.8 | 2.4125 | 0.7311 |
| 2-Methylbutylamine | 15.8 | 4.2 | 6.9 | 0.0 | 115.1 | 2.4269 | 0.7354 |
| 3-Methylbutylamine | 15.2 | 4.4 | 7.0 | 0.0 | 116.3 | 2.5100 | 0.7606 |
| Ethylpropylamine | 15.3 | 3.9 | 5.3 | 0.0 | 119.5 | 2.5612 | 0.7761 |
| 1-Ethylpropylamine | 15.3 | 3.9 | 5.3 | 0.0 | 119.5 | 2.5612 | 0.7761 |
| Isobutylamine | 15.0 | 4.9 | 7.5 | 0.0 | 100.1 | 2.6758 | 0.8108 |
| Octylamine | 16.1 | 3.9 | 4.8 | 0.0 | 165.1 | 2.6851 | 0.8137 |
| N-Chlorodimethylamine | 16.0 | 7.8 | 7.9 | 0.0 | 87.4 | 2.7295 | 0.8271 |
| Isopropyl Amine (2-Propan Amine) | 14.8 | 4.4 | 6.6 | 0.0 | 86.8 | 2.7677 | 0.8387 |
| 1,3-Propanediamine, N,N-Diethyl- | 15.9 | 4.5 | 7.8 | 0.0 | 158.7 | 2.7946 | 0.8468 |
| Methyl-Butylamine | 15.3 | 3.5 | 5.1 | 0.0 | 119.8 | 2.9732 | 0.9010 |
| Nonylamine | 16.1 | 3.6 | 4.7 | 0.0 | 181.3 | 2.9883 | 0.9055 |
| Bis-(2,2,2-Trifluoro-Ethyl)-Amine | 14.4 | 5.9 | 4.2 | 0.0 | 135.0 | 3.0282 | 0.9176 |
| N,N-Dichloromethyl Amine | 16.5 | 7.5 | 8.0 | 0.0 | 90.8 | 3.0480 | 0.9236 |
| Undecylamine | 16.1 | 3.5 | 4.8 | 0.0 | 214.3 | 3.0480 | 0.9236 |
| N-Ethyl-2-Methylallylamine | 15.4 | 3.3 | 6.0 | 0.0 | 128.9 | 3.0741 | 0.9315 |
| N,N'-Dimethylpiperazine | 16.9 | 4.4 | 5.4 | 0.0 | 130.2 | 3.0757 | 0.9320 |
| n-Butyl Amine | 16.2 | 4.5 | 8.0 | 0.0 | 98.8 | 3.0871 | 0.9355 |
| Methylheptylamine | 15.6 | 3.2 | 5.0 | 0.0 | 169.0 | 3.1843 | 0.9649 |
| Methylisopropylamine | 14.9 | 3.5 | 5.7 | 0.0 | 102.9 | 3.2249 | 0.9772 |
| Bornylamine | 16.9 | 4.3 | 4.9 | 0.0 | 166.8 | 3.2249 | 0.9772 |
| 2,2,2-Trifluoro-Ethylamine | 14.6 | 7.7 | 7.6 | 0.0 | 81.5 | 3.2265 | 0.9777 |
| Ethanamine, 2,2-Dufluoro-N,N-Bis(Trifluoromethyl)- | 14.9 | 6.2 | 2.9 | 0.0 | 146.5 | 3.2265 | 0.9777 |
| Propylisopropylamine | 15.2 | 3.3 | 5.0 | 0.0 | 136.6 | 3.2388 | 0.9815 |
| N,N-Dichloroethyl Amine | 16.8 | 7.6 | 7.7 | 0.0 | 98.3 | 3.2450 | 0.9833 |
| Propyl Amine | 16.0 | 4.9 | 8.6 | 0.0 | 83.0 | 3.2757 | 0.9926 |
| Cyclopentylamine | 17.1 | 4.8 | 6.5 | 0.0 | 97.9 | 3.2757 | 0.9926 |
| Ethanolamine (MEA) | 17.0 | 15.5 | 21.0 | 0.0 | 60.3 | 18.0413 | 5.4671 |

From Table 5.4 it is clear that, based on HSP theory, MEA on its own is not an ideal solvent for CO₂. The set of solvents with RED values less than 1 represents the group predicted to have the best potential for absorbing CO₂. The HSPiP program was used to visualize the above set of solvents w.r.t. the target solute (CO₂) in a 3D viewing space. The visualization is shown in Figure 5.1.



(a)



(b)

Figure 5.1 – (a) Screenshot of the 3D HSPiP solvent-solute analysis of the solvents with RED values between 0 and 1 (with CO₂ selected as the target solute), (b) Screenshot of the planar analysis of the 3D rendering.

From Figure 5.1 it is clear that all of the solvents with RED values less than 1 are positioned within the solubility sphere, i.e. within the interaction radius of the target solute. It is also clear that MEA falls well

outside the interaction radius of the target solute (i.e. CO₂). This is the primary advantage of the HSP approach: only 3 values are required for each solvent to quickly screen through large datasets and identify the solvents best suited for the desired application. Furthermore, it can easily be visualized in a 3D viewing space. The simplicity of the model theory is its key feature. The relatively small differences in HSP component values (δ_D , δ_P and δ_H) between the solvents and the target solute are an indication that all of the above solvents are expected to be “good” solvents for absorbing CO₂. All solvents with an RED value greater than 1 are classified as “bad” solvents. The solvents presented in Table 5.4 can be isolated and analyzed separately to refine the search for an optimal solvent blend formulation. The remaining solvents (i.e. with RED values greater than 1) should however not be neglected entirely. It is still possible that a specific combination of “bad” solvents could yield a “good” solvent blend.

5.3. Searching for Solvent Blend Formulations w.r.t. a Particular Target Solute

The EquiSolv solvent optimizer offers numerous options to be specified in the search for an optimal solvent blend formulation, translating to countless possible design configurations. It would not be practically feasible to validate the model hypothesis for every possible design configuration. For the purpose of this study, the design configuration was specified as follow:

- Gauss-Seidel iteration with the calculation loop set to terminate at either 10000 iterations or a 5% error estimate;
- Analyzing for a 2-component blend;
- Using a square calculation algorithm;
- Excluding the proposed δ_1 parameter;
- Analyzing for up to a 25% variance from ideality;
- Excluding the test for the blend component inter-miscibility;
- Rounding the final values to 4 significant numbers;
- Searching for amine-amine based blend formulations with CO₂ as the target solute.

For this setup configuration the EquiSolv solvent optimizer analyzed a total of 88209 possible blend formulations and found 2685 formulations for which the HSP values are within specification. The program was able to screen through the entire set of 88209 blend formulations in a period of 10

minutes. This compares extremely well with the HSPiP program taking up to 5 minutes to perform a similar search for a significantly smaller dataset.

Six solvent blends were randomly selected from the predicted 2685 formulations to be used in the model hypothesis tests. The blend formulations were randomly selected based on their respective RED values. The selection was split into three categories: (i) two of the blends should have RED values close to 0, (ii) the next two should have RED values close to 0.5, and (iii) the final two blends should have RED values close to 1. As it would not be practical to include the entire list of 2685 predicted formulations in this document, a condensed selection containing the six randomly selected blends (highlighted in red) is presented in Table B.11 (Appendix B). A summary of the six selected blend formulations as well as their predicted volume percentage contributions and respective HSP values are shown in Table 5.5. The blends are shown in descending order of expected CO₂ absorption capacity (ranked numbers 1 to 6 respectively).

Table 5.5 – Summary of the six blend formulations random selected from the EquiSolv solvent optimizer predictions.

| Rank _{Pred} | Constituent 1 | Constituent 2 | x ₁ [vol%] | x ₂ [vol%] | x ₃ [vol%] | δ _D [MPa ^{0.5}] | δ _P [MPa ^{0.5}] | δ _H [MPa ^{0.5}] | RED |
|----------------------|-----------------|------------------------------|-----------------------|-----------------------|-----------------------|--------------------------------------|--------------------------------------|--------------------------------------|--------|
| 1 | Di-p-Tolylamine | Dimethyl ethanolamine (DMEA) | 0.5597 | 0.0723 | 0.6320 | 15.70 | 6.30 | 5.70 | 0.0019 |
| 2 | Trioctylamine | Monoethanolamine (MEA) | 0.8339 | 0.0934 | 0.9273 | 15.70 | 6.30 | 5.70 | 0.0037 |
| 3 | sec-Butylamine | Auramine | 0.3345 | 0.4309 | 0.7654 | 15.80 | 6.30 | 5.00 | 0.2179 |
| 4 | Tryptamine | Diisobutylamine | 0.5006 | 0.2962 | 0.7968 | 15.70 | 5.70 | 6.10 | 0.2235 |
| 5 | Auramine | Hexylamine | 0.2813 | 0.5545 | 0.8358 | 15.70 | 5.50 | 5.00 | 0.3257 |
| 6 | Hexylamine | 2,4-Dichlorobenzylamine | 0.0902 | 0.6799 | 0.7701 | 17.10 | 6.30 | 6.40 | 0.8614 |

From Table 5.5, the predicted HSP values for the first two blends, i.e. Di-p-tolylamine mixed with Dimethyl ethanolamine (DMEA) and Trioctylamine mixed with Monoethanolamine (MEA), appear to be an exact match to the HSP values of the target solute (CO₂). The non-zero RED values (0.0019 and 0.0037 respectively) however indicate that their HSP values are not an exact match to the HSP values of CO₂. The blend HSP values presented in Table 5.5 are rounded to one significant number. This would explain why the first two blends would appear to be ideal solvents for CO₂, yet both have non-zero RED values. Nevertheless, the variances from zero RED values for both blends are very small. Based on this, it is expected that both of these blends will have a high CO₂ absorption capacity. From their respective RED values, blend numbers 3 and 4 (sec-Butylamine mixed with Auramine, and Tryptamine mixed with

Diisobutylamine) are expected to have measurably lower CO₂ absorption capacities than blend numbers 1 and 2. Similarly, blend numbers 5 and 6 (Auramine mixed with Hexylamine, and Hexylamine mixed with 2,4-Dichlorobenzylamine) are expected to have measurably lower CO₂ absorption capacities than blend numbers 3 and 4. Hence, for the research hypothesis to be successfully rejected, results from the experimental work (see Chapter 6) should rank the six blends, in decreasing order of CO₂ absorption capacity.

From Table 5.5 it can also be seen that, for all six blend formulations, the sum of the volume percentage contributions (x_i) does not add up to 1 (i.e. 100vol%). This error is due to an invalid assumption made in deriving the iterative algorithm used in the solvent optimizer. A block flow diagram of the iterative algorithm used is shown in Figure 5.2.

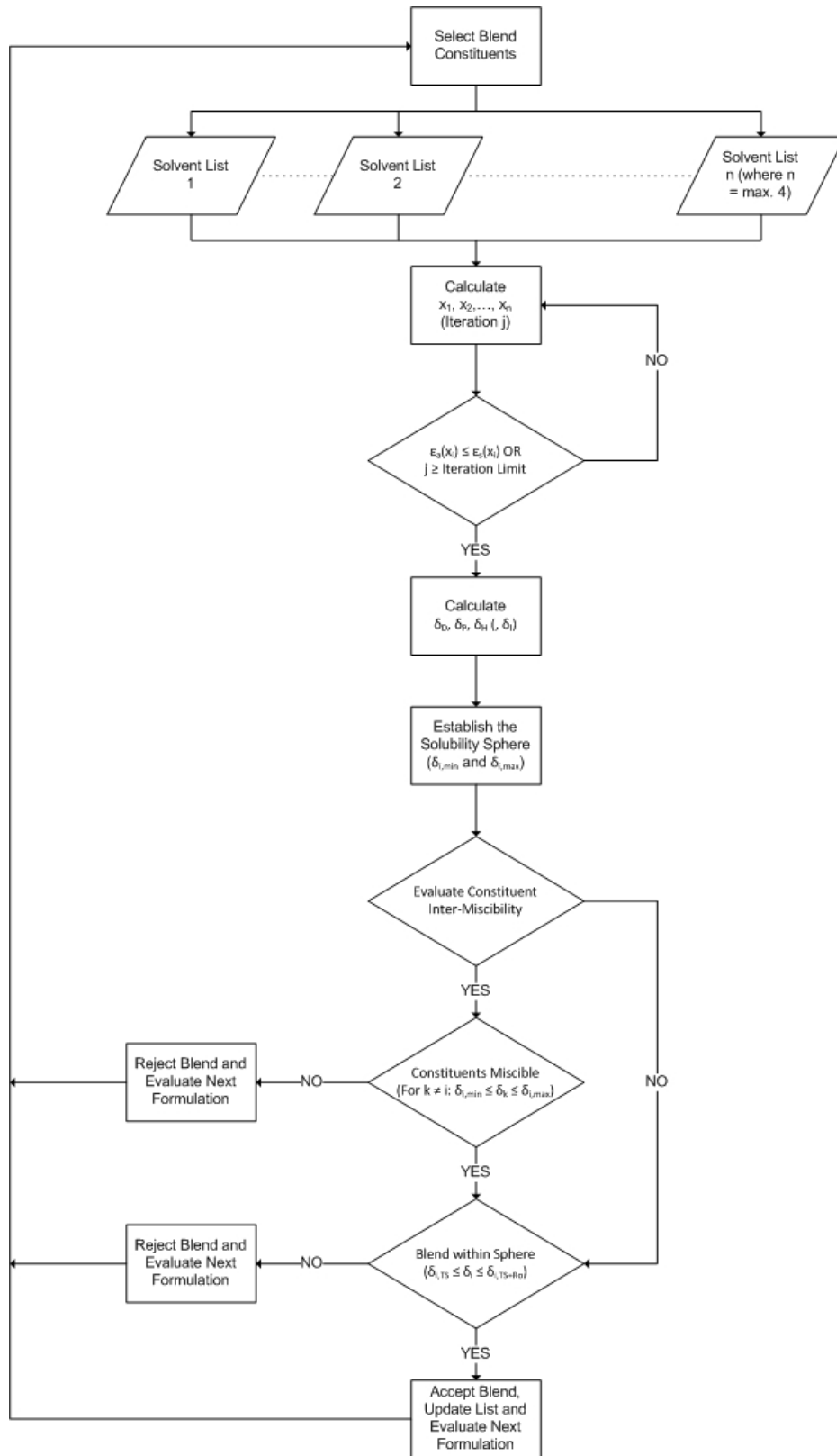


Figure 5.2 – A block flow diagram of the original iterative algorithm used by the EquiSolv solvent optimizer for Gauss-Seidel iteration.

From Figure 5.2 it is clear that the algorithm will accept blend formulations irrespective of their x_t values, as long as their HSP component values are positioned within the solubility sphere. The algorithm never check's the sum of the volume percentage contributions (x_t). This is due to the primary assumption made in deriving the algorithm. The algorithm was derived based on three fundamental assumptions, including:

- The sum of the volume percentage contributions (x_t) for all blend formulations analyzed amount to unity;
- From the first assumption, the primary stop criterion (ϵ_s) is based on the respective constituent volume percentage contributions (x_i);
- Blend formulations are accepted (or rejected) base on the inter-miscibility of the constituents (if evaluated) and/or the relative position of the blend HSP values w.r.t. the solubility sphere (i.e. whether or not the blends are located inside the solubility sphere).

From the results presented in Table 5.5 it is clear that the first assumption is invalid. The sum of the volume percentage contributions (x_t) does not amount to unity for any of the six blend formulations predicted. From this it can be concluded that, for all six formulations, the calculation loops were terminated prematurely (i.e. before the values of the respective constituent volume percentage contributions (x_i) have attained their true value). Hence it can be concluded that the second assumption is also invalid. The third assumption however holds true irrespective of the validity of the first to assumptions. Although the first two assumptions are invalid, it has no effect on the fundamental theory of the HSP approach (i.e. ranking the performance of solvents based on their RED values). It merely affects the constituents of the blend formulations predicted. Hence the EquiSolv program retains its credibility. After studying the model results, a new algorithm is proposed for the iterative process. The assumptions made in deriving the new algorithm are as follow:

- The sum of the volume percentage contributions (x_t) does not amount to unity for all possible blend formulations;
- From the first assumption, the primary stop criterion (ϵ_s) is based on the blend RED value (i.e. searching for an absolute minimum RED value);
- As a first stage of evaluation, a blend will be accepted if the volume percentage contribution for each constituent (x_i) is between 0 and 1, and the sum of the volume percentage contributions (x_t) is equal to 0;

- Blends that pass the first stage of evaluation will be accepted (or rejected) based on the inter-miscibility of the constituents (if evaluated) and/or the relative position of the blend HSP values w.r.t. the solubility sphere (i.e. whether or not the blends are located inside the solubility sphere).

A block flow diagram of the revised iterative algorithm is shown in Figure 5.3. The revised iterative algorithm will ensure that the sum of the volume percentage contributions for all predicted formulations will amount to unity. Furthermore, as with the current algorithm, the HSP values for all of the predicted formulations will be positioned within the solubility sphere. It is recommended that the algorithm currently used by the EquiSolv solvent optimizer (Figure 5.2) be upgraded to the revised algorithm (Figure 5.3). Upgrading the EquiSolv program to the revised algorithm however would require a significant amount of time for development.

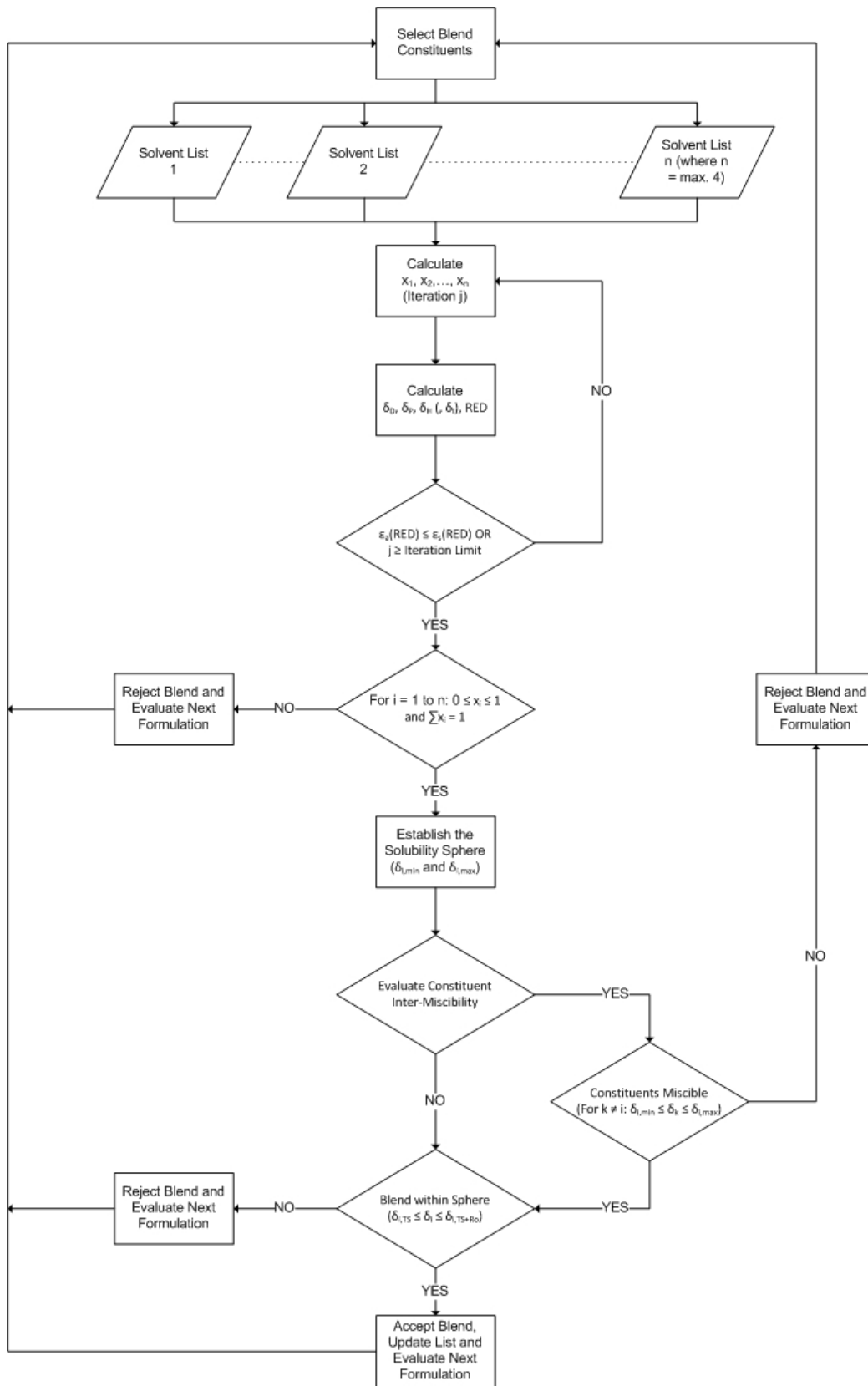


Figure 5.3 – A block flow diagram of the updated iterative algorithm.

The fundamental model theory of the HSP approach is based on minimizing the difference in HSP component values between materials, irrespective of the materials and/or compositions selected. Hence, the current algorithm used by the EquiSolv solvent optimizer retains its credibility. The blend formulations predicted are not incorrect; the sum of their volume percentage contributions might just not amount to unity. To correct for this, the volume percentage contributions can either be normalized to unity (i.e. $x_i = 1$) or balanced with an additional constituent (e.g. water). Both of these approaches were used to balance the volume percentage contributions for each of the six blend formulations. The results for the normalized approach are presented in Table 5.6.

Table 5.6 – Summary of the six blend formulations randomly selected normalized to a sum of volume fractions equal to 1.

| Rank _{Pred} | Constituent 1 | Constituent 2 | x_1 [vol%] | x_2 [vol%] | x_i [vol%] | δ_D [MPa ^{0.5}] | δ_P [MPa ^{0.5}] | δ_H [MPa ^{0.5}] | RED |
|----------------------|-----------------|------------------------------|--------------|--------------|--------------|----------------------------------|----------------------------------|----------------------------------|--------|
| 1 | Trioctylamine | Monoethanolamine (MEA) | 0.8993 | 0.1007 | 1.0000 | 16.30 | 5.00 | 6.70 | 0.6072 |
| 2 | Auramine | Hexylamine | 0.3366 | 0.6634 | 1.0000 | 17.20 | 6.00 | 5.50 | 0.9002 |
| 3 | Tryptamine | Diisobutylamine | 0.6283 | 0.3717 | 1.0000 | 17.60 | 6.40 | 6.80 | 1.1955 |
| 4 | sec-Butylamine | Auramine | 0.4370 | 0.5630 | 1.0000 | 18.00 | 7.20 | 5.70 | 1.4204 |
| 5 | Hexylamine | 2,4-Dichlorobenzylamine | 0.1171 | 0.8829 | 1.0000 | 19.50 | 7.70 | 7.10 | 2.3554 |
| 6 | Di-p-Tolylamine | Dimethyl ethanolamine (DMEA) | 0.8856 | 0.1144 | 1.0000 | 19.70 | 5.30 | 5.40 | 2.4370 |

From Table 5.6, it is clear that the x_i value for each blend amounts to 1. Altering the blend compositions does however change the blend HSP component values, and by default their RED values. Hence, the ranking position of each blend's expected CO₂ absorption capacity must be revised. The blends are shown in decreasing order of expected CO₂ absorption capacity. The results for the alternative approach (i.e. including an additional constituent to balance the volume percentage contributions) are presented in Table 5.7. For the purpose of this study water was selected as the additional constituent in all six solvent formulation

Table 5.7 – Summary of the six blend formulations randomly selected balanced with water to a sum of volume fractions equal to 1.

| Rank _{Pred} | Constituent 1 | Constituent 2 | Constituent 3 | x_1 [vol%] | x_2 [vol%] | x_3 [vol%] | x_i [vol%] | δ_D [MPa ^{0.5}] | δ_P [MPa ^{0.5}] | δ_H [MPa ^{0.5}] | RED |
|----------------------|-----------------|------------------------------|---------------|--------------|--------------|--------------|--------------|----------------------------------|----------------------------------|----------------------------------|--------|
| 1 | Trioctylamine | Monoethanolamine (MEA) | Water | 0.8339 | 0.0934 | 0.0727 | 1.0000 | 16.20 | 6.50 | 13.10 | 2.2735 |
| 2 | Auramine | Hexylamine | Water | 0.2813 | 0.5545 | 0.1642 | 1.0000 | 16.90 | 8.50 | 17.90 | 3.8134 |
| 3 | Tryptamine | Diisobutylamine | Water | 0.5006 | 0.2962 | 0.2032 | 1.0000 | 17.20 | 9.20 | 20.00 | 4.5174 |
| 4 | sec-Butylamine | Auramine | Water | 0.3345 | 0.4309 | 0.2346 | 1.0000 | 17.40 | 10.00 | 21.10 | 4.9099 |
| 5 | Hexylamine | 2,4-Dichlorobenzylamine | Water | 0.0902 | 0.6799 | 0.2299 | 1.0000 | 18.60 | 10.20 | 21.20 | 5.1612 |
| 6 | Di-p-Tolylamine | Dimethyl ethanolamine (DMEA) | Water | 0.5597 | 0.0723 | 0.3680 | 1.0000 | 18.30 | 10.60 | 26.00 | 6.4779 |

From Table 5.7 it is clear that the x_i values for all six blends amount to 1. Similar to the normalized approach; altering the blend compositions change the HSP component values. The rank of each blend's expected CO₂ absorption capacity must be revised again. Again the blends are shown in decreasing order of expected CO₂ absorption capacity.

The predicted blend compositions were used to synthesize the six blend formulations for the water-balanced case (Table 5.7). The synthesized blends were used to test the research hypothesis. For the null hypothesis (H_0) to be rejected, the ranking of the six blends, in decreasing order of experimentally measured CO₂ absorption capacity, should match the predicted order of expected CO₂ absorption capacity. The experimental results are presented and discussed in Chapter 6.

5.4. Using the EquiSolv Quick Blend Calculator

The EquiSolv quick blend calculator is available in two versions, i.e. (i) the option to calculate both the HSP values and composition of a specific blend formulation, and (ii) the option to calculate the HSP values of a specific blend formulation for a given composition. For the purpose of this study, the latter was used to calculate the HSP component values for the 30wt% aqueous MEA solution conventionally used in CO₂ absorption processes. The algorithms used in the EquiSolv program are all based on volume percentage contributions (i.e. vol%). Hence, the composition of the MEA solution had to be converted from weight percentage to volume percentage contributions. The results for the volume percentage contributions are presented in Table 5.8.

Table 5.8 – Results for converting the conventional 30wt% MEA solution composition to volume percentage contributions.

| | y_i [wt%] | m_i [g] | ρ_i [g/cm ³] | V_i [cm ³] | x_i [vol%] |
|------------------|-------------|------------|-------------------------------|--------------------------|--------------|
| MEA | 0.3 | 30 | 1.012 | 29.644 | 0.298 |
| H ₂ O | 0.7 | 70 | 1.000 | 70.000 | 0.702 |
| Total | 1 | 100 | - | 99.644 | 1 |

The volume percentage contributions (x_i) presented in Table 5.8 (i.e. 0.298 and 0.702 for MEA and water respectively) were used to specify the composition of the aqueous MEA solution in the quick blend

calculator. A square calculation algorithm was applied, with the proposed δ_i parameter excluded from the calculation. The results for the HSP component values calculated for the blend are presented in Table 5.9. The HSP values for CO₂ are also shown as comparison to the calculated blend HSP values.

Table 5.9 – Summary of HSP values calculated for the conventional 30wt% MEA solution using the quick blend calculator.

| | x_i [vol%] | δ_D [MPa ^{0.5}] | δ_P [MPa ^{0.5}] | δ_H [MPa ^{0.5}] |
|------------------|--------------|----------------------------------|----------------------------------|----------------------------------|
| MEA | 0.298 | 17.0 | 15.5 | 21.0 |
| H ₂ O | 0.702 | 15.5 | 16.0 | 42.3 |
| Blend | | 15.7 | 15.9 | 37.3 |
| CO ₂ | | 15.7 | 6.3 | 5.7 |

From Table 5.9, it is clear that the dispersion bond parameter (δ_D) calculated for the blend is an exact match to that of CO₂. The values calculated for the polar and hydrogen bond parameters (δ_P and δ_H respectively) of the blend vary significantly from the δ_P and δ_H parameters of CO₂. There is a 152% difference between the δ_P parameters for the blend and CO₂ respectively, and a 554% difference between the δ_H parameters. The RED value calculated for the blend is 9.99. Based on HSP theory, this formulation is classified as an extremely poor solvent for CO₂. Industry applications of the conventional 30wt% aqueous MEA solvent to capture CO₂ however suggest otherwise, achieving CO₂-capture rates up to 90% and rich stream loadings of 0.49 mol CO₂/mol solvent (Oexmann et al., 2008). There could be a number of explanations for this contradiction, including:

- The HSP analysis was conducted with parameter values obtained for a temperature of 25°C whilst industrial applications are operated at temperatures in the range 60-110°C (Wang et al., 2010);
- HSP theory considers only the equilibrium thermodynamics, neglecting the effects of chemical reactions between the amine and CO₂, as well as between the water and CO₂.

HSP parameter values decrease with an increase in temperature (see Section 3.3.2.3 in Chapter 3). Hence, it is expected that increasing the temperature would decrease the difference between the HSP values of the MEA blend and CO₂ respectively. To investigate the effect of temperature on the model predictions, the HSPiP program was used to obtain the adjusted HSP values for MEA and water at 60°C and 110°C. Results from the HSPiP program suggests that the HSP values for CO₂ remains unchanged for these changes in temperature (i.e. $\delta_D = 15.7$ MPa^{0.5}, $\delta_P = 6.3$ MPa^{0.5} and $\delta_H = 5.7$ MPa^{0.5}). The altered HSP

values for MEA and water was used to calculate the blend HSP values at 60°C and 110°C. The results for the HSP values as well as the respective RED values are presented in Table 5.10.

Table 5.10 – Summary of the quick blend calculator predictions for the conventional 30wt% MEA solution at 60 and 110°C.

| Temperature [°C] | Material | δ_D [MPa ^{0.5}] | δ_P [MPa ^{0.5}] | δ_H [MPa ^{0.5}] | RED |
|------------------|------------------|----------------------------------|----------------------------------|----------------------------------|--------|
| 60 | MEA | 16.4 | 15.3 | 19.8 | |
| | H ₂ O | 14.8 | 15.7 | 39.8 | |
| | Blend | 15.29 | 15.58 | 35.05 | 9.3327 |
| 110 | MEA | 15.5 | 15 | 18.1 | |
| | H ₂ O | 13.9 | 15.3 | 36.1 | |
| | Blend | 14.4 | 15.21 | 31.82 | 8.4003 |

From Table 5.10 it is clear that the blend HSP values do decrease at the increased temperature conditions, hence the decreased RED values. The blend RED values for both temperature increments (60°C and 110°C) are still extremely high. Based on this, it can be concluded that the contradiction discussed earlier is due to the HSP theory neglecting the effects of chemical reactions between materials. CO₂ reacts with aqueous amine solutions to form either bicarbonate or carbamate byproducts, or both (da Silva & Svendsen, 2007). These reactions could have a significant effect on the dissolution behaviour of CO₂ absorbing into the solvent. HSP theory cannot predict the effects of such interactions on the dissolution behaviour of materials in each other. The possibility of chemical reactions between materials should be considered when applying partial solubility parameter theory to screen solvents.

The HSP theory can however be used to explain the high energy requirements involved with the conventional 30wt% MEA solvent. The HSP values presented in Tables 5.9 and 5.10 show large differences between the δ_P and δ_H parameters calculated for the blend and CO₂ respectively. HSP theory states that increasing differences between the parameters of materials translate to increased energy requirements to break the individual bonds and create holes in the solvent for the solute to dissolve in. Hence, the high RED values indicate that a significant amount of energy is required to absorb (or desorb) CO₂ in (or from) the solvent.

Clearly there are serious limitations to the HSP approach. It should be kept in mind however that the partial solubility parameter approach is intended to be used as a simplified solvent screening method, and not as an all-encompassing process design model. Ideally, the solubility parameter theory should be integrated with a dynamic process design model. Such a model would be able to analyze and find the absolute optimal solvent (formulation) for the desired application.

6. Results & Discussion: Experimental

The experimental plan was structured to test the research hypothesis through random solvent sample CO₂ absorption experiments. The plan was devised into three stages: (i) reference sample tests, (ii) hypothesis validation tests, and (iii) ionic liquid (IL) sample tests. All of the experiments were conducted at a temperature of 25°C and a pressure of 1 atm. The purpose of the reference sample tests is to validate the experimental setup and procedure. This is done by comparing the measured sample CO₂ absorption capacity to data presented in literature.

The hypothesis validation tests will be used to either reject or accept the research hypothesis. The null hypothesis (H₀) and alternative hypothesis (H₁) for this study was formulated as follow:

H₀: Partial solubility parameters cannot be used to accurately describe the equilibrium behaviour of carbon dioxide (CO₂) reactively absorbing into task specific designed solvents.

H₁: It is possible to use partial solubility parameters to predict the equilibrium behaviour of CO₂ reactively absorbing into task specific designed solvents.

A set of solvent blend formulations was randomly selected from predictions based on partial solubility parameter theory, and ranked in decreasing order of expected CO₂ absorption capacity. To conclusively reject the null hypothesis, the measured CO₂ absorption capacities should match the predicted ranking order.

Three ionic liquids were selected for preliminary CO₂ absorption tests. The purpose of the experiments is to investigate both the absorption capacities of the ILs themselves, as well as the effect of including ILs in amine-based blends on the absorption capacity of such blends. A set of four amine-IL blends was synthesized to investigate the phenomenon of the latter. Results from these experiments served as supplement to the hypothesis tests.

6.1. Reference Solvent Sample Results

Three solvent blends commonly used in industry to separate CO₂ from gas streams were selected as reference solvents. The main purpose of the reference solvents is to set a standard to which the performance of all further solvent blends is compared. Another purpose of the reference solvents is to compare their absorption performance measured using the experimental setup, to the performance values found in literature for the same solvent blends. The three blends selected include:

- An aqueous solution of 30wt% monoethanolamine (MEA);
- An aqueous solution of 30wt% potassium bicarbonate (K₂CO₃);
- An aqueous solution of 22.1wt% K₂CO₃ and 13.8wt% piperazine (PZ).

The typical rich loading values (mol CO₂/mol solvent) found in literature for these solvent blends are 0.49, 1.612 and 1.101 respectively (Oexmann et al., 2008). For the first experimental run, an aqueous solution of 30wt% MEA was injected into a pure CO₂ atmosphere and allowed to interact for a period of 30000 seconds (about 8 hours). The main purpose of the first run was to investigate the time required for the system to attain a state of equilibrium. From the pressure versus time (P-v-t) data it was concluded that this is achieved within a period of 5000 seconds (about 80 minutes). A cropped section view of the complete P-v-t graph is shown for the period 0-2000 seconds (Figure 6.1).

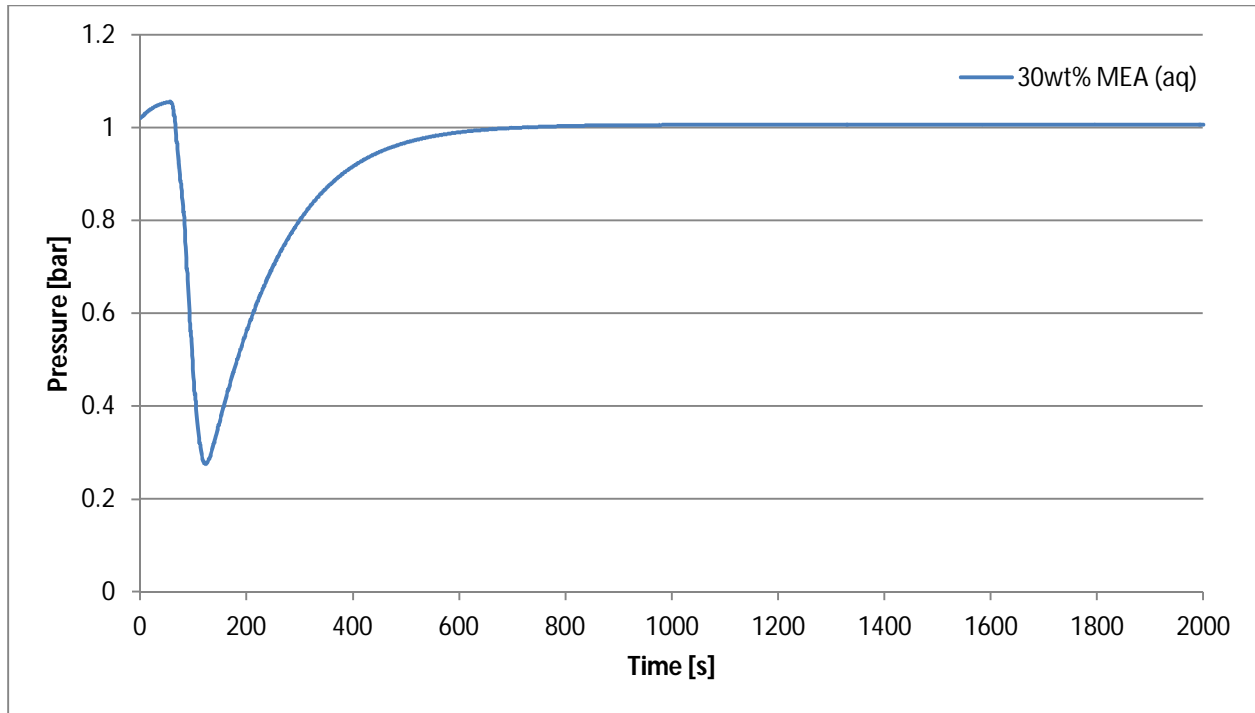


Figure 6.1 – A cropped section view of the P-v-t graph for Run 1 (30wt% MEA (aq) exposed for 50000s).

From Figure 6.1 it can be seen that this system attains a state of equilibrium approximately 1000 seconds after injecting the solvent. For the purpose of this study, all further experimental runs were conducted for a period of 2000 seconds (about 30 minutes).

Next, the absorption behaviour of the solvent was analyzed. Figure 6.1 shows a slight increase in the system pressure at the time that the solvent is injected into the pure CO₂ atmosphere contained within the equilibrium cell (t = 0 seconds). This increase is due to the injected solvent decreasing the volume available for the CO₂ gas. A fraction of the CO₂ is absorbed as it comes into contact with the solvent, causing the pressure to decrease. The pressure continues to decrease until it reaches an absolute minimum. At this point the solvent has absorbed the maximum amount of CO₂ that it can. Typically, upon reaching an absolute minimum, the pressure will increase slightly and stabilize at some value below atmospheric pressure. This slight increase in pressure is due to:

- An increase in temperature caused by an exothermic reaction between the solvent and the CO₂ gas;

- CO₂ gas desorbing due to solvent degradation and/or reversible reactions between the solvent and the CO₂ gas.

Individually, or in combination, the phenomenon above will cause only a slight increase in pressure from the absolute minimum pressure. Figure 6.1 however shows a considerable increase in the pressure until equilibrium is reached at atmospheric pressure. This could be due to leakages in the system. For the purpose of this study however it was assumed that the magnitude of the error resulting from leaks is the same for each experimental run. The absolute minimum pressure reading found for each experimental run was taken as the equilibrium pressure in the data analysis process. The pressure reading just prior to injecting the solvent sample was taken as the initial pressure. The pressure readings were chosen such to discard the effect of leakages in the system, as well as the magnitude of the pressure increase caused by injecting the solvent sample. This would allow the loading calculated for different solvent samples to be compared with each other.

The Peng-Robinson Equation of State (PR-EoS) was used to determine the rich loading of each solvent blend (sample calculations are presented in Appendix F). The loading of the 30wt% MEA (aq) solvent was determined to be 0.0051 mol CO₂/mol solvent. This is significantly less than the values found in literature, i.e. 0.49 mol CO₂/mol solvent. This difference could be due to:

- Differences in the temperatures at which the values were obtained: The measured value was obtained at a temperature of 25°C, while the literature value was obtained at 48°C;
- Differences in operating conditions: The measured value was obtained for batch operation, whereas the literature value was obtained for a continuously operated system;
- Differences in CO₂ feed concentration: The measured value was obtained for a pure CO₂ atmosphere (99.95%), whereas the literature value was obtained for 13% CO₂ in the feed gas.

Individually, or in combination, the above factors could have a significant effect on the amount of CO₂ absorbed by the solvent. A second sample of a 30wt% MEA (aq) solution was prepared and tested to evaluate the repeatability of the experimental procedure. The P-v-t data for the second sample is shown in Figure 6.2.

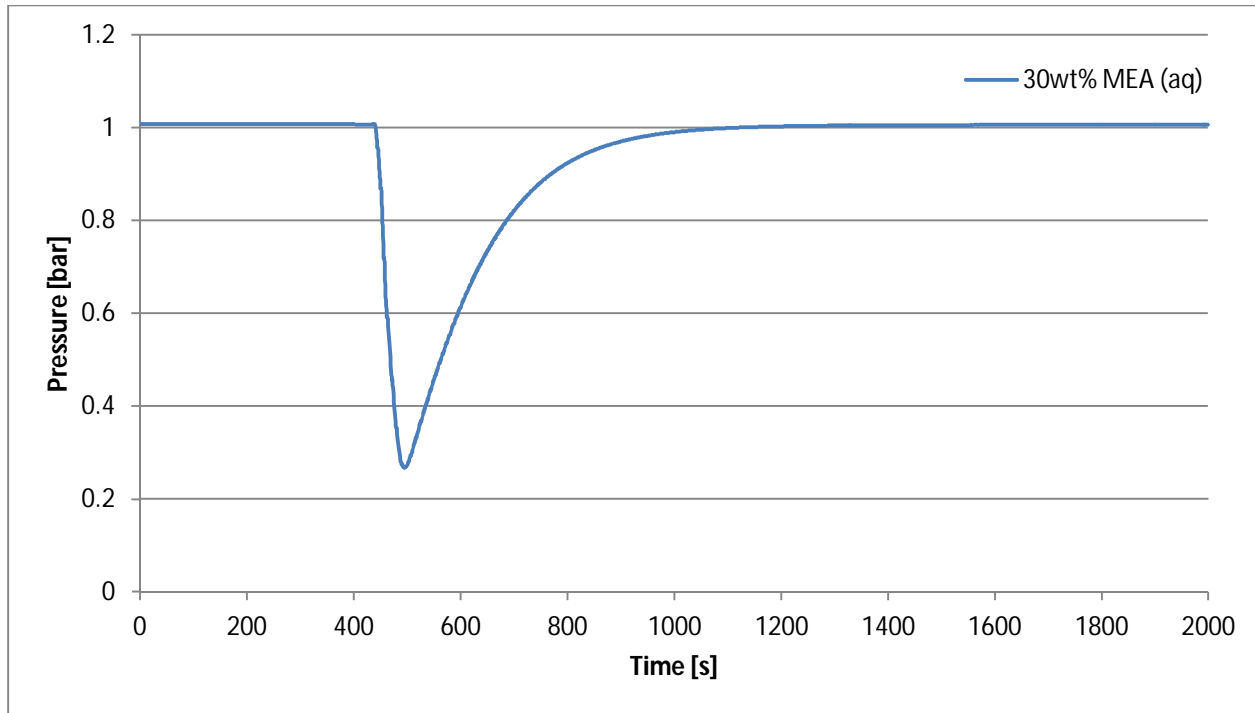


Figure 6.2 – P-v-t graph for Run 2 (the repeated experimental run for 30wt% MEA (aq) exposed for 2000s).

Figure 6.2 shows similar P-v-t behaviour for the second solvent sample as was seen for the first (Figure 6.1). The loading of the second sample was calculated to be 0.0051 mol CO₂/mol solvent. This is exactly the same as the loading calculated for the first sample. Based on this, the experimental procedure was concluded to be repeatable.

The second reference solvent tested was an aqueous solution of 30wt% K₂CO₃. This blend is sometimes used as an alternative to the conventional 30wt% MEA (aq) solution. The P-v-t data obtained for the 30wt% K₂CO₃ (aq) solvent solution is shown in Figure 6.3.

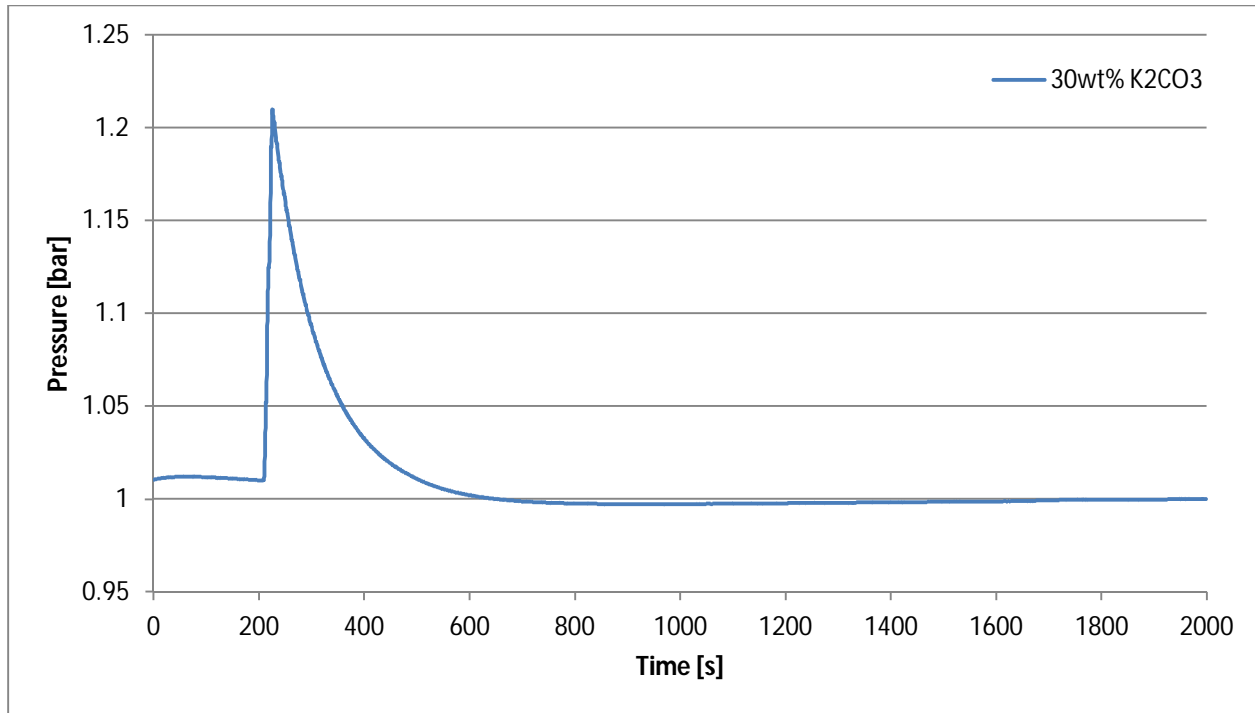


Figure 6.3 – P-v-t graph for Run 3 (30wt% K_2CO_3 (aq) exposed for 2000s).

Figure 6.3 shows a substantial increase in pressure at the time of solvent injection ($t \approx 200$ seconds). This increase is significantly more than that seen for the 30wt% MEA (aq) solution (Figures 6.1 and 6.2). This could be due to slower reactions kinetics and/or slower solvation between the gas and the K_2CO_3 solution compared to the MEA solution. Upon reaching an absolute maximum ($P \approx 1.2$ bar), the pressure steadily decreases to near atmospheric pressure. This decrease is primarily due to CO_2 gas being absorbed into the solvent. Results from the pressure tests however suggest that it could also be partly due to leaks in the system. For this solvent, the P-v-t behaviour never exhibits a significant dip below atmospheric pressure, but rather stabilizes at near atmospheric pressure on its descent from an absolute maximum. This could be attributed to slow reaction kinetics between the gas and the solvent, as well as the possibility of leaks in the system. The magnitude of the error resulting from leaks is expected to be insignificant to the overall absorption performance measured. The kinetics observed in Figure 6.3 suggests that the pressure would have dipped only slightly below atmospheric pressure before attaining equilibrium. Based on this it is assumed that the error made in the data analysis due to leaks in the system is negligible.

The loading of the 30wt% K_2CO_3 (aq) solution was determined to be 0.0014 mol CO_2 /mol solvent. This loading is significantly less than the values presented in literature (1.612 mol CO_2 /mol solvent). A second sample of the 30wt% K_2CO_3 (aq) solution was synthesized and tested as a supplementary repeatability test. The P-v-t data for the second sample is shown in Figure 6.4.

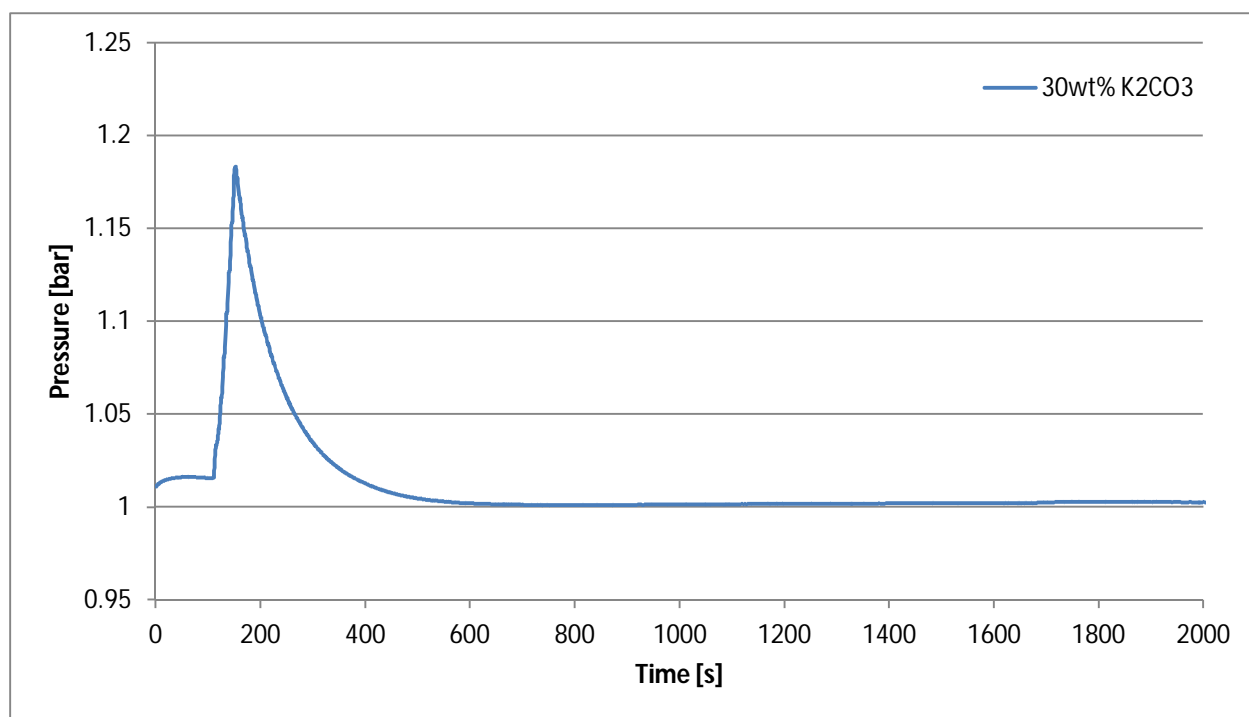


Figure 6.4 – P-v-t graph for Run 4 (the repeated experimental run for 30wt% K_2CO_3 (aq) exposed for 2000s).

Figure 6.4 shows similar P-v-t behaviour for the second K_2CO_3 solution as that seen for the first sample (Figure 6.3). The loading of the second sample was determined to be 0.0014 mol CO_2 /mol solvent. This is exactly the same as the loading determined for the first sample. This confirms the repeatability of the experimental procedure for a second solvent solution. Hence, it can be assumed that the procedure will be repeatable for any solvent system.

The third reference solvent is an aqueous piperazine (PZ) promoted K_2CO_3 blend. The blend composition was suggested by Oexmann *et al.* (2008) to be 2.5M PZ and 2.5M K_2CO_3 , translating to 13.8wt% PZ and

22.1wt% K_2CO_3 . The piperazine promoted blend is a suggested alternative to improve the absorption performance of the 30wt% K_2CO_3 (aq) solvent to above that of the conventional 30wt% MEA (aq) solvent. The P-v-t data for the PZ promoted K_2CO_3 solution is shown in Figure 6.5.

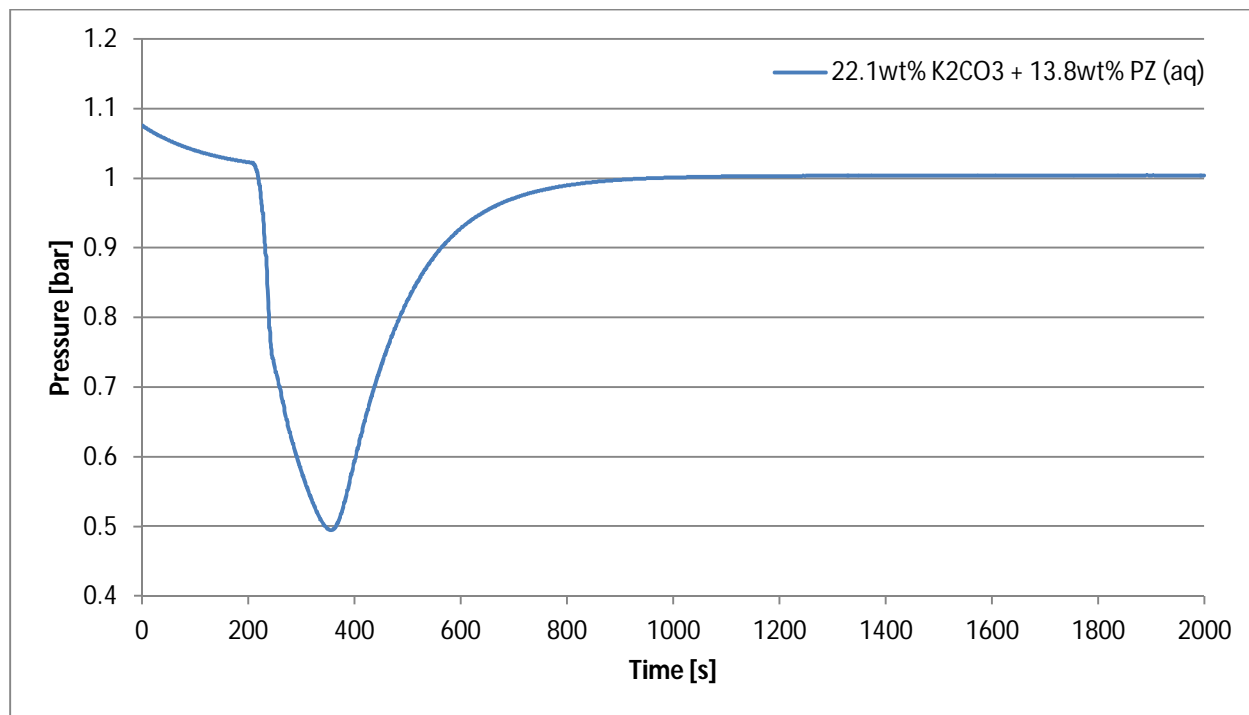


Figure 6.5 – P-v-t graph for Run 5 (an aqueous solution of 22.1wt% K_2CO_3 and 13.8wt% Piperazine (PZ) exposed for 2000s).

Figure 6.5 shows very similar P-v-t behaviour for the piperazine promoted solvent as that seen for the 30wt% MEA (aq) solvent. Following injection, this solvent however displays an initial gradual decrease in pressure and then the sudden considerable drop to the absolute minimum pressure. The presence of two consecutive descending pressure tendencies could be indicative of two absorption reactions. From the P-v-t behaviour seen for the 30wt% K_2CO_3 (aq) solvent, the initial gradual decrease is most likely due to CO_2 absorbing into the K_2CO_3 . The sudden considerable pressure decrease is expected to be the result of secondary absorption reactions between the CO_2 and the piperazine in the blend. Upon reaching the absolute minimum, the pressure gradually returns to near atmospheric pressure. The loading for the solvent was determined to be 0.0046 mol CO_2 /mol solvent. As with the first two reference solvents, the

measured loading of the PZ promoted K_2CO_3 solvent is significantly less than the values presented in literature (1.101 mol CO_2 /mol solvent).

None of the measured loadings match the literature values closely. It should be noted that the values found in literature were obtained for continuously operated CO_2 absorption processes, i.e. an unlimited supply of solvent, as well as CO_2 gas. The values measured experimentally however were obtained for a batch-wise operated system containing a limited quantity of solvent and CO_2 gas. Hence, it would be impossible for the experimental system to attain solvent loadings similar to that found in literature. Based on the repeatability of the experimental procedure, the measured loading values however are still accepted as valid reference standards. The absorption performance of all further solvent samples is compared to the loading values of the reference solvents.

6.2. Hypothesis Test Results

The main objective of the experimental plan is to test the research hypothesis that partial solubility parameters cannot be used to predict solvent formulations for CO_2 absorption processes. Six solvent formulations were randomly selected from EquiSolv solvent optimizer predictions for CO_2 absorbing solvent solutions. The solvents were synthesized and their absorption performance measured. The six formulations selected for synthesis, in decreasing order of predicted CO_2 absorption performance, are summarized in Table 6.1.

Table 6.1 – Summary of the solvent formulations randomly selected for synthesis and experimental testing.

| Rank _{Pred} | Constituent 1 | Constituent 2 | Constituent 3 | x_1 [vol%] | x_2 [vol%] | x_3 [vol%] | δ_D [MPa ^{0.5}] | δ_P [MPa ^{0.5}] | δ_H [MPa ^{0.5}] | RED |
|----------------------|-----------------|------------------------------|---------------|--------------|--------------|--------------|----------------------------------|----------------------------------|----------------------------------|--------|
| 1 | Trioctylamine | Monoethanolamine (MEA) | Water | 0.8339 | 0.0934 | 0.0727 | 16.20 | 6.50 | 13.10 | 2.2735 |
| 2 | Auramine | Hexylamine | Water | 0.2813 | 0.5545 | 0.1642 | 16.90 | 8.50 | 17.90 | 3.8134 |
| 3 | Tryptamine | Diisobutylamine | Water | 0.5006 | 0.2962 | 0.2032 | 17.20 | 9.20 | 20.00 | 4.5174 |
| 4 | sec-Butylamine | Auramine | Water | 0.3345 | 0.4309 | 0.2346 | 17.40 | 10.00 | 21.10 | 4.9099 |
| 5 | Hexylamine | 2,4-Dichlorobenzylamine | Water | 0.0902 | 0.6799 | 0.2299 | 18.60 | 10.20 | 21.20 | 5.1612 |
| 6 | Di-p-Tolylamine | Dimethyl ethanolamine (DMEA) | Water | 0.5597 | 0.0723 | 0.3680 | 18.30 | 10.60 | 26.00 | 6.4779 |

To conclusively reject the null hypothesis, the measured absorption performances in decreasing order of solvent loadings should match the predicted solvent rankings based on their respective RED values. The amount of solvent injected varied for each sample due to differences in the solvent viscosities (see Appendix E for a summary of the experimental data). The solvents were synthesized and tested in the order indicated in Table 6.1. The P-v-t data obtained for the first solvent formulation is shown in Figure 6.6.

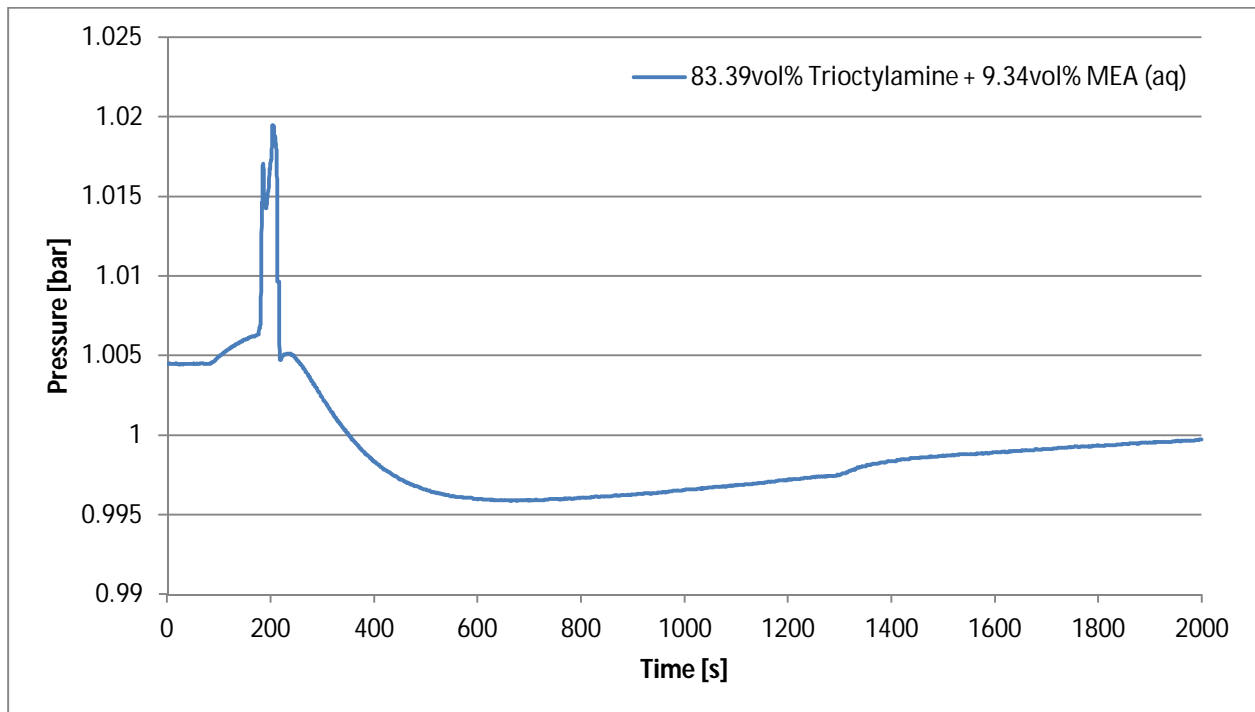


Figure 6.6 – P-v-t graph for Run 6 (an aqueous solution of 83.39vol% Trioctylamine and 9.34vol% Monoethanolamine (MEA) exposed for 2000s).

Figure 6.6 shows similar P-v-t behaviour for this solvent formulation as was seen for the 30wt% MEA (aq) and PZ promoted K_2CO_3 (aq) reference solvents. There are however clear discrepancies with the initial pressure spikes. Following the point of injection, Figure 6.6 shows a gradual increase in pressure followed by a sudden spike to an absolute maximum. This spike however contains a brief drop in the pressure before increasing to the absolute maximum. Both the initial gradual increase, as well as the brief drop in pressure could be attributed to delays in injecting the solvent sample due to a high solvent

sample density. A high solvent density makes it difficult to force the sample through the needle of the syringe used to inject it into the equilibrium cell.

As expected, upon reaching an absolute minimum pressure at approximately 0.995 bar the pressure returns to near atmospheric pressure due to leaks in the system. The P-v-t trend observed in Figure 6.6 exhibits a much more gradual return to atmospheric pressure as that observed for the 30wt% MEA (aq) solvent. This could be the result of a significantly smaller pressure driving force observed for the Trioctylamine-MEA solvent compared to the conventional MEA solvent (Figure 6.1). The significant difference in absolute pressure minima observed for the two cases could be due to different rates of diffusion for the solvents. Although Figure 6.6 suggests that the system has not yet attained a state of equilibrium after the assumed period of 2000 seconds, this has no effect on the data analysis of the solvent's absorption performance. As stated earlier, the data analysis only considers the initial and absolute minimum pressures; discarding the effect of leaks. Using the PR-EoS, the loading of the Trioctylamine-MEA (aq) solvent formulation was determined to be 0.0153 mol CO₂/mol solvent. Irrespective of the solvent's eventual overall ranking, this is already a significant (more than 50%) improvement over the performance of the conventional reference solvents. The P-v-t data for the second solvent formulation (an aqueous solution of Auramine and Hexylamine) is shown in Figure 6.7.

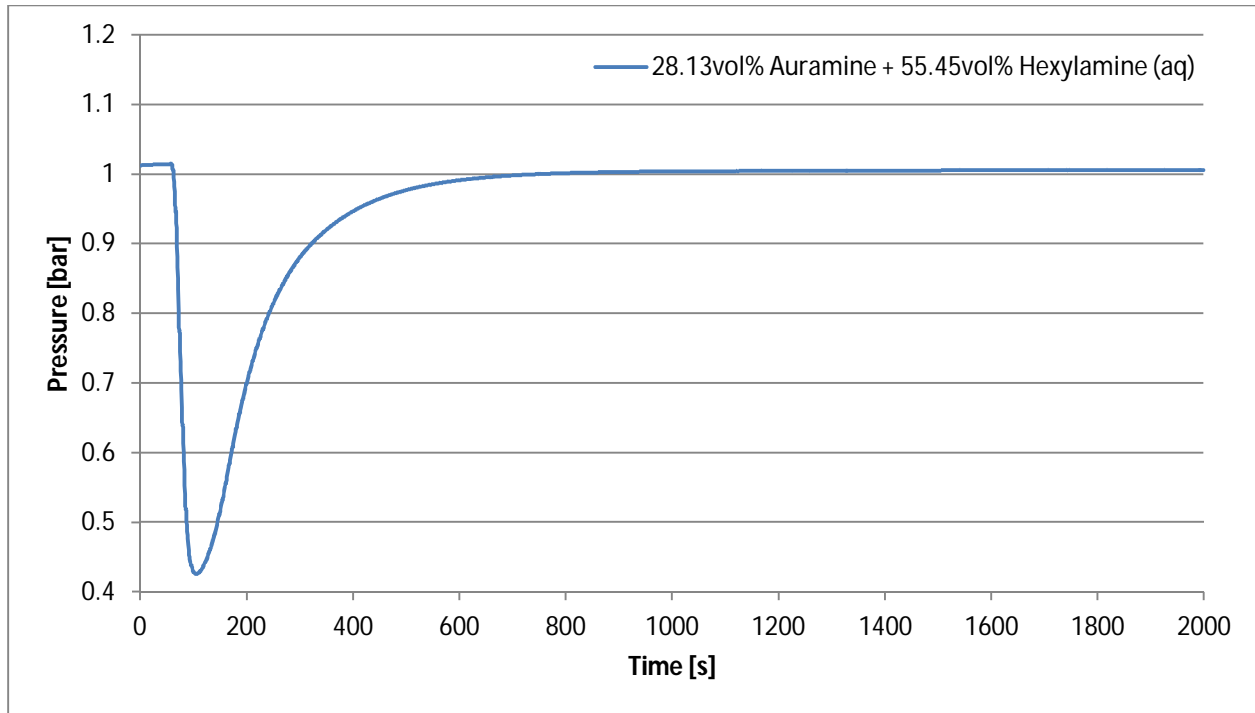


Figure 6.7 – P-v-t graph for Run 7 (an aqueous solution of 28.13vol% Auramine and 55.45vol% Hexylamine exposed for 2000s).

Figure 6.7 shows almost exactly the same PT behaviour for this solvent as was seen for the conventional 30wt% MEA (aq) solvent. The only difference between the trends observed for the two solvents being the lack of an initial pressure increase in Figure 6.7. This is indicative of extremely fast reaction kinetics between the solvent and the CO₂ gas. The solvent effectively absorbed CO₂ as it was being injected into the equilibrium cell. Based on this, it is expected that the solvent would have a very high CO₂ absorption capacity. The solvent loading was determined to be 0.0421 mol CO₂/mol solvent. As expected, this is significantly higher than the loadings measured for any of the previous solvents. From Figure 6.7 it is clear that the assumption of attaining equilibrium within a period of 2000 seconds is valid for this solvent. The P-v-t data obtained for the third solvent formulation is presented in Figure 6.8.

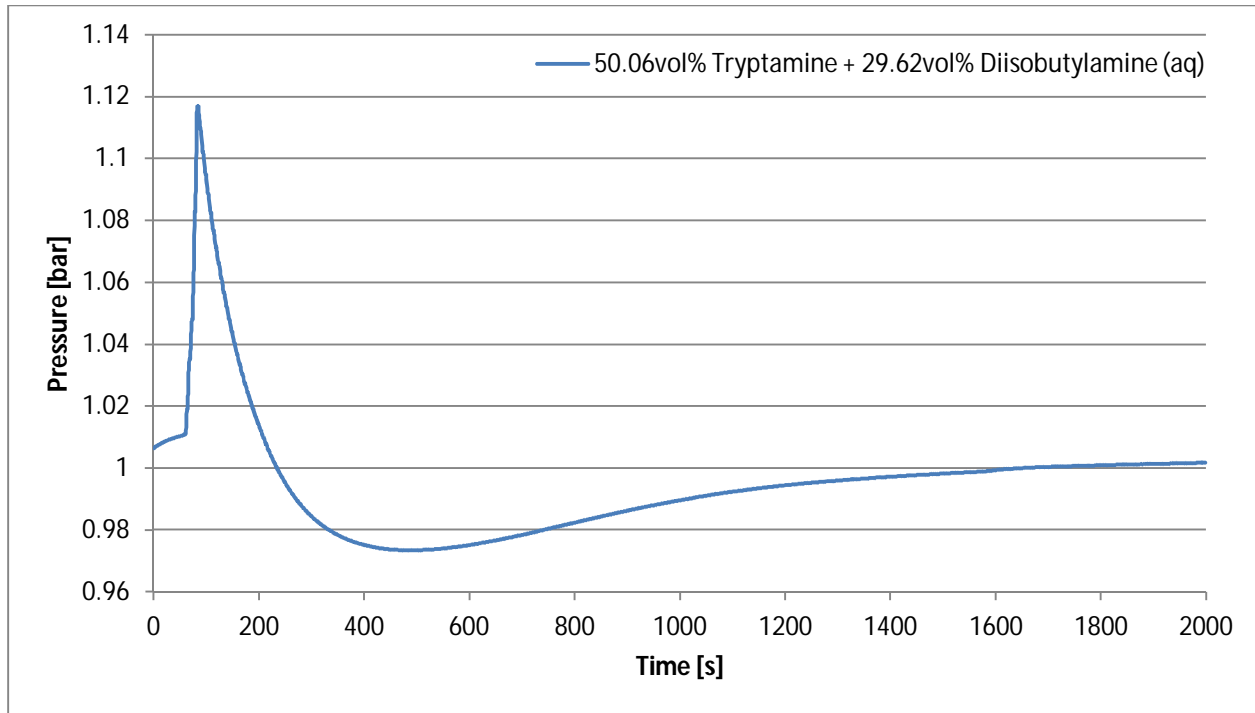


Figure 6.8 – P-v-t graph for Run 8 (an aqueous solution of 50.06vol% Tryptamine and 29.62vol% Diisobutylamine exposed for 2000s).

The P-v-t data for the Tryptamine-Diisobutylamine (aq) solvent follows a similar trend to that seen for the Trioctylamine-MEA (aq) solvent. At the point of injection the pressure increases gradually for a brief period before it quickly jumps to an absolute maximum. Hereafter the pressure gradually decreases to an absolute minimum before returning to near atmospheric pressure. As with the Trioctylamine-MEA (aq) solvent, the brief gradual initial increase is attributed to delays in injecting the solvent. Again it appears that the assumption of attaining equilibrium within a period of 2000 seconds is valid. The solvent rich loading was calculated to be 0.0145 mol CO₂/mol solvent. As with the two prior solvent formulations, this is a significant improvement in absorption performance compared with the reference standards. P-v-t data for the fourth solvent formulation is shown in Figure 6.9.

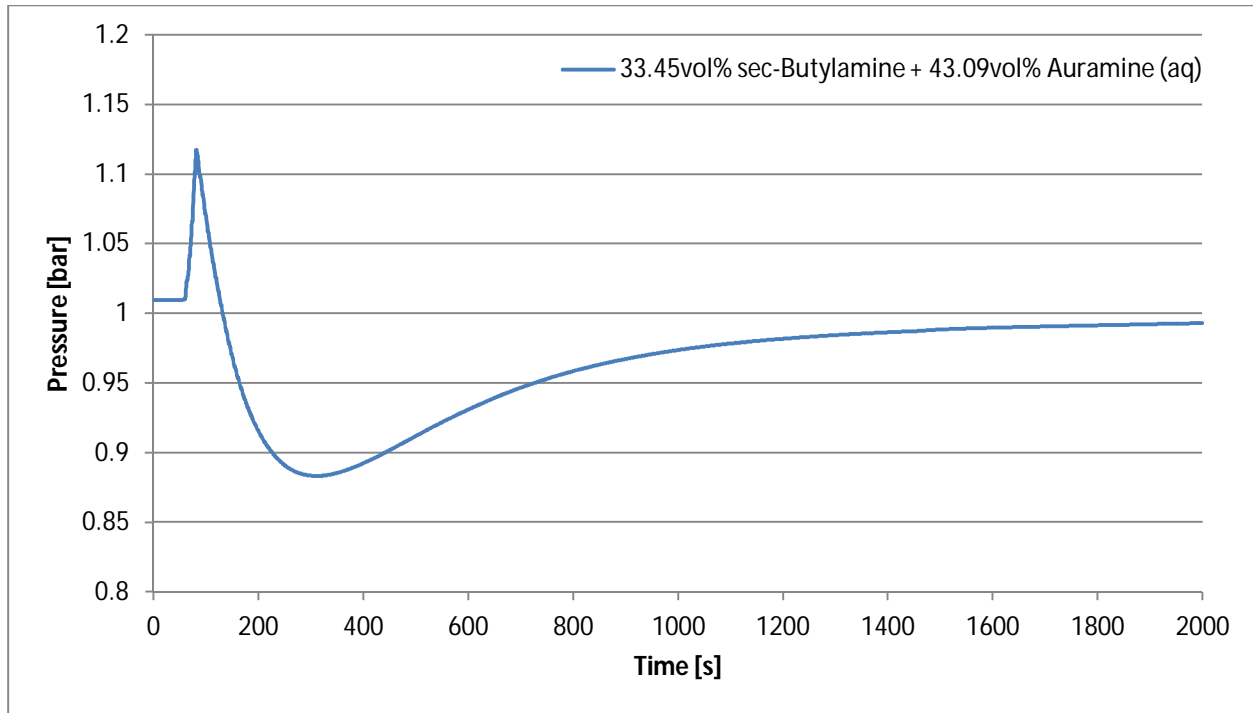


Figure 6.9 – P-v-t graph for Run 9 (an aqueous solution of 33.45vol% sec-Butylamine and 43.09vol% Auramine exposed for 2000s).

Figure 6.9 shows similar P-v-t behaviour for the aqueous sec-Butylamine-Auramine solvent as was seen for the Trioctylamine-MEA (aq) and Tryptamine-Diisobutylamine (aq) solvents. The solvent rich loading was determined to be 0.0116 mol CO₂/mol solvent. This translates to a 56% improvement in absorption performance compared with the 30wt% MEA (aq) solvent typically used in CO₂ absorption processes (60.3% in the case of the PZ promoted K₂CO₃ solvent, and 87.9% in the case of the 30wt% K₂CO₃ (aq) solvent). Based on the results of the first four solvent formulations, partial solubility parameter theory exhibits enormous potential in predicting alternative solvent blend formulations for CO₂ recovery processes. The P-v-t data obtained for the fifth solvent formulation, i.e. an aqueous solution of Hexylamine and 2,4-Dichlorobenzylamine, is shown in Figure 6.10.

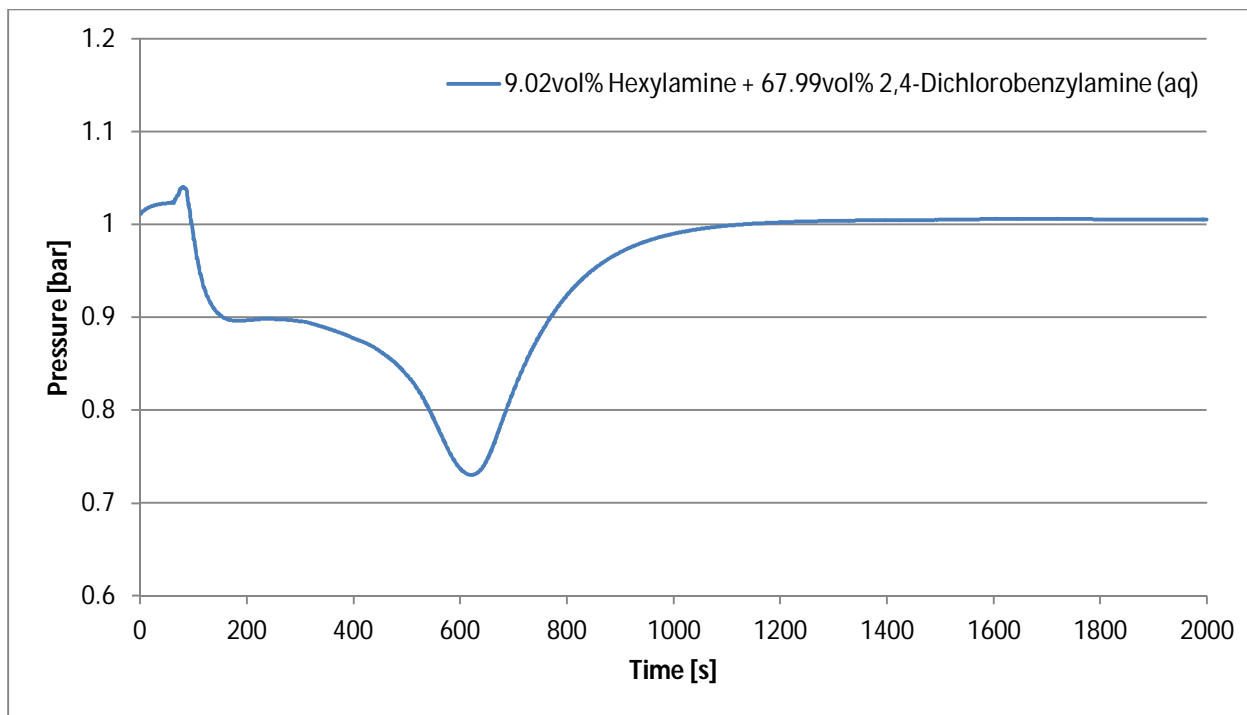


Figure 6.10 – P-v-t graph for Run 10 (an aqueous solution of 9.02vol% Hexylamine and 67.99vol% 2,4-Dichlorobenzylamine exposed for 2000s).

Figure 6.10 shows an unusual trend for the P-v-t behaviour of the solvent. The initial pressure increase as well as the eventual return to near atmospheric pressure are expected and have been discussed already. It is the trend of the pressure decrease from the absolute maximum to the absolute minimum that is interesting. Following the initial increase at the point of injection, the pressure decreases and stabilizes at a local minimum at approximately 0.9 bar for a brief period before gradually decreasing further to the absolute minimum pressure. This presence of two separate pressure troughs could be explained by two stages of absorption occurring. This could be attributed to incomplete mixing between the solvent constituents, i.e. a not completely homogeneous solution. Initially a fraction of the CO_2 is absorbed by a part of the solvent primarily comprised of one of the constituents. This is followed by a second fraction of the gas being absorbed by the remaining part primarily comprised of the other constituent. The local minimum then represents the maximum absorption capacity of the first element.

The loading for the solvent was determined to be 0.0104 mol CO₂/mol solvent. Although less than the previous four solvent formulations, this is still significantly higher than the loadings measured for the three reference standards. P-v-t data for the sixth solvent formulation is presented in Figure 6.11.

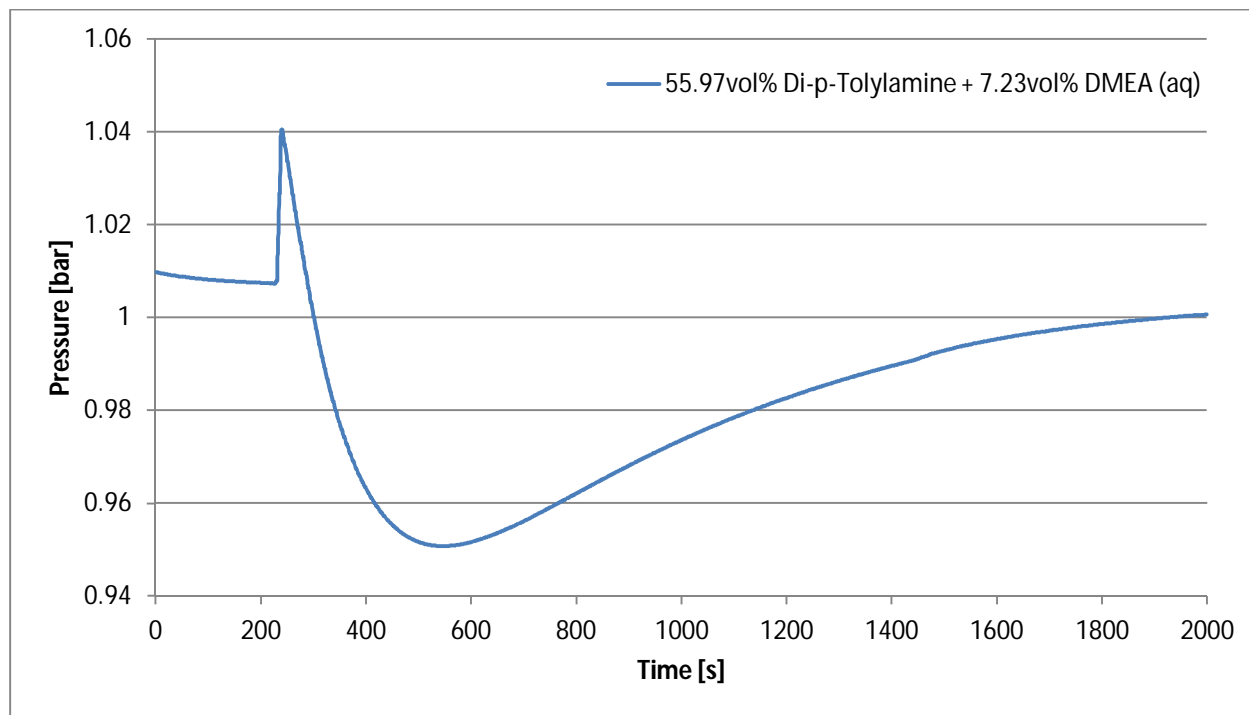


Figure 6.11 – P-v-t graph for Run 11 (an aqueous solution of 55.97vol% Di-p-Tolylamine and 7.23vol% Dimethyl ethanolamine (DMEA) exposed for 2000s).

The P-v-t behaviour obtained for the aqueous Di-p-Tolylamine-DMEA solvent clearly follows the expected trend. The slight decrease in pressure for the period 0-200 seconds (prior to injection) is attributed to noise in the pressure transmitter readings. This decrease however has no effect on the data analysis. Although it appears that the system has not yet reached equilibrium at $t = 2000$ seconds, this also has no effect on the data analysis of the solvent's absorption performance. The solvent rich loading was determined to be 0.0062 mol CO₂/mol solvent. As was expected from the EquiSolv predictions, the loading of this solvent is the lowest of all six solvent formulations. It compares closely to that of the conventional 30wt% MEA (aq) solvent. The measured loadings for all six solvent formulations are summarized in Table 6.2. The measured ranking position of each blend, in order of decreasing loading capacity, is shown in the far right-hand column.

Table 6.2 – Summary of the CO₂ absorption capacities (rich loadings) experimentally measured for the six randomly selected blend formulations.

| Rank _{pred} | Constituent 1 | Constituent 2 | Constituent 3 | x ₁ [vol%] | x ₂ [vol%] | x ₃ [vol%] | δ _D [MPa ^{0.5}] | δ _P [MPa ^{0.5}] | δ _H [MPa ^{0.5}] | RED | I ^{rich} [mol CO ₂ /mol soln] | Rank _{calc} |
|----------------------|-----------------|------------------------------|---------------|-----------------------|-----------------------|-----------------------|--------------------------------------|--------------------------------------|--------------------------------------|--------|---|----------------------|
| 1 | Trioctylamine | Monoethanolamine (MEA) | Water | 0.8339 | 0.0934 | 0.0727 | 16.20 | 6.50 | 13.10 | 2.2735 | 0.0153 | 2 |
| 2 | Auramine | Hexylamine | Water | 0.2813 | 0.5545 | 0.1642 | 16.90 | 8.50 | 17.90 | 3.8134 | 0.0421 | 1 |
| 3 | Tryptamine | Diisobutylamine | Water | 0.5006 | 0.2962 | 0.2032 | 17.20 | 9.20 | 20.00 | 4.5174 | 0.0145 | 3 |
| 4 | sec-Butylamine | Auramine | Water | 0.3345 | 0.4309 | 0.2346 | 17.40 | 10.00 | 21.10 | 4.9099 | 0.0116 | 4 |
| 5 | Hexylamine | 2,4-Dichlorobenzylamine | Water | 0.0902 | 0.6799 | 0.2299 | 18.60 | 10.20 | 21.20 | 5.1612 | 0.0104 | 5 |
| 6 | Di-p-Tolylamine | Dimethyl ethanolamine (DMEA) | Water | 0.5597 | 0.0723 | 0.3680 | 18.30 | 10.60 | 26.00 | 6.4779 | 0.0062 | 6 |

To conclusively reject the null hypothesis, the predicted ranking position of each blend should match the measured ranking position, i.e. the position indicated in the far left-hand column of Table 6.2 should match the position indicated in the far right-hand column. From Table 6.2, this is true for the last four solvent formulations. The measured ranking positions of the first two solvent blends however are the exact opposite of their predicted ranking. Kendall's coefficient of concordance (W) was used to evaluate the agreement between predicted and measured ranking positions. This non-parametric statistical test makes no assumption regarding the nature of the probability distribution of sample data (Legendre, 2005). Dr. Lidia Auret of the University of Stellenbosch developed MATLAB code based on Kendall's coefficient of concordance. The procedure was used to perform the statistical hypothesis test on the data presented in Table 6.2 using MATLAB R2010b. A copy of the code is presented in Appendix I. The results obtained from the statistical analysis are summarized in Table 6.3.

Table 6.3 – Summary of the MATLAB results obtained for the Kendall coefficient of concordance statistical test conducted for the results of the experimental hypothesis test results.

| | |
|------------------------|-----------------|
| n (Number of Objects): | 6 |
| m (Number of Columns): | 2 |
| Wref: | 0.9714 |
| chi2ref: | 9.7143 |
| Wperm: | [1000x1 double] |
| chi2perm: | [1000x1 double] |
| P: | 0.0130 |

For the purpose of this study the threshold of statistical significance (α) was chosen to be 0.05, i.e. a 95% confidence level. From Table 6.3 it is clear that the p-value is significantly less than the value chosen for α . This indicates that the set of predicted and measured data contains concordant ranking results. Based on this the null hypothesis (H_0) can conclusively be rejected in favour of the alternative hypothesis

(H_1). It is clear that partial solubility parameters have the potential to accurately describe the equilibrium behaviour of CO_2 absorbing in task specific designed solvents. Hence partial solubility parameters show great promise to be used as basis in solvent screening models for CO_2 absorption.

The discrepancy observed in the ranking results of the first two solvent formulations prevents the null hypothesis to be rejected entirely. Based on the results of the last four solvents however it can be rejected with great confidence. The difference observed between the predicted and measured ranking position of the first two solvents could be due to experimental error including:

- Error made in measuring the solvent sample injected;
- Error arising due to differences in the magnitude of the leaks observed for each experimental run.

A larger set of solvent formulations would be needed to investigate the possibility of such errors and conclusively reject (or accept) the null hypothesis. A comparison of the measured loadings for each of the six solvent formulations to that of the three reference solvents are given in Figure 6.12.

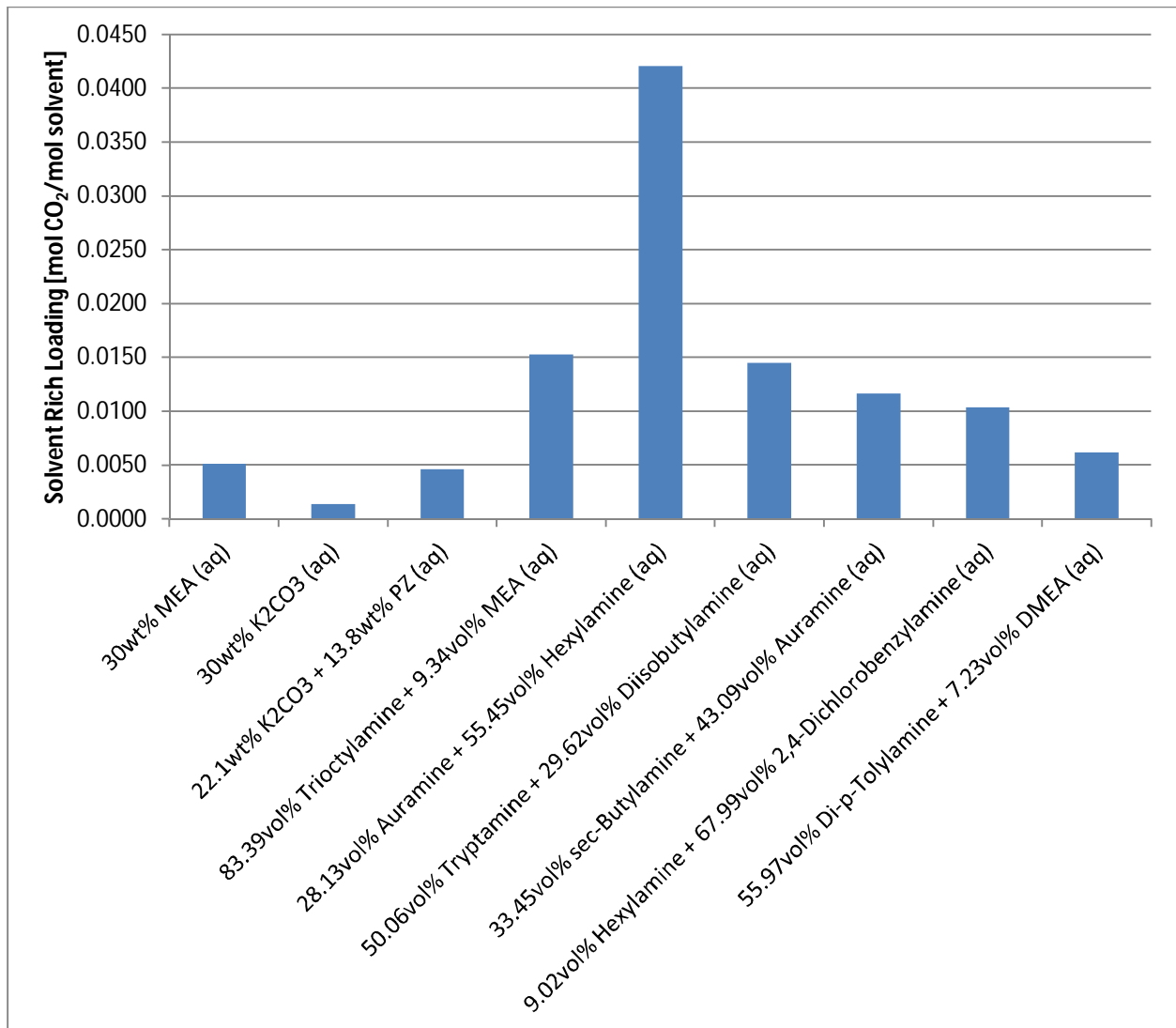


Figure 6.12 – Comparison of the solvent rich loadings for the six randomly selected solvent formulations to the loadings measured for the three reference solvent blends.

As predicted, all of the alternative solvent formulations exhibited improved absorption performance compared with the reference standard solvents. An improvement of 97% was seen for the aqueous Auramine-Hexylamine solvent compared with the 30wt% K₂CO₃ (aq) solvent. It is clear that partial solubility parameter theory has the potential to significantly improve the absorption performance of CO₂ recovery processes through efficient solvent screening.

6.3. Ionic Liquid CO₂ Absorption Results

Recently ionic liquids (ILs) have started to be considered as possible alternatives to conventional solvents used in CO₂ recovery processes. Three ILs were identified for preliminary CO₂ absorption experiments to evaluate the performance of ILs. The ILs selected include:

- 1-Butyl-3-methylimidazolium hexafluorophosphate (or [bmim][PF₆]);
- 1-Butyl-3-methylimidazolium tetrafluoroborate (or [bmim][BF₄]);
- And 1-Octyl-3-methylimidazolium hexafluorophosphate (or [omim][PF₆]).

The ILs were selected based on the fact that their respective Hansen partial solubility parameters are available in literature. This allowed the EquiSolv program to be used in predicting the absorption behaviour of CO₂ in each of the selected ILs. Two sets of experiments were conducted to evaluate the absorption performance of ILs. The first set of experiments tested the performance of each individual IL to absorb CO₂, whereas the second set of experiments tested the performance of amine-IL based solvents to absorb CO₂. For the first set, an aqueous solution of 60wt% IL was synthesized for each of the ILs investigated. The P-v-t data obtained for the first IL solvent is shown in Figure 6.13.

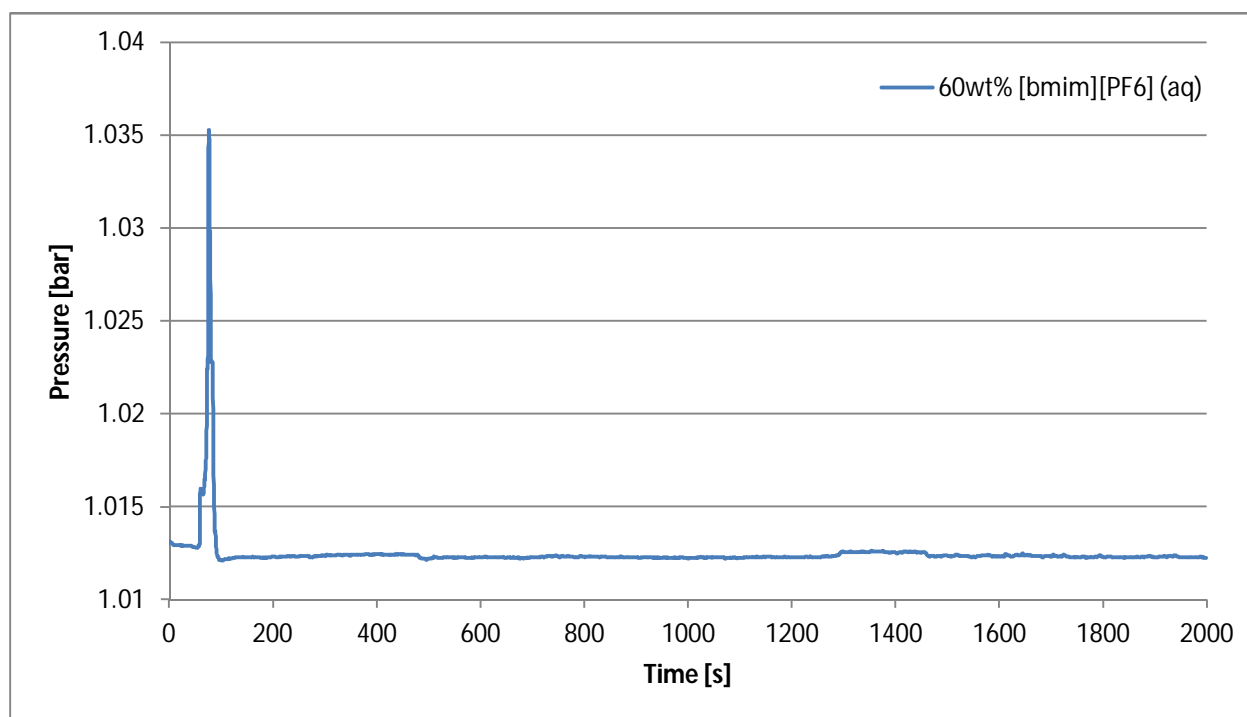


Figure 6.13 – P-v-t graph for Run 12 (60wt% [bmim][PF₆] (aq) exposed for 2000s).

Figure 6.13 clearly shows a sudden spike in the pressure at the point of injection. This increase is expected, as injecting the solvent would decrease the volume available for the CO₂ gas inside the equilibrium cell. Upon reaching an absolute maximum at approximately 1.035 bar, the pressure immediately returns to near atmospheric pressure. Based on the magnitude of the pressure spike (approximately 0.02 bar), the sudden decrease in pressure is attributed almost entirely to CO₂ absorbing into the solvent rather than leaks in the system. The fact that the pressure never dips below atmospheric pressure before returning to it however is attributed to a combination of slow kinetics and leaks in the system. The loading of the aqueous [bmim][PF₆] solvent was determined to be 0.0060 mol CO₂/mol solvent. Although a slight improvement, this still compares closely to the loadings observed for the three reference standards. P-v-t data for the second aqueous IL solvent is shown in Figure 6.14.

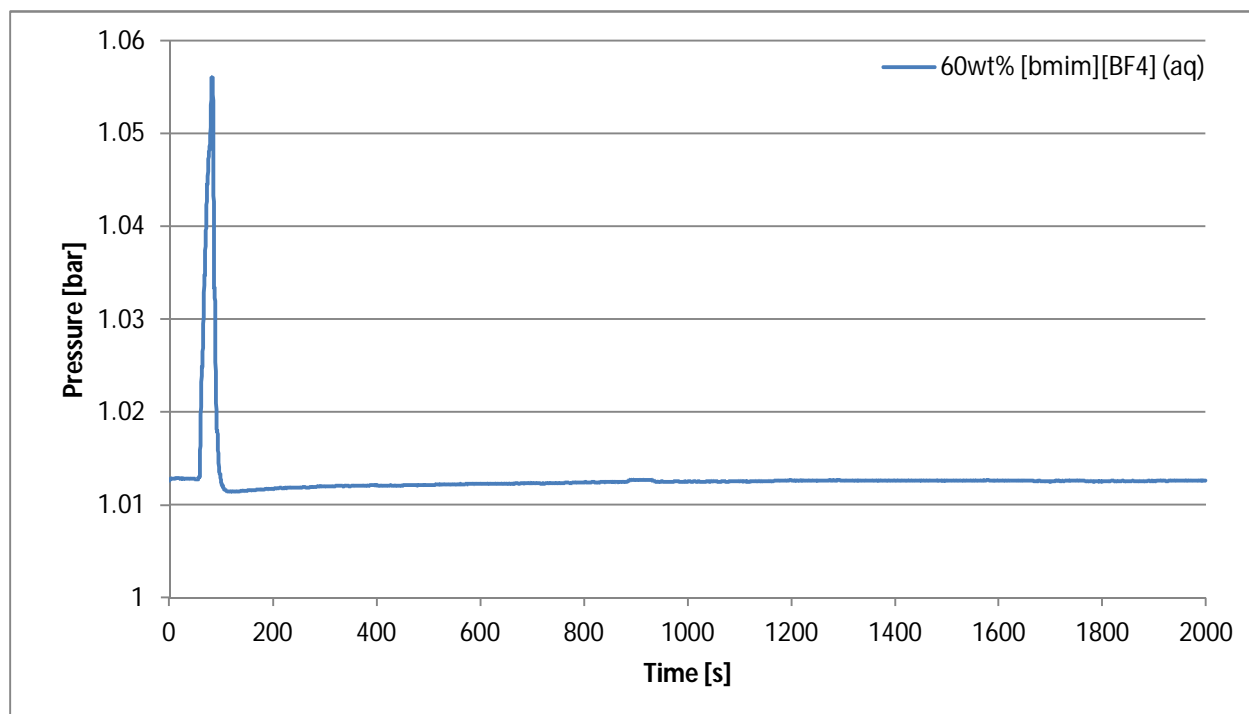


Figure 6.14 – P-v-t graph for Run 13 (60wt% [bmim][BF₄] (aq) exposed for 2000s).

Figure 6.14 shows a similar trend for the P-v-t behaviour of the aqueous [bmim][BF₄] solvent as was seen for the aqueous [bmim][PF₆] solvent (Figure 6.13). Although the pressure increase here is slightly more than that observed for the previous IL solvent, the explanation given for the sudden pressure

decrease of the latter holds true for the [bmim][BF₄] solvent. The loading of the [bmim][BF₄] solvent was determined to be 0.0053 mol CO₂/mol solvent. This is almost exactly the loading value observed for the 30wt% MEA (aq) reference solvent, translating to an almost negligible improvement over the conventional solvent. The P-v-t data obtained for the third IL solvent, i.e. 60wt% [omim][PF₆] (aq), is given in Figure 6.15.

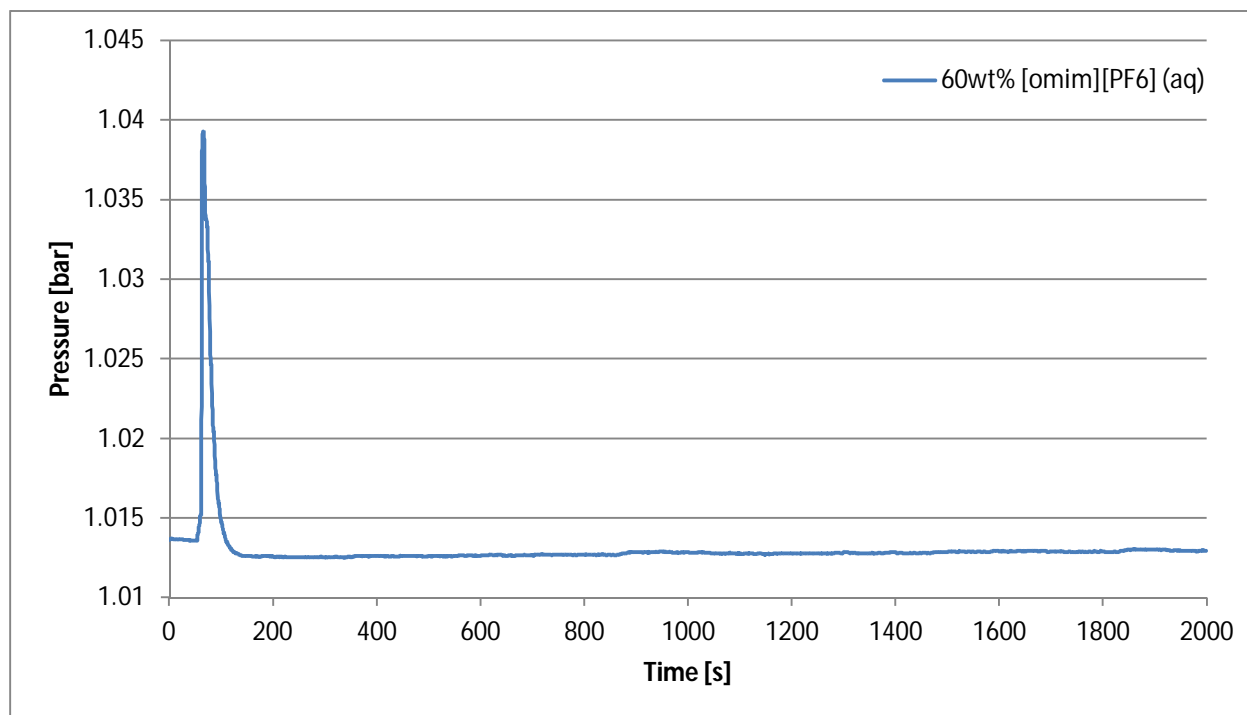


Figure 6.15 – P-v-t graph for Run 14 (60wt% [omim][PF₆] (aq) exposed for 2000s).

A similar P-v-t trend is observed for the third IL solvent as for the first two IL solvents, with a sudden pressure spike at the point of injection immediately returning to near atmospheric pressure (Figure 6.15). The loading of the aqueous [omim][PF₆] solvent was determined to be 0.0078 mol CO₂/mol solvent. This is a 34.6% improvement in absorption compared with the 30wt% MEA (aq) solvent conventionally used to recover CO₂. Although none were major, each of the aqueous IL solvents showed an improvement in CO₂ absorption compared with the three reference solvents. Furthermore, from Figures 6.13 to 6.15 it is clear that the assumption that equilibrium is attained within a period of 2000 seconds is valid.

The second set of IL-based experiments evaluated the absorption performance of IL solvents when combined with an amine. The EquiSolv solvent optimizer was used to predict amine-IL-based solvents for CO₂ capture and four solvent formulations were randomly selected. As with the hypothesis test solvents (see Section 6.2), the four IL-based solvent formulations were ranked in decreasing order of expected loading capacity based on their respective RED values. The four solvent formulations are summarized in Table 6.4.

Table 6.4 – Summary of the four IL-based solvent formulations randomly selected for synthesis and experimental testing.

| Rank _{pred} | Constituent 1 | Constituent 2 | x ₁ [vol%] | x ₂ [vol%] | δ _D [MPa ^{0.5}] | δ _P [MPa ^{0.5}] | δ _H [MPa ^{0.5}] | RED |
|----------------------|-------------------------|--------------------------|-----------------------|-----------------------|--------------------------------------|--------------------------------------|--------------------------------------|--------|
| 1 | Diisobutylamine | [omim][PF ₆] | 0.8845 | 0.1155 | 15.70 | 6.30 | 5.74 | 0.0117 |
| 2 | Diisobutylamine | [bmim][PF ₆] | 0.8812 | 0.1188 | 15.70 | 6.30 | 5.83 | 0.0404 |
| 3 | 2,4-Dichlorobenzylamine | [omim][PF ₆] | 0.6011 | 0.3989 | 15.71 | 6.30 | 5.94 | 0.0544 |
| 4 | MEA | [bmim][BF ₄] | 0.7800 | 0.2200 | 18.48 | 16.33 | 19.13 | 6.9678 |

The second set of IL-based experiments was designed with a secondary purpose in mind, i.e. to serve as a supplementary independent test of the null hypothesis. The four IL-based solvents were determined and ranked according to the same method used for the original hypothesis test solvents. Thus, as an additional test, the null hypothesis can be conclusively rejected if the calculated solvent ranking (in order of decreasing CO₂ loading) matches the predicted ranking (Table 6.4). P-v-t data for the first amine-IL solvent formulation (Diisobutylamine and [omim][PF₆]) is shown in Figure 6.16.

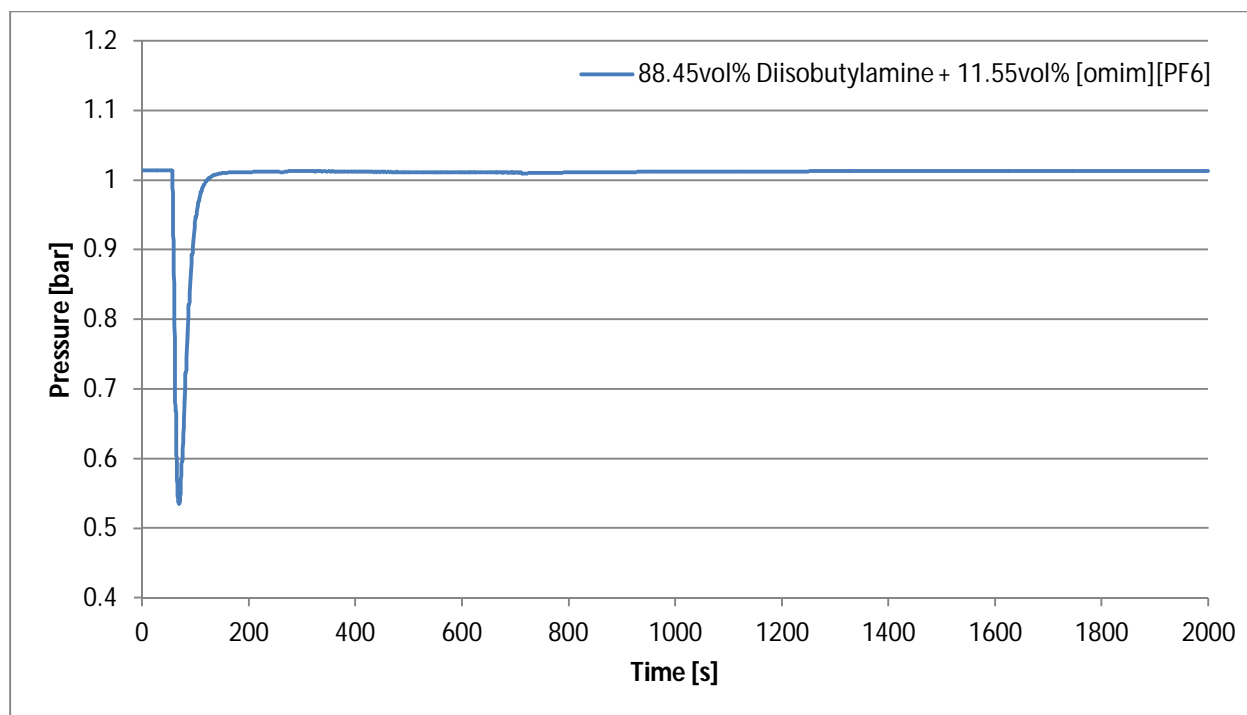


Figure 6.16 – P-v-t graph for Run 15 (a solution of 88.45vol% Diisobutylamine and 11.55vol% [omim][PF₆] exposed for 2000s).

Figure 6.16 shows a similar trend for the P-v-t behaviour of the Diisobutylamine-[omim][PF₆] solvent as was seen for the aqueous Auramine-Hexylamine solvent tested in the original hypothesis test experiments (Figure 6.7). The P-v-t behaviour observed here for the amine-IL solvent however exhibits a much quicker return to near atmospheric pressure than that seen for the amine-amine solvent tested earlier. This could be attributed to:

- Slower kinetics allowing the leaks to dominate the return to atmospheric pressure;
- Fewer, or even the absence of, side-reactions counteracting the effect of leaks in the system;
- A higher cell temperature at the absolute minimum due to more exothermic reactions.

The more rapid return to atmospheric pressure could also be due to a combination of the phenomenon described above. The solvent loading was determined to be 0.0372 mol CO₂/mol solvent. This is a significant improvement compared with the reference standards (an 86.3% improvement compared with the conventional 30wt% MEA (aq) solvent). The P-v-t data obtained for the second amine-IL-based solvent is shown in Figure 6.17.

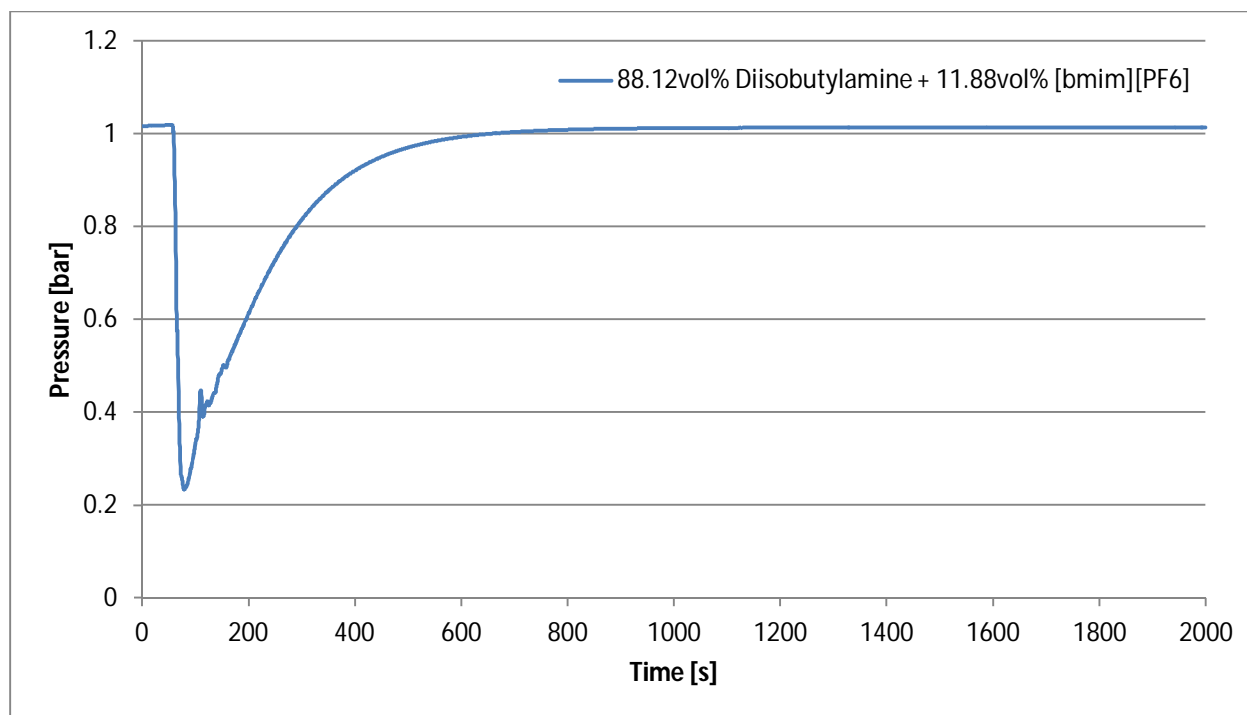


Figure 6.17 – P-v-t graph for Run 16 (a solution of 88.12vol% Diisobutylamine and 11.88vol% [bmim][PF₆] exposed for 2000s).

The P-v-t data for the Diisobutylamine-[bmim][PF₆] solvent follows the same trend as that observed for the aqueous Auramine-Hexylamine solvent investigated in the original hypothesis test experiments. In contrast with the previous amine-IL solvent, this solvent exhibits the same gradual return from the absolute minimum to atmospheric pressure as that seen for the amine-amine-based solvent. Figure 6.17 however shows a slight decrease in the pressure during its ascent to atmospheric pressure. This quick drop in pressure could be the result of a secondary absorption phase occurring. This could be due to byproducts formed during the absorption process. The solvent loading was determined to be 0.0314 mol CO₂/mol solvent. As for the previous solvent, this is a considerable improvement in absorption capacity compared with the three reference solvents. P-v-t data for the third amine-IL-based solvent (2,4-Dichlorobenzylamine and [omim][PF₆]) is shown in Figure 6.18.

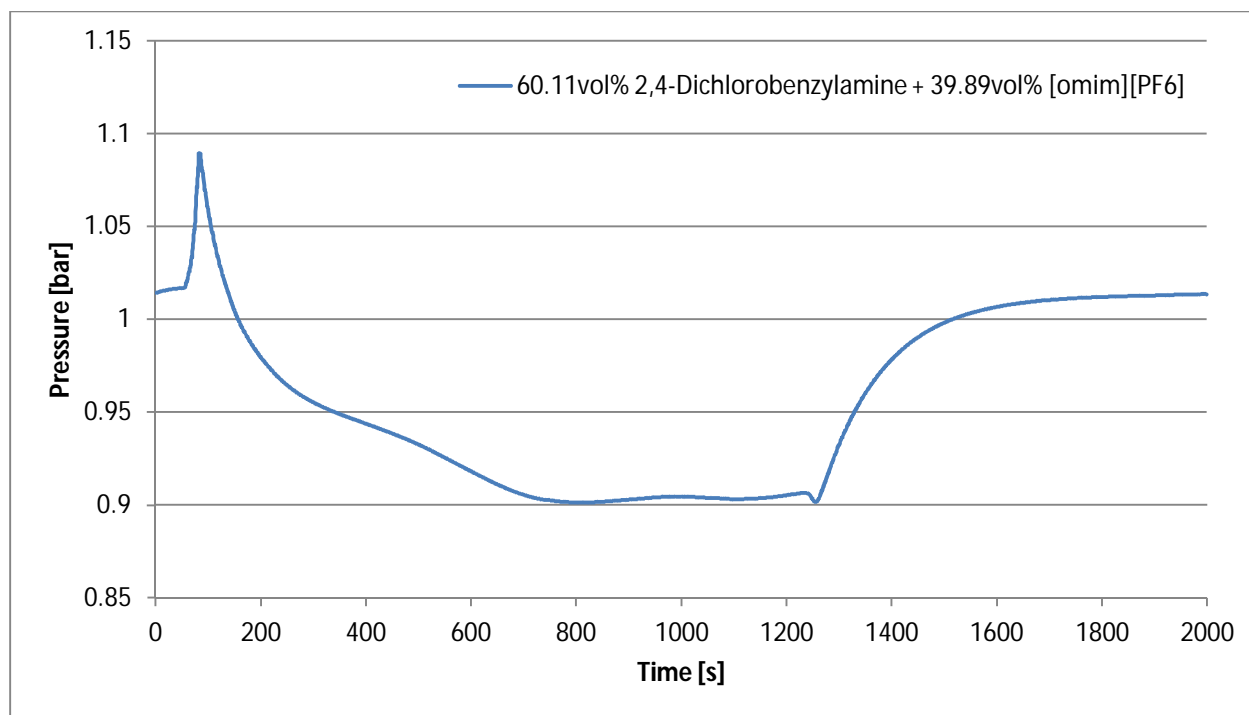


Figure 6.18 – P-v-t graph for Run 17 (a solution of 60.11vol% 2,4-Dichlorobenzylamine and 39.89vol% [omim][PF₆] exposed for 2000s).

The P-v-t behaviour seen in Figure 6.18 is very similar to the trend observed for the Hexylamine-2,4-Dichlorobenzylamine solvent investigated in the original hypothesis test experiments. The pressure decreases from an absolute maximum through a series of local minimum points before gradually returning to near atmospheric pressure. The presence of multiple local minimum points on the pressure curve is indicative of multiple absorption phases due to various absorption reactions and rates between the separate solvent elements and the CO₂ gas. In both amine-amine and amine-IL-based solvent cases, the presence of multiple local minima is observed only when 2,4-Dichlorobenzylamine is one of the solvent elements. The loading of the 2,4-Dichlorobenzylamine-[omim][PF₆] solvent was determined to be 0.0217 mol CO₂/mol solvent. Again this is a significant improvement in absorption capacity compared with the reference standards. The P-v-t data for the fourth amine-IL-based solvent is shown in Figure 6.19.

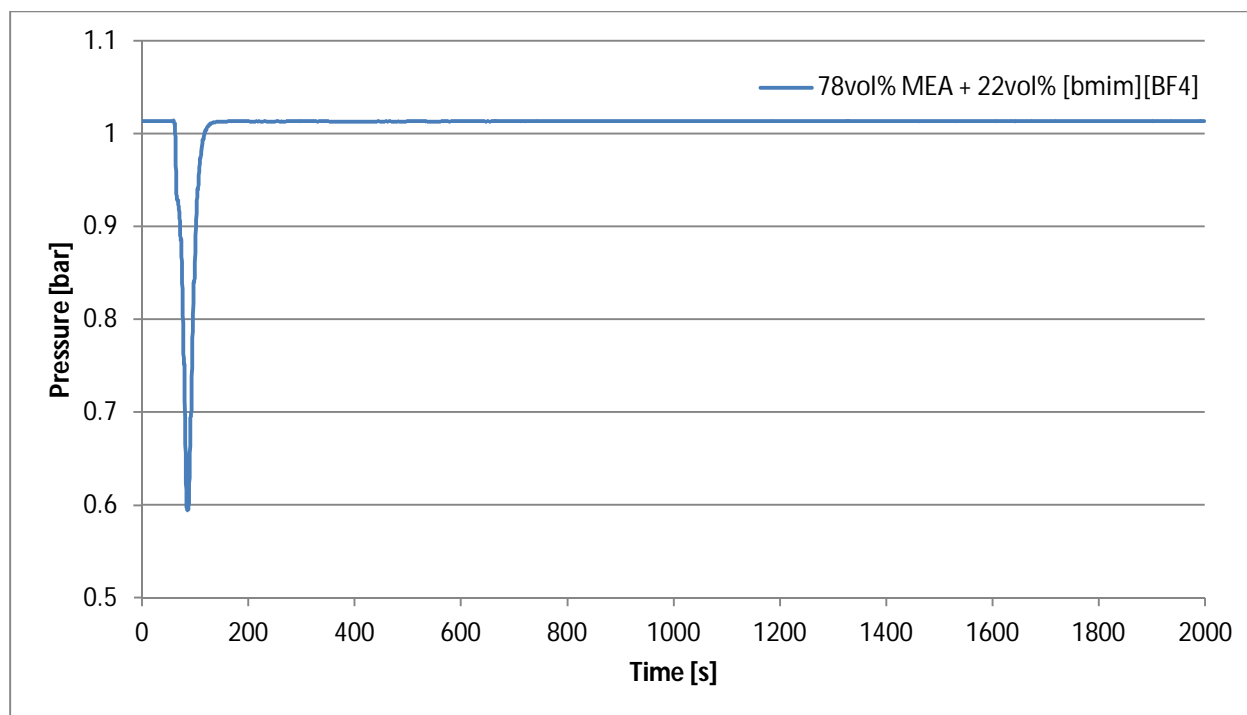


Figure 6.19 – P-v-t graph for Run 18 (a solution of 78vol% Monoethanolamine (MEA) and 22vol% [bmim][BF₄] exposed for 2000s).

The P-v-t behaviour of the MEA-[bmim][BF₄] solvent (Figure 6.19) exhibits a similar trend as that seen for the first amine-IL-based solvent (Figure 6.16). The solvent loading was determined to be 0.0104 mol CO₂/mol solvent. Although this is less than the loadings observed for the previous four solvents, it is still a considerable improvement in absorption capacity compared with the reference solvents. The calculated loadings of the four amine-IL-based solvents are summarized in Table 6.5. The calculated solvent ranking positions are indicated in the far right-hand column.

Table 6.5 – Summary of the CO₂ absorption capacities experimentally measured for the four amine-IL blend formulations.

| Rank _{Pred} | Constituent 1 | Constituent 2 | x ₁ [vol%] | x ₂ [vol%] | δ _D [MPa ^{0.5}] | δ _p [MPa ^{0.5}] | δ _H [MPa ^{0.5}] | RED | I _{rich} [mol CO ₂ /mol soln] | Rank _{Calc} |
|----------------------|-------------------------|--------------------------|-----------------------|-----------------------|--------------------------------------|--------------------------------------|--------------------------------------|--------|---|----------------------|
| 1 | Diisobutylamine | [omim][PF ₆] | 0.8845 | 0.1155 | 15.70 | 6.30 | 5.74 | 0.0117 | 0.0372 | 1 |
| 2 | Diisobutylamine | [bmim][PF ₆] | 0.8812 | 0.1188 | 15.70 | 6.30 | 5.83 | 0.0404 | 0.0314 | 2 |
| 3 | 2,4-Dichlorobenzylamine | [omim][PF ₆] | 0.6011 | 0.3989 | 15.71 | 6.30 | 5.94 | 0.0544 | 0.0217 | 3 |
| 4 | MEA | [bmim][BF ₄] | 0.7800 | 0.2200 | 18.48 | 16.33 | 19.13 | 6.9678 | 0.0104 | 4 |

From Table 6.5 it is clear that the calculated ranking position of each solvent, in order of decreasing solvent loading, match the ranking position predicted. Based on this, the null hypothesis is conclusively rejected. However, a second statistical test based on the Kendal coefficient of concordance was conducted to assess the agreement between the combined predicted and measured ranking data obtained in both experimental hypothesis tests. A summary of the results obtained for the test is presented in Table 6.6.

Table 6.6 – Summary of the results obtained for the Kendall coefficient of concordance statistical test conducted for the results of the combined experimental hypothesis test results.

| | |
|------------------------|-----------------|
| n (Number of Objects): | 10 |
| m (Number of Columns): | 2 |
| Wref: | 0.9939 |
| chi2ref: | 17.8909 |
| Wperm: | [1000x1 double] |
| chi2perm: | [1000x1 double] |
| P: | 1.0000e-003 |

From Table 6.6 it is clear that the p-value is significantly less than the value chosen for the threshold of statistical significance (i.e. $\alpha = 0.05$). Based on this the null hypothesis is conclusively rejected in favour of the alternative hypothesis. Hence, it can be concluded with great confidence that partial solubility parameter theory can be used to accurately screen solvents for alternative formulations to be used in CO₂ recovery processes. Figure 6.20 presents a comparison between the absorption performance of the seven IL-based solvents and the three reference solvents.

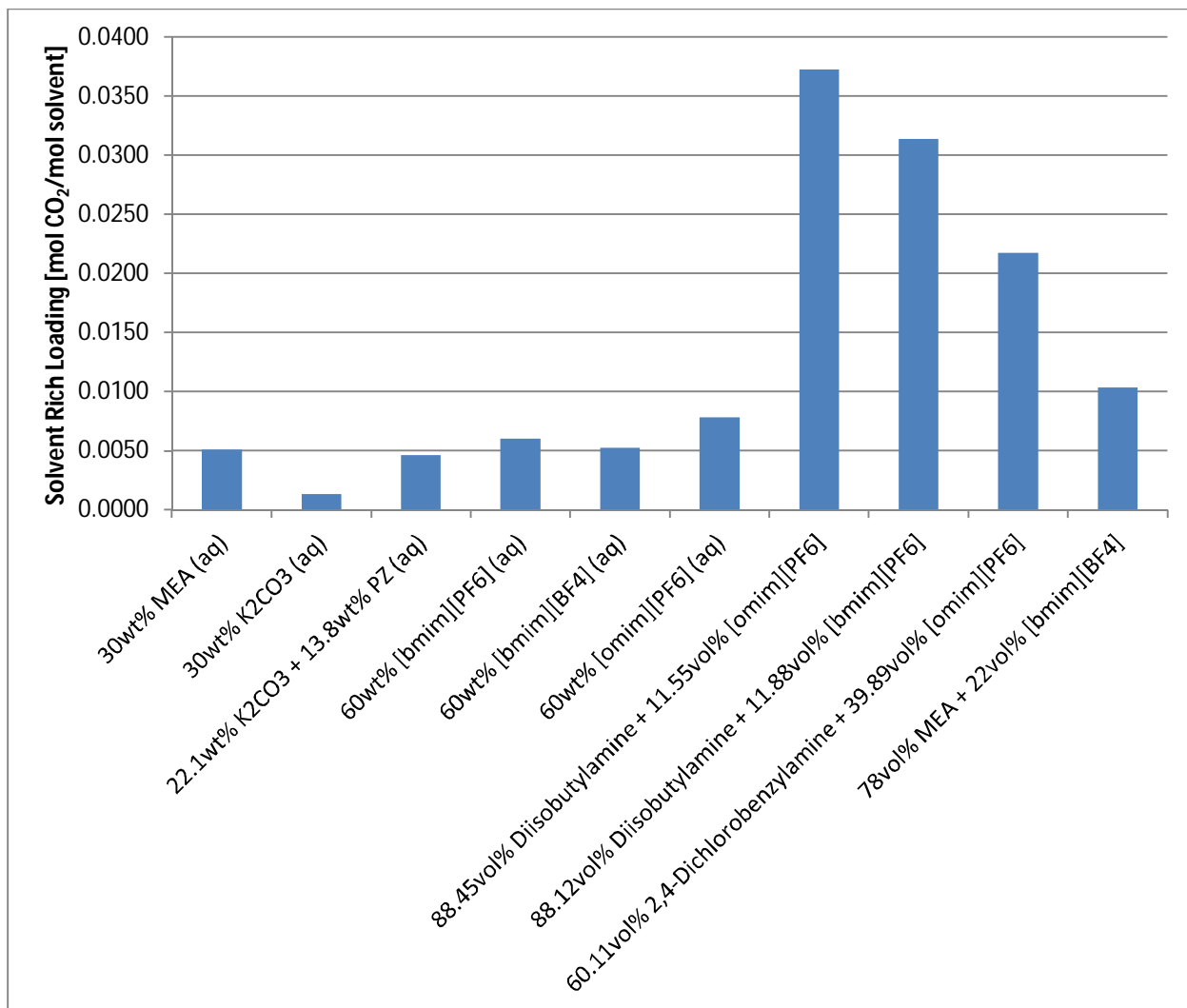


Figure 6.20 – Comparison of the solvent rich loadings for the seven IL solvent blends to the loadings measured for the three reference solvent blends.

It is clear that ILs have great potential as alternative solvents for absorbing CO₂. Compared with the 30wt% K₂CO₃ (aq) solvent, the Diisobutylamine-[omim][PF₆] solvent showed an improvement of 96% for the absorption capacity. Results obtained for the preliminary IL absorption experiments suggest that future work in solvent selection for CO₂ recovery processes should consider ionic liquids either as alternative, or as additive to the conventional alkanolamine solvents used. The low CO₂ loadings observed for the aqueous IL solvents is attributed to the high viscosities of the ILs. This should be kept in mind when evaluating alternative solvent formulations containing high concentrations of ILs.

6.4. Pressure Test Results

The pressure versus time (P-v-t) data presented for the various absorption experiments clearly suggest the presence of leaks in the experimental setup. A series of pressure tests were conducted to investigate the existence and severity of leaks in the setup. The tests comprised three positive force, and three negative force pressure tests. The complete set of P-v-t data obtained is presented in Appendix G. P-v-t data for one of the negative force tests is shown in Figure 6.21.

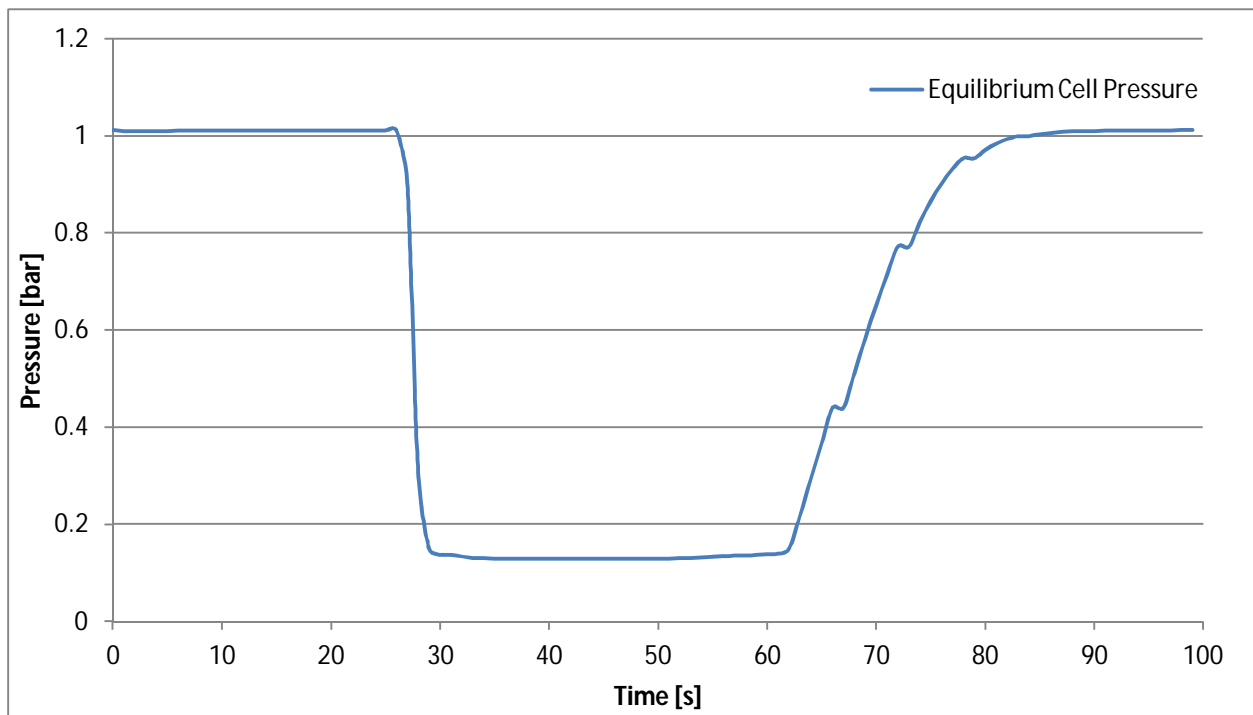


Figure 6.21 – P-v-t data obtained for one of the pressure test runs (negative force exerted).

The system was put under partial vacuum for a period of about 30 seconds and then sealed off at $t \approx 65$ seconds. Figure 6.21 clearly shows that the system pressure quickly returns to atmospheric pressure once it is sealed off. This is evidence of leaks present in the system, most likely through the solvent and/or pressure sampling points. Leaks at the sampling points could result from:

- Inadequate sealing at the sampling point capping, and/or;
- Inadequate sealing from the GC septums.

The magnitude of the leak seen in Figure 6.21 would suggest that the majority of the leak result from inadequate sealing at the solvent and/or pressure sampling point capping(s). A second set of pressure tests were conducted to test this theory. Vacuum grease was applied to both sampling points to provide additional sealing, and a third absorption experiment was conducted for the 30wt% MEA (aq) solution. The P-v-t data is presented in Figure 6.22.

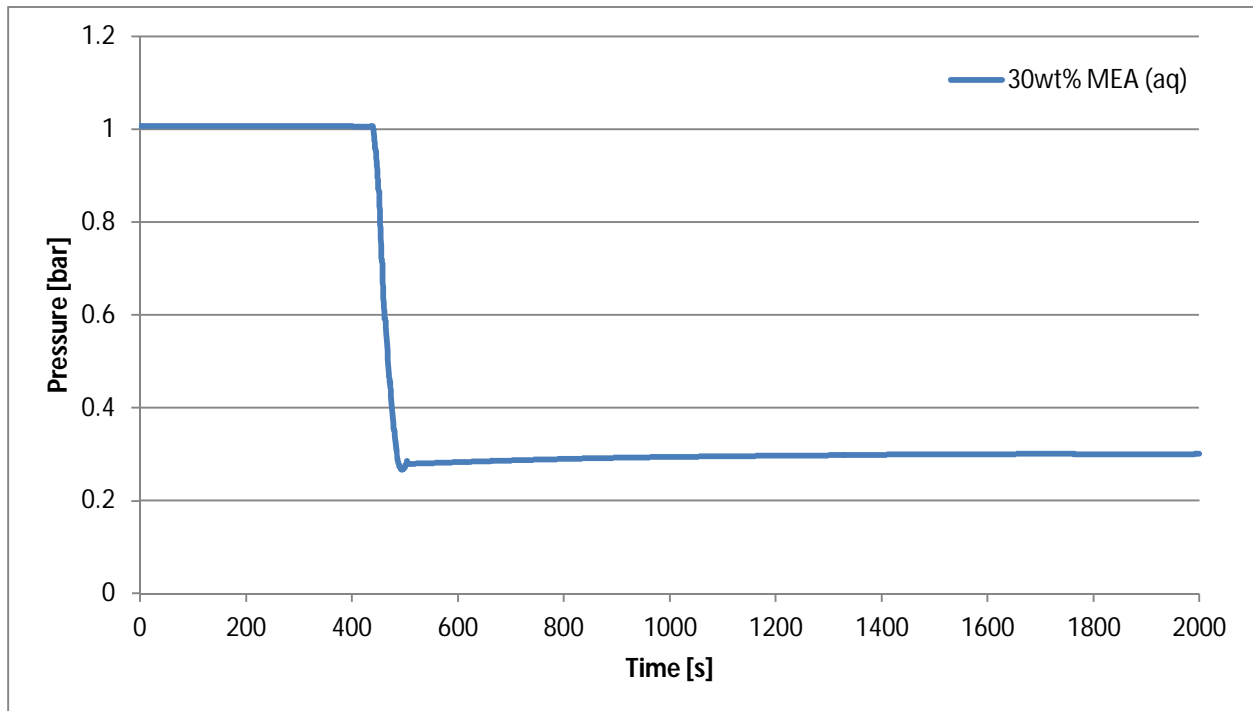


Figure 6.22 – P-v-t graph for Run 19 (the third experimental run for 30wt% MEA (aq) exposed for 2000s).

From Figure 6.22 it is clear that there are no (or at least insignificant) leaks present in the system – the pressure decreases as CO₂ is absorbed by the solvent until a minimum pressure is attained, at which the pressure stabilizes. A fourth run for the 30wt% MEA (aq) was conducted to investigate the effect of subsequent puncturing of the GC membranes on the propagation of leaks in the experimental setup. The P-v-t data is presented in Figure 6.23.

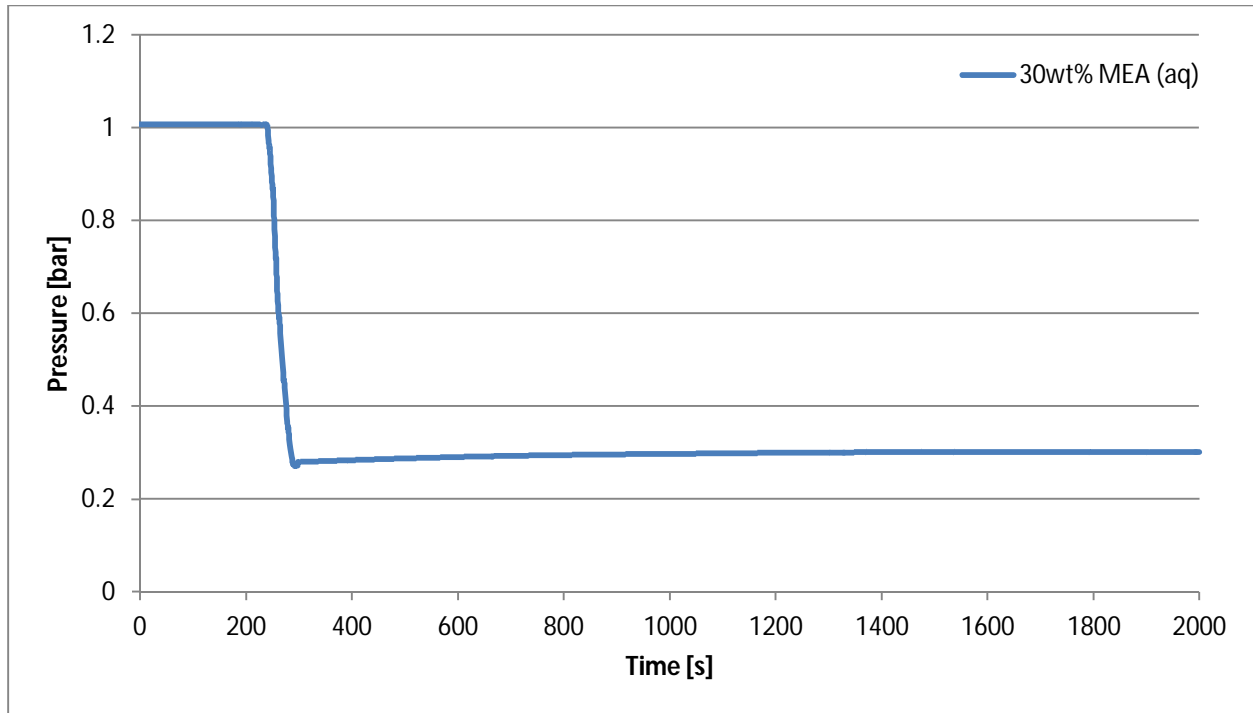


Figure 6.23 – P-v-t graph for Run 20 (the fourth experimental run for 30wt% MEA (aq) exposed for 2000s).

Figure 6.23 exhibits a similar trend in P-v-t behaviour as that seen in Figure 6.22. The difference between the absolute pressure minimum observed in Figures 6.22 and 6.23 was calculated to be about 1.5%. This clearly indicates that subsequent puncturing of the GC membranes have an insignificant effect on the propagation of leaks in the system.

Furthermore, the absolute minimum pressure readings found for the above two runs were compared to that found for the initial two experimental runs with the 30wt% MEA (aq) solution. The absolute minima readings for the first initial two runs were approximately 0.29 and 0.27 bar respectively. This compares extremely well with the values found for the pressure test runs; approximately 0.27 bar in both cases. Based on this it can be concluded that the magnitude of the error made during data analysis resulting from leaks in the system will be the same for each experimental run.

7. Conclusions

7.1. Modeling CO₂ Solubility

The ionic bond energies of 74 commercially available ionic liquids (ILs) were quantified using a molecular orbital approach. Due to a lack of IL physical property data in literature, the proposed ionic bond partial solubility parameter (δ_i) could only be calculated for four of the ILs. As expected, the magnitude of the δ_i parameters proved the ionic forces to dominate the molecular interactions of ILs. Hence it is of paramount importance to include the δ_i parameter when predicting the equilibrium behaviour of systems containing materials with strong ionic molecular interactions, e.g. ILs.

The proposed 4-set model was fitted to the partial solubility parameter data obtained for four ILs. The coefficient of ionic interaction (c_i) was found to be almost constant for the set of ILs considered. Based on the results a value of 0.001 was assumed for c_i and the model used to calculate the total (Hildebrand) solubility parameter for each of the ILs considered. The model was able to predict the parameter values with an average error of 0.036%. A larger set of IL parameter data is required however to thoroughly evaluate, and possibly revise, the model fit.

A number of limitations were discovered for the HSPiP program. The EquiSolv package was developed to address some of these limitations, including:

- The limit on the number of solvents that the HSPiP program can analyze;
- The limit on the number of solvent constituents that the HSPiP program can analyze;
- The lack of an ionic bond parameter (δ_i) in the HSPiP model theory.

The HSPiP analysis is limited to three-constituent solvent formulations. For datasets including more than about 80000 possible solvent combinations however, the program is limited to two-constituent blends. Trial runs were conducted to evaluate the capabilities of the EquiSolv program. The program was shown to successfully analyze up to four-constituent solvent formulations from approximately 400 million possible combinations. This is a substantial improvement compared to the capabilities of the HSPiP program.

Additionally, the solvent solubility parameter data can be used to examine the miscibility of the solvent constituents in each other. This is vital to establish whether or not it is possible to synthesize a predicted solvent formulation. Furthermore the HSPiP 3D visualizer was used to validate the predictions made by the EquiSolv program for solvents with RED values in the range 0 to 1. The results proved all of these solvents to fall within the solubility sphere of the target solute.

Results from the EquiSolv solvent optimizer did however show an inaccuracy in the calculations. The sum of the volume percentage contributions (x_i) calculated for the solvent formulations did not amount to unity for all predictions. This was attributed to an invalid assumption made in deriving the iterative algorithm used in the program. Fundamentally, the algorithm was based on the assumption that the x_i value of all possible solvent formulations would amount to unity. The algorithm assumptions were revised and an alternative algorithm was proposed. The inaccuracy however has no effect on the fundamental partial solubility parameter theory. It merely alters the solvent constituents predicted.

The EquiSolv quick blend calculator was used to evaluate the equilibrium behaviour of CO₂ absorbing into the conventionally used 30wt% MEA (aq) solvent. Based on partial solubility parameter theory, this solution is predicted to be an extremely “poor” solvent for absorbing CO₂ (RED = 9.99). The solvent however has been used successfully in industry for decades to recover CO₂ from gas stream. This does not prove partial solubility parameter theory to be incorrect. Instead, results from the model predictions merely suggest that this is not nearly the best choice of solvent for the desired application, i.e. absorbing CO₂.

Partial solubility parameters (specifically Hansen solubility parameters) have enormous potential to be in screening solvents for CO₂ absorption. The theory adheres to all of the specified design criteria:

- It is easy to understand;
- It is easy to apply;
- It circumvents the need for extensive material property data and/or data regression;
- It can be applied to quickly screen through massive datasets;

- It has the potential to be modified to include additional interaction parameters.

The theory should however be applied with caution. It should be kept in mind that it neglects the possibility and/or existence of chemical reactions between the materials considered. Nevertheless, it can be argued that dissolution is required before reaction can occur. Hence partial solubility parameter theory still has the potential to provide a good initial prediction of alternative solvent formulations with improved absorption performances.

7.2. CO₂ Absorption Experiments

The experimental plan was designed to achieve 3 main objectives, including:

- To establish a set of reference standard solvent loadings to which the performance of all other solvent formulations can be compared;
- To test the research hypothesis through random solvent sample CO₂ absorption experiments;
- To do a preliminary evaluation of the absorption performance of ionic liquids (ILs).

Three solvents commonly used in industry to recover CO₂ from gas streams were identified as reference solvent samples. Although none of the measured values closely match the values from literature, the discrepancies were attributed to the differences in operating conditions (i.e. the measured values were obtained for batch-wise operation, whilst the literature values were obtained for continuously operated processes). The limited resources available in the batch system make it impossible for the solvents to attain similar loadings as that obtained for the continuous system with unlimited resources. Nevertheless, the loadings measured for the remaining test samples were compared to the loadings measured for the three reference samples. Loading values obtained from repeated runs for the first two solvents were identical to the values found initially.

Six solvent formulations were randomly selected from predictions made by the EquiSolv solvent blend optimizer for CO₂ absorbing solvents. Water was used to balance the volume percentage contributions for each of the formulations. The solvents were synthesized for absorption experiments to determine the CO₂ loading of each formulation. The solvents were ranked in order of decreasing absorption

performance, i.e. decreasing loading values. For four of the solvents, the ranking positions based on their RED values matched the experimentally determined positions exactly. The determined positions of the remaining two solvents however were the exact opposite of their predicted positions. Kendall's coefficient of concordance was used to statistically test the null hypothesis. The p-value was calculated to be 0.01 (significantly less than the value chosen for the threshold of statistical significance, i.e. $\alpha = 0.05$). Based on this the null hypothesis can conclusively be rejected.

Next, three commercially available ILs were selected for CO₂ absorption experiments. The IL-based experiments were designed with a dual purpose: (i) to evaluate the absorption performance of aqueous IL solvents, and (ii) to serve as an additional hypothesis test. The loadings measured for the aqueous IL (60wt%) solvents showed only a slight improvement in absorption performance compared to the loadings measured for the reference solvents. Four amine-IL-based solvent formulations were randomly selected from predictions made by the EquiSolv solvent optimizer. The solvents were synthesized for absorption experiments in a second phase hypothesis test. The ranking of the solvents adhered to the same logic applied for the first hypothesis test. Results showed the predicted solvent ranking order to match the experimentally determined order exactly. Based on this, the null hypothesis is rejected conclusively.

A second statistical test based on Kendall's coefficient of concordance was conducted to test the null hypothesis against the combined data obtained for both experimental hypothesis tests. The p-value was found to be 0.001. Again, this is significantly less than the value chosen for α (i.e. 0.05). Based on this the null hypothesis is conclusively rejected in favour of the alternative hypothesis. Thus it can be concluded that partial solubility parameter theory can be used to accurately describe the equilibrium behaviour of CO₂ absorbing in task specific designed solvents. Hence, partial solubility parameters show great promise to be used as basis for solvent screening for CO₂ absorption.

Furthermore, based on their respective RED values, all of the predicted alternative solvent formulations were expected to exhibit improved absorption performance compared with the reference solvents. The solvent loadings measured experimentally validated this prediction. Thus, it is clear that partial solubility

parameter theory has enormous potential to be used in screening solvents for CO₂ recovery processes. Although it was found that leaks were present in the system, it was shown that the effect of the leaks was negligible on the data analysis of the absorption experiments.

8. Recommendations

8.1. Future Work on CO₂ Solubility Modeling

Due to the lack of available physical property data, the δ_i parameter could only be calculated for four of the 74 ILs for which the ionic bond energies were quantified. Future work should focus on quantifying the molar volumes of ILs in particular. Furthermore, the Hansen solubility parameters (δ_D , δ_P and δ_H) should also be assigned for a larger set of ILs. It is paramount that a larger dataset of ILs be comprised to thoroughly evaluate the proposed 4-set partial solubility parameter model. The proposed 4D visualization theory should also be tested properly.

The key feature of ILs is that they can be designed to achieve the desired physical properties through proper selection of the cation-anion combination. It has been suggested that there are at least 10^{18} possible cation-anion combinations. It is vital that the proposed 4-set parameter model be extended to consider the effect of cation-anion selection in the solvent screening process. In essence, each partial solubility parameter (i.e. δ_D , δ_P , δ_H and δ_i) should be devised into their respective contributions from the cation and anion elements:

$$\delta_i = f(\delta_{i,CAT}, \delta_{i,AN}) \quad [8.1]$$

Where the subscript i denote the solubility parameter component considered. A large dataset of 4-set parameter values is required to quantify the cation-anion interaction model (Eqn. 8.1). Data from literature suggests that the molecular interactions are dominated by selection of the anion. Including a model for cation-anion screening would make it possible to find the optimal IL additive (or substitute) for the considered application.

Next, the EquiSolv program should be upgraded to the revised iterative algorithm. This would ensure that the x_t values of all predicted blends amount to unity. Furthermore, this would improve the overall efficiency of the program to search for the optimal solvent formulation. The program should also be

upgraded to allow for temperature and pressure increment changes. This could be done by applying the derivative-form equations presented by Hansen. The temperature and pressure-dependencies of the δ_1 parameter should also be derived and included in the program.

8.2. Future Experimental Work and Model Validation

A volumetric method was used to determine the amount of CO₂ absorbed by each solvent. A solvent sample of known volume was injected into a pure CO₂ atmosphere of known volume. Pressure tests however revealed the presence of leaks in the system. It is recommended that the leaks in the system are fixed and the experimental work reevaluated. Varying solvent viscosities proved to be an obstacle when injecting some of the solvents. It is recommended that the experimental setup be redesigned to first load the solvent sample, followed by injecting the CO₂ gas. This should surmount issues arising from leaks as well as high solvent viscosities. Such a setup might however require the use of a gas flow meter to quantify the amount of CO₂ gas injected.

All of the absorption experiments were conducted at 25°C as this is the temperature for which the solubility parameter data is available. Once the EquiSolv program has been updated, solvent data should be generated for alternate temperature increments and the absorption experiments repeated. This would make it possible to screen solvent formulations for the optimum solvent-operating condition combination. The loadings of larger solvent formulation sets should also be quantified to thoroughly test the research hypothesis. Furthermore, the experimental plan should be expanded to evaluate the ability of the EquiSolv program to describe the miscibility of the solvent constituents in each other. This can be done by examining solvent formulations predicted by including the test for constituent inter-miscibility.

Finally, a number of predicted solvent formulations should be randomly selected for pilot plant tests. It is vital to evaluate the performance of these solvents under continuous operation at pilot-plant scale to determine the ability of partial solubility parameter theory to accurately predict alternative solvents that will minimize the energy requirements of CO₂ recovery processes.

References

Abbott, S., Hansen, C.M., Yamamoto, H. & Valpey, R.S., 2010. *Hansen Solubility Parameters in Practice*. 3rd ed. Hansen-Solubility.com.

Aboudheir, A. & ElMoudir, W., 2009. Performance of Formulated Solvent in Handling of Enriched CO₂ Flue Gas Stream. *Energy Procedia*, 1, pp.195-204.

Aboudheir, A., Tontiwachwuthikul, P., Chakma, A. & Idem, R., 2003. Kinetics of the reactive absorption of carbon dioxide in high CO₂-loaded, concentrated aqueous monoethanolamine solutions. *Chemical Engineering and Technology*, 58, pp.5195-210.

Anderson, J.L. et al., 2007. Ionic liquids as CO₂ capture media. In *CHEMRAWN-XVII Conference on Greenhouse Gases Mitigation and Utilization*. Western Cape Province, South Africa, 2007.

Aronu, U.E. et al., 2011. Equilibrium absorption of carbon dioxide by amino acid salt and amine amino acid salt solutions. *Energy Procedia*, 4, pp.109-16.

Aronu, U.E., Svendsen, H.F. & Karl, A.H., 2010. Investigation of amine amino acid salts for carbon dioxide absorption. *International Journal of Greenhouse Gas Control*, p.doi:10.1016/j.ijggc.2010.04.003.

Aronu, U.E. et al., 2009. Amine Amino Acid Salt for Carbon Dioxide Absorption. In *The 5th Trondheim Conference on CO₂ Capture, Transport and Storage*., 2009.

Astarita, G., Savage, D.W. & Bisio, A., 1983. *Gas treating with chemical solvents*. New York: John Wiley.

Baltus, R.E. et al., 2004. Low-Pressure Solubility of Carbon Dioxide in Room-Temperature Ionic Liquids Measured with a Quartz Crystal Microbalance. *The Journal of Physical Chemistry*, 108, p.721.

Bates, E.D., Mayton, R.D., Ntai, I. & Davis, J.H., 2002. CO₂ Capture by a Task-Specific Ionic Liquid. *Journal of the American Chemical Society*, 124, p.926.

Cabaco, M.I., Besnard, M., Danten, Y. & Coutinho, J.A.P., 2011. Solubility of CO₂ in 1-Butyl-3-methylimidazolium-trifluoro Acetate Ionic Liquid Studied by Raman Spectroscopy and DFT Investigations. *The Journal of Physical Chemistry*, 115, pp.3538-50.

- Carapellucci, R. & Milazzo, A., 2003. Membrane systems for CO₂ capture and their integration with gas turbine plants. *Proceedings of the Institute of Mechanical Engineers Part A: Journal of Power and Energy*, 217, pp.505-17.
- CCC, 2008. *Building a Low Carbon Economy - The UK's Contribution to Tackling Climate Change*. TSO, London: <http://www.theccc.org.uk> Committee on Climate Change.
- Chakma, A., 1995. Separation of CO₂ and SO₂ from flue gas streams by liquid membranes. *Energy Conversion and Management*, 36, pp.405-10.
- Chakraborty, A.K., Astarita, G. & Bischoff, K.B., 1986. CO₂ absorption in aqueous solutions of hindered amines. *Chemical Engineering Science*, 41, pp.997-1000.
- Chakravati, S., Gupta, A. & Hunek, B., 2001. Advanced technology for the capture of carbon dioxide from flue gases. In *1st National Conference on Carbon Sequestration*. Washington, DC, 2001.
- Chapel, D.G. & Mariz, C.L., 1999. Recovery of CO₂ from flue gases: commercial trends. In *Originally presented at the Canadian society of chemical engineers annual meeting.*, 1999.
- Chapra, S.C., 2008. *Applied Numerical Methods with MATLAB for Engineers and Scientists*. 2nd ed. McGraw-Hill.
- Cheng, H.H. & Tan, C.S., 2009. Carbon dioxide capture by blended alkanolamines in rotating packed bed. *Energy Procedia*, 1(1), pp.925-32.
- Cullinane, J.T. & Rochelle, G.T., 2005. Thermodynamics of aqueous potassium carbonate, piperazine, and carbon dioxide. *Fluid Phase Equilibria*, 227, pp.197-213.
- da Silva, E.F. & Svendsen, H.F., 2007. Computational chemistry study of reactions, equilibrium and kinetics of chemical CO₂ absorption. *International Journal of Greenhouse Gas Control*, 1, pp.151-57.
- Danckwerts, P.V., 1970. *Gas-Liquid Reactions*. NY, USA: McGraw-Hill.
- Darde, V., Thomsen, K., van Well, W.J.M. & Stenby, E.H., 2010. Chilled ammonia process for CO₂ capture. *International Journal of Greenhouse Gas Control*, 4, pp.131-36.
- Davidson, R.M., 2007. CCC/125 *Post-combustion Carbon Capture from Coal Fired Plants - Solvent Scrubbing*.

- Davison, J., 2007. Performance and costs of power plants with capture and storage of CO₂. *Energy*, 32, pp.1163-76.
- Davis, J. & Rochelle, G., 2009. Thermal degradation of monoethanolamine at stripper conditions. *Energy Procedia*, 1(1), pp.327-33.
- De Marignan, A.L., 2008. *CO₂ capture and storage: The IFP-steered European Castor project is a tremendous success.* [Online] Available at: <http://www.ifpenergiesnouvelles.com/actualites/communiqués-de-presse/le-projet-europeen-castor-plebiscite> [Accessed 25 September 2011].
- Dragos, L., Nada, O., Flueraru, C. & Scarlat, N., 1996. Romanian research for CO₂ recovery. *Energy Conversion and Management*, 37, pp.923-28.
- Dugas, E.R., 2006. *Pilot plant study of carbon dioxide capture by aqueous monoethanolamine.* MSc Thesis. Austin, USA: University of Texas.
- Edali, M., Aboudheir, A. & Idem, R., 2009. Kinetics of carbon dioxide absorption into mixed aqueous solutions of MDEA and MEA using laminar jet apparatus and a numerically solved 2D absorption rate/kinetics model. *International Journal of Greenhouse Gas Control*, 3, pp.550-60.
- Elwell, L.C. & Grant, W.S., 2006. Technology options for capturing CO₂-Special Reports. *Power*, 150(8).
- Enkvist, P.A., Naucér, T. & Rosander, J., 2007. A cost curve for greenhouse gas reduction. *The McKinsey Quarterly*, pp.37-45.
- Erga, O., Juliussenb, O. & Lidal, H., 1995. CO₂ recovery by means of aqueous amines. *Energy Conservation and Management*, 36, pp.387-92.
- Feng, Z. et al., 2010. Absorption of CO₂ in the aqueous solutions of functionalized ionic liquids and MDEA. *Chemical Engineering Journal*, 160, pp.691-97.
- Fernandes, A.M. et al., 2011. Evaluation of Cation-Anion Interaction Strength in Ionic Liquids. *The Journal of Physical Chemistry*, 115, pp.4033-41.
- Feron, P.H.M., 2010. Exploring the potential for improvement of the energy performance of coal fired power plants with post-combustion capture of carbon dioxide. *International Journal of Greenhouse Gas Control*, 4, pp.152-60.

Feron, P.H.M. & Hendriks, C.A., 2005. CO₂ capture process principles and costs. *Oil and Gas Science and Technology-Rev*, 60(3), pp.451-59.

Finkenrath, M., 2011. Cost and Performance of Carbon Dioxide Capture from Power Generation. *International Energy Agency*, p.http://www.iea.org/papers/2011/costperf_ccs_powergen.pdf.

Freeman, S.A. et al., 2010. Carbon dioxide capture with concentrated, aqueous piperazine. *International Journal of Greenhouse Gas Control*, 4, pp.119-24.

freevec.org, 2010. freevec.org. [Online] Available at: http://freevec.org/function/inverse_matrix_4x4_using_partitioning [Accessed 2 August 2010].

Freguia, S. & Rochelle, G.T., 2003. Modeling of CO₂ capture by aqueous monoethanolamine. In *AIChE Symposium Ser. 49.*, 2003.

Freund, P., 2003. Making deep reductions in CO₂ emissions from coal-fired power plants using capture and storage of CO₂. *Proceedings of the Institute of Mechanical Engineers Part A: Journal of Power and Energy*, 217, pp.1-8.

Gertenbach, R.M., 2009. *Methane and Carbon Dioxide Sorption Studies on South African Coals*. Master of Science in Engineering Thesis. University of Stellenbosch.

Hansen, C.M., 2007. *Hansen solubility parameters: a user's handbook*. 2nd ed. CRC Press, ISBN: 9780849372483.

Hansen, C.M., 2011. *Hansen Solubility Parameters*. [Online] Available at: <http://hansen-solubility.com/index.php?id=11> [Accessed 9 October 2011].

Herzog, H., Caldeira, K. & Adams, E., 2000. Carbon Sequestration via Direct Injection. *Encyclopedia of Ocean Sciences*.

Herzog, H.J. & Drake, E.M., 1996. Carbon dioxide recovery and disposal from large energy systems. *Annual Review of Energy and the Environment*, 21, pp.145-66.

Husson-Borg, P., Majer, V. & Costa Gomes, M.F., 2003. Solubilities of Oxygen and Carbon Dioxide in Butyl Methyl Imidazolium Tetrafluoroborate as a Function of Temperature and at Pressures Close to Atmospheric Pressure. *Journal of Chemical Engineering Data*, 48, p.480.

HyperChem, 2011. *HyperChem Professional Help Files*. HyperChem.

iCap, 2010. *The iCap project*. [Online] Available at: <http://icapco2.org/> [Accessed 25 September 2011].

Idem, R. et al., 2006. Pilot plant studies of the CO₂ capture performance of aqueous MEA and mixed MEA/MDEA solvents at the University of Regina CO₂ capture technology development plant and the Boundary Dam CO₂ capture demonstration plant. *Industrial and Engineering Chemistry Research*, 45, pp.2414-20.

IEA, 1993. *The Capture of Carbon Dioxide from Fossil Fuel Fired Power Stations*. Cheltenham, UK: IEA GHG; IEA GHG/SR2.

IEA, 2007. *International Energy Outlook 2007*. <http://www.eia.doe.gov/oiaf/ieo/index.html>.

IEA, 2009. How the energy sector can deliver on a climate agreement in Copenhagen. In *Special early excerpt of the World Energy Outlook 2009 for the Bangkok UNFCCC meeting*, http://www.iea.org/weo/docs/weo2009/climate_change_excerpt.pdf, 2009. International Energy Agency.

IPCC, 2005. *Intergovernmental Panel on Climate Change (IPCC) Special Report on Carbon Dioxide Capture and Storage*. Cambridge, UK: Cambridge University press.

Jassim, M.S., Rochelle, G., Eimer, D. & Ramshaw, C., 2009. Carbon dioxide absorption and desorption in aqueous monoethanolamine solutions in a rotating packed bed. *Industrial and Engineering Chemistry Research*, 46, pp.2823-33.

Kenig, E.Y., Scheider, R. & Górak, A., 2001. Reactive absorption: optimal process design via optimal modelling. *Chemical Engineering and Technology*, 56, pp.343-50.

Kishimoto, S. et al., 2009. Current status of MHI's CO₂ recovery technology and optimization of CO₂ recovery plant with a PC fired power plant. *Energy Procedia*, 1, pp.1091-98.

Kittel, J. et al., 2009. Corrosion in MEA units for CO₂ capture: pilot plant studies. *Energy Procedia*, 1(1), pp.791-97.

Knudsen, J.N., Vilhelmsen, P.J., Jensen, J.N. & Beide, O., 2008. *CASTOR SP2: Experiments on Pilot Plant*. [Online] Dong Energy and Vattenfall Available at: http://www.encapco2.org/CECD/castor_knudsen.pdf [Accessed 25 September 2011].

Knuutila, H., Aronu, U.E., Kvamsdal, H.M. & Chikukwa, A., 2011. Post combustion CO₂ capture with an amino acid salt. *Energy Procedia*, 4, pp.1550-57.

Kohl, A.L. & Nielsen, R.B., 1997. *Gas purification*. 5th ed. Houston, Texas: Gulf Publisher.

Koretsky, M.D., 2004. *Engineering and Chemical Thermodynamics*. John Wiley & Sons.

Kucka, L., Müller, I., Kenig, E.Y. & Górak, A., 2003. On the modelling and simulation of sour gas absorption by aqueous amine solutions. *Chemical Engineering and Technology*, 58, pp.3571-78.

Kumar, P., Hogendoorn, J., Versteeg, G.F. & Feron, P.H.M., 2003. Kinetics of the reaction of CO₂ with aqueous potassium salt of taurine and glycine. *The American Institute of Chemical Engineers Journal*, 49(1), pp.203-13.

Kvamsdal, H.M., Jakobsen, J.P. & Hoff, K.A., 2009. Dynamic modelling and simulation of a CO₂ absorber column for post-combustion CO₂ capture. *Chemical Engineering and Processing: Process Intensification*, 48, pp.135-44.

Lawal, A. et al., 2010. Dynamic modelling and analysis of post-combustion CO₂ chemical absorption process for coal-fired power plants. *Fuel*, 89(10), pp.2791-801.

Lawal, A., Wang, M., Stephenson, P. & Yeung, H., 2009a. Dynamic modelling of CO₂ absorption for post-combustion capture in coal-fired power plants. *Fuel*, 88(12), pp.2455-62.

Lawal, A., Wang, M., Stephenson, P. & Yeung, H., 2009b. Dynamic modelling and simulation of CO₂ chemical absorption process for coal-fired power plants. *Computer Aided Chemical Engineering*, 27, pp.1725-30.

Lee, S.H. & Lee, S.B., 2005. The Hildebrand solubility parameters, cohesive energy densities and internal energies of 1-alkyl-3-methylimidazolium-based room temperature ionic liquids. *Chemical Communications, RSC*, doi: 10.1039/b503740a, pp.3469-71.

Legendre, P., 2005. Species Associations: The Kendall Coefficient of Concordance Revisited. *American Statistical Association and the International Biometric Society Journal of Agricultural, Biological, and Environmental Statistics*, 10(2), p.226–245.

Lin, C.C. & Liu, W.T., 2007. Mass transfer characteristics of a high-voidage rotating packed bed. *Journal of Industrial and Engineering Chemistry*, 13(1), pp.71-78.

- Llovell, F. et al., 2010. Thermodynamic characterization of ionic liquids and their mixtures with supercritical carbon dioxide. In Reverchon, E., ed. *Ninth Conference on Supercritical Fluids and Their Applications*. Sorrento, Italy, 2010.
- Lucquiaud, M. & Gibbins, J., 2010. Effective retrofitting of post-combustion CO₂ capture to coal-fired power plants and insensitivity of CO₂ abatement costs to base plant efficiency. *International Journal of Greenhouse Gas Control*, p.doi:10.1016/j.ijggc.2010.09.003.
- Marciniak, A., 2010. The Solubility Parameters of Ionic Liquids. *International Journal of Molecular Sciences*, 11, pp.1973-90.
- Mathews, J., 2007. Seven steps to curb global warming. *Energy Policy*, 35, pp.4247-59.
- Mattedi, S. et al., 2011. High pressure CO₂ solubility in N-methyl-2-hydroxyethylammonium protic ionic liquids. *The Journal of Supercritical Fluids*, 56, pp.224-30.
- Mofarahi, M., Khojasteh, Y., Khaledi, H. & Farahnak, A., 2008. Design of CO₂ absorption plant for recovery of CO₂ from flue gases of gas turbine. *Energy*, 33, pp.1311-19.
- Noeres, C., Kenig, E.Y. & Górak, A., 2003. Modelling of reactive separation processes: reactive absorption and reactive distillation. *Chemical Engineering Progress*, 42, pp.157-78.
- Notz, R. et al., 2010. A short-cut method for assessing absorbents for post-combustion carbon dioxide capture. *International Journal of Greenhouse Gas Control*, p.doi:10.1016/j.ijggc.2010.03.008.
- Nyquist, S. & Ruys, J., 2009. CO₂ abatement: Exploring options for oil and natural gas companies. *The McKinsey Quarterly*, pp.39-43.
- NZEC, 2009. *The joint China-UK near zero emissions coal (NZEC) Initiative*. [Online] Available at: <http://www.nzec.info/en/assets/Reports/China-UK-NZEC-English-031109.pdf> [Accessed 25 September 2011].
- Oexmann, J., Hensel, C. & Kather, A., 2008. Post-combustion CO₂-capture from coal-fired power plants: Preliminary evaluation of an integrated chemical absorption process with piperazine-promoted potassium carbonate. *International Journal of Greenhouse Gas Control*, 2, pp.539-52.

Oexmann, J. & Kather, A., 2010. Minimising the regeneration heat duty of post-combustion CO₂ capture by wet chemical absorption: The misguided focus on low heat of absorption solvents. *International Journal of Greenhouse Gas Control*, 4, pp.36-43.

Oyenekan, B.A., 2007. *Modeling of strippers for CO₂ capture by aqueous amines*. PhD Thesis. Austin, USA: The University of Texas.

Oyenekan, B.A. & Rochelle, G.T., 2007. Alternative stripper configurations for CO₂ capture by aqueous amines. *American Institute of Chemical Engineers Journal*, 53(12), pp.3144-54.

Panayiotou, S.C., 2008. Prediction of Hansen Solubility Parameters with a New Group-Contribution Method. *International Journal of Thermophysics*, 29(2), pp.568-85.

Pires, J.C.M., Martins, F.G., Alvim-Ferraz, M.C.M. & Simões, M., 2011. Recent developments on carbon capture and storage: An overview. *Chemical Engineering Research and Design*, 89, pp.1446-60.

Rao, A.B., Rubin, E.S. & Berkenpas, M.B., 2004. *An Integrated Modelling Framework for Carbon Management Technologies*. Pittsburgh, Pennsylvania: Carnegie Mellon University.

Raynal, L., Bouillon, P.A., Gomez, A. & Broutin, P., 2011. From MEA to demixing solvents and future steps; a roadmap for lowering the cost of post-combustion carbon capture. *Chemical Engineering Journal*, p.doi:10.1016/j.cej.2011.01.008.

Resnik, K.P., Yeh, J.T. & Pennline, H.W., 2004. Aqua ammonia process for simultaneous removal of CO₂, SO₂ and NO_x. *International Journal of Environmental Technology and Management*, 4, pp.89-104.

Retief, F.J.G., 2009. *Investigating the Effect of the Supercritical Region on the Adsorption of Carbon Dioxide & Methane on Dry South African Coals*. Undergraduate Thesis. University of Stellenbosch.

Riahi, K., Rubin, E.S. & Schrattenholzer, L., 2004. Prospects for carbon capture and sequestration technologies assuming their technological learning. *Energy*, 29, pp.1309-18.

Rogers, R.D. & Seddon, K.R., 2002. *Ionic Liquids: Industrial Applications to Green Chemistry*. Washington D.C.: American Chemical Society.

Rydén, M. & Lyngfelt, A., 2006. Using steam reforming to produce hydrogen with carbon dioxide capture by chemical-looping combustion. *International Journal of Hydrogen Energy*, 31, pp.1271-83.

- Sada, T., Fujii, M. & Yoshida, K., 1992. Development of flue gas CO₂ recovery technology. *Energy Conversion and Management*, 33, pp.317-24.
- Saha, S. & Chakma, A., 1992. Separation of CO₂ from gas mixture with liquid membrane. *Energy Conversion and Management*, 33, pp.413-20.
- Schneider, R., Kenig, E.Y. & Górak, A., 1999. Dynamic modelling of reactive absorption with the Maxwell-Stefan approach. *Chemical Engineering Research and Design*, 77, pp.633-38.
- Scovazzo, P. et al., 2004. Regular Solution Theory and CO₂ Gas Solubility in Room-Temperature Ionic Liquids. *Industrial and Engineering Chemistry Research*, 43, p.6855.
- Shao, R. & Stangeland, A., 2009. *Amines Used in CO₂ Capture*. Oslo, Norway: The Bellona Foundation.
- Shiflett, M.B. & Yokozeki, A., 2005. Solubilities and Diffusivities of Carbon Dioxide in Ionic Liquids: [bmim][PF₆] and [bmim][BF₄]. *Industrial and Engineering Chemistry Research*, 44, pp.4453-64.
- Singh, P., Niederer, J.P.M. & Versteeg, G.F., 2007. Structure and activity relationships for amine based CO₂ absorbents - I. *International Journal of Greenhouse Gas Control*, 1, pp.5-10.
- Singh, P., Niederer, J.P.M. & Versteeg, G.F., 2009. Structure and activity relationships for amine-based CO₂ absorbents - II. *Chemical Engineering Research and Design*, 87, pp.135-44.
- Singh, P. & Versteeg, G.F., 2008. Structure and activity relationships for CO₂ regeneration from aqueous amine-based absorbents. *Process Safety and Environment Protection*, 86, pp.347-59.
- Stewart, C. & Hessami, M., 2005. A study of methods for carbon dioxide capture and sequestration-the Sustainability of a photosynthetic bioreactor approach. *Energy Conversion and Management*, 46, pp.403-20.
- Thitakamol, B., Veawab, A. & Aroonwilas, A., 2007. Environmental impacts of absorption-based CO₂ capture unit for post-combustion treatment of flue gas from coal-fired power plant. *International Journal of Greenhouse Gas Control*, 1, pp.318-42.
- Tobiesen, F.A. & Svendsen, H.F., 2006. Study of a modified amine-based regeneration unit. *Industrial and Engineering Chemistry Research*, 45, pp.2489-96.

UNEP, 2005. *United Nations Environment Programme, Introduction to Climate Change*. <http://www.grida.no/climate/vital/06.htm> (accessed October 2010).

Uyanga, I.J. & Idem, R.O., 2007. Studies of SO₂- and O₂-induced degradation of aqueous MEA during CO₂ capture from power plant flue gas streams. *Industrial and Engineering Chemistry Research*, 46(8), pp.2558-66.

Vaidya, P.D. & Kenig, E.Y., 2007. CO₂-alkanolamine reaction kinetics: a review of recent studies. *Chemistry - A European Journal*, 30, pp.1467-74.

Van Holst, J., Versteeg, G.F., Brillman, D.W.F. & Hogendoorn, J.A., 2009. Kinetic study CO₂ with various amino acid salts in aqueous solution. *Chemical Engineering Science*, 64(1), pp.59-68.

Vega, L.F., Vilaseca, O., Llovel, F. & Andreu, S., 2008. Modeling Ionic Liquids and the Solubility of Gases in them: recent advances and perspectives. *Fluid Phase Equilibria*, p.doi:10.1016/j.fluid.2010.02.006.

Wang, M. et al., 2010. Post-combustion CO₂ capture with chemical absorption: A state-of-the-art review. *Chemical Engineering Research and Design*, doi:10.1016/j.cherd.2010.11.005.

Wappel, D., Gronald, G., Kalb, R. & Draxler, J., 2009. Ionic liquids for post-combustion CO₂ absorption. *International Journal of Greenhouse Gas Control*, p.doi:10.1016/j.ijggc.2009.11.012.

Wasserscheid, P. & Welton, T., 2008. *Ionic Liquids in Synthesis*. 2nd ed. Wiley-VCH, ISBN: 9783527312399.

Wilson, M.A., Wrubesk, R.M. & Yarborough, L., 1992. Recovery of CO₂ from power plant flue gases using amines. *Energy Conversion and Management*, 33, pp.325-31.

Wong, S., Payzant, J., Bioletti, R. & Feng, X., 2002. www.arc.ab.ca CO₂ separation technology in enhanced oil recovery: a state-of-the-art technical and economic review. Final Report. Alberta Research Council.

Yamasaki, A., 2003. An overview of CO₂ mitigation options for global warming - Emphasizing CO₂ sequestration options. *Journal of Chemical Engineering of Japan*, 36(4), pp.361-75.

Yang, H. et al., 2008. Progress in carbon dioxide separation and capture: A review. *Journal of Environmental Sciences*, 20, pp.14-27.

Yu, G. et al., 2006. Design of Task-Specific Ionic Liquids for Capturing CO₂: A Molecular Orbital Study. *Industrial and Engineering Chemistry Research*, 45, pp.2875-80.

Zhao, Z., Cui, X., Ma, J. & Li, R., 2007. Adsorption of carbon dioxide on alkali-modified zeolite 13X adsorbents. *International Journal of Greenhouse Gas Control*, 1, pp.355-59.

Ziaii, S., Rochelle, G.T. & Edgar, T.F., 2009. Dynamic modelling to minimise the energy use for CO₂ capture in power plant aqueous monoethanolamine. *Industrial and Engineering Chemistry Research*, 48, pp.6105-11.

Appendix A: EquiSolv Fundamentals

A.1. Introduction

The EquiSolv solvent blend optimizer offers the option to use either matrix-manipulation or Gauss-Seidel iteration as basis for screening alternative solvent formulations. Both approaches allow analysis for up to four blend constituents, either including or excluding the proposed δ_i parameter. Furthermore, both approaches offer the option to use either linear or square calculation methods.

The matrix-manipulation approach calculates the blend composition directly, reducing the time required for analysis. This approach however could yield significant noise as well as other discrepancies in the predicted data. In contrast the iterative approach will increase the time of calculation, but improved accuracy and considerably less noise and discrepancies.

The solvent-solute distances (R_a) are calculated using the same set of equations for both approaches. See Chapter 3 for a detailed discussion on the equations used to calculate the R_a values for either 3D or 4D visualizations. A detailed discussion is given below on the step-by-step procedures employed by the EquiSolv program for either matrix or iterative analysis methods.

A.2. Solvent Blend Calculations: Matrix Manipulation

Matrix manipulation is used to solve directly for the blend composition from a set of linear algebraic equations. The calculated composition is used to determine the partial solubility parameter values for the blend. This is done for every possible solvent formulation. The blends are then either accepted or rejected based on their calculated RED values. A block flow diagram of the basic algorithm employed in the matrix-manipulation approach is shown in Figure A.1.

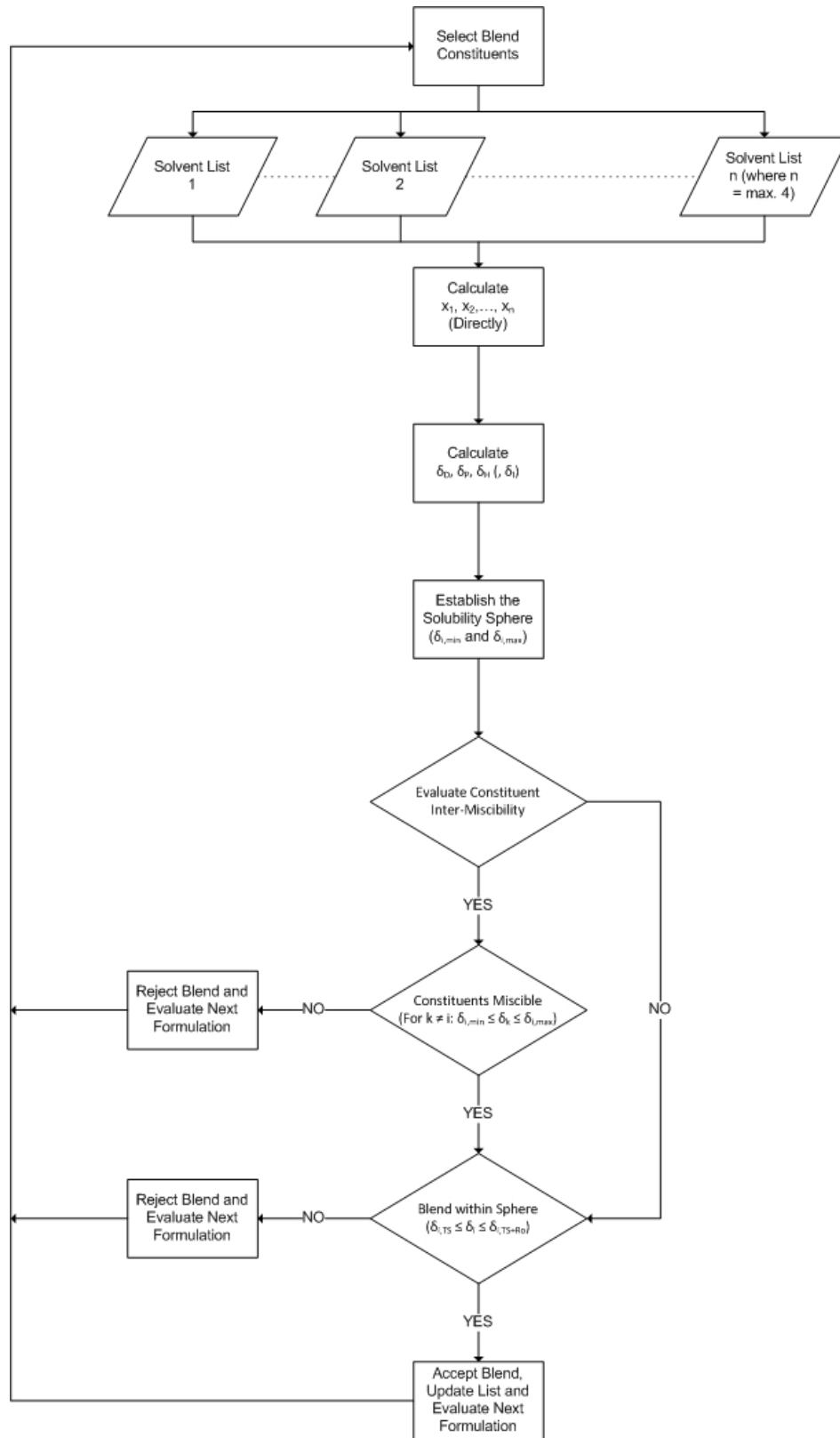


Figure A.1 – A block flow diagram of the algorithm used by the EquiSolv solvent optimizer for matrix manipulation calculations.

A.2.1. Two-Component Blends

A.2.1.1. Linear Calculation Method

The first step in solving matrix manipulation-based calculations is to establish the set of linear algebraic equations. The left-hand side (LHS) of the equations is comprised of the partial solubility parameter component contributions. The right-hand side (RHS) of the equations is a column vector of the partial solubility parameter values for the target solute. The dispersion and polar interaction parameters (δ_D and δ_P) are isolated to form a two-by-two matrix for the two-component blend analysis. The set of linear equations used by the EquiSolv program to solve for the composition of two-component blends is expressed as follow:

$$\begin{pmatrix} x_1 \cdot \delta_{D,1} & x_2 \cdot \delta_{D,2} \\ x_1 \cdot \delta_{P,1} & x_2 \cdot \delta_{P,2} \end{pmatrix} = \begin{pmatrix} \delta_{D,TS} \\ \delta_{P,TS} \end{pmatrix} \quad [\text{A.1.}]$$

Where x is the volume percentage contribution of the constituent considered, δ is the partial solubility parameter value, the subscripts D and P denotes the dispersion and polar interactions respectively, the subscript TS denote the target solute, and

$$\mathbf{M} = \begin{pmatrix} \delta_{D,1} & \delta_{D,2} \\ \delta_{P,1} & \delta_{P,2} \end{pmatrix} \quad [\text{A.2.}]$$

$$\mathbf{B} = \begin{pmatrix} \delta_{D,TS} \\ \delta_{P,TS} \end{pmatrix} \quad [\text{A.3.}]$$

With the set of linear equations defined, the determinant of the two-by-two (2x2) matrix on the LHS is determined as follows:

$$\text{Det } \mathbf{M} = \delta_{D,1}\delta_{P,2} - \delta_{D,2}\delta_{P,1} \quad [\text{A.4.}]$$

The determinant in turn, is used to calculate the inverse of the 2x2 matrix, \mathbf{M} . The inverse is defined as follow:

$$\mathbf{M}^{-1} = \frac{1}{\text{Det } \mathbf{M}} \begin{pmatrix} \delta_{P,2} & -\delta_{D,2} \\ -\delta_{P,1} & \delta_{D,1} \end{pmatrix} \quad [\text{A.5.}]$$

To yield:

$$\mathbf{M}^{-1} = \begin{pmatrix} M_{11}^* & M_{12}^* \\ M_{21}^* & M_{22}^* \end{pmatrix} \quad [\text{A.6.}]$$

The composition of the two-component blend is calculated directly from the inverse of the matrix \mathbf{M} . The volume percentage contributions (i.e. volume fractions) of the solvent constituents considered is calculated as follow:

$$x_1 = M_{11}^* \delta_{D,TS} + M_{12}^* \delta_{P,TS} \quad [\text{A.7.}]$$

$$x_2 = M_{21}^* \delta_{D,TS} + M_{22}^* \delta_{P,TS} \quad [\text{A.8.}]$$

Next, the blend partial solubility parameter component values are calculated from the calculated blend composition:

$$\delta_{D,calc} = x_1 \delta_{D,1} + x_2 \delta_{D,2} \quad [\text{A.9.}]$$

$$\delta_{P,calc} = x_1 \delta_{P,1} + x_2 \delta_{P,2} \quad [\text{A.10.}]$$

$$\delta_{H,Calc} = x_1\delta_{H,1} + x_2\delta_{H,2} \quad [A.11.]$$

$$\delta_{I,Calc} = x_1\delta_{I,1} + x_2\delta_{I,2} \quad [A.12.]$$

Where the subscripts H and I denotes the hydrogen bond and ionic interactions respectively, and the subscript Calc denote the calculated parameter values. It is vital to check whether or not the partial solubility parameters assigned to the blend are located within the specified solubility sphere. This is done by evaluating the RED value calculated for the blend. A RED value in the range 0-1 would indicate that the blend parameters are located within the solubility sphere. The EquiSolv solvent optimizer however offers a second option called the “variance from ideality”. Essentially this is a second solubility sphere constructed around the partial solubility parameter values of the target the solute. The range of this sphere however can be adjusted, as opposed to the range of the standard sphere that is fixed on the solute interaction radius (Ro). The range of the second sphere is calculated as follow:

$$\delta_{i,tar\ min} = \delta_i - \left[\left(\frac{VI}{100} \right) \cdot \delta_i \right] \quad [A.13.]$$

$$\delta_{i,tar\ max} = \delta_i + \left[\left(\frac{VI}{100} \right) \cdot \delta_i \right] \quad [A.14.]$$

Where the subscript i denote the partial solubility parameter component considered, the subscripts tar min and tar max denotes the lower and upper limits of the calculated range respectively, and VI is the variance from ideality specified by the user. To be accepted, the partial solubility parameters calculated for the blend must fall in the range between the lower and upper limits calculated:

$$\delta_{i,tar\ min} \leq \delta_{i,Calc} \leq \delta_{i,tar\ max} \quad [A.15.]$$

The EquiSolv solvent optimizer also offers the option to examine the miscibility of the solvent blend constituents in each other. This is done by constructing a set of solubility spheres around the partial solubility parameters of each of the constituents considered. The ranges of the interaction spheres are calculated as follow:

$$\delta_{i,min} = \delta_i - \left[\left(1 - \left(\frac{CL}{100} \right) \right) \cdot \delta_i \right] \quad [A.16.]$$

$$\delta_{i,max} = \delta_i + \left[\left(1 - \left(\frac{CL}{100} \right) \right) \cdot \delta_i \right] \quad [A.17.]$$

Where the subscripts min and max denotes the lower and upper limits of the ranges respectively, and CL is the confidence level specified by the user. The confidence level represents the minimum acceptable range of interaction between the constituents. For constituents to be miscible in each other, their respective solubility spheres should overlap. Mathematically, this is expressed as follow:

$$\delta_{ij+1,min} \leq \delta_{ij,Calc} \leq \delta_{ij+1,max} \quad [A.18.]$$

$$\delta_{ij-1,min} \leq \delta_{ij,Calc} \leq \delta_{ij-1,max} \quad [A.19.]$$

A.2.1.2. Square Calculation Method

The same set of equations described above for the linear calculation method is applied to the square calculation method. The only difference between the two methods is in the set of linear equations established at the start of the process. For the square method, the values of the partial solubility parameter components considered is raised to the power of two, (i.e. squared). The set of linear equations used for the square method is expressed as follow:

$$\begin{pmatrix} x_1 \cdot \delta_{D,1}^2 & x_2 \cdot \delta_{D,2}^2 \\ x_1 \cdot \delta_{P,1}^2 & x_2 \cdot \delta_{P,2}^2 \end{pmatrix} = \begin{pmatrix} \delta_{D,TS}^2 \\ \delta_{P,TS}^2 \end{pmatrix} \quad [\text{A.20.}]$$

A.2.2. Three-Component Blends

A.2.2.1. Linear Calculation Method

A procedure similar to that described above for two-component calculations is used to solve for the compositions and partial solubility parameter values of three-component blends. The matrix of linear algebraic equations used for linear three-component calculations is defined as follow:

$$\begin{pmatrix} x_1 \cdot \delta_{D,1} & x_2 \cdot \delta_{D,2} & x_3 \cdot \delta_{D,3} \\ x_1 \cdot \delta_{P,1} & x_2 \cdot \delta_{P,2} & x_3 \cdot \delta_{P,3} \\ x_1 \cdot \delta_{H,1} & x_2 \cdot \delta_{H,2} & x_3 \cdot \delta_{H,3} \end{pmatrix} = \begin{pmatrix} \delta_{D,TS} \\ \delta_{P,TS} \\ \delta_{H,TS} \end{pmatrix} \quad [\text{A.21.}]$$

Where

$$\mathbf{M} = \begin{pmatrix} \delta_{D,1} & \delta_{D,2} & \delta_{D,3} \\ \delta_{P,1} & \delta_{P,2} & \delta_{P,3} \\ \delta_{H,1} & \delta_{H,2} & \delta_{H,3} \end{pmatrix} \quad [\text{A.22.}]$$

$$\mathbf{B} = \begin{pmatrix} \delta_{D,TS} \\ \delta_{P,TS} \\ \delta_{H,TS} \end{pmatrix} \quad [\text{A.23.}]$$

From this, the determinant of the three-by-three (3x3) matrix comprising the LHS of the equations is calculated as follow:

$$\begin{aligned} \text{Det } \mathbf{M} = & (\delta_{D,1}\delta_{P,2}\delta_{H,3} + \delta_{D,2}\delta_{P,3}\delta_{H,1} + \delta_{D,3}\delta_{P,1}\delta_{H,2}) \\ & - (\delta_{D,3}\delta_{P,2}\delta_{H,1} + \delta_{D,1}\delta_{P,3}\delta_{H,2} + \delta_{D,2}\delta_{P,1}\delta_{H,3}) \end{aligned} \quad [\text{A.24.}]$$

Next, a set of cofactors is determined. The cofactors are required to calculate the inverse of the matrix, **M**. A total of 9 cofactors are calculated:

$$C_{11} = (\delta_{D,2}\delta_{H,3} - \delta_{H,2}\delta_{P,3}) \quad [A.25.]$$

$$C_{21} = -(\delta_{D,2}\delta_{H,3} - \delta_{H,2}\delta_{D,3}) \quad [A.26.]$$

$$C_{31} = (\delta_{D,2}\delta_{P,3} - \delta_{P,2}\delta_{D,3}) \quad [A.27.]$$

$$C_{12} = -(\delta_{P,1}\delta_{H,3} - \delta_{H,1}\delta_{P,3}) \quad [A.28.]$$

$$C_{22} = (\delta_{D,1}\delta_{H,3} - \delta_{H,1}\delta_{D,3}) \quad [A.29.]$$

$$C_{32} = -(\delta_{D,1}\delta_{P,3} - \delta_{P,1}\delta_{D,3}) \quad [A.30.]$$

$$C_{13} = (\delta_{P,1}\delta_{H,2} - \delta_{H,1}\delta_{P,2}) \quad [A.31.]$$

$$C_{23} = -(\delta_{D,1}\delta_{H,2} - \delta_{H,1}\delta_{D,2}) \quad [A.32.]$$

$$C_{33} = (\delta_{D,1}\delta_{P,2} - \delta_{P,1}\delta_{D,2}) \quad [A.33.]$$

The values calculated from Eqns. A.25 to A.33 are used to establish a matrix of cofactors. The matrix in turn is multiplied by the reciprocal of the determinant calculated for the matrix, **M**. This yields the inverse of the matrix, **M**:

$$\mathbf{M}^{-1} = \frac{1}{\text{Det } \mathbf{M}} \cdot \begin{pmatrix} C_{11} & C_{12} & C_{13} \\ C_{21} & C_{22} & C_{23} \\ C_{31} & C_{32} & C_{33} \end{pmatrix} \quad [\text{A.34.}]$$

To yield:

$$\mathbf{M}^{-1} = \begin{pmatrix} C_{11}^* & C_{12}^* & C_{13}^* \\ C_{21}^* & C_{22}^* & C_{23}^* \\ C_{31}^* & C_{32}^* & C_{33}^* \end{pmatrix} \quad [\text{A.35.}]$$

The inverse is multiplied by the column vector for the partial solubility parameter values of the target solute to obtain a column vector for the volume percentage contributions of the blend constituents:

$$\{x\} = \mathbf{M}^{-1} \cdot \mathbf{B} \quad [\text{A.36.}]$$

From this, the volume percentage contributions of the blend constituents can be expressed as follow:

$$x_1 = C_{11}^* \delta_{D,TS} + C_{12}^* \delta_{P,TS} + C_{13}^* \delta_{H,TS} \quad [\text{A.37.}]$$

$$x_2 = C_{21}^* \delta_{D,TS} + C_{22}^* \delta_{P,TS} + C_{23}^* \delta_{H,TS} \quad [\text{A.38.}]$$

$$x_3 = C_{31}^* \delta_{D,TS} + C_{32}^* \delta_{P,TS} + C_{33}^* \delta_{H,TS} \quad [\text{A.39.}]$$

The procedure used to calculate and evaluate the partial solubility parameter values of the blend is similar to that described earlier for two-component blends.

A.2.2.2. Square Calculation Method

The set of linear equations used for squared three-component blend calculations is expressed as follow:

$$\begin{pmatrix} x_1 \cdot \delta_{D,1}^2 & x_2 \cdot \delta_{D,2}^2 & x_3 \cdot \delta_{D,3}^2 \\ x_1 \cdot \delta_{P,1}^2 & x_2 \cdot \delta_{P,2}^2 & x_3 \cdot \delta_{P,3}^2 \\ x_1 \cdot \delta_{H,1}^2 & x_2 \cdot \delta_{H,2}^2 & x_3 \cdot \delta_{H,3}^2 \end{pmatrix} = \begin{pmatrix} \delta_{D,TS}^2 \\ \delta_{P,TS}^2 \\ \delta_{H,TS}^2 \end{pmatrix} \quad [\text{A.40.}]$$

A.2.3. Four-Component Blends

A.2.3.1. Linear Calculation Method

The set of equations used for linear four-component calculations is expressed as follow:

$$\begin{pmatrix} x_1 \cdot \delta_{D,1} & x_2 \cdot \delta_{D,2} & x_3 \cdot \delta_{D,3} & x_4 \cdot \delta_{D,4} \\ x_1 \cdot \delta_{P,1} & x_2 \cdot \delta_{P,2} & x_3 \cdot \delta_{P,3} & x_4 \cdot \delta_{P,4} \\ x_1 \cdot \delta_{H,1} & x_2 \cdot \delta_{H,2} & x_3 \cdot \delta_{H,3} & x_4 \cdot \delta_{H,4} \\ x_1 \cdot \delta_{I,1} & x_2 \cdot \delta_{I,2} & x_3 \cdot \delta_{I,3} & x_4 \cdot \delta_{I,4} \end{pmatrix} = \begin{pmatrix} \delta_{D,TS} \\ \delta_{P,TS} \\ \delta_{H,TS} \\ \delta_{I,TS} \end{pmatrix} \quad [\text{A.41.}]$$

Where

$$\mathbf{M} = \begin{pmatrix} \delta_{D,1} & \delta_{D,2} & \delta_{D,3} & \delta_{D,4} \\ \delta_{P,1} & \delta_{P,2} & \delta_{P,3} & \delta_{P,4} \\ \delta_{H,1} & \delta_{H,2} & \delta_{H,3} & \delta_{H,4} \\ \delta_{I,1} & \delta_{I,2} & \delta_{I,3} & \delta_{I,4} \end{pmatrix} \quad [\text{A.42.}]$$

$$\mathbf{B} = \begin{pmatrix} \delta_{D,TS} \\ \delta_{P,TS} \\ \delta_{H,TS} \\ \delta_{I,TS} \end{pmatrix} \quad [\text{A.43.}]$$

For two- and three-component calculations, the inverse of the matrix, \mathbf{M} , is calculated directly. For four-component calculations however, the inverse is calculated by using partitioning (freevec.org, 2010). The four-by-four (4x4) matrix comprising the LHS of the equations is partitioned into four 2x2 matrices:

$$\mathbf{M} = \begin{pmatrix} \mathbf{P} & \mathbf{Q} \\ \mathbf{R} & \mathbf{S} \end{pmatrix} \quad [\text{A.44.}]$$

Where

$$\mathbf{P} = \begin{pmatrix} \delta_{D,1} & \delta_{D,2} \\ \delta_{P,1} & \delta_{P,2} \end{pmatrix} \quad [\text{A.45.}]$$

$$\mathbf{Q} = \begin{pmatrix} \delta_{H,1} & \delta_{H,2} \\ \delta_{I,1} & \delta_{I,2} \end{pmatrix} \quad [\text{A.46.}]$$

$$\mathbf{R} = \begin{pmatrix} \delta_{D,3} & \delta_{D,4} \\ \delta_{P,3} & \delta_{P,4} \end{pmatrix} \quad [\text{A.47.}]$$

$$\mathbf{S} = \begin{pmatrix} \delta_{H,3} & \delta_{H,4} \\ \delta_{I,3} & \delta_{I,4} \end{pmatrix} \quad [\text{A.48.}]$$

From this, the inverse of the matrix, \mathbf{M} , is defined as follow:

$$\mathbf{M}^{-1} = \begin{pmatrix} \bar{\mathbf{P}} & \bar{\mathbf{Q}} \\ \bar{\mathbf{R}} & \bar{\mathbf{S}} \end{pmatrix} \quad [\text{A.49.}]$$

Where

$$\bar{P} = P^{-1} - (P^{-1} \cdot Q) \cdot \bar{R} \quad [A.50.]$$

$$\bar{Q} = -(P^{-1} \cdot Q) \cdot \bar{S} \quad [A.51.]$$

$$\bar{R} = -\bar{S} \cdot (R \cdot P^{-1}) \quad [A.52.]$$

$$\bar{S} = (S - R \cdot P^{-1} \cdot Q)^{-1} \quad [A.53.]$$

Based on this, the inverse of the matrix, \mathbf{M} , can be expressed as follow:

$$M^{-1} = \begin{pmatrix} \bar{P}_{11} & \bar{P}_{12} & \bar{Q}_{11} & \bar{Q}_{12} \\ \bar{P}_{21} & \bar{P}_{22} & \bar{Q}_{21} & \bar{Q}_{22} \\ \bar{R}_{11} & \bar{R}_{12} & \bar{S}_{11} & \bar{S}_{12} \\ \bar{R}_{21} & \bar{R}_{22} & \bar{S}_{21} & \bar{S}_{22} \end{pmatrix} \quad [A.54.]$$

Next, the volume percentage contributions of the blend constituents can be calculated according to the following equations:

$$x_1 = \bar{P}_{11}\delta_{D,TS} + \bar{P}_{12}\delta_{P,TS} + \bar{Q}_{11}\delta_{H,TS} + \bar{Q}_{12}\delta_{I,TS} \quad [A.55.]$$

$$x_2 = \bar{P}_{21}\delta_{D,TS} + \bar{P}_{22}\delta_{P,TS} + \bar{Q}_{21}\delta_{H,TS} + \bar{Q}_{22}\delta_{I,TS} \quad [A.56.]$$

$$x_3 = \bar{R}_{11}\delta_{D,TS} + \bar{R}_{12}\delta_{P,TS} + \bar{S}_{11}\delta_{H,TS} + \bar{S}_{12}\delta_{I,TS} \quad [A.57.]$$

$$x_4 = \bar{R}_{21}\delta_{D,TS} + \bar{R}_{22}\delta_{P,TS} + \bar{S}_{21}\delta_{H,TS} + \bar{S}_{22}\delta_{I,TS} \quad [\text{A.58.}]$$

As for three-component calculations, the procedure used to calculate and evaluate the partial solubility parameter values of the blend is similar to that described earlier for two-component blends.

A.2.3.2. Square Calculation Method

The set of equations used for squared four-component calculations is expressed as follow:

$$\begin{pmatrix} x_1 \cdot \delta_{D,1}^2 & x_2 \cdot \delta_{D,2}^2 & x_3 \cdot \delta_{D,3}^2 & x_4 \cdot \delta_{D,4}^2 \\ x_1 \cdot \delta_{P,1}^2 & x_2 \cdot \delta_{P,2}^2 & x_3 \cdot \delta_{P,3}^2 & x_4 \cdot \delta_{P,4}^2 \\ x_1 \cdot \delta_{H,1}^2 & x_2 \cdot \delta_{H,2}^2 & x_3 \cdot \delta_{H,3}^2 & x_4 \cdot \delta_{H,4}^2 \\ x_1 \cdot \delta_{I,1}^2 & x_2 \cdot \delta_{I,2}^2 & x_3 \cdot \delta_{I,3}^2 & x_4 \cdot \delta_{I,4}^2 \end{pmatrix} = \begin{pmatrix} \delta_{D,TS}^2 \\ \delta_{P,TS}^2 \\ \delta_{H,TS}^2 \\ \delta_{I,TS}^2 \end{pmatrix} \quad [\text{A.59.}]$$

A.3. Solvent Blend Calculations: Gauss-Seidel Iteration

In addition to matrix manipulation, the EquiSolv solvent optimizer also offers the option to use Gauss-Seidel iteration as basis for screening solvent formulations. Although the iterative approach increases the calculation time required to screen through a selected set of data, it does however improve the accuracy of calculations as well as reduce noise in the resulting data. A block flow diagram of the algorithm applied by the EquiSolv program for the iterative process is presented in Figure A.2.

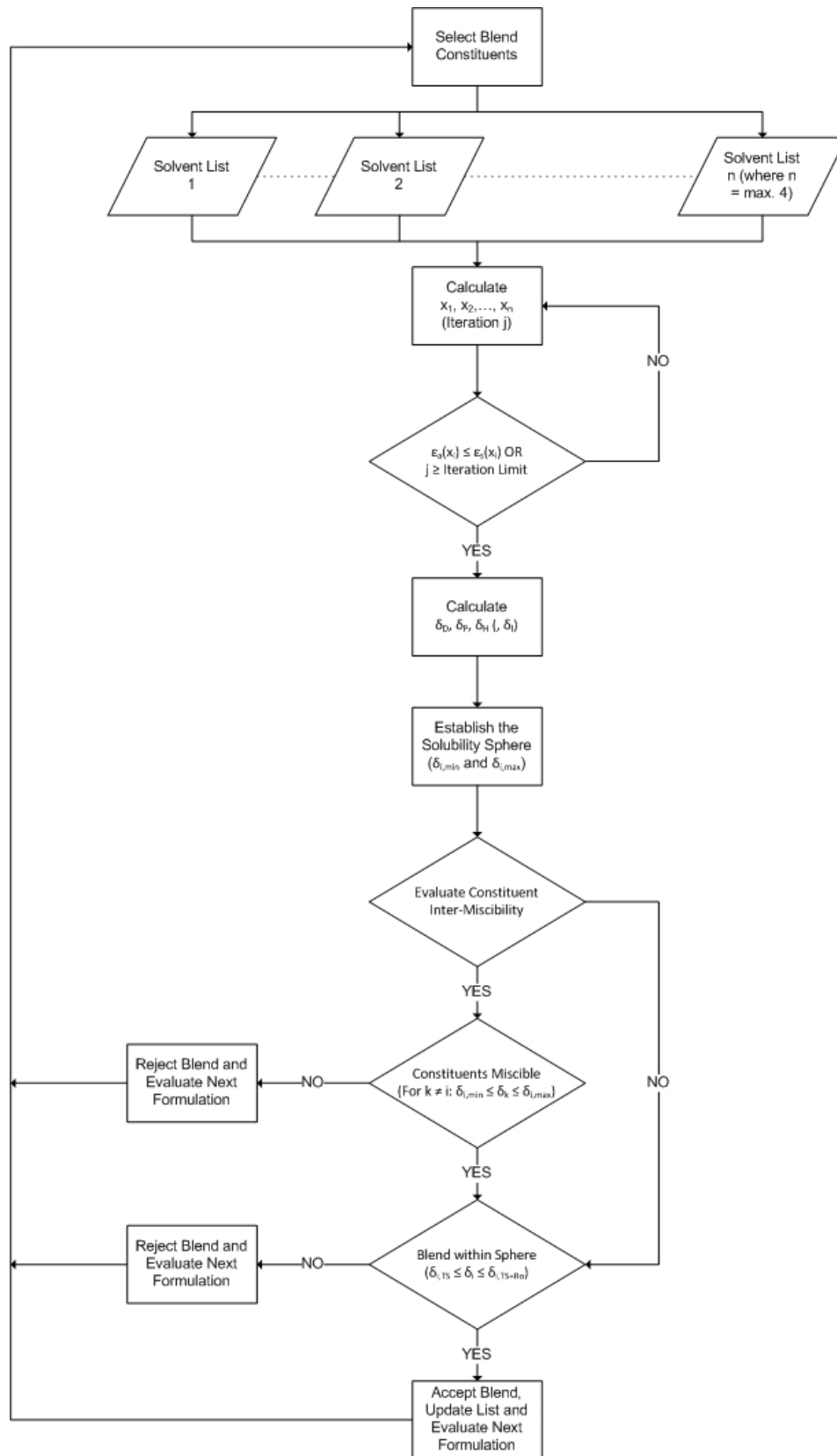


Figure A.2 – A block flow diagram of the iterative algorithm used by the EquiSolv solvent optimizer for Gauss-Seidel iteration.

The set of linear equations used for two-, three- or four component calculations, both linear and square methods, is similar to that described earlier for the matrix analysis of each case. The volume percentage contributions of the blend constituents are calculated sequentially using an iterative method of forward substitution:

$$x_i^{(k)} = \frac{1}{a_{ii}} \left(b_i - \sum_{j>i} a_{ij} x_j^{(k-1)} - \sum_{j<i} a_{ij} x_j^{(k)} \right), i \text{ and } j = 1, 2, \dots, n. \quad [\text{A.60.}]$$

Where x is the volume percentage contribution, a is the element from the LHS matrix, b is the element from RHS matrix, the subscripts i and j denotes the constituents considered, and the superscript k denote the current iteration number. For each iteration, the convergence between of the volume percentage contributions is defined as follow:

$$\varepsilon_i = \left| \frac{x^{(k)} - x^{(k-1)}}{x^{(k)}} \right| \times 100, i = 2, 3, \dots, n. \quad [\text{A.61.}]$$

Where ε is the convergence between the volume percentage contributions calculated for two following iterations and the subscript i denote the constituent considered. The procedure used to calculate and evaluate the partial solubility parameter values of the blend is similar to that described earlier for matrix-approach calculations.

A.3.1. Two-Component Blends

For two-component calculations, the volume percentage contributions for the constituents considered are calculated as follow:

$$x_1^k = \frac{1}{\delta_{D,1}} [\delta_{D,TS} - (\delta_{D,2} \cdot x_2^{k-1})] \quad [\text{A.62.}]$$

$$x_2^k = \frac{1}{\delta_{P,2}} [\delta_{P,TS} - (\delta_{P,1} \cdot x_1^k)] \quad [\text{A.63.}]$$

A.3.2. Three-Component Blends

The volume percentage contributions for the constituents considered in three-component calculations are calculated as follow:

$$x_1^k = \frac{1}{\delta_{D,1}} [\delta_{D,TS} - (\delta_{D,2} \cdot x_2^{k-1}) - (\delta_{D,3} \cdot x_3^{k-1})] \quad [\text{A.64.}]$$

$$x_2^k = \frac{1}{\delta_{P,2}} [\delta_{P,TS} - (\delta_{P,1} \cdot x_1^k) - (\delta_{P,3} \cdot x_3^{k-1})] \quad [\text{A.65.}]$$

$$x_3^k = \frac{1}{\delta_{H,3}} [\delta_{H,TS} - (\delta_{H,1} \cdot x_1^k) - (\delta_{H,2} \cdot x_2^k)] \quad [\text{A.66.}]$$

A.3.3. Four-Component Blends

The volume percentage contributions for the constituents considered in four-component calculations are calculated as follow:

$$x_1^k = \frac{1}{\delta_{D,1}} [\delta_{D,TS} - (\delta_{D,2} \cdot x_2^{k-1}) - (\delta_{D,3} \cdot x_3^{k-1}) - (\delta_{D,4} \cdot x_4^{k-1})] \quad [\text{A.67.}]$$

$$x_2^k = \frac{1}{\delta_{P,2}} [\delta_{P,TS} - (\delta_{P,1} \cdot x_1^k) - (\delta_{P,3} \cdot x_3^{k-1}) - (\delta_{P,4} \cdot x_4^{k-1})] \quad [\text{A.68.}]$$

$$x_3^k = \frac{1}{\delta_{H,3}} [\delta_{H,TS} - (\delta_{H,1} \cdot x_1^k) - (\delta_{H,2} \cdot x_2^k) - (\delta_{H,4} \cdot x_4^{k-1})] \quad [\text{A.69.}]$$

$$x_4^k = \frac{1}{\delta_{I,3}} [\delta_{I,TS} - (\delta_{I,1} \cdot x_1^k) - (\delta_{I,2} \cdot x_2^k) - (\delta_{I,3} \cdot x_3^k)] \quad [\text{A.70.}]$$

Appendix B: Modeling Data

Table B.1 – Summary of the molecular mechanics (MM+) calculation results for the ionic bond energies of the 74 selected ionic liquids.

| Ionic Liquid (Sigma-Aldrich) | Molecular Mechanics (MM+) Geometry Optimization | | | | | | | |
|--|---|-------|--------------|-------|--------------|-------|---------------------------|------------------------|
| | Cation | | Anion | | Component | | Ionic Bond Energy | |
| | E [kcal/mol] | Grad | E [kcal/mol] | Grad | E [kcal/mol] | Grad | E _i [kcal/mol] | E _i [J/mol] |
| 1,2,3-Trimethylimidazolium methyl sulfate | 7.956 | 0.086 | 14.616 | 0.096 | 41.266 | 0.087 | 18.694 | 78267.578 |
| 1,2,3-Trimethylimidazolium trifluoromethanesulfonate | 7.956 | 0.086 | 22.763 | 0.069 | 28.934 | 0.068 | -1.785 | -7473.444 |
| 1,2-Dimethyl-3-propylimidazolium bis(trifluoromethylsulfonyl)imide | 9.039 | 0.090 | 45.677 | 0.094 | 67.085 | 0.099 | 12.370 | 51789.847 |
| 1,2-Dimethyl-3-propylimidazolium tris(trifluoromethylsulfonyl)methide | 9.039 | 0.090 | 92.364 | 0.096 | 95.669 | 0.099 | -5.733 | -24004.241 |
| 1,3-Dimethylimidazolium methyl sulfate | 9.168 | 0.055 | 14.616 | 0.096 | 20.055 | 0.094 | -3.729 | -15612.284 |
| 1-Allyl-3-methylimidazolium chloride | 8.168 | 0.098 | 0.000 | 0.000 | 6.549 | 0.093 | -1.619 | -6780.117 |
| 1-Benzyl-3-methylimidazolium chloride | 6.680 | 0.093 | 0.000 | 0.000 | 5.386 | 0.095 | -1.295 | -5421.185 |
| 1-Benzyl-3-methylimidazolium hexafluorophosphate | 6.680 | 0.093 | 12.883 | 0.055 | 12.204 | 0.098 | -7.359 | -30811.350 |
| 1-Benzyl-3-methylimidazolium tetrafluoroborate | 6.680 | 0.093 | 0.000 | 0.030 | 17.366 | 0.096 | 10.685 | 44736.986 |
| 1-Butyl-1-(3,3,4,4,5,5,6,6,7,7,8,8,8-tridecafluorooctyl)-imidazolium hexafluorophosphate | 29.114 | 0.099 | 12.883 | 0.055 | 74.477 | 0.095 | 32.480 | 135986.544 |
| 1-Butyl-2,3-dimethylimidazolium chloride | 9.632 | 0.093 | 0.000 | 0.000 | 16.526 | 0.099 | 6.894 | 28861.377 |
| 1-Butyl-2,3-dimethylimidazolium hexafluorophosphate | 9.632 | 0.093 | 12.883 | 0.055 | 14.387 | 0.093 | -8.128 | -34031.250 |
| 1-Butyl-2,3-dimethylimidazolium tetrafluoroborate | 9.632 | 0.093 | 0.000 | 0.030 | 9.611 | 0.099 | -0.022 | -91.354 |
| 1-Butyl-3-methylimidazolium acetate | 11.819 | 0.091 | -0.208 | 0.074 | 10.814 | 0.097 | -0.797 | -3335.127 |
| 1-Butyl-3-methylimidazolium bis(trifluoromethylsulfonyl)imide | 11.819 | 0.091 | 45.677 | 0.094 | 64.682 | 0.094 | 7.187 | 30088.013 |
| 1-Butyl-3-methylimidazolium bromide | 11.819 | 0.091 | 0.000 | 0.000 | 11.033 | 0.093 | -0.785 | -3287.678 |
| 1-Butyl-3-methylimidazolium chloride | 11.819 | 0.091 | 0.000 | 0.000 | 10.850 | 0.094 | -0.969 | -4055.018 |
| 1-Butyl-3-methylimidazolium dicyanamide | 11.819 | 0.091 | 4.895 | 0.057 | 16.601 | 0.085 | -0.113 | -473.615 |
| 1-Butyl-3-methylimidazolium hexafluorophosphate | 11.819 | 0.091 | 12.883 | 0.055 | 17.246 | 0.080 | -7.455 | -31212.690 |
| 1-Butyl-3-methylimidazolium hydrogen sulfate | 11.819 | 0.091 | 7.778 | 0.079 | 17.703 | 0.097 | -1.894 | -7927.758 |
| 1-Butyl-3-methylimidazolium methanesulfonate | 11.819 | 0.091 | 3.457 | 0.097 | 40.678 | 0.095 | 25.403 | 106355.989 |
| 1-Butyl-3-methylimidazolium methyl sulfate | 11.819 | 0.091 | 14.616 | 0.096 | 21.097 | 0.098 | -5.338 | -22348.964 |
| 1-Butyl-3-methylimidazolium nitrate | 11.819 | 0.091 | 0.000 | 0.024 | 7.940 | 0.096 | -3.879 | -16238.706 |
| 1-Butyl-3-methylimidazolium octyl sulfate | 11.819 | 0.091 | 19.143 | 0.090 | 25.475 | 0.099 | -5.487 | -22973.611 |
| 1-Butyl-3-methylimidazolium tetrachloroaluminate | 11.819 | 0.091 | 0.000 | 0.006 | 5.329 | 0.095 | -6.490 | -27169.856 |
| 1-Butyl-3-methylimidazolium tetrafluoroborate | 11.819 | 0.091 | 0.000 | 0.040 | 10.419 | 0.087 | -1.399 | -5858.999 |
| 1-Butyl-3-methylimidazolium thiocyanate | 11.819 | 0.091 | 0.000 | 0.009 | 10.929 | 0.100 | -0.890 | -3725.912 |
| 1-Butyl-3-methylimidazolium tosylate | 11.819 | 0.091 | 16.328 | 0.078 | 18.963 | 0.095 | -9.183 | -38447.867 |
| 1-Butyl-3-methylimidazolium trifluoromethanesulfonate | 11.819 | 0.091 | 22.763 | 0.069 | 31.975 | 0.100 | -2.607 | -10915.227 |
| 1-Butyl-3-methylpyridinium bis(trifluoromethylsulfonyl)imide | 14.513 | 0.089 | 45.677 | 0.094 | 59.046 | 0.097 | -1.143 | -4785.480 |
| 1-Butyl-4-methylpyridinium bromide | 8.747 | 0.096 | 0.000 | 0.000 | 11.720 | 0.099 | 2.973 | 12447.729 |
| 1-Butyl-4-methylpyridinium chloride | 8.747 | 0.096 | 0.000 | 0.000 | 14.376 | 0.097 | 5.629 | 23569.131 |
| 1-Butyl-4-methylpyridinium tetrafluoroborate | 8.747 | 0.096 | 0.000 | 0.040 | 13.628 | 0.096 | 4.882 | 20438.731 |
| 1-Butylpyridinium bromide | 12.883 | 0.082 | 0.000 | 0.000 | 11.325 | 0.094 | -1.558 | -6524.384 |
| 1-Dodecyl-3-methylimidazolium iodide | 16.919 | 0.090 | 0.000 | 0.000 | 26.135 | 0.098 | 9.216 | 38584.961 |
| 1-Ethyl-2,3-dimethylimidazolium chloride | 8.469 | 0.098 | 0.000 | 0.000 | 6.982 | 0.093 | -1.487 | -6227.511 |
| 1-Ethyl-2,3-dimethylimidazolium ethyl sulfate | 8.469 | 0.098 | 15.330 | 0.092 | 23.304 | 0.100 | -0.495 | -2072.698 |
| 1-Ethyl-2,3-dimethylimidazolium trifluoromethanesulfonate | 9.465 | 0.090 | 22.763 | 0.069 | 30.831 | 0.097 | -1.398 | -5851.915 |
| 1-Ethyl-3-methylimidazolium acetate | 10.570 | 0.098 | -0.208 | 0.074 | 10.168 | 0.096 | -0.194 | -911.505 |
| 1-Ethyl-3-methylimidazolium bis(pentafluoroethylsulfonyl)imide | 10.570 | 0.098 | 52.628 | 0.090 | 80.642 | 0.100 | 17.444 | 73034.871 |
| 1-Ethyl-3-methylimidazolium bis(trifluoromethylsulfonyl)imide | 10.570 | 0.098 | 45.677 | 0.094 | 56.113 | 0.085 | -0.133 | -556.307 |
| 1-Ethyl-3-methylimidazolium bromide | 10.570 | 0.098 | 0.000 | 0.000 | 9.910 | 0.097 | -0.660 | -2763.668 |
| 1-Ethyl-3-methylimidazolium chloride | 10.570 | 0.098 | 0.000 | 0.000 | 10.015 | 0.091 | -0.555 | -2323.529 |
| 1-Ethyl-3-methylimidazolium dicyanamide | 10.570 | 0.098 | 4.895 | 0.057 | 9.269 | 0.100 | -6.196 | -25939.498 |
| 1-Ethyl-3-methylimidazolium ethyl sulfate | 10.570 | 0.098 | 15.330 | 0.092 | 39.140 | 0.094 | 13.240 | 55433.096 |
| 1-Ethyl-3-methylimidazolium hexafluorophosphate | 10.570 | 0.098 | 12.883 | 0.055 | 14.750 | 0.099 | -8.702 | -36433.561 |
| 1-Ethyl-3-methylimidazolium hydrogen sulfate | 10.570 | 0.098 | 7.778 | 0.079 | 37.086 | 0.097 | 18.738 | 78450.149 |
| 1-Ethyl-3-methylimidazolium methanesulfonate | 10.570 | 0.098 | 3.457 | 0.097 | 9.236 | 0.099 | -4.790 | -20054.850 |
| 1-Ethyl-3-methylimidazolium methyl sulfate | 10.570 | 0.098 | 14.616 | 0.096 | 20.225 | 0.098 | -4.961 | -20770.986 |
| 1-Ethyl-3-methylimidazolium nitrate | 10.570 | 0.098 | 0.000 | 0.024 | 10.278 | 0.099 | -0.292 | -1222.022 |
| 1-Ethyl-3-methylimidazolium tetrachloroaluminate | 10.570 | 0.098 | 0.000 | 0.006 | 4.451 | 0.086 | -6.119 | -25617.714 |
| 1-Ethyl-3-methylimidazolium tetrafluoroborate | 10.570 | 0.098 | 0.000 | 0.040 | 9.970 | 0.099 | -0.600 | -2511.970 |
| 1-Ethyl-3-methylimidazolium thiocyanate | 10.570 | 0.098 | 0.000 | 0.009 | 9.617 | 0.098 | -0.953 | -3988.658 |
| 1-Ethyl-3-methylimidazolium tosylate | 10.570 | 0.098 | 16.328 | 0.078 | 23.717 | 0.089 | -3.181 | -13316.052 |
| 1-Ethyl-3-methylimidazolium trifluoromethanesulfonate | 10.570 | 0.098 | 22.763 | 0.069 | 32.835 | 0.098 | -0.498 | -2085.593 |

Table B.2 – Summary of the molecular mechanics (MM+) calculation results for the ionic bond energies of the 74 selected ionic liquids (continued).

| Ionic Liquid (Sigma-Aldrich) | Molecular Mechanics (MM+) Geometry Optimization | | | | | | | |
|---|---|-------|--------------|-------|--------------|-------|---------------------------|------------------------|
| | Cation | | Anion | | Component | | Ionic Bond Energy | |
| | E [kcal/mol] | Grad | E [kcal/mol] | Grad | E [kcal/mol] | Grad | E _i [kcal/mol] | E _i [J/mol] |
| 1-Hexyl-3-methylimidazolium chloride | 13.079 | 0.097 | 0.000 | 0.000 | 12.596 | 0.099 | -0.483 | -2023.877 |
| 1-Hexyl-3-methylimidazolium hexafluorophosphate | 13.079 | 0.097 | 12.883 | 0.055 | 16.191 | 0.095 | -9.771 | -40910.031 |
| 1-Hexyl-3-methylimidazolium tetrafluoroborate | 13.079 | 0.097 | 0.000 | 0.040 | 11.931 | 0.093 | -1.149 | -4808.545 |
| 1-Hexyl-3-methylimidazolium trifluoromethanesulfonate | 13.079 | 0.097 | 22.763 | 0.069 | 34.098 | 0.091 | -1.745 | -7305.648 |
| 1-Methyl-3-(3,3,4,4,5,5,6,6,7,7,8,8,8-tridecafluorooctyl)-imidazolium hexafluorophosphate | 68.389 | 0.096 | 12.883 | 0.055 | 74.785 | 0.096 | -6.487 | -27158.761 |
| 1-Methyl-3-octylimidazolium chloride | 14.375 | 0.099 | 0.000 | 0.000 | 14.269 | 0.087 | -0.105 | -441.143 |
| 1-Methyl-3-octylimidazolium hexafluorophosphate | 14.375 | 0.099 | 12.883 | 0.055 | 33.524 | 0.096 | 6.267 | 26237.241 |
| 1-Methyl-3-octylimidazolium tetrafluoroborate | 14.375 | 0.099 | 0.000 | 0.040 | 13.653 | 0.092 | -0.721 | -3018.953 |
| 1-Methyl-3-octylimidazolium trifluoromethanesulfonate | 14.375 | 0.099 | 22.763 | 0.069 | 35.354 | 0.095 | -1.783 | -7466.456 |
| 1-Methylimidazolium chloride | 16.108 | 0.093 | 0.000 | 0.000 | 15.536 | 0.079 | -0.572 | -2396.115 |
| 1-Methylimidazolium hydrogen sulfate | 16.108 | 0.093 | 7.778 | 0.079 | 37.832 | 0.084 | 13.946 | 58387.411 |
| 3-(Triphenylphosphonio)propane-1-sulfonic acid | 12.960 | 0.092 | 16.328 | 0.078 | 19.733 | 0.098 | -9.555 | -40002.282 |
| 3-Methyl-1-propylpyridinium bis(trifluoromethylsulfonyl)imide | 13.894 | 0.097 | 45.677 | 0.094 | 59.509 | 0.098 | -0.061 | -256.818 |
| 4-(3-Butyl-1-imidazolyl)-1-butanefluoroborate triflate | 12.220 | 0.098 | 22.763 | 0.087 | 28.821 | 0.099 | -6.162 | -25799.246 |
| Tetrabutylphosphonium bromide | 17.331 | 0.089 | 0.000 | 0.000 | 16.353 | 0.100 | -0.979 | -4098.166 |
| Tetrabutylphosphonium chloride | 17.331 | 0.089 | 0.000 | 0.000 | 16.240 | 0.099 | -1.091 | -4567.884 |
| Tetrabutylphosphonium methanesulfonate | 17.331 | 0.089 | 3.457 | 0.097 | 16.364 | 0.099 | -4.424 | -18523.697 |
| Tetrabutylphosphonium p-toluenesulfonate | 17.331 | 0.089 | 16.328 | 0.093 | 26.614 | 0.096 | -7.045 | -29495.947 |
| Tetrabutylphosphonium tetrafluoroborate | 17.331 | 0.089 | 0.000 | 0.040 | 15.731 | 0.088 | -1.601 | -6702.257 |

Table B.3 – Summary of the semi-empirical (AM1) calculation results for the ionic bond energies of the 74 selected ionic liquids.

| Ionic Liquid (Sigma-Aldrich) | Semi-Empirical Approach (AM1) Geometry Optimization | | | | | | | |
|---|---|-------|--------------|-------|--------------|-------|---------------------------|------------------------|
| | Cation | | Anion | | Component | | Ionic Bond Energy | |
| | E [kcal/mol] | Grad | E [kcal/mol] | Grad | E [kcal/mol] | Grad | E _i [kcal/mol] | E _j [J/mol] |
| 1,2,3-Trimethylimidazolium methyl sulfate | -1734.549 | 0.097 | -860.271 | 0.072 | -2565.034 | 0.093 | 29.786 | 124706.301 |
| 1,2,3-Trimethylimidazolium trifluoromethanesulfonate | -1734.549 | 0.097 | -803.447 | 0.084 | -2515.702 | 0.098 | 22.295 | 93341.846 |
| 1,2-Dimethyl-3-propylimidazolium bis(trifluoromethylsulfonyl)imide | -2200.107 | 0.094 | -1472.491 | 0.081 | -3736.053 | 0.096 | -63.455 | -265670.505 |
| 1,2-Dimethyl-3-propylimidazolium tris(trifluoromethylsulfonyl)methide | -2200.107 | 0.094 | -2115.650 | 0.089 | -4377.459 | 0.092 | -61.702 | -258331.170 |
| 1,3-Dimethylimidazolium methyl sulfate | -1350.209 | 0.100 | -860.271 | 0.072 | -2296.114 | 0.100 | -85.634 | -358527.109 |
| 1-Allyl-3-methylimidazolium chloride | -1778.729 | 0.098 | -66.659 | 0.000 | -1968.866 | 0.091 | -123.479 | -516970.902 |
| 1-Benzyl-3-methylimidazolium chloride | -2559.629 | 0.089 | -66.659 | 0.000 | -2746.299 | 0.094 | -120.011 | -502455.097 |
| 1-Benzyl-3-methylimidazolium hexafluorophosphate | -2559.629 | 0.089 | -693.356 | 0.029 | -3326.351 | 0.087 | -73.366 | -307163.073 |
| 1-Benzyl-3-methylimidazolium tetrafluoroborate | -2559.629 | 0.089 | -608.733 | 0.041 | -3247.886 | 0.098 | -79.524 | -332945.782 |
| 1-Butyl-1-(3,3,4,4,5,5,6,6,7,7,8,8,8-tridecafluorooctyl)-imidazolium hexafluorophosphate | -4304.892 | 0.089 | -693.356 | 0.029 | -5076.130 | 0.098 | -77.882 | -326068.662 |
| 1-Butyl-2,3-dimethylimidazolium chloride | -2482.261 | 0.097 | -66.659 | 0.000 | -2662.744 | 0.095 | -113.824 | -476549.717 |
| 1-Butyl-2,3-dimethylimidazolium hexafluorophosphate | -2482.261 | 0.097 | -693.356 | 0.029 | -3241.844 | 0.098 | -66.226 | -277270.672 |
| 1-Butyl-2,3-dimethylimidazolium tetrafluoroborate | -2482.261 | 0.097 | -608.733 | 0.041 | -3162.108 | 0.093 | -71.114 | -297733.724 |
| 1-Butyl-3-methylimidazolium acetate | -2197.101 | 0.099 | -732.681 | 0.055 | -3017.128 | 0.088 | -87.346 | -365693.113 |
| 1-Butyl-3-methylimidazolium bis(trifluoromethylsulfonyl)imide | -2197.101 | 0.099 | -1472.491 | 0.081 | -3726.878 | 0.066 | -57.286 | -239841.323 |
| 1-Butyl-3-methylimidazolium bromide | -2197.101 | 0.099 | -47.151 | 0.000 | -2339.901 | 0.099 | -95.649 | -400457.609 |
| 1-Butyl-3-methylimidazolium chloride | -2197.101 | 0.099 | -66.659 | 0.000 | -2360.330 | 0.074 | -96.571 | -404316.517 |
| 1-Butyl-3-methylimidazolium dicyanamide | -2197.101 | 0.099 | -647.533 | 0.080 | -2910.846 | 0.078 | -66.212 | -272712.058 |
| 1-Butyl-3-methylimidazolium hexafluorophosphate | -2197.101 | 0.099 | -693.356 | 0.029 | -2965.057 | 0.092 | -74.600 | -312331.589 |
| 1-Butyl-3-methylimidazolium hydrogen sulfate | -2197.101 | 0.099 | -590.708 | 0.094 | -2863.723 | 0.097 | -75.914 | -317832.112 |
| 1-Butyl-3-methylimidazolium methanesulfonate | -2197.101 | 0.099 | -737.532 | 0.066 | -3011.918 | 0.095 | -77.285 | -323572.535 |
| 1-Butyl-3-methylimidazolium methyl sulfate | -2197.101 | 0.099 | -860.271 | 0.072 | -3139.246 | 0.096 | -81.875 | -342786.686 |
| 1-Butyl-3-methylimidazolium nitrate | -2197.101 | 0.099 | -380.557 | 0.090 | -2660.738 | 0.074 | -83.081 | -347837.136 |
| 1-Butyl-3-methylimidazolium octyl sulfate | -2197.101 | 0.099 | -2833.421 | 0.089 | -5110.395 | 0.094 | -79.874 | -334409.043 |
| 1-Butyl-3-methylimidazolium tetrachloroaluminate | -2197.101 | 0.099 | -446.132 | 0.004 | -2717.177 | 0.086 | -73.944 | -309583.839 |
| 1-Butyl-3-methylimidazolium tetrafluoroborate | -2197.101 | 0.099 | -608.733 | 0.035 | -2878.923 | 0.088 | -73.089 | -306005.443 |
| 1-Butyl-3-methylimidazolium thiocyanate | -2197.101 | 0.099 | -364.499 | 0.015 | -2637.429 | 0.098 | -75.829 | -317477.496 |
| 1-Butyl-3-methylimidazolium tosylate | -2197.101 | 0.099 | -1948.789 | 0.089 | -4230.835 | 0.095 | -84.945 | -355642.872 |
| 1-Butyl-3-methylimidazolium trifluoromethanesulfonate | -2197.101 | 0.099 | -803.447 | 0.084 | -3069.287 | 0.096 | -68.739 | -287792.757 |
| 1-Butyl-3-methylpyridinium bis(trifluoromethylsulfonyl)imide | -2500.448 | 0.082 | -1472.491 | 0.081 | -4038.084 | 0.099 | -65.144 | -272741.470 |
| 1-Butyl-4-methylpyridinium bromide | -2502.178 | 0.083 | -47.151 | 0.000 | -2638.505 | 0.098 | -89.176 | -373355.244 |
| 1-Butyl-4-methylpyridinium chloride | -2502.178 | 0.083 | -66.659 | 0.000 | -2657.231 | 0.083 | -88.395 | -370086.665 |
| 1-Butyl-4-methylpyridinium tetrafluoroborate | -2502.178 | 0.083 | -608.733 | 0.035 | -3187.257 | 0.092 | -76.347 | -319643.291 |
| 1-Butylpyridinium bromide | -2216.601 | 0.091 | -47.151 | 0.000 | -2389.850 | 0.094 | -126.098 | -527936.362 |
| 1-Dodecyl-3-methylimidazolium iodide | -4453.121 | 0.100 | -27.745 | 0.000 | -4574.527 | 0.094 | -93.662 | -392138.581 |
| 1-Ethyl-2,3-dimethylimidazolium chloride | -1917.792 | 0.090 | -66.659 | 0.000 | -2096.352 | 0.081 | -111.901 | -468498.221 |
| 1-Ethyl-2,3-dimethylimidazolium ethyl sulfate | -1917.792 | 0.090 | -1141.090 | 0.073 | -3130.297 | 0.099 | -71.416 | -298998.116 |
| 1-Ethyl-2,3-dimethylimidazolium trifluoromethanesulfonate | -1917.480 | 0.077 | -803.447 | 0.084 | -2787.508 | 0.093 | -66.581 | -278757.379 |
| 1-Ethyl-3-methylimidazolium acetate | -1632.390 | 0.091 | -732.681 | 0.055 | -2452.026 | 0.089 | -86.955 | -364055.265 |
| 1-Ethyl-3-methylimidazolium bis(pentafluoroethylsulfonyl)imide | -1632.390 | 0.091 | -2073.219 | 0.094 | -3774.179 | 0.096 | -68.570 | -287082.688 |
| 1-Ethyl-3-methylimidazolium bis(trifluoromethylsulfonyl)imide | -1632.390 | 0.091 | -1472.491 | 0.081 | -3168.434 | 0.070 | -63.553 | -266079.548 |
| 1-Ethyl-3-methylimidazolium bromide | -1632.390 | 0.091 | -47.151 | 0.000 | -1776.609 | 0.092 | -97.068 | -406396.902 |
| 1-Ethyl-3-methylimidazolium chloride | -1632.390 | 0.091 | -66.659 | 0.000 | -1795.677 | 0.092 | -96.628 | -404555.579 |
| 1-Ethyl-3-methylimidazolium dicyanamide | -1632.390 | 0.091 | -647.533 | 0.080 | -2354.236 | 0.087 | -74.313 | -311126.230 |
| 1-Ethyl-3-methylimidazolium ethyl sulfate | -1632.390 | 0.091 | -1141.090 | 0.073 | -2856.661 | 0.094 | -83.181 | -348257.065 |
| 1-Ethyl-3-methylimidazolium hexafluorophosphate | -1632.390 | 0.091 | -693.356 | 0.029 | -2401.696 | 0.093 | -75.950 | -317981.997 |
| 1-Ethyl-3-methylimidazolium hydrogen sulfate | -1632.390 | 0.091 | -590.708 | 0.094 | -2309.423 | 0.095 | -86.325 | -361419.301 |
| 1-Ethyl-3-methylimidazolium methanesulfonate | -1632.390 | 0.091 | -737.532 | 0.066 | -2456.301 | 0.094 | -86.379 | -361644.547 |
| 1-Ethyl-3-methylimidazolium methyl sulfate | -1632.390 | 0.091 | -860.271 | 0.072 | -2578.304 | 0.098 | -85.643 | -358563.534 |
| 1-Ethyl-3-methylimidazolium nitrate | -1632.390 | 0.091 | -380.557 | 0.090 | -2088.147 | 0.089 | -75.200 | -314841.532 |
| 1-Ethyl-3-methylimidazolium tetrachloroaluminate | -1632.390 | 0.091 | -446.132 | 0.004 | -2153.091 | 0.098 | -74.569 | -312200.963 |
| 1-Ethyl-3-methylimidazolium tetrafluoroborate | -1632.390 | 0.091 | -608.733 | 0.035 | -2315.204 | 0.084 | -74.081 | -310158.677 |
| 1-Ethyl-3-methylimidazolium thiocyanate | -1632.390 | 0.091 | -364.499 | 0.015 | -2073.425 | 0.100 | -76.536 | -320436.676 |
| 1-Ethyl-3-methylimidazolium tosylate | -1632.390 | 0.091 | -1948.789 | 0.089 | -3668.505 | 0.100 | -87.326 | -365611.472 |
| 1-Ethyl-3-methylimidazolium trifluoromethane | -1632.390 | 0.091 | -803.448 | 0.084 | -2504.234 | 0.096 | -68.396 | -286356.291 |
| 1-Ethyl-3-methylimidazolium trifluoromethanesulfonate | -1632.390 | 0.091 | -803.447 | 0.084 | -2502.428 | 0.096 | -66.591 | -278798.828 |
| 1-Hexyl-3-methylimidazolium chloride | -2761.179 | 0.087 | -66.659 | 0.000 | -2923.252 | 0.088 | -95.414 | -399473.310 |
| 1-Hexyl-3-methylimidazolium hexafluorophosphate | -2761.179 | 0.087 | -693.356 | 0.029 | -3527.800 | 0.099 | -72.845 | -304981.369 |
| 1-Hexyl-3-methylimidazolium tetrafluoroborate | -2761.179 | 0.087 | -608.733 | 0.035 | -3442.999 | 0.095 | -73.087 | -305993.720 |
| 1-Hexyl-3-methylimidazolium trifluoromethanesulfonate | -2761.179 | 0.087 | -803.447 | 0.084 | -3632.062 | 0.094 | -67.435 | -282332.845 |
| 1-Methyl-3-(3,3,4,4,5,5,6,6,7,7,8,8,8-tridecafluorooctyl)-imidazolium hexafluorophosphate | -3457.718 | 0.086 | -693.356 | 0.029 | -4216.789 | 0.098 | -65.714 | -275127.905 |
| 1-Methyl-3-octylimidazolium chloride | -3325.146 | 0.100 | -66.659 | 0.000 | -3487.217 | 0.093 | -95.412 | -399465.355 |
| 1-Methyl-3-octylimidazolium hexafluorophosphate | -3325.146 | 0.100 | -693.356 | 0.029 | -4093.068 | 0.087 | -74.566 | -312187.565 |
| 1-Methyl-3-octylimidazolium tetrafluoroborate | -3325.146 | 0.100 | -608.733 | 0.035 | -4006.408 | 0.100 | -72.530 | -303661.294 |
| 1-Methyl-3-octylimidazolium trifluoromethanesulfonate | -3325.146 | 0.100 | -803.447 | 0.084 | -4196.555 | 0.092 | -67.962 | -284537.576 |
| 1-Methylimidazolium chloride | -1076.674 | 0.081 | -66.659 | 0.000 | -1243.316 | 0.097 | -99.983 | -418601.633 |
| 1-Methylimidazolium hydrogen sulfate | -1076.674 | 0.081 | -590.708 | 0.094 | -1758.563 | 0.100 | -91.180 | -381747.959 |
| 3-(Triphenylphosphonio)propane-1-sulfonic acid | -5005.937 | 0.100 | -1948.789 | 0.089 | -7006.707 | 0.083 | -51.981 | -217631.568 |
| 3-Methyl-1-propylpyridinium bis(trifluoromethylsulfonyl)imide | -2218.262 | 0.076 | -1472.491 | 0.081 | -3749.190 | 0.092 | -58.437 | -244659.410 |
| 4-(3-Butyl-1-imidazolium)-1-butanedisulfonic acid triflate | -3400.207 | 0.095 | -803.448 | 0.089 | -4281.576 | 0.098 | -77.921 | -326234.875 |
| Tetrabutylphosphonium bromide | -4673.176 | 0.099 | -47.151 | 0.000 | -4833.077 | 0.097 | -112.570 | -472052.334 |
| Tetrabutylphosphonium chloride | -4673.176 | 0.099 | -66.659 | 0.000 | -4850.248 | 0.095 | -110.414 | -462274.231 |
| Tetrabutylphosphonium methanesulfonate | -4673.176 | 0.099 | -737.532 | 0.066 | -5494.762 | 0.098 | -84.054 | -351911.660 |
| Tetrabutylphosphonium p-toluenesulfonate | -4673.176 | 0.099 | -1948.789 | 0.089 | -6697.937 | 0.088 | -75.973 | -318079.967 |
| Tetrabutylphosphonium tetrafluoroborate | -4673.176 | 0.099 | -608.733 | 0.035 | -5360.920 | 0.081 | -79.012 | -330802.596 |

Table B.4 – Summary of the Ab-Initio calculation results using a minimal basis set (STO-3G) geometry optimization for the ionic bond energies of the 74 selected ionic liquids.

| Ionic Liquid (Sigma-Aldrich) | Ab-Initio Approach: Minimal Base Set (STO-3G) Geometry Optimization | | | | | | | |
|---|---|----------|--------------|----------|--------------|----------|-------------------------|------------------------|
| | Cation | | Anion | | Component | | Ionic Bond Energy | |
| | E [kcal/mol] | SCF Grad | E [kcal/mol] | SCF Grad | E [kcal/mol] | SCF Grad | E _i [kJ/mol] | E _j [J/mol] |
| 1,2,3-Trimethylimidazolium methyl sulfate | -212233.367 | 0.092 | -456350.367 | 0.066 | -668736.610 | 0.098 | -152.875 | -640044.756 |
| 1,2,3-Trimethylimidazolium trifluoromethanesulfonate | -212233.367 | 0.092 | -593497.229 | 0.049 | -805876.996 | 0.095 | -146.400 | -612936.885 |
| 1,2-Dimethyl-3-propylimidazolium bis(trifluoromethylsulfonyl)imide | -260656.064 | 0.095 | -1128180.656 | 0.088 | -1388951.323 | 0.084 | -114.603 | -479813.603 |
| 1,2-Dimethyl-3-propylimidazolium tris(trifluoromethylsulfonyl)methide | -260656.064 | 0.095 | -1665187.797 | 0.092 | -1925912.978 | 0.092 | -69.118 | -289378.108 |
| 1,3-Dimethylimidazolium methyl sulfate | -188013.718 | 0.086 | -456350.367 | 0.066 | -644504.390 | 0.087 | -140.305 | -587419.699 |
| 1-Allyl-3-methylimidazolium chloride | -235665.806 | 0.091 | -285190.791 | 0.000 | -520988.765 | 0.098 | -132.167 | -553348.842 |
| 1-Benzyl-3-methylimidazolium chloride | -330305.047 | 0.097 | -285190.791 | 0.000 | -615624.948 | 0.081 | -129.110 | -540547.101 |
| 1-Benzyl-3-methylimidazolium hexafluorophosphate | -330305.047 | 0.097 | -580409.485 | 0.045 | -910824.835 | 0.084 | -110.303 | -461807.243 |
| 1-Benzyl-3-methylimidazolium tetrafluoroborate | -330305.047 | 0.097 | -261429.508 | 0.074 | -591855.127 | 0.081 | -120.572 | -504800.879 |
| 1-Butyl-1-(3,3,4,4,5,5,6,6,7,7,8,8,8-tridecafluorooctyl)-imidazolium hexafluorophosphate | -1225115.549 | 0.077 | -580409.485 | 0.045 | -1805637.593 | 0.089 | -112.559 | -471253.427 |
| 1-Butyl-2,3-dimethylimidazolium chloride | -284865.802 | 0.096 | -285190.791 | 0.000 | -570181.262 | 0.093 | -124.668 | -521952.204 |
| 1-Butyl-2,3-dimethylimidazolium hexafluorophosphate | -284865.802 | 0.096 | -580409.485 | 0.045 | -865363.415 | 0.099 | -88.129 | -368970.588 |
| 1-Butyl-2,3-dimethylimidazolium tetrafluoroborate | -284865.802 | 0.096 | -261429.508 | 0.074 | -546394.680 | 0.095 | -99.370 | -416034.026 |
| 1-Butyl-3-methylimidazolium acetate | -260645.594 | 0.088 | -140592.467 | 0.074 | -401375.433 | 0.084 | -137.371 | -575134.042 |
| 1-Butyl-3-methylimidazolium bis(trifluoromethylsulfonyl)imide | -260645.594 | 0.088 | -1128180.656 | 0.088 | -1388949.256 | 0.076 | -123.006 | -514990.961 |
| 1-Butyl-3-methylimidazolium bromide | -260645.594 | 0.088 | -1597261.406 | 0.000 | -1858010.034 | 0.091 | -103.033 | -431372.179 |
| 1-Butyl-3-methylimidazolium chloride | -260645.594 | 0.088 | -285190.791 | 0.000 | -545935.282 | 0.088 | -98.896 | -414052.301 |
| 1-Butyl-3-methylimidazolium dicyanamide | -260645.594 | 0.088 | -148016.490 | 0.075 | -408743.515 | 0.086 | -81.430 | -340925.556 |
| 1-Butyl-3-methylimidazolium hexafluorophosphate | -260645.594 | 0.088 | -580409.485 | 0.045 | -841165.659 | 0.093 | -110.579 | -462965.744 |
| 1-Butyl-3-methylimidazolium hydrogen sulfate | -260645.594 | 0.088 | -432139.533 | 0.050 | -692896.830 | 0.085 | -111.702 | -467664.760 |
| 1-Butyl-3-methylimidazolium methanesulfonate | -260645.594 | 0.088 | -410017.509 | 0.092 | -670784.458 | 0.096 | -121.354 | -508077.496 |
| 1-Butyl-3-methylimidazolium methyl sulfate | -260645.594 | 0.088 | -456350.367 | 0.066 | -717155.133 | 0.100 | -159.171 | -666407.335 |
| 1-Butyl-3-methylimidazolium nitrate | -260645.594 | 0.088 | -172545.703 | 0.065 | -433346.522 | 0.096 | -155.225 | -469884.961 |
| 1-Butyl-3-methylimidazolium octyl sulfate | -260645.594 | 0.088 | -625818.446 | 0.091 | -886622.683 | 0.073 | -158.643 | -664194.880 |
| 1-Butyl-3-methylimidazolium tetrachloroaluminate | -260645.594 | 0.088 | -1291236.008 | 0.027 | -1551951.058 | 0.099 | -69.456 | -290792.137 |
| 1-Butyl-3-methylimidazolium tetrafluoroborate | -260645.594 | 0.088 | -261429.508 | 0.071 | -522178.140 | 0.094 | -103.038 | -431391.396 |
| 1-Butyl-3-methylimidazolium thiocyanate | -260645.594 | 0.088 | -303824.303 | 0.051 | -564559.193 | 0.097 | -89.296 | -373858.120 |
| 1-Butyl-3-methylimidazolium tosylate | -260645.594 | 0.088 | -552311.689 | 0.085 | -813098.860 | 0.083 | -141.576 | -592740.138 |
| 1-Butyl-3-methylimidazolium trifluoromethanesulfonate | -260645.594 | 0.088 | -593497.229 | 0.049 | -854249.344 | 0.097 | -106.521 | -445974.750 |
| 1-Butyl-3-methylpyridinium bis(trifluoromethylsulfonyl)imide | -274227.836 | 0.084 | -1128180.656 | 0.088 | -1402528.905 | 0.082 | -125.414 | -525074.034 |
| 1-Butyl-4-methylpyridinium bromide | -274227.239 | 0.089 | -1597261.406 | 0.000 | -1871583.291 | 0.097 | -94.645 | -396254.825 |
| 1-Butyl-4-methylpyridinium chloride | -274227.239 | 0.089 | -285190.791 | 0.000 | -559505.048 | 0.090 | -87.018 | -364320.398 |
| 1-Butyl-4-methylpyridinium tetrafluoroborate | -274227.239 | 0.089 | -261429.508 | 0.071 | -535765.350 | 0.076 | -108.604 | -454693.649 |
| 1-Butylpyridinium bromide | -250010.542 | 0.098 | -1597261.406 | 0.000 | -1847430.093 | 0.088 | -158.144 | -662107.951 |
| 1-Dodecyl-3-methylimidazolium iodide | -454321.540 | 0.092 | -4301226.885 | 0.000 | -4755634.662 | 0.074 | -86.237 | -361050.597 |
| 1-Ethyl-2,3-dimethylimidazolium chloride | -236445.892 | 0.072 | -285190.791 | 0.000 | -521762.328 | 0.096 | -125.645 | -526041.302 |
| 1-Ethyl-2,3-dimethylimidazolium ethyl sulfate | -236445.892 | 0.072 | -480561.667 | 0.057 | -717115.091 | 0.081 | -107.533 | -450210.902 |
| 1-Ethyl-2,3-dimethylimidazolium trifluoromethanesulfonate | -236444.774 | 0.081 | -593497.229 | 0.049 | -830046.772 | 0.099 | -104.770 | -438641.658 |
| 1-Ethyl-3-methylimidazolium acetate | -212226.661 | 0.097 | -140592.467 | 0.074 | -352956.950 | 0.095 | -137.821 | -577019.385 |
| 1-Ethyl-3-methylimidazolium bis(pentafluoroethylsulfonyl)imide | -212226.661 | 0.097 | -1421211.134 | 0.077 | -1633546.449 | 0.094 | -108.654 | -454906.075 |
| 1-Ethyl-3-methylimidazolium bis(trifluoromethylsulfonyl)imide | -212226.661 | 0.097 | -1128180.656 | 0.088 | -1340526.904 | 0.073 | -119.587 | -506299.715 |
| 1-Ethyl-3-methylimidazolium bromide | -212226.661 | 0.097 | -1597261.406 | 0.000 | -1809639.308 | 0.077 | -151.241 | -633204.103 |
| 1-Ethyl-3-methylimidazolium chloride | -212226.661 | 0.097 | -285190.791 | 0.000 | -497516.273 | 0.096 | -98.821 | -413735.445 |
| 1-Ethyl-3-methylimidazolium dicyanamide | -212226.661 | 0.097 | -148016.490 | 0.075 | -360365.543 | 0.088 | -122.392 | -512421.918 |
| 1-Ethyl-3-methylimidazolium ethyl sulfate | -212226.661 | 0.097 | -480561.667 | 0.057 | -692946.914 | 0.092 | -158.586 | -663956.441 |
| 1-Ethyl-3-methylimidazolium hexafluorophosphate | -212226.661 | 0.097 | -580409.485 | 0.045 | -792747.347 | 0.093 | -111.201 | -465566.711 |
| 1-Ethyl-3-methylimidazolium hydrogen sulfate | -212226.661 | 0.097 | -432139.533 | 0.050 | -644525.308 | 0.099 | -159.113 | -666163.626 |
| 1-Ethyl-3-methylimidazolium methanesulfonate | -212226.661 | 0.097 | -410017.509 | 0.092 | -622412.387 | 0.092 | -168.216 | -704275.286 |
| 1-Ethyl-3-methylimidazolium methyl sulfate | -212226.661 | 0.097 | -456350.367 | 0.066 | -668736.179 | 0.092 | -159.151 | -666320.456 |
| 1-Ethyl-3-methylimidazolium nitrate | -212226.661 | 0.097 | -172545.703 | 0.065 | -384882.912 | 0.095 | -110.548 | -462835.654 |
| 1-Ethyl-3-methylimidazolium tetrachloroaluminate | -212226.661 | 0.097 | -1291236.008 | 0.027 | -1503531.589 | 0.079 | -68.920 | -288550.270 |
| 1-Ethyl-3-methylimidazolium tetrafluoroborate | -212226.661 | 0.097 | -261429.508 | 0.071 | -473759.006 | 0.089 | -102.836 | -430547.800 |
| 1-Ethyl-3-methylimidazolium thiocyanate | -212226.661 | 0.097 | -303824.303 | 0.051 | -516141.716 | 0.093 | -90.753 | -379956.785 |
| 1-Ethyl-3-methylimidazolium tosylate | -212226.661 | 0.097 | -552311.689 | 0.085 | -764682.602 | 0.086 | -144.252 | -603942.089 |
| 1-Ethyl-3-methylimidazolium trifluoromethane | -212226.661 | 0.097 | -593497.229 | 0.080 | -805825.210 | 0.099 | -101.320 | -424201.093 |
| 1-Ethyl-3-methylimidazolium trifluoromethanesulfonate | -212226.661 | 0.097 | -593497.229 | 0.049 | -805830.765 | 0.088 | -106.876 | -447459.653 |
| 1-Hexyl-3-methylimidazolium chloride | -309064.714 | 0.089 | -285190.791 | 0.000 | -594354.167 | 0.089 | -98.662 | -413070.835 |
| 1-Hexyl-3-methylimidazolium hexafluorophosphate | -309064.714 | 0.089 | -580409.485 | 0.045 | -889584.725 | 0.081 | -110.526 | -462743.915 |
| 1-Hexyl-3-methylimidazolium tetrafluoroborate | -309064.714 | 0.089 | -261429.508 | 0.071 | -570595.092 | 0.089 | -102.870 | -430690.542 |
| 1-Hexyl-3-methylimidazolium trifluoromethanesulfonate | -309064.714 | 0.089 | -593497.229 | 0.049 | -902662.946 | 0.095 | -101.004 | -422874.662 |
| 1-Methyl-3-(3,3,4,4,5,5,6,6,7,7,8,8,8-tridecafluorooctyl)-imidazolium hexafluorophosphate | -1152482.221 | 0.080 | -580409.485 | 0.045 | -1732978.659 | 0.092 | -86.953 | -364048.905 |
| 1-Methyl-3-octylimidazolium chloride | -357483.699 | 0.099 | -285190.791 | 0.000 | -642769.394 | 0.095 | -94.903 | -397334.712 |
| 1-Methyl-3-octylimidazolium hexafluorophosphate | -357483.699 | 0.099 | -580409.485 | 0.045 | -938003.219 | 0.095 | -110.035 | -460686.552 |
| 1-Methyl-3-octylimidazolium tetrafluoroborate | -357483.699 | 0.099 | -261429.508 | 0.071 | -619015.303 | 0.080 | -102.095 | -427444.442 |
| 1-Methyl-3-octylimidazolium trifluoromethanesulfonate | -357483.699 | 0.099 | -593497.229 | 0.049 | -951085.571 | 0.095 | -104.643 | -438110.923 |
| 1-Methylimidazolium chloride | -163798.567 | 0.072 | -285190.791 | 0.000 | -449091.625 | 0.088 | -102.266 | -428161.888 |
| 1-Methylimidazolium hydrogen sulfate | -163798.567 | 0.072 | -432139.533 | 0.050 | -596106.467 | 0.093 | -168.367 | -704905.104 |
| 3-(Triphenylphosphonio)propane-1-sulfonic acid | -1097831.330 | 0.076 | -552311.689 | 0.085 | -1650232.453 | 0.065 | -89.434 | -374435.051 |
| 3-Methyl-1-propylpyridinium bis(trifluoromethylsulfonyl)imide | -250012.875 | 0.091 | -1128180.656 | 0.088 | -1378321.315 | 0.094 | -127.784 | -534996.931 |
| 4-(3-Butyl-1-imidazolyl)-1-butanesulfonic acid triflate | -718812.554 | 0.095 | -593497.229 | 0.086 | -1312424.627 | 0.091 | -114.845 | -480823.299 |
| Tetrabutylphosphonium bromide | -600151.187 | 0.099 | -1597261.406 | 0.000 | -2197516.553 | 0.081 | -103.959 | -435248.135 |
| Tetrabutylphosphonium chloride | -600151.187 | 0.099 | -285190.791 | 0.000 | -885441.897 | 0.084 | -99.919 | -418332.895 |
| Tetrabutylphosphonium methanesulfonate | -600151.187 | 0.099 | -410017.509 | 0.092 | -1010271.681 | 0.083 | -102.985 | -431168.838 |
| Tetrabutylphosphonium p-toluenesulfonate | -600151.187 | 0.099 | -552311.689 | 0.085 | -1152569.673 | 0.075 | -96.796 | -405260.105 |
| Tetrabutylphosphonium tetrafluoroborate | -600151.187 | 0.099 | -261429.508 | 0.071 | -861682.518 | 0.099 | -101.823 | -426304.664 |

Table B.5 – Summary of the Ab-Initio calculation results using a small basis set (3-21G) geometry optimization with MP2 correction for the ionic bond energies of the 74 selected ionic liquids.

| Ionic Liquid (Sigma-Aldrich) | Ab-Initio Approach: Small Base Set (3-21G) with MP2 Correlation Single Point Calculation | | | | | | | |
|---|--|-----------------------------|--------------|-----------------------------|------------------------------|-----------------------------|---------------------------|------------------------|
| | Cation | | Anion | | Component | | Ionic Bond Energy | |
| | E [kcal/mol] | E _{MP2} [kcal/mol] | E [kcal/mol] | E _{MP2} [kcal/mol] | E [kcal/mol] | E _{MP2} [kcal/mol] | E _i [kcal/mol] | E _j [J/mol] |
| 1,2,3-Trimethylimidazolium methyl sulfate | -214095.620 | -479.035 | -460071.660 | -417.803 | -674246.114 | -904.441 | -86.437 | -361886.845 |
| 1,2,3-Trimethylimidazolium trifluoromethanesulfonate | -214095.620 | -479.035 | -598584.441 | -554.524 | -817639.748 | -1594.260 | -5520.388 | -23112363.609 |
| 1,2-Dimethyl-3-propylimidazolium bis(trifluoromethylsulfonyl)imide | -262935.558 | -596.353 | -1137622.199 | -1030.456 | -1400616.435 | -1638.492 | -70.361 | -294581.604 |
| 1,2-Dimethyl-3-propylimidazolium tris(trifluoromethylsulfonyl)methide | -262935.558 | -596.353 | -1679026.769 | -1485.965 | -1942071.842 | -2128.284 | -155.481 | -650957.827 |
| 1,3-Dimethylimidazolium methyl sulfate | -190927.579 | -624.221 | -460071.660 | -417.803 | -649828.642 | -843.132 | 1369.490 | 573362.366 |
| 1-Allyl-3-methylimidazolium chloride | -239333.396 | -787.132 | -287023.591 | -29.860 | -524848.027 | -566.517 | 1759.434 | 7366273.037 |
| 1-Benzyl-3-methylimidazolium chloride | -333240.443 | -750.959 | -287023.591 | -29.860 | -620328.053 | -785.266 | -68.466 | -286649.311 |
| 1-Benzyl-3-methylimidazolium hexafluorophosphate | -333240.443 | -750.959 | -585725.114 | -490.597 | -919029.931 | -1251.546 | -74.365 | -311345.104 |
| 1-Benzyl-3-methylimidazolium tetrafluoroborate | -333240.443 | -750.959 | -264190.808 | -327.912 | -597506.386 | -1086.265 | -82.528 | -345523.044 |
| 1-Butyl-1-(3,3,4,4,5,5,6,6,7,7,8,8,8-tridecafluorooctyl)-imidazolium hexafluorophosphate | -1749479.079 | -2363.235 | -585725.114 | -490.597 | Calculation Session Time Out | n/a | n/a | n/a |
| 1-Butyl-2,3-dimethylimidazolium chloride | -287353.685 | -654.807 | -287023.591 | -29.860 | -574443.371 | -691.885 | -73.314 | -306947.369 |
| 1-Butyl-2,3-dimethylimidazolium hexafluorophosphate | -287353.685 | -654.807 | -585725.114 | -490.597 | -873157.702 | -1157.178 | -90.678 | -379643.019 |
| 1-Butyl-2,3-dimethylimidazolium tetrafluoroborate | -287353.685 | -654.807 | -264190.808 | -327.912 | -551615.515 | 992.962 | 1904.659 | 7974288.461 |
| 1-Butyl-3-methylimidazolium acetate | -262926.227 | -595.768 | -93841.323 | -49.115 | -405075.890 | -873.188 | -48536.645 | -203209734.042 |
| 1-Butyl-3-methylimidazolium bis(trifluoromethylsulfonyl)imide | -262926.227 | -595.768 | -1137622.199 | -1030.456 | -1400604.261 | -1633.517 | -63.128 | -264299.694 |
| 1-Butyl-3-methylimidazolium bromide | -262926.227 | -595.768 | -1606505.205 | -20.199 | -1869502.357 | -625.835 | -80.192 | -338255.876 |
| 1-Butyl-3-methylimidazolium chloride | -262926.227 | -595.768 | -287023.591 | -29.860 | -550030.197 | -632.079 | -86.831 | -362536.353 |
| 1-Butyl-3-methylimidazolium dicyanamide | -262926.227 | -595.768 | -149500.662 | -324.973 | -412504.148 | -925.386 | -81.904 | -342910.484 |
| 1-Butyl-3-methylimidazolium hexafluorophosphate | -262926.227 | -595.768 | -585725.114 | -490.597 | -848716.331 | -1097.235 | -75.861 | -317608.801 |
| 1-Butyl-3-methylimidazolium hydrogen sulfate | -262926.227 | -595.768 | -435655.965 | -358.047 | -698650.443 | -954.632 | -69.068 | -289170.798 |
| 1-Butyl-3-methylimidazolium methanesulfonate | -262926.227 | -595.768 | -413268.986 | -332.119 | -676286.568 | -941.460 | -104.928 | -439304.446 |
| 1-Butyl-3-methylimidazolium methyl sulfate | -262926.227 | -595.768 | -460071.660 | -417.803 | -723071.070 | -1019.073 | -78.686 | -329435.508 |
| 1-Butyl-3-methylimidazolium nitrate | -262926.227 | -595.768 | -174322.725 | -323.835 | -437333.796 | -936.138 | -101.379 | -424447.272 |
| 1-Butyl-3-methylimidazolium octyl sulfate | -262926.227 | -595.768 | -631000.204 | -826.599 | -213414.819 | -266.720 | 681667.259 | 2853955448.043 |
| 1-Butyl-3-methylimidazolium tetrachloroaluminate | -262926.227 | -595.768 | -1299199.524 | -140.157 | -1562196.914 | -740.539 | -75.777 | -317256.311 |
| 1-Butyl-3-methylimidazolium tetrafluoroborate | -262926.227 | -595.768 | -264190.808 | -327.912 | -442624.162 | -736.432 | 84680.121 | 354532639.242 |
| 1-Butyl-3-methylimidazolium thiocyanate | -262926.227 | -595.768 | -306014.425 | -164.222 | -568998.517 | -772.802 | -70.677 | -295903.936 |
| 1-Butyl-3-methylimidazolium tosylate | -262926.227 | -595.768 | -556847.688 | -666.174 | -819865.064 | -1268.015 | -97.221 | -407039.807 |
| 1-Butyl-3-methylimidazolium trifluoromethanesulfonate | -262926.227 | -595.768 | -598584.441 | -554.524 | -861586.422 | -1161.440 | -86.903 | -363837.199 |
| 1-Butyl-3-methylpyridinium bis(trifluoromethylsulfonyl)imide | -27618.425 | -638.580 | -1137622.199 | -1030.456 | -1414309.003 | -1682.256 | -81.599 | -341633.318 |
| 1-Butyl-4-methylpyridinium bromide | -276620.980 | -636.658 | -1606505.205 | -20.199 | -1883210.823 | -667.391 | -95.172 | -398458.932 |
| 1-Butyl-4-methylpyridinium chloride | -276620.980 | -636.658 | -287023.591 | -29.860 | -563720.084 | -671.754 | -80.750 | -338077.743 |
| 1-Butyl-4-methylpyridinium tetrafluoroborate | -276620.980 | -636.658 | -264190.808 | -327.912 | -540886.375 | -974.052 | -84.068 | -351971.698 |
| 1-Butylpyridinium bromide | -252196.789 | -577.730 | -1606505.205 | -20.199 | -1858789.572 | -607.131 | -96.781 | -405194.545 |
| 1-Dodecyl-3-methylimidazolium iodide | -458268.703 | -1062.787 | -4322251.676 | -20.568 | -3902176.220 | -721.070 | 878706.444 | 3678904935.102 |
| 1-Ethyl-2,3-dimethylimidazolium chloride | -238516.861 | -537.981 | -287023.591 | -29.860 | -525607.155 | -575.436 | -74.298 | -311066.255 |
| 1-Ethyl-2,3-dimethylimidazolium ethyl sulfate | -238516.861 | -537.981 | -484492.924 | -476.320 | -723080.770 | -1024.593 | -81.275 | -340277.530 |
| 1-Ethyl-2,3-dimethylimidazolium trifluoromethanesulfonate | -238516.861 | -537.981 | -598584.441 | -554.524 | -837177.597 | -1109.458 | -94.081 | -393891.731 |
| 1-Ethyl-3-methylimidazolium acetate | -214090.285 | -479.069 | -93841.323 | -49.115 | -356239.650 | -756.309 | -48536.168 | -203207737.392 |
| 1-Ethyl-3-methylimidazolium bis(pentafluoroethylsulfonyl)imide | -214090.285 | -479.069 | -1433547.748 | -1448.581 | -1647712.311 | -1940.156 | -86.785 | -363346.393 |
| 1-Ethyl-3-methylimidazolium bis(trifluoromethylsulfonyl)imide | -214090.285 | -479.069 | -1137622.199 | -1030.456 | -1351760.391 | -1515.591 | -53.973 | -225972.104 |
| 1-Ethyl-3-methylimidazolium bromide | -214090.285 | -479.069 | -1606505.205 | -20.199 | -1820661.357 | -505.649 | -72.249 | -302484.911 |
| 1-Ethyl-3-methylimidazolium chloride | -214090.285 | -479.069 | -287023.591 | -29.860 | -501193.850 | -515.363 | -86.410 | -361774.084 |
| 1-Ethyl-3-methylimidazolium dicyanamide | -214090.285 | -479.069 | -149500.662 | -324.973 | -363667.899 | -807.098 | -80.010 | -334978.551 |
| 1-Ethyl-3-methylimidazolium ethyl sulfate | -214090.285 | -479.069 | -484492.924 | -476.320 | -698658.482 | -959.127 | -79.011 | -330795.989 |
| 1-Ethyl-3-methylimidazolium hexafluorophosphate | -214090.285 | -479.069 | -585725.114 | -490.597 | -799879.761 | -979.820 | -74.517 | -311984.015 |
| 1-Ethyl-3-methylimidazolium hydrogen sulfate | -214090.285 | -479.069 | -435655.965 | -358.047 | -649816.039 | -838.318 | -70.992 | -297223.274 |
| 1-Ethyl-3-methylimidazolium methanesulfonate | -214090.285 | -479.069 | -413268.986 | -332.119 | -627452.899 | -817.427 | -99.867 | -418117.840 |
| 1-Ethyl-3-methylimidazolium methyl sulfate | -214090.285 | -479.069 | -460071.660 | -417.803 | -674236.220 | -902.808 | -80.213 | -335829.274 |
| 1-Ethyl-3-methylimidazolium nitrate | -214090.285 | -479.069 | -174322.725 | -323.835 | -388503.285 | -819.989 | -107.361 | -449489.265 |
| 1-Ethyl-3-methylimidazolium tetrachloroaluminate | -214090.285 | -479.069 | -1299199.524 | -140.157 | -1511360.722 | -623.785 | -75.473 | -315984.367 |
| 1-Ethyl-3-methylimidazolium tetrafluoroborate | -214090.285 | -479.069 | -264190.808 | -327.912 | -478355.236 | -817.072 | -84.235 | -352668.135 |
| 1-Ethyl-3-methylimidazolium thiocyanate | -214090.285 | -479.069 | -306014.425 | -164.222 | -520152.676 | -655.451 | -60.126 | -251731.685 |
| 1-Ethyl-3-methylimidazolium tosylate | -214090.285 | -479.069 | -556847.688 | -666.174 | -771037.057 | -1150.533 | -104.374 | -436985.736 |
| 1-Ethyl-3-methylimidazolium trifluoromethane | -214090.285 | -479.069 | -545390.715 | -448.299 | -812744.336 | -1044.546 | -53380.515 | -223489699.619 |
| 1-Ethyl-3-methylimidazolium trifluoromethanesulfonate | -214090.285 | -479.069 | -598584.441 | -554.524 | -812752.422 | -1049.391 | -93.496 | -391444.195 |
| 1-Hexyl-3-methylimidazolium chloride | -311762.043 | -712.578 | -287023.591 | -29.860 | -598865.754 | -748.873 | -86.556 | -362386.088 |
| 1-Hexyl-3-methylimidazolium hexafluorophosphate | -311762.043 | -712.578 | -585725.114 | -490.597 | -590993.735 | -1035.226 | 306661.370 | 1283907764.543 |
| 1-Hexyl-3-methylimidazolium tetrafluoroborate | -311762.043 | -712.578 | -264190.808 | -327.912 | -452933.728 | -70.655 | 123988.957 | 519108048.139 |
| 1-Hexyl-3-methylimidazolium trifluoromethanesulfonate | -311762.043 | -712.578 | -598584.441 | -554.524 | -910412.842 | -1276.351 | -75.608 | -316550.994 |
| 1-Methyl-3-(3,3,4,4,5,5,6,6,7,7,8,8,8-tridecafluorooctyl)-imidazolium hexafluorophosphate | -1163618.890 | -1801.071 | -585725.114 | -490.597 | -210241.032 | -196.057 | 1541198.582 | 6452579369.443 |
| 1-Methyl-3-octylimidazolium chloride | -360597.672 | -829.324 | -287023.591 | -29.860 | -647695.879 | -865.355 | -80.788 | -338235.654 |
| 1-Methyl-3-octylimidazolium hexafluorophosphate | -360597.672 | -829.324 | -585725.114 | -490.597 | -302431.190 | -995.852 | 644215.664 | 2697158803.630 |
| 1-Methyl-3-octylimidazolium tetrafluoroborate | -360597.672 | -829.324 | -264190.808 | -327.912 | -128945.007 | -299.091 | 496701.619 | 2079554611.053 |
| 1-Methyl-3-octylimidazolium trifluoromethanesulfonate | -360597.672 | -829.324 | -598584.441 | -554.524 | -768250.656 | -978.039 | 191337.265 | 801077098.007 |
| 1-Methylimidazolium chloride | -165249.299 | -361.853 | -287023.591 | -29.860 | -452355.632 | -398.238 | -89.267 | -373738.660 |
| 1-Methylimidazolium hydrogen sulfate | -165249.299 | -361.853 | -435655.965 | -358.047 | -601012.988 | -725.801 | -113.626 | -475719.104 |
| 3-(Triphenylphosphonio)propane-1-sulfonic acid | -1106553.011 | -1499.506 | -556847.688 | -666.174 | -1662652.960 | -1377.051 | 1536.369 | 6432358.874 |
| 3-Methyl-1-propylpyridinium bis(trifluoromethylsulfonyl)imide | -252200.152 | -580.283 | -1137622.199 | -1030.456 | -1389885.375 | -1619.436 | -71.720 | -300272.916 |
| 4-(3-Butyl-1-imidazolyl)-1-butanefluoric acid triflate | -724644.670 | -1040.994 | -533729.841 | -420.979 | -1323337.686 | -1622.680 | -65123.808 | -272655982.952 |
| Tetrabutylphosphonium bromide | -604793.599 | -985.306 | -1606505.205 | -20.199 | -2211382.357 | -1014.762 | -92.882 | -388563.701 |
| Tetrabutylphosphonium chloride | -604793.599 | -985.306 | -287023.591 | -29.860 | -891904.007 | -1021.372 | -93.022 | -389457.484 |
| Tetrabutylphosphonium methanesulfonate | -604793.599 | -985.306 | -413268.986 | -332.119 | -1018166.248 | -1335.637 | -121.875 | -510255.654 |
| Tetrabutylphosphonium p-toluenesulfonate | -604793.599 | -985.306 | -556847.688 | -666.174 | -1161686.455 | -1611.488 | -5.175 | -21664.346 |
| Tetrabutylphosphonium tetrafluoroborate | -604793.599 | -985.306 | -264190.808 | -327.912 | -869071.728 | -1326.004 | -100.106 | -419116.044 |

Table B.6 – Summary of the RED values calculated for the collective list of solvents analyzed in the EquiSolv package.

| Solvent Name | δ_D [MPa ^{0.5}] | δ_P [MPa ^{0.5}] | δ_H [MPa ^{0.5}] | δ_I [MPa ^{0.5}] | V_m [cm ³ /mol] | Ra | RED |
|--|----------------------------------|----------------------------------|----------------------------------|----------------------------------|------------------------------|--------|--------|
| 1,1-Dimethylpropylamine | 15.1 | 5.8 | 6.4 | 0.0 | 114.3 | 1.4765 | 0.4474 |
| Pentylamine | 15.6 | 4.7 | 6.7 | 0.0 | 115.4 | 1.8974 | 0.5750 |
| Heptylamine | 15.7 | 4.4 | 6.4 | 0.0 | 148.4 | 2.0248 | 0.6136 |
| Diallyl Amine | 15.6 | 4.5 | 6.7 | 0.0 | 124.3 | 2.0688 | 0.6269 |
| 2-Ethylhexyl Amine | 15.7 | 4.2 | 6.1 | 0.0 | 163.3 | 2.1378 | 0.6478 |
| Methyl-Propylamine | 15.2 | 4.2 | 5.7 | 0.0 | 102.8 | 2.3259 | 0.7048 |
| Hexylamine | 15.8 | 4.0 | 6.1 | 0.0 | 132.1 | 2.3431 | 0.7100 |
| sec-Butylamine | 15.7 | 4.6 | 7.4 | 0.0 | 98.9 | 2.4042 | 0.7285 |
| (+/-)-sec-Butylamine | 15.7 | 4.6 | 7.4 | 0.0 | 98.9 | 2.4042 | 0.7285 |
| Methylethylamine | 15.0 | 4.4 | 6.2 | 0.0 | 85.8 | 2.4125 | 0.7311 |
| 2-Methylbutylamine | 15.8 | 4.2 | 6.9 | 0.0 | 115.1 | 2.4269 | 0.7354 |
| 3-Methylbutylamine | 15.2 | 4.4 | 7.0 | 0.0 | 116.3 | 2.5100 | 0.7606 |
| Ethylpropylamine | 15.3 | 3.9 | 5.3 | 0.0 | 119.5 | 2.5612 | 0.7761 |
| 1-Ethylpropylamine | 15.3 | 3.9 | 5.3 | 0.0 | 119.5 | 2.5612 | 0.7761 |
| Isobutylamine | 15.0 | 4.9 | 7.5 | 0.0 | 100.1 | 2.6758 | 0.8108 |
| Octylamine | 16.1 | 3.9 | 4.8 | 0.0 | 165.1 | 2.6851 | 0.8137 |
| N-Chlorodimethylamine | 16.0 | 7.8 | 7.9 | 0.0 | 87.4 | 2.7295 | 0.8271 |
| Isopropyl Amine (2-Propan Amine) | 14.8 | 4.4 | 6.6 | 0.0 | 86.8 | 2.7677 | 0.8387 |
| 1,3-Propanediamine, N,N-Diethyl- | 15.9 | 4.5 | 7.8 | 0.0 | 158.7 | 2.7946 | 0.8468 |
| Methyl-Butylamine | 15.3 | 3.5 | 5.1 | 0.0 | 119.8 | 2.9732 | 0.9010 |
| Nonylamine | 16.1 | 3.6 | 4.7 | 0.0 | 181.3 | 2.9883 | 0.9055 |
| Bis-(2,2,2-Trifluoro-Ethyl)-Amine | 14.4 | 5.9 | 4.2 | 0.0 | 135.0 | 3.0282 | 0.9176 |
| N,N-Dichloromethyl Amine | 16.5 | 7.5 | 8.0 | 0.0 | 90.8 | 3.0480 | 0.9236 |
| Undecylamine | 16.1 | 3.5 | 4.8 | 0.0 | 214.3 | 3.0480 | 0.9236 |
| N-Ethyl-2-Methylallylamine | 15.4 | 3.3 | 6.0 | 0.0 | 128.9 | 3.0741 | 0.9315 |
| N,N?-Dimethylpiperazine | 16.9 | 4.4 | 5.4 | 0.0 | 130.2 | 3.0757 | 0.9320 |
| n-Butyl Amine | 16.2 | 4.5 | 8.0 | 0.0 | 98.8 | 3.0871 | 0.9355 |
| Methylheptylamine | 15.6 | 3.2 | 5.0 | 0.0 | 169.0 | 3.1843 | 0.9649 |
| Methylisopropylamine | 14.9 | 3.5 | 5.7 | 0.0 | 102.9 | 3.2249 | 0.9772 |
| Bornylamine | 16.9 | 4.3 | 4.9 | 0.0 | 166.8 | 3.2249 | 0.9772 |
| 2,2,2-Trifluoro-Ethylamine | 14.6 | 7.7 | 7.6 | 0.0 | 81.5 | 3.2265 | 0.9777 |
| Ethanamine, 2,2-Dufluoro-N,N-Bis(Trifluoromethyl)- | 14.9 | 6.2 | 2.9 | 0.0 | 146.5 | 3.2265 | 0.9777 |
| Propylisopropylamine | 15.2 | 3.3 | 5.0 | 0.0 | 136.6 | 3.2388 | 0.9815 |
| N,N-Dichloroethyl Amine | 16.8 | 7.6 | 7.7 | 0.0 | 98.3 | 3.2450 | 0.9833 |
| Propyl Amine | 16.0 | 4.9 | 8.6 | 0.0 | 83.0 | 3.2757 | 0.9926 |
| Cyclopentylamine | 17.1 | 4.8 | 6.5 | 0.0 | 97.9 | 3.2757 | 0.9926 |
| 2-Popen-1-Amine, N,N-Di-2-Popenyl- | 15.7 | 3.0 | 5.6 | 0.0 | 170.3 | 3.3015 | 1.0005 |
| Methylpentylamine | 15.4 | 3.1 | 5.0 | 0.0 | 136.0 | 3.3302 | 1.0092 |
| Decylamine | 16.2 | 3.3 | 4.5 | 0.0 | 198.0 | 3.3823 | 1.0249 |
| Ethylbutylamine | 15.3 | 3.1 | 4.9 | 0.0 | 136.6 | 3.3941 | 1.0285 |
| Ethylheptylamine | 15.6 | 3.0 | 4.9 | 0.0 | 185.7 | 3.4015 | 1.0308 |
| Ethylloctylamine | 15.0 | 3.2 | 5.8 | 0.0 | 197.9 | 3.4029 | 1.0312 |
| Ethylisopropylamine | 15.0 | 3.2 | 5.3 | 0.0 | 119.6 | 3.4249 | 1.0378 |
| 2,2-Dimethylpropylamine | 15.0 | 3.2 | 6.7 | 0.0 | 115.7 | 3.5454 | 1.0744 |
| Piperazine (PZ) | 17.3 | 4.8 | 6.0 | 0.0 | 129.4 | 3.5468 | 1.0748 |
| Methanamine, n-(Difluoromethyl)-1,1,1-Trifluoro-n-(Trifluoromethyl)- | 14.7 | 5.7 | 2.8 | 0.0 | 130.3 | 3.5735 | 1.0829 |
| Methyl-Tert-Butylamine | 14.9 | 3.1 | 5.4 | 0.0 | 120.7 | 3.5903 | 1.0880 |
| Ethyl-sec-Butylamine | 15.5 | 2.8 | 5.0 | 0.0 | 136.2 | 3.5917 | 1.0884 |
| Ethylpentylamine | 15.4 | 2.9 | 4.7 | 0.0 | 152.7 | 3.5944 | 1.0892 |
| Ethylisobutylamine | 15.0 | 3.0 | 5.1 | 0.0 | 137.4 | 3.6346 | 1.1014 |
| 1-Hexanamine, 2-Ethyl- | 14.8 | 3.1 | 5.9 | 0.0 | 164.9 | 3.6770 | 1.1142 |
| Tert-Butylamine | 14.7 | 3.5 | 7.1 | 0.0 | 99.6 | 3.7148 | 1.1257 |
| Methylhexylamine | 15.6 | 2.7 | 4.7 | 0.0 | 152.6 | 3.7417 | 1.1338 |
| 1-Methylbutylamine | 14.3 | 4.4 | 7.3 | 0.0 | 115.0 | 3.7430 | 1.1342 |
| Methylloctylamine | 15.9 | 2.8 | 4.2 | 0.0 | 185.7 | 3.8288 | 1.1602 |
| Dibutyl Amine | 15.0 | 3.0 | 4.3 | 0.0 | 170.7 | 3.8484 | 1.1662 |
| 2,5-Dimethylpiperazine | 17.4 | 5.4 | 7.3 | 0.0 | 127.6 | 3.8639 | 1.1709 |
| Dimethyl-Propylamine | 15.5 | 2.8 | 4.1 | 0.0 | 121.7 | 3.8691 | 1.1725 |
| Tripropylamine | 15.7 | 2.9 | 3.8 | 0.0 | 189.1 | 3.8949 | 1.1803 |

Table B.7 – Summary of the RED values calculated for the collective list of solvents analyzed in the EquiSolv package (continued).

| Solvent Name | δ_D [MPa ^{0.5}] | δ_P [MPa ^{0.5}] | δ_H [MPa ^{0.5}] | δ_I [MPa ^{0.5}] | V_m [cm ³ /mol] | Ra | RED |
|--|----------------------------------|----------------------------------|----------------------------------|----------------------------------|------------------------------|--------|--------|
| Methylundecylamine | 16.0 | 2.7 | 4.3 | 0.0 | 234.8 | 3.9090 | 1.1845 |
| Dimethyl-1,1-Dimethylpropylamine | 15.3 | 3.1 | 3.6 | 0.0 | 153.8 | 3.9102 | 1.1849 |
| Perfluor-Tert-Butylamine | 13.9 | 7.0 | 4.3 | 0.0 | 146.3 | 3.9256 | 1.1896 |
| Methanediamine, N,N,N',N'-Tetramethyl- | 15.9 | 2.4 | 5.9 | 0.0 | 131.7 | 3.9256 | 1.1896 |
| Methyldipropylamine | 15.6 | 2.8 | 3.9 | 0.0 | 155.4 | 3.9408 | 1.1942 |
| Pentadecylamine | 16.3 | 3.0 | 3.9 | 0.0 | 280.2 | 3.9459 | 1.1957 |
| Dimethylethylamine | 15.4 | 2.7 | 4.2 | 0.0 | 104.7 | 3.9459 | 1.1957 |
| Dodecylamine | 16.3 | 3.1 | 3.7 | 0.0 | 231.0 | 3.9598 | 1.1999 |
| Ethanamine, N,N-Bis(Trifluoromethyl)- | 14.4 | 5.0 | 3.0 | 0.0 | 138.3 | 3.9674 | 1.2022 |
| Methanamine, 1,1,1-Trifluoro-N-Methyl-n-(Trifluoromethyl)- | 14.3 | 7.1 | 3.0 | 0.0 | 121.6 | 3.9711 | 1.2034 |
| Methylethylpropylamine | 15.5 | 2.7 | 4.0 | 0.0 | 138.4 | 4.0012 | 1.2125 |
| 1-Phenylethyl Amine | 17.3 | 4.2 | 6.9 | 0.0 | 126.6 | 4.0112 | 1.2155 |
| 3-Pentanamine | 14.2 | 4.1 | 7.2 | 0.0 | 114.7 | 4.0112 | 1.2155 |
| Diethylpropylamine | 15.5 | 2.6 | 3.9 | 0.0 | 155.1 | 4.1340 | 1.2527 |
| Diisopentylamine | 15.2 | 2.4 | 4.7 | 0.0 | 204.6 | 4.1485 | 1.2571 |
| Tetramethylethylenediamine | 16.0 | 2.2 | 5.5 | 0.0 | 148.4 | 4.1485 | 1.2571 |
| Amphetamine | 17.5 | 4.3 | 6.3 | 0.0 | 148.1 | 4.1617 | 1.2611 |
| Methyldiethylamine | 15.4 | 2.5 | 4.1 | 0.0 | 121.4 | 4.1665 | 1.2626 |
| Diisobutylamine | 14.9 | 2.5 | 4.8 | 0.0 | 172.3 | 4.2202 | 1.2788 |
| N-Methyl-2-Heptanamine | 15.4 | 2.2 | 4.9 | 0.0 | 168.7 | 4.2202 | 1.2788 |
| Dimethylheptylamine | 15.7 | 2.3 | 4.1 | 0.0 | 187.8 | 4.3081 | 1.3055 |
| 3-Methyl Mercaptopropyl Amine | 16.9 | 7.1 | 9.2 | 0.0 | 111.8 | 4.3186 | 1.3087 |
| Diethyl Amine | 14.9 | 2.3 | 6.1 | 0.0 | 104.1 | 4.3267 | 1.3111 |
| 1,2-Dimethylpropylamine | 14.1 | 3.8 | 7.2 | 0.0 | 115.1 | 4.3290 | 1.3118 |
| Hexamethylenediamine | 16.6 | 8.0 | 9.3 | 0.0 | 135.4 | 4.3692 | 1.3240 |
| Diethylheptylamine | 15.7 | 2.3 | 3.9 | 0.0 | 221.3 | 4.3863 | 1.3292 |
| Tetradecylamine | 16.4 | 2.7 | 3.6 | 0.0 | 263.8 | 4.3966 | 1.3323 |
| Methyl-sec-Butylamine | 14.3 | 2.9 | 5.3 | 0.0 | 119.5 | 4.4227 | 1.3402 |
| Cyclohexylamine | 17.2 | 3.1 | 6.5 | 0.0 | 115.0 | 4.4587 | 1.3511 |
| N-Methylcyclohexylamine | 16.8 | 2.6 | 4.5 | 0.0 | 133.6 | 4.4688 | 1.3542 |
| Methyldodecylamine | 16.2 | 2.4 | 3.7 | 0.0 | 251.6 | 4.4956 | 1.3623 |
| Dimethylbutylamine | 15.5 | 2.2 | 3.8 | 0.0 | 138.7 | 4.5365 | 1.3747 |
| Dimethylisobutylamine | 15.2 | 2.1 | 4.1 | 0.0 | 139.5 | 4.6043 | 1.3952 |
| Diethyloctylamine | 15.9 | 1.9 | 4.4 | 0.0 | 238.0 | 4.6054 | 1.3956 |
| Dimethylpentylamine | 15.6 | 2.1 | 3.8 | 0.0 | 154.9 | 4.6141 | 1.3982 |
| Diethylisopropylamine | 15.4 | 2.1 | 3.8 | 0.0 | 155.2 | 4.6487 | 1.4087 |
| Dimethyl-3-Methylbutylamine | 15.3 | 2.0 | 4.1 | 0.0 | 155.7 | 4.6573 | 1.4113 |
| Methylethylbutylamine | 15.5 | 2.1 | 3.7 | 0.0 | 155.4 | 4.6690 | 1.4148 |
| Dipentylamine | 15.6 | 2.2 | 3.4 | 0.0 | 202.9 | 4.7053 | 1.4258 |
| Dimethyloctylamine | 16.0 | 2.0 | 3.8 | 0.0 | 204.6 | 4.7392 | 1.4361 |
| Hexadecylamine | 16.5 | 2.6 | 3.2 | 0.0 | 296.9 | 4.7434 | 1.4374 |
| Diethyldecylamine | 16.0 | 1.8 | 4.3 | 0.0 | 270.8 | 4.7508 | 1.4396 |
| 3,5-Bis(Trifluoromethyl)Benzylamine | 17.5 | 5.7 | 2.6 | 0.0 | 174.7 | 4.7885 | 1.4511 |
| Diethylbutylamine | 15.6 | 2.0 | 3.6 | 0.0 | 172.1 | 4.7896 | 1.4514 |
| Diethylhexadecylamine | 16.3 | 1.7 | 5.1 | 0.0 | 369.7 | 4.7917 | 1.4520 |
| Heptadecylamine | 16.5 | 2.5 | 3.2 | 0.0 | 313.0 | 4.8218 | 1.4612 |
| Diheptylamine | 15.7 | 2.6 | 2.6 | 0.0 | 268.9 | 4.8270 | 1.4627 |
| Dimethylhexylamine | 15.8 | 1.9 | 3.7 | 0.0 | 171.5 | 4.8374 | 1.4659 |
| Methylisobutylamine | 14.6 | 2.0 | 5.1 | 0.0 | 120.1 | 4.8672 | 1.4749 |
| Butylcyclohexylamine | 16.5 | 2.0 | 4.0 | 0.0 | 184.4 | 4.8929 | 1.4827 |
| Methyldiisopropylamine | 15.2 | 1.9 | 3.8 | 0.0 | 155.5 | 4.8959 | 1.4836 |
| Ethyl-Tert-Butylamine | 14.7 | 1.9 | 4.9 | 0.0 | 136.9 | 4.8990 | 1.4845 |
| Octadecylamine | 16.5 | 2.4 | 3.2 | 0.0 | 329.7 | 4.9010 | 1.4852 |
| 2,2'-Dimethyl-4,4'-Methylenebis(Cyclohexylamine) | 17.7 | 3.4 | 5.7 | 0.0 | 251.8 | 4.9406 | 1.4972 |
| Allyl Amine | 15.5 | 5.7 | 10.6 | 0.0 | 74.9 | 4.9528 | 1.5008 |
| Dimethyldodecylamine | 16.2 | 1.8 | 3.8 | 0.0 | 270.4 | 4.9860 | 1.5109 |
| Dimethyldecylamine | 16.1 | 1.8 | 3.7 | 0.0 | 237.4 | 4.9890 | 1.5118 |
| Dimethyl-1,2-Dimethylpropylamine | 15.3 | 1.6 | 4.2 | 0.0 | 154.5 | 4.9980 | 1.5145 |
| Tricosylamine | 16.5 | 2.4 | 3.0 | 0.0 | 411.9 | 5.0060 | 1.5170 |

Table B.8 – Summary of the RED values calculated for the collective list of solvents analyzed in the EquiSolv package (continued).

| Solvent Name | δ_D [MPa ^{0.5}] | δ_P [MPa ^{0.5}] | δ_H [MPa ^{0.5}] | δ_I [MPa ^{0.5}] | V_m [cm ³ /mol] | Ra | RED |
|--|----------------------------------|----------------------------------|----------------------------------|----------------------------------|------------------------------|--------|--------|
| Diethylhexylamine | 15.7 | 1.8 | 3.5 | 0.0 | 205.0 | 5.0090 | 1.5179 |
| N,N'-Di-Tert-Butylethylenediamine | 14.9 | 1.5 | 5.9 | 0.0 | 212.8 | 5.0636 | 1.5344 |
| Diethylamine | 15.8 | 1.9 | 3.2 | 0.0 | 236.2 | 5.0646 | 1.5347 |
| Triisobutylamine | 15.1 | 1.7 | 3.8 | 0.0 | 242.7 | 5.1196 | 1.5514 |
| 3-Methoxyisopropylamine | 14.3 | 6.1 | 10.0 | 0.0 | 104.7 | 5.1352 | 1.5561 |
| Dimethyltetradecylamine | 16.3 | 1.7 | 3.7 | 0.0 | 303.2 | 5.1575 | 1.5629 |
| Methyloctadecylamine | 16.4 | 1.9 | 3.4 | 0.0 | 350.2 | 5.1585 | 1.5632 |
| Dimethylhexadecylamine | 16.4 | 1.7 | 3.8 | 0.0 | 336.3 | 5.1701 | 1.5667 |
| Dipropyl Amine | 15.3 | 1.4 | 4.1 | 0.0 | 136.9 | 5.2163 | 1.5807 |
| Cis-1,2-Cyclohexanediamine | 17.3 | 6.7 | 9.8 | 0.0 | 119.1 | 5.2163 | 1.5807 |
| Trans-1,2-Cyclohexanediamine | 17.3 | 6.7 | 9.8 | 0.0 | 119.1 | 5.2163 | 1.5807 |
| n-Nitrosodimethylamine | 15.6 | 11.4 | 4.6 | 0.0 | 79.0 | 5.2211 | 1.5822 |
| Ethyl Amine | 15.0 | 5.6 | 10.7 | 0.0 | 65.6 | 5.2393 | 1.5877 |
| Eicosylamine | 16.6 | 2.3 | 2.8 | 0.0 | 362.7 | 5.2583 | 1.5934 |
| Cyclopropylamine | 17.6 | 7.7 | 9.1 | 0.0 | 66.8 | 5.2877 | 1.6023 |
| Benzylethylamine | 17.9 | 3.4 | 5.0 | 0.0 | 147.3 | 5.3160 | 1.6109 |
| Trimethyl Amine | 14.6 | 3.4 | 1.8 | 0.0 | 90.2 | 5.3348 | 1.6166 |
| Dimethyleicosylamine | 16.5 | 1.5 | 3.8 | 0.0 | 402.2 | 5.4046 | 1.6378 |
| Diisopropylamine | 14.8 | 1.7 | 3.5 | 0.0 | 141.9 | 5.4074 | 1.6386 |
| Benzenamine, 2-(Trifluoromethyl)- | 18.3 | 5.7 | 7.1 | 0.0 | 126.8 | 5.4185 | 1.6420 |
| Dioctylamine | 16.1 | 1.9 | 2.4 | 0.0 | 302.3 | 5.5579 | 1.6842 |
| Dinonylamine | 16.1 | 1.8 | 2.5 | 0.0 | 334.6 | 5.5794 | 1.6907 |
| Dimethyl-2,2-Dimethylpropylamine | 15.2 | 1.1 | 3.8 | 0.0 | 155.2 | 5.6258 | 1.7048 |
| Benzenemethanamine, N-Methyl- | 18.2 | 3.7 | 5.3 | 0.0 | 130.6 | 5.6498 | 1.7121 |
| Didecylamine | 16.2 | 1.7 | 2.5 | 0.0 | 367.9 | 5.6921 | 1.7249 |
| Dimethyl-Tert-Butylamine | 15.0 | 1.1 | 3.8 | 0.0 | 139.0 | 5.7105 | 1.7305 |
| Dimethyl Amine | 15.3 | 4.8 | 11.2 | 0.0 | 67.3 | 5.7567 | 1.7445 |
| 1,2-Benzenediamine, N,N,N',N'-Tetamethyl- | 18.4 | 4.3 | 5.0 | 0.0 | 168.7 | 5.8009 | 1.7578 |
| Nonacosylamine | 16.7 | 1.9 | 2.4 | 0.0 | 510.6 | 5.8523 | 1.7734 |
| Dimethyl-2-Methylbutylamine | 13.9 | 1.9 | 3.9 | 0.0 | 154.5 | 5.9632 | 1.8070 |
| Di-2-Ethylhexyl Amine | 15.6 | 0.8 | 3.2 | 0.0 | 301.5 | 6.0448 | 1.8318 |
| Tritriacontylamine | 16.7 | 1.7 | 2.3 | 0.0 | 576.5 | 6.0597 | 1.8363 |
| (R)-N,N,à-Trimethyl Benzyl Amine | 17.7 | 2.0 | 4.2 | 0.0 | 166.0 | 6.0614 | 1.8368 |
| Ditridecylamine | 16.4 | 1.6 | 2.1 | 0.0 | 466.4 | 6.0836 | 1.8435 |
| Methyl-(2,2,3,3,3-Pentafluoro-Propyl)-Amine | 12.8 | 5.5 | 3.9 | 0.0 | 131.0 | 6.1254 | 1.8562 |
| Didodecylamine | 16.4 | 1.6 | 2.0 | 0.0 | 434.0 | 6.1433 | 1.8616 |
| Ditetradecylamine | 16.4 | 1.5 | 2.1 | 0.0 | 499.7 | 6.1612 | 1.8670 |
| Vinyl Amine | 15.7 | 7.2 | 11.8 | 0.0 | 51.8 | 6.1660 | 1.8685 |
| Dicyclohexylamine | 17.5 | 1.7 | 3.7 | 0.0 | 198.2 | 6.1741 | 1.8709 |
| Dehydroabietylamine | 18.4 | 3.6 | 4.4 | 0.0 | 289.6 | 6.1758 | 1.8715 |
| à-Methylbenzylamine | 18.7 | 4.9 | 6.3 | 0.0 | 125.8 | 6.1903 | 1.8758 |
| Phenethylamine | 18.7 | 4.7 | 6.5 | 0.0 | 126.7 | 6.2610 | 1.8973 |
| N,N-Dimethylpyridin-2-Amine | 18.8 | 5.6 | 6.3 | 0.0 | 122.1 | 6.2682 | 1.8995 |
| N,N-Dimethylbenzyl Amine | 18.1 | 2.6 | 4.0 | 0.0 | 149.4 | 6.2944 | 1.9074 |
| Dimethyl-sec-Butylamine | 13.6 | 1.9 | 4.0 | 0.0 | 138.4 | 6.3159 | 1.9139 |
| Triethylenediamine | 18.3 | 6.0 | 9.3 | 0.0 | 115.5 | 6.3317 | 1.9187 |
| 2,2,3,3,4,4,4-Heptafluoro-Butylamine | 13.1 | 2.8 | 4.2 | 0.0 | 136.4 | 6.4452 | 1.9531 |
| Isopentylidene Isopentyl Amine | 15.5 | 3.2 | 0.0 | 0.0 | 201.0 | 6.5008 | 1.9699 |
| 2,2,3,3,3-Pentafluoro-Propylamine | 12.5 | 5.1 | 5.5 | 0.0 | 110.4 | 6.5146 | 1.9741 |
| n-Aminoethyl Piperazine | 15.6 | 6.9 | 12.2 | 0.0 | 132.2 | 6.5307 | 1.9790 |
| Tripenylamine | 15.8 | 1.3 | 1.5 | 0.0 | 288.7 | 6.5330 | 1.9797 |
| Trihexylamine | 16.0 | 1.2 | 1.6 | 0.0 | 338.6 | 6.5711 | 1.9912 |
| Trinonylamine | 16.3 | 1.2 | 1.4 | 0.0 | 486.3 | 6.7779 | 2.0539 |
| Tributylamine | 15.7 | 1.3 | 1.0 | 0.0 | 240.2 | 6.8622 | 2.0795 |
| Tritetradecylamine | 16.5 | 1.1 | 1.4 | 0.0 | 733.8 | 6.9347 | 2.1014 |
| Trioctylamine | 16.2 | 1.2 | 1.1 | 0.0 | 437.8 | 6.9405 | 2.1032 |
| Tritridecylamine | 16.5 | 1.1 | 1.3 | 0.0 | 683.9 | 6.9971 | 2.1203 |
| n-(1,3-Dimethylbutyl)-N'-Phenyl-Paraphenylenediamine | 18.8 | 3.1 | 6.9 | 0.0 | 262.2 | 7.0795 | 2.1453 |
| Tryptamine | 19.0 | 7.8 | 7.8 | 0.0 | 147.3 | 7.0866 | 2.1475 |

Table B.9 – Summary of the RED values calculated for the collective list of solvents analyzed in the EquiSolv package (continued).

| Solvent Name | δ_D [MPa ^{0.5}] | δ_P [MPa ^{0.5}] | δ_H [MPa ^{0.5}] | δ_I [MPa ^{0.5}] | V_m [cm ³ /mol] | Ra | RED |
|---|----------------------------------|----------------------------------|----------------------------------|----------------------------------|------------------------------|---------|--------|
| Tridodecylamine | 16.5 | 1.1 | 1.1 | 0.0 | 635.4 | 7.1246 | 2.1590 |
| Triundecylamine | 16.3 | 1.7 | 0.3 | 0.0 | 585.2 | 7.1944 | 2.1801 |
| Benzenamine, Ar-Octyl-n-(Octylphenyl)- | 18.1 | 1.8 | 2.7 | 0.0 | 421.6 | 7.2312 | 2.1913 |
| 4-Octylbenzenamine | 17.9 | 2.2 | 1.6 | 0.0 | 226.8 | 7.2787 | 2.2057 |
| Benzenamine, N,N,3-Timethyl- | 18.6 | 2.6 | 3.3 | 0.0 | 145.1 | 7.2863 | 2.2080 |
| Benzhydrlamine | 19.1 | 3.5 | 5.9 | 0.0 | 172.0 | 7.3566 | 2.2293 |
| Chlorpheniramine | 19.1 | 3.3 | 6.4 | 0.0 | 249.6 | 7.4653 | 2.2622 |
| 4-Chlorobenzylamine | 19.4 | 6.2 | 6.7 | 0.0 | 122.7 | 7.4679 | 2.2630 |
| Triethylamine | 15.5 | 0.4 | 1.0 | 0.0 | 139.7 | 7.5538 | 2.2890 |
| Bromopheniramine | 19.3 | 4.0 | 5.5 | 0.0 | 251.1 | 7.5611 | 2.2912 |
| 1,3,5-Triazine-2,4,6-Triamine, N,N,N,N,N,N -Hexakis(Methoxy | 17.6 | 9.7 | 11.4 | 0.0 | 331.1 | 7.6479 | 2.3175 |
| 1,4-Butanediamine | 16.6 | 11.3 | 11.3 | 0.0 | 102.6 | 7.7201 | 2.3394 |
| Imipramine | 19.5 | 5.6 | 4.4 | 0.0 | 269.2 | 7.7421 | 2.3461 |
| Benzyl Amine | 19.0 | 4.6 | 9.4 | 0.0 | 109.2 | 7.7550 | 2.3500 |
| 1-Naphthalenamine, N,N-Dimethyl- | 19.3 | 3.0 | 4.7 | 0.0 | 163.9 | 7.9831 | 2.4191 |
| Desipramine | 19.7 | 6.3 | 5.1 | 0.0 | 250.4 | 8.0225 | 2.4311 |
| Dibenzylamine | 19.4 | 3.0 | 4.7 | 0.0 | 192.1 | 8.1639 | 2.4739 |
| 1-Naphthalenamine, N-Ethyl- | 19.4 | 2.8 | 6.6 | 0.0 | 162.4 | 8.2353 | 2.4955 |
| Pentaethylene Hexamine | 16.6 | 5.3 | 13.7 | 0.0 | 235.8 | 8.2608 | 2.5033 |
| Auramine | 19.6 | 8.7 | 3.9 | 0.0 | 242.1 | 8.3570 | 2.5324 |
| Cysteamine | 17.1 | 8.6 | 13.3 | 0.0 | 78.4 | 8.4196 | 2.5514 |
| Tetraethylenepentamine | 16.5 | 5.7 | 14.0 | 0.0 | 194.2 | 8.4741 | 2.5679 |
| N,N-Diphenylethylamine | 19.6 | 3.2 | 3.8 | 0.0 | 191.4 | 8.6058 | 2.6078 |
| 2,4-Dichlorobenzylamine | 19.9 | 7.5 | 7.4 | 0.0 | 134.6 | 8.6539 | 2.6224 |
| Dimethyl Ethanolamine (DMEA) | 16.1 | 9.2 | 14.0 | 0.0 | 101.1 | 8.8284 | 2.6753 |
| Triethylene Tetramine | 16.5 | 6.3 | 14.4 | 0.0 | 152.7 | 8.8459 | 2.6806 |
| Diethylenetriamine | 16.7 | 7.1 | 14.3 | 0.0 | 108.1 | 8.8657 | 2.6866 |
| Ethyl Carbylamine | 15.6 | 15.2 | 5.8 | 0.0 | 74.4 | 8.9028 | 2.6978 |
| Histamine | 18.2 | 7.4 | 13.0 | 0.0 | 104.4 | 8.9163 | 2.7019 |
| Diphenylamine | 20.0 | 3.3 | 5.9 | 0.0 | 159.7 | 9.1104 | 2.7607 |
| N-Methyldiphenylamine | 20.0 | 3.3 | 3.9 | 0.0 | 174.7 | 9.2844 | 2.8135 |
| Methyl-1-Naphthylamine | 19.8 | 2.0 | 4.5 | 0.0 | 145.7 | 9.3365 | 2.8292 |
| 4,6-Dimethylpyrimidinamine | 18.9 | 11.3 | 10.4 | 0.0 | 114.5 | 9.3835 | 2.8435 |
| Dinitramine | 19.9 | 10.5 | 4.6 | 0.0 | 229.1 | 9.4557 | 2.8654 |
| Di-p-Tolylamine | 20.1 | 4.5 | 2.7 | 0.0 | 188.3 | 9.4700 | 2.8697 |
| N-Methylpyridinamine | 19.4 | 7.1 | 11.6 | 0.0 | 103.9 | 9.4979 | 2.8782 |
| Tribenzylamine | 19.9 | 2.2 | 3.7 | 0.0 | 272.4 | 9.5588 | 2.8966 |
| 1-Isoquinolinamine | 20.1 | 7.6 | 9.5 | 0.0 | 124.1 | 9.6732 | 2.9313 |
| 3-Quinolinamine | 20.1 | 7.6 | 9.5 | 0.0 | 124.1 | 9.6732 | 2.9313 |
| Benzenamine, 2,3,4-Trichloro- | 20.5 | 7.2 | 8.3 | 0.0 | 130.4 | 9.9865 | 3.0262 |
| Benzenamine, n-Nitroso-n-Phenyl- | 20.3 | 9.8 | 3.9 | 0.0 | 165.7 | 10.0065 | 3.0323 |
| Methylethanolamine | 16.0 | 5.4 | 15.7 | 0.0 | 83.6 | 10.0583 | 3.0480 |
| Perfluorotripropylamine | 12.2 | 1.0 | 0.7 | 0.0 | 303.2 | 10.1040 | 3.0618 |
| 1-Naphthylamine | 20.3 | 3.6 | 8.9 | 0.0 | 128.8 | 10.1079 | 3.0630 |
| 2-Naphthylamine | 20.3 | 3.6 | 8.9 | 0.0 | 128.8 | 10.1079 | 3.0630 |
| Perfluorotributylamine | 12.8 | 0.0 | 0.3 | 0.0 | 381.3 | 10.1237 | 3.0678 |
| 1,3-Propanediamine | 16.1 | 9.4 | 15.4 | 0.0 | 85.9 | 10.2147 | 3.0954 |
| 2-Methoxy-5-Methylbenzenamine | 19.7 | 5.9 | 12.3 | 0.0 | 130.7 | 10.3788 | 3.1451 |
| p-Phenylenediamine | 20.7 | 6.6 | 8.9 | 0.0 | 98.9 | 10.5038 | 3.1830 |
| Methyl Amine | 14.4 | 7.0 | 16.0 | 0.0 | 44.7 | 10.6461 | 3.2261 |
| Glycocamine | 16.7 | 16.2 | 9.3 | 0.0 | 85.7 | 10.7224 | 3.2492 |
| o-Nitrodiphenylamine | 20.9 | 9.1 | 6.4 | 0.0 | 172.5 | 10.7931 | 3.2706 |
| 1-Naphthalenamine, n-Phenyl- | 20.8 | 2.7 | 6.1 | 0.0 | 191.0 | 10.8240 | 3.2800 |
| n-Phenyl-2-Naphthylamine | 20.8 | 2.7 | 6.1 | 0.0 | 191.0 | 10.8240 | 3.2800 |
| Tyramine | 18.7 | 6.9 | 14.7 | 0.0 | 129.1 | 10.8333 | 3.2828 |
| 4,4'-Dinitrodiphenylamine | 21.0 | 8.4 | 6.5 | 0.0 | 188.9 | 10.8356 | 3.2835 |
| Tris-Pentafluoroethyl-Amine | 11.0 | 2.9 | 1.4 | 0.0 | 225.1 | 10.8816 | 3.2975 |
| Triphenylamine | 20.8 | 3.0 | 3.7 | 0.0 | 220.0 | 10.9055 | 3.3047 |
| p-Nitrodiphenylamine | 21.0 | 8.9 | 6.3 | 0.0 | 172.7 | 10.9307 | 3.3123 |
| p-Aminodiphenylamine | 21.1 | 4.8 | 7.8 | 0.0 | 161.0 | 11.1041 | 3.3649 |
| Benzenamine, 4,4'-Methylenebis- | 20.9 | 4.6 | 2.1 | 0.0 | 176.3 | 11.1360 | 3.3745 |
| 1,2-Propanediamine | 12.8 | 7.5 | 15.2 | 0.0 | 85.6 | 11.1951 | 3.3925 |

Table B.10 – Summary of the RED values calculated for the collective list of solvents analyzed in the EquiSolv package (continued).

| Solvent Name | δ_D [MPa ^{0.5}] | δ_P [MPa ^{0.5}] | δ_H [MPa ^{0.5}] | δ_I [MPa ^{0.5}] | V_m [cm ³ /mol] | Ra | RED |
|---|----------------------------------|----------------------------------|----------------------------------|----------------------------------|------------------------------|---------|---------|
| Toluene-2,5-Diamine (2,5-Diaminotoluene) | 20.5 | 5.3 | 11.5 | 0.0 | 114.0 | 11.2606 | 3.4123 |
| Benzenamine, 4-Methyl-3-Nitro- | 20.5 | 11.0 | 9.3 | 0.0 | 125.7 | 11.2787 | 3.4178 |
| Benzenamine, 2-Methyl-5-Nitro- | 20.5 | 11.0 | 9.3 | 0.0 | 125.7 | 11.2787 | 3.4178 |
| Benzenamine, 4-Methyl-2-Nitro- | 20.5 | 11.0 | 9.3 | 0.0 | 125.7 | 11.2787 | 3.4178 |
| Benzenamine, 2-Methyl-4-Nitro- | 20.5 | 11.0 | 9.3 | 0.0 | 125.7 | 11.2787 | 3.4178 |
| Benzenamine, 3-Methyl-4-Nitro- | 20.5 | 11.0 | 9.3 | 0.0 | 125.7 | 11.2787 | 3.4178 |
| N-(2-Hydroxyethyl)Piperazine | 15.7 | 7.7 | 16.9 | 0.0 | 125.6 | 11.2872 | 3.4204 |
| N,N'-Diphenyl-p-Phenylenediamine | 21.2 | 3.7 | 7.3 | 0.0 | 223.2 | 11.4158 | 3.4593 |
| 3-Pyridinamine | 20.1 | 9.1 | 12.8 | 0.0 | 87.1 | 11.6486 | 3.5299 |
| Ethylenediamine | 16.6 | 8.8 | 17.0 | 0.0 | 67.3 | 11.7124 | 3.5492 |
| 2,5-Dichloro-1,4-Benzenediamine | 21.0 | 6.4 | 10.9 | 0.0 | 122.3 | 11.8072 | 3.5779 |
| 3-Hydroxydiphenylamine | 20.6 | 4.9 | 12.5 | 0.0 | 158.7 | 12.0100 | 3.6394 |
| Hexamethylenetetramine | 19.4 | 7.0 | 16.0 | 0.0 | 105.3 | 12.7020 | 3.8491 |
| n-Aminoethyl Ethanolamine | 16.6 | 6.6 | 18.3 | 0.0 | 104.6 | 12.7315 | 3.8580 |
| Benzenamine, 4-Methoxy-2-Nitro- | 20.6 | 11.7 | 12.4 | 0.0 | 131.0 | 13.0419 | 3.9521 |
| 1,8-Naphthalenediamine | 19.7 | 3.7 | 15.9 | 0.0 | 136.3 | 13.2212 | 4.0064 |
| Toluene Diamine (2,6-Toluene Diamine) | 20.5 | 6.4 | 14.8 | 0.0 | 114.0 | 13.2280 | 4.0085 |
| Toluenediamine | 20.5 | 6.4 | 14.8 | 0.0 | 114.0 | 13.2280 | 4.0085 |
| 1H-Indol-5-Amine | 21.3 | 8.6 | 12.8 | 0.0 | 113.5 | 13.4588 | 4.0784 |
| 4-Methoxy-M-Phenylenediamine | 20.7 | 6.7 | 14.8 | 0.0 | 119.3 | 13.5266 | 4.0990 |
| Diethanolamine (DEA) | 17.2 | 7.0 | 19.0 | 0.0 | 96.2 | 13.6521 | 4.1370 |
| Benzenamine, 2,4,6-Tribromo- | 21.7 | 9.4 | 11.6 | 0.0 | 134.9 | 13.7266 | 4.1596 |
| Laevo-Glutamine | 16.4 | 12.6 | 18.0 | 0.0 | 114.6 | 13.8903 | 4.2092 |
| Methyl Diethanolamine | 16.8 | 7.4 | 19.4 | 0.0 | 116.9 | 13.9191 | 4.2179 |
| 1-Octyl-3-methylimidazolium hexafluorophosphate | 20.0 | 16.5 | 10.0 | 40.9 | 276.0 | 14.0175 | 4.2477 |
| o-Phenylenediamine | 20.5 | 7.0 | 16.3 | 0.0 | 98.7 | 14.3182 | 4.3388 |
| m-Phenylenediamine | 20.8 | 5.4 | 15.8 | 0.0 | 98.7 | 14.3826 | 4.3584 |
| 4-Chloro-M-Phenylenediamine | 21.1 | 8.2 | 15.8 | 0.0 | 110.7 | 14.9084 | 4.5177 |
| Dopamine | 18.2 | 10.3 | 19.5 | 0.0 | 180.0 | 15.2132 | 4.6101 |
| Ethylenediaminetetraacetic Acid | 17.4 | 7.7 | 20.7 | 0.0 | 207.5 | 15.4441 | 4.6800 |
| Triethanolamine (TEA) | 17.3 | 7.6 | 21.0 | 0.0 | 133.0 | 15.6850 | 4.7530 |
| 1-Butyl-3-methylimidazolium hexafluorophosphate | 21.0 | 17.2 | 10.9 | 47.2 | 207.6 | 16.0689 | 4.8694 |
| 2,5-Pyridinediamine | 20.4 | 10.4 | 18.1 | 0.0 | 92.5 | 16.0913 | 4.8762 |
| Benzenamine, 2,3,4,5-Tetrachloro- | 22.9 | 13.9 | 6.7 | 0.0 | 141.6 | 16.3132 | 4.9434 |
| 2-Pyrimidinamine | 20.6 | 14.5 | 16.8 | 0.0 | 80.9 | 16.9260 | 5.1291 |
| Dimethyl Ethanolamine/Methacrylic Acid | 17.2 | 18.8 | 17.6 | 0.0 | 999.0 | 17.5174 | 5.3083 |
| N,N-Diethylhydroxylamine | 15.5 | 1.1 | 22.6 | 0.0 | 103.6 | 17.6864 | 5.3595 |
| Ethanolamine (MEA) | 17.0 | 15.5 | 21.0 | 0.0 | 60.3 | 18.0413 | 5.4671 |
| Dimethyl Isopropanol Amine/Acetic Acid | 16.6 | 19.4 | 18.0 | 0.0 | 999.0 | 18.0593 | 5.4725 |
| 5-Nitropyrimidinamine | 20.9 | 19.1 | 14.2 | 0.0 | 98.0 | 18.5540 | 5.6224 |
| n-Butyl Amine/Acetic Acid | 16.0 | 20.3 | 18.4 | 0.0 | 999.0 | 18.9116 | 5.7308 |
| Diethyl Amine/Acetic Acid | 16.0 | 20.3 | 18.4 | 0.0 | 999.0 | 18.9116 | 5.7308 |
| Diethyl Ethanolamine/Acetic Acid | 16.0 | 20.3 | 18.4 | 0.0 | 999.0 | 18.9116 | 5.7308 |
| Ethanolamine/Acetic Acid | 17.2 | 20.3 | 18.4 | 0.0 | 999.0 | 19.1387 | 5.7996 |
| Triethanolamine/Acetic Acid | 17.2 | 20.3 | 18.4 | 0.0 | 999.0 | 19.1387 | 5.7996 |
| Dimethyl Ethanolamine/Acetic Acid | 16.8 | 19.8 | 19.8 | 0.0 | 999.0 | 19.6443 | 5.9528 |
| 1-Butyl-3-methylimidazolium tetrafluoroborate | 23.0 | 19.0 | 10.0 | 46.3 | 201.4 | 19.8227 | 6.0069 |
| Diisopropanolamine | 16.0 | 19.2 | 21.2 | 0.0 | 131.8 | 20.1747 | 6.1135 |
| 2-Thiazolamine | 20.2 | 19.0 | 18.6 | 0.0 | 78.3 | 20.2163 | 6.1262 |
| O,n-Dimethylhydroxylamine | 14.5 | 0.9 | 25.4 | 0.0 | 81.1 | 20.5672 | 6.2325 |
| 1-Butyl-3-methylimidazolium chloride | 19.1 | 20.7 | 20.7 | 48.6 | 175.0 | 21.8769 | 6.6294 |
| 1H-1,2,4-Triazol-3-Amine | 20.0 | 9.5 | 25.7 | 0.0 | 65.8 | 22.0045 | 6.6680 |
| Dimethyl Ethanolamine/p-Toluene Sulfonic Acid | 17.2 | 21.5 | 22.5 | 0.0 | 999.0 | 22.8534 | 6.9253 |
| Dimethyl Ethanolamine/Thioglycolic Acid | 17.2 | 21.5 | 22.5 | 0.0 | 999.0 | 22.8534 | 6.9253 |
| Dimethyl Ethanolamine/Formic Acid | 17.2 | 21.5 | 22.5 | 0.0 | 999.0 | 22.8534 | 6.9253 |
| 3-Methoxypropyl Amine/Acetic Acid | 17.2 | 22.5 | 23.5 | 0.0 | 999.0 | 24.2545 | 7.3498 |
| Lactoyl Ethanolamine | 17.8 | 18.3 | 30.4 | 0.0 | 107.8 | 27.7800 | 8.4182 |
| Melamine | 21.8 | 20.3 | 31.7 | 0.0 | 85.6 | 31.9506 | 9.6820 |
| Lactoyl Ethanolamine Phosphate | 18.4 | 26.0 | 33.5 | 0.0 | 140.2 | 34.4977 | 10.4538 |
| Water | 15.5 | 16.0 | 42.3 | 0.0 | 18.0 | 37.8657 | 11.4745 |
| Gluconyl Ethanolamine | 18.2 | 18.1 | 45.0 | 0.0 | 151.3 | 41.3368 | 12.5263 |
| Gluconyl Ethanolamine Phosphate | 18.8 | 24.1 | 46.8 | 0.0 | 183.7 | 45.2160 | 13.7018 |

Table B.11 – Summary of the blend formulations randomly selected from the solvent optimizer predictions (with the six blend formulations selected for synthesis highlighted in red).

| Solvent Constituent 1 | Solvent Constituent 2 | x ₁ [vol%] | x ₂ [vol%] | x _{tot} [vol%] | x ₁ [*] [vol%] | x ₂ [*] [vol%] | x _{tot} [*] [vol%] | δ _D [MPa ^{0.5}] | δ _P [MPa ^{0.5}] | δ _H [MPa ^{0.5}] | RED |
|------------------------------------|-----------------------------------|-----------------------|-----------------------|-------------------------|------------------------------------|------------------------------------|--------------------------------------|--------------------------------------|--------------------------------------|--------------------------------------|--------|
| Di-p-Tolylamine | Dimethyl Ethanolamine/Acetic Acid | 0.5597 | 0.0723 | 0.632 | 0.8856 | 0.1144 | 1 | 15.7 | 6.3 | 5.69 | 0.0019 |
| Diethylhexadecylamine | Glycocylamine | 0.7781 | 0.1427 | 0.9208 | 0.845 | 0.155 | 1 | 15.7 | 6.3 | 5.71 | 0.0025 |
| Imipramine | Dimethyl Ethanolamine/Acetic Acid | 0.6094 | 0.0525 | 0.6619 | 0.9207 | 0.0793 | 1 | 15.7 | 6.3 | 5.69 | 0.0031 |
| Triundecylamine | 4,6-Dimethylpyrimidinamine | 0.5261 | 0.2989 | 0.825 | 0.6377 | 0.3623 | 1 | 15.7 | 6.3 | 5.69 | 0.0032 |
| Pentadecylamine | Benzenamine, 4-Methyl-3-Nitro- | 0.4641 | 0.2935 | 0.7576 | 0.6126 | 0.3874 | 1 | 15.71 | 6.3 | 5.7 | 0.0033 |
| Pentadecylamine | Benzenamine, 2-Methyl-5-Nitro- | 0.4641 | 0.2935 | 0.7576 | 0.6126 | 0.3874 | 1 | 15.71 | 6.3 | 5.7 | 0.0033 |
| Pentadecylamine | Benzenamine, 4-Methyl-2-Nitro- | 0.4641 | 0.2935 | 0.7576 | 0.6126 | 0.3874 | 1 | 15.71 | 6.3 | 5.7 | 0.0033 |
| Pentadecylamine | Benzenamine, 2-Methyl-4-Nitro- | 0.4641 | 0.2935 | 0.7576 | 0.6126 | 0.3874 | 1 | 15.71 | 6.3 | 5.7 | 0.0033 |
| Pentadecylamine | Benzenamine, 3-Methyl-4-Nitro- | 0.4641 | 0.2935 | 0.7576 | 0.6126 | 0.3874 | 1 | 15.71 | 6.3 | 5.7 | 0.0033 |
| Methyl-Tert-Butylamine | Ethyl Carbylamine | 0.9663 | 0.1316 | 1.0979 | 0.8801 | 0.1199 | 1 | 15.7 | 6.3 | 5.71 | 0.0033 |
| Trioctylamine | n-Butyl Amine/Acetic Acid | 0.8482 | 0.0933 | 0.9415 | 0.9009 | 0.0991 | 1 | 15.7 | 6.3 | 5.71 | 0.0033 |
| Trioctylamine | Diethyl Amine/Acetic Acid | 0.8482 | 0.0933 | 0.9415 | 0.9009 | 0.0991 | 1 | 15.7 | 6.3 | 5.71 | 0.0033 |
| Trioctylamine | Diethyl Ethanolamine/Acetic Acid | 0.8482 | 0.0933 | 0.9415 | 0.9009 | 0.0991 | 1 | 15.7 | 6.3 | 5.71 | 0.0033 |
| N,N-Dimethylbenzyl Amine | Benzenamine, 4-Methyl-3-Nitro- | 0.3574 | 0.308 | 0.6654 | 0.5371 | 0.4629 | 1 | 15.7 | 6.3 | 5.69 | 0.0036 |
| N,N-Dimethylbenzyl Amine | Benzenamine, 2-Methyl-5-Nitro- | 0.3574 | 0.308 | 0.6654 | 0.5371 | 0.4629 | 1 | 15.7 | 6.3 | 5.69 | 0.0036 |
| N,N-Dimethylbenzyl Amine | Benzenamine, 4-Methyl-2-Nitro- | 0.3574 | 0.308 | 0.6654 | 0.5371 | 0.4629 | 1 | 15.7 | 6.3 | 5.69 | 0.0036 |
| N,N-Dimethylbenzyl Amine | Benzenamine, 2-Methyl-4-Nitro- | 0.3574 | 0.308 | 0.6654 | 0.5371 | 0.4629 | 1 | 15.7 | 6.3 | 5.69 | 0.0036 |
| N,N-Dimethylbenzyl Amine | Benzenamine, 3-Methyl-4-Nitro- | 0.3574 | 0.308 | 0.6654 | 0.5371 | 0.4629 | 1 | 15.7 | 6.3 | 5.69 | 0.0036 |
| Trioctylamine | Ethanolamine/Acetic Acid | 0.8339 | 0.0934 | 0.9273 | 0.8993 | 0.1007 | 1 | 15.7 | 6.3 | 5.71 | 0.0037 |
| Trioctylamine | Triethanolamine/Acetic Acid | 0.8339 | 0.0934 | 0.9273 | 0.8993 | 0.1007 | 1 | 15.7 | 6.3 | 5.71 | 0.0037 |
| Isopentylidene Isopentyl Amine | 3-Methoxypropyl Amine/Acetic Acid | 0.9532 | 0.0591 | 1.0123 | 0.9416 | 0.0584 | 1 | 15.7 | 6.3 | 5.71 | 0.0039 |
| Tripropylamine | Benzenamine, 4-Methyl-3-Nitro- | 0.5008 | 0.2932 | 0.794 | 0.6307 | 0.3693 | 1 | 15.71 | 6.3 | 5.71 | 0.0042 |
| Tripropylamine | Benzenamine, 2-Methyl-5-Nitro- | 0.5008 | 0.2932 | 0.794 | 0.6307 | 0.3693 | 1 | 15.71 | 6.3 | 5.71 | 0.0042 |
| | | | | | | | | | | | |
| 1-Phenylethyl Amine | p-Nitrodiphenylamine | 0.1296 | 0.4722 | 0.6018 | 0.2154 | 0.7846 | 1 | 15.72 | 6.3 | 4.99 | 0.215 |
| Methylpentylamine | n-Nitrosodimethylamine | 0.787 | 0.2472 | 1.0342 | 0.761 | 0.239 | 1 | 15.71 | 6.3 | 4.99 | 0.2151 |
| Piperazine (PZ) | o-Nitrodiphenylamine | 0.2157 | 0.4193 | 0.635 | 0.3397 | 0.6603 | 1 | 15.74 | 6.3 | 4.99 | 0.2152 |
| p-Nitrodiphenylamine | Lactoyl Ethanolamine Phosphate | 0.5542 | 0.0062 | 0.5604 | 0.9889 | 0.0111 | 1 | 15.7 | 6.93 | 5.38 | 0.2153 |
| Bis-(2,2,2-Trifluoro-Ethyl)-Amine | 1,2-Propanediamine | 1.1887 | 0.0199 | 1.2086 | 0.9835 | 0.0165 | 1 | 15.8 | 6.52 | 5.06 | 0.2154 |
| Diocetylamine | 5-Nitropyrimidinamine | 0.7807 | 0.1011 | 0.8818 | 0.8853 | 0.1147 | 1 | 15.7 | 6.3 | 4.99 | 0.2157 |
| 2-Ethylhexyl Amine | p-Nitrodiphenylamine | 0.1754 | 0.462 | 0.6374 | 0.2752 | 0.7248 | 1 | 15.72 | 6.3 | 4.99 | 0.2165 |
| Ethyl-Tert-Butylamine | Benzenamine, 2,3,4,5-Tetrachloro- | 0.6735 | 0.1928 | 0.8663 | 0.7774 | 0.2226 | 1 | 15.7 | 6.3 | 4.98 | 0.2174 |
| sec-Butylamine | Auramine | 0.3345 | 0.4309 | 0.7654 | 0.437 | 0.563 | 1 | 15.75 | 6.3 | 4.99 | 0.2179 |
| (+)-sec-Butylamine | Auramine | 0.3345 | 0.4309 | 0.7654 | 0.437 | 0.563 | 1 | 15.75 | 6.3 | 4.99 | 0.2179 |
| Cyclopentylamine | p-Nitrodiphenylamine | 0.1604 | 0.4544 | 0.6148 | 0.2609 | 0.7391 | 1 | 15.73 | 6.3 | 4.98 | 0.2184 |
| 4,4'-Dinitrodiphenylamine | Tryptamine | 0.5261 | 0.0422 | 0.5683 | 0.9257 | 0.0743 | 1 | 15.72 | 6.3 | 4.98 | 0.2188 |
| Trimethyl Amine | 2,2,3,3,3-Pentafluoro-Propylamine | 0.4145 | 1.012 | 1.4265 | 0.2906 | 0.7094 | 1 | 15.7 | 5.58 | 5.65 | 0.2193 |
| 4,4'-Dinitrodiphenylamine | Cyclopropylamine | 0.545 | 0.0208 | 0.5658 | 0.9632 | 0.0368 | 1 | 15.71 | 6.3 | 4.97 | 0.2198 |
| Isopentylidene Isopentyl Amine | Ethanolamine/Acetic Acid | 0.9361 | 0.0731 | 1.0092 | 0.9276 | 0.0724 | 1 | 15.7 | 6.3 | 4.97 | 0.2198 |
| Isopentylidene Isopentyl Amine | Triethanolamine/Acetic Acid | 0.9361 | 0.0731 | 1.0092 | 0.9276 | 0.0724 | 1 | 15.7 | 6.3 | 4.97 | 0.2198 |
| 4,4'-Dinitrodiphenylamine | 1,3-Propanediamine | 0.5559 | 0.0053 | 0.5612 | 0.9906 | 0.0094 | 1 | 15.7 | 6.3 | 4.97 | 0.2199 |
| p-Nitrodiphenylamine | 2,5-Dichloro-1,4-Benzenediamine | 0.5206 | 0.0378 | 0.5584 | 0.9323 | 0.0677 | 1 | 15.69 | 6.54 | 5.02 | 0.22 |
| Propylisopropylamine | Benzenamine, 2,3,4,5-Tetrachloro- | 0.6894 | 0.1666 | 0.856 | 0.8054 | 0.1946 | 1 | 15.7 | 6.3 | 4.97 | 0.2208 |
| Ethylisopropylamine | o-Nitrodiphenylamine | 0.2201 | 0.4521 | 0.6722 | 0.3274 | 0.6726 | 1 | 15.72 | 6.3 | 4.97 | 0.2214 |
| 4,4'-Dinitrodiphenylamine | Gluconyl Ethanolamine Phosphate | 0.5585 | 0.0005 | 0.559 | 0.9991 | 0.0009 | 1 | 15.7 | 6.3 | 4.97 | 0.2215 |
| 2,2-Dimethylpropylamine | Benzenamine, n-Nitroso-n-Phenyl- | 0.4257 | 0.3679 | 0.7936 | 0.5364 | 0.4636 | 1 | 15.73 | 6.3 | 4.97 | 0.2218 |
| 2-Popen-1-Amine, N,N-Di-2-Popenyl- | o-Nitrodiphenylamine | 0.1877 | 0.4589 | 0.6466 | 0.2903 | 0.7097 | 1 | 15.71 | 6.3 | 4.97 | 0.2218 |
| Phenethylamine | o-Nitrodiphenylamine | 0.1615 | 0.4362 | 0.5977 | 0.2702 | 0.7298 | 1 | 15.72 | 6.3 | 4.97 | 0.2218 |
| Methylpentylamine | Perfluor-Tert-Buthylamine | 0.454 | 0.721 | 1.175 | 0.3864 | 0.6136 | 1 | 15.72 | 6.3 | 4.97 | 0.222 |
| Imipramine | 1,1-Dimethylpropylamine | 0.1102 | 0.8973 | 1.0075 | 0.1094 | 0.8906 | 1 | 15.7 | 5.8 | 6.24 | 0.2221 |
| Ethylpropylamine | o-Nitrodiphenylamine | 0.2452 | 0.4343 | 0.6795 | 0.3609 | 0.6391 | 1 | 15.72 | 6.3 | 4.97 | 0.2223 |
| 1-Ethylpropylamine | o-Nitrodiphenylamine | 0.2452 | 0.4343 | 0.6795 | 0.3609 | 0.6391 | 1 | 15.72 | 6.3 | 4.97 | 0.2223 |
| Nonacosylamine | 5-Nitropyrimidinamine | 0.7247 | 0.1016 | 0.8263 | 0.877 | 0.123 | 1 | 15.7 | 6.3 | 4.97 | 0.2224 |
| Tryptamine | Diisobutylamine | 0.5006 | 0.2962 | 0.7968 | 0.6283 | 0.3717 | 1 | 15.7 | 5.68 | 6.11 | 0.2235 |
| Isopentylidene Isopentyl Amine | n-Butyl Amine/Acetic Acid | 0.9485 | 0.0727 | 1.0212 | 0.9288 | 0.0712 | 1 | 15.7 | 6.3 | 4.96 | 0.2239 |
| Isopentylidene Isopentyl Amine | Diethyl Amine/Acetic Acid | 0.9485 | 0.0727 | 1.0212 | 0.9288 | 0.0712 | 1 | 15.7 | 6.3 | 4.96 | 0.2239 |
| Isopentylidene Isopentyl Amine | Diethyl Ethanolamine/Acetic Acid | 0.9485 | 0.0727 | 1.0212 | 0.9288 | 0.0712 | 1 | 15.7 | 6.3 | 4.96 | 0.2239 |
| | | | | | | | | | | | |
| Auramine | Hexylamine | 0.2813 | 0.5545 | 0.8358 | 0.3366 | 0.6634 | 1 | 15.7 | 5.49 | 4.99 | 0.3257 |
| | | | | | | | | | | | |
| | | | | | | | | | | | |
| à-Methylbenzylamine | 2,4-Dichlorobenzylamine | 0.0644 | 0.6781 | 0.7425 | 0.0867 | 0.9133 | 1 | 17.06 | 6.3 | 6.3 | 0.8442 |
| N,N'-Dimethylpiperazine | 2,4-Dichlorobenzylamine | 0.0793 | 0.6783 | 0.7576 | 0.1047 | 0.8953 | 1 | 17.07 | 6.3 | 6.28 | 0.8467 |
| Bornylamine | 2,4-Dichlorobenzylamine | 0.0786 | 0.6798 | 0.7584 | 0.1036 | 0.8964 | 1 | 17.08 | 6.3 | 6.25 | 0.8518 |
| Ethylpropylamine | 2,4-Dichlorobenzylamine | 0.0957 | 0.6797 | 0.7754 | 0.1234 | 0.8766 | 1 | 17.08 | 6.3 | 6.32 | 0.8543 |
| 1-Ethylpropylamine | 2,4-Dichlorobenzylamine | 0.0957 | 0.6797 | 0.7754 | 0.1234 | 0.8766 | 1 | 17.08 | 6.3 | 6.32 | 0.8543 |
| Hexylamine | 2,4-Dichlorobenzylamine | 0.0902 | 0.6799 | 0.7701 | 0.1171 | 0.8829 | 1 | 17.08 | 6.3 | 6.37 | 0.8614 |
| Phenethylamine | 2,4-Dichlorobenzylamine | 0.0647 | 0.6802 | 0.7449 | 0.0869 | 0.9131 | 1 | 17.09 | 6.3 | 6.32 | 0.862 |
| Amphetamine | 2,4-Dichlorobenzylamine | 0.0764 | 0.6805 | 0.7569 | 0.1009 | 0.8991 | 1 | 17.11 | 6.3 | 6.35 | 0.8791 |
| Octylamine | 2,4-Dichlorobenzylamine | 0.0908 | 0.681 | 0.7718 | 0.1176 | 0.8824 | 1 | 17.12 | 6.3 | 6.28 | 0.8803 |

Appendix C: Experimental Procedure

The experimental procedure consists of seven primary steps:

- C.1. Absorbent sample preparation;
- C.2. Preparing the experimental environment;
- C.3. Setting experimental conditions;
- C.4. Performing an experimental run;
- C.5. Experimental data acquisition;
- C.6. Equilibrium absorbent sampling for GC analysis;
- C.7. System cleanup and preparation for the next experimental run.

Each of the primary experimental procedure steps is discussed below with reference to Figure C.1.

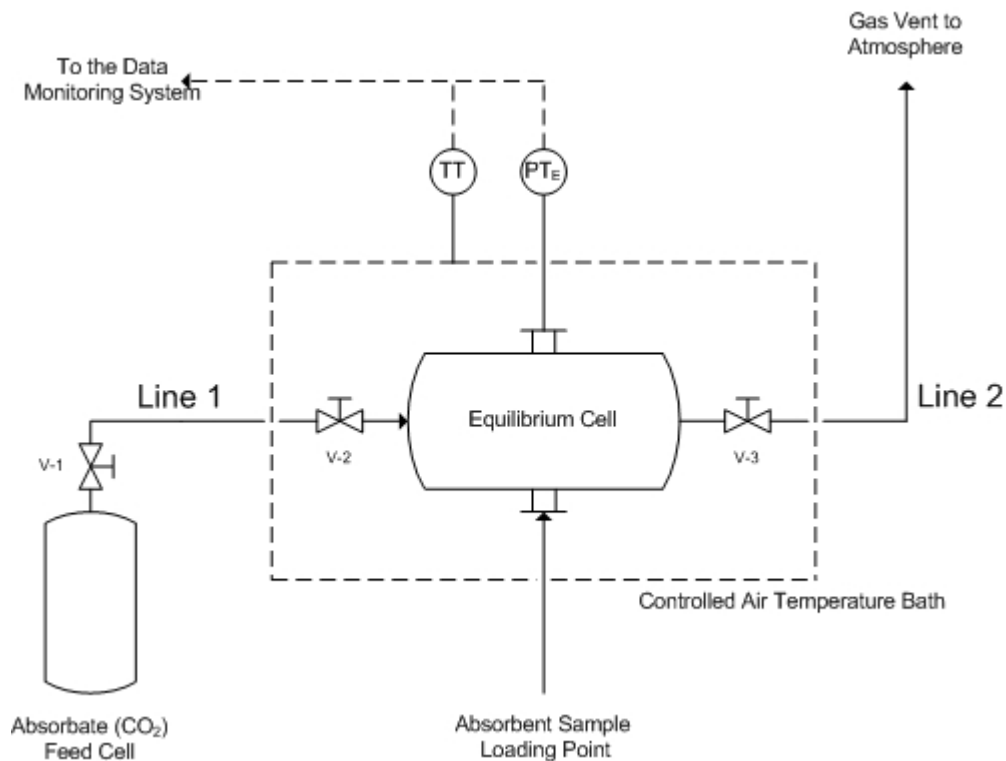


Figure C.1 – Schematic of the experimental setup design.

C.1. Absorbent Sample Preparation

- C.1.1. A total sample volume of 30ml is prepared for each absorbent sample considered;
- C.1.2. Each absorbent sample is prepared 24h prior to the considered experimental run;
- C.1.3. Mix the individual components together in the required ratio, i.e. the specified weight or volume percentages;
- C.1.4. Stir the contents of the sample vial using a vortex machine for a few seconds;
- C.1.5. Store the prepared sample in a refrigerator.

C.2. Preparing the Experimental Environment

- C.2.1. Reset the data monitoring system (DMS);
- C.2.2. Connect the CO₂ cylinder feed line (Line 1) to the experimental setup via the connection point at valve V-2;
- C.2.3. Ensure that valves V-2 and V-3 are open;
- C.2.4. Ensure that the CO₂ vent line (Line 2) is properly connected to the experimental setup via the connection point at valve V-3, and that the vent line is open to the atmosphere;
- C.2.5. Slowly open the CO₂ feed cylinder valve (V-1) by a small amount and check that the CO₂ is flowing through the system and out at the vent line (Line 2);
- C.2.6. Allow the CO₂ to flow through the system for approximately 5min to remove any air from the system. This is to create a pure CO₂ atmosphere in the equilibrium cell;
- C.2.7. After the 5min period, simultaneously close-off valves V-1 and V-3 to retain the created CO₂ atmosphere in the system. Once the valves are closed, close-off valve V-2 to create an isolated CO₂ atmosphere within the equilibrium cell;
- C.2.8. Check that the data monitoring system is giving a stable reading for the equilibrium cell pressure transmitter (PT_E). The pressure reading should stabilize around atmospheric pressure. If the pressure reading is not equal to atmospheric pressure use either the CO₂ feed (V-2) or vent (V-3) to increase or decrease the system pressure respectively.

C.3. Setting the Experimental Conditions

The experimental conditions must be set approximately 30 minutes before commencing with an experimental run (section C.4). This is to allow the operating conditions to reach and attain a state of equilibrium at the specified set points.

- C.3.1. Adjust the set point of the temperature transmitter on the data monitoring system to the desired value;
- C.3.2. Ensure that the pressure transmitter data log is cleared on the data monitoring system.

C.4. Performing an Experimental Run

- C.4.1. Start the DMS recording procedure;
- C.4.2. Draw a 5ml sample of the prepared absorbent sample using the gas-tight Hamilton syringe;
- C.4.3. Insert the needle of the syringe through the absorbent sample loading point and inject the entire 5ml sample into the equilibrium cell;
- C.4.4. Allow a 2h period of time for the CO₂ to absorb into the absorbent sample and attain a state of equilibrium.
- C.4.5. Use the standard data acquisition sheet (Appendix D) to record the initial state operating conditions and sample specification data.

C.5. Experimental Data Acquisition

- C.5.1. Once a state of equilibrium is attained (2h period), stop the DMS recording procedure and save the experimental run data to an .xls file; the system temperature, pressure and time steps are saved.
- C.5.2. Use the standard data acquisition sheet (Appendix D) to record the final state operating conditions.

C.6. Equilibrium Absorbent Sampling for GC analysis

- C.6.1. Ensure that the gas-tight Hamilton syringe is cleaned before proceeding with the absorbent sampling;
- C.6.2. Insert the syringe needle through the absorbent sample loading point and draw a 1ml sample for GC analysis;
- C.6.3. Inject the sample into a GC sample container and label the sample;
- C.6.4. Repeat steps C.6.2. and C.6.3. for three samples.

C.7. System Cleanup and Preparation for the next Experimental Run

- C.7.1. Remove the CO₂ cylinder feed line (Line 1) from the connection point at valve V-2;
- C.7.2. Remove the CO₂ vent line (Line 2) from the connection point at valve V-3;
- C.7.3. The equilibrium cell is attached to the experimental setup by two cable ties. Cut the ties and slowly remove the equilibrium cell from the experimental setup, ensuring that the PT_E connection point is not damaged in the process;
- C.7.4. Remove the PT_E and absorbent sample loading point screw caps and membranes from the equilibrium cell;
- C.7.5. Remove the absorbent sample from the equilibrium cell and wash the cell with water and acetone. Allow the cell to dry before reattaching it to the experimental setup;
- C.7.6. Reattach the equilibrium cell to the experimental setup using two new cable ties.

Appendix D: Experimental Run Data Sheet

Experimental Data Sheet Run no. ____

| | | |
|-------------|-------------|--|
| Date | Initial | |
| | Equilibrium | |

| | | |
|-------------|-------------|--|
| Time | Initial | |
| | Equilibrium | |

| | | | | | |
|-----------------------------------|--|---|--|---|--|
| Number of blend components | | | | | |
| 2 | | 3 | | 4 | |

| | |
|----------------------------------|--|
| Names of blend components | |
| 1 | |
| 2 | |
| 3 | |
| 4 | |

| | | |
|------------------------------------|-------------|--|
| System Operating Conditions | | |
| Temperature [°C] | | |
| Pressure [mbar] | Initial | |
| | Equilibrium | |

| | |
|-----------------------|--|
| GC Sample Data | |
| Sample 1 Code | |
| Sample 2 Code | |
| Sample 3 Code | |

Appendix E: Experimental Data

Table E.1 – Summary of the experimental data for the six solvent formulations synthesized.

| Run No. | Constituent 1 | Constituent 2 | Constituent 3 | ρ_1 [g/cm ³] | ρ_2 [g/cm ³] | ρ_3 [g/cm ³] | V_{sample} [cm ³] | P_{ini} [bar] | P_{eq} [bar] | n_{abs} [mol] | I_{rich} [mol CO ₂ /mol solvent] |
|---------|--------------------------------|--------------------------|------------------|-------------------------------|-------------------------------|-------------------------------|--|------------------------|-----------------------|------------------------|--|
| 1 | MEA | H ₂ O | - | 1.0120 | 1.0000 | - | 5.0000 | 1.0218 | 0.2756 | 0.00084 | 0.00518 |
| 2 | MEA | H ₂ O | - | 1.0120 | 1.0000 | - | 5.0000 | 1.0064 | 0.2677 | 0.00083 | 0.00512 |
| 3 | K ₂ CO ₃ | H ₂ O | - | 2.1700 | 1.0000 | - | 5.0000 | 1.0101 | 0.9974 | 0.00022 | 0.00136 |
| 4 | K ₂ CO ₃ | H ₂ O | - | 2.1700 | 1.0000 | - | 5.0000 | 1.0132 | 1.0010 | 0.00022 | 0.00136 |
| 5 | K ₂ CO ₃ | PZ | H ₂ O | 2.1700 | 1.1000 | 1.0000 | 5.0000 | 1.0132 | 0.4948 | 0.00065 | 0.00462 |
| 6 | Trioctylamine | MEA | H ₂ O | 0.8090 | 1.0120 | 1.0000 | 5.0000 | 1.0146 | 0.9959 | 0.00022 | 0.01526 |
| 7 | Auramine | Hexylamine | H ₂ O | 0.9445 | 0.7660 | 1.0000 | 2.7000 | 1.0133 | 0.4262 | 0.00066 | 0.04207 |
| 8 | Tryptamine | Diisobutylamine | H ₂ O | 1.0990 | 0.7630 | 1.0000 | 0.5000 | 1.0103 | 0.9735 | 0.00006 | 0.01447 |
| 9 | sec-Butylamine | Auramine | H ₂ O | 0.7240 | 0.9445 | 1.0000 | 5.0000 | 1.0145 | 0.8833 | 0.00032 | 0.01164 |
| 10 | Hexylamine | 2,4-Dichlorobenzylamine | H ₂ O | 0.7660 | 1.3000 | 1.0000 | 5.0000 | 1.0133 | 0.7307 | 0.00045 | 0.01038 |
| 11 | Di-p-Tolylamine | DMEA | H ₂ O | 1.0490 | 0.8900 | 1.0000 | 5.0000 | 1.0138 | 0.9598 | 0.00025 | 0.00620 |
| 12 | [bmim][PF ₆] | H ₂ O | - | 1.3800 | 1.0000 | - | 2.0000 | 1.0132 | 1.0121 | 0.00008 | 0.00602 |
| 13 | [bmim][BF ₄] | H ₂ O | - | 1.2077 | 1.0000 | - | 5.0000 | 1.0130 | 1.0115 | 0.00021 | 0.00525 |
| 14 | [omim][PF ₆] | H ₂ O | - | 1.2345 | 1.0000 | - | 1.0000 | 1.0137 | 1.0125 | 0.00004 | 0.00783 |
| 15 | Diisobutylamine | [omim][PF ₆] | - | 0.7630 | 1.2345 | - | 3.0000 | 1.0139 | 0.5353 | 0.00057 | 0.03724 |
| 16 | Diisobutylamine | [bmim][PF ₆] | - | 0.7630 | 1.3800 | - | 5.0000 | 1.0155 | 0.2339 | 0.00087 | 0.03137 |
| 17 | 2,4-Dichlorobenzylamine | [omim][PF ₆] | - | 1.3000 | 1.2345 | - | 1.0000 | 1.0140 | 0.9013 | 0.00016 | 0.02173 |
| 18 | MEA | [bmim][BF ₄] | - | 1.0120 | 1.2077 | - | 5.0000 | 1.0137 | 0.5948 | 0.00056 | 0.01036 |

Appendix F: Sample Calculations

Sample calculations are presented to explain, step-by-step, the data analysis procedure used to determine the CO₂ loadings of the solvent formulations investigated. The sample calculations are done for the first absorption experiment, i.e. for the 30wt% MEA (aq) solvent. All calculations were done using Microsoft Excel. None of the values were rounded to less significant numbers during the calculation process.

The first step is to determine the void volume available for CO₂ gas inside the equilibrium cell once the solvent sample has been injected. The volume of the cell was determined to be 25.87 cm³. For the first run, 5ml (or cm³) of the solvent was injected into the cell. From this, the void volume is determined to be:

$$V_{void,1} = V_{cell} - V_{sample,1} = 25.87 - 5.00 = 20.87 \text{ cm}^3$$

Next, the various components of the Peng-Robinson Equation of State (PR-EoS) must be calculated. First, the PR-EoS attractive parameter, *a*, is calculated:

$$a = \frac{0.45724R^2T_c^2}{P_c} = \frac{0.45724 \times 8.314^2 \times 304.1^2}{7380000} = 0.396041535 \frac{J \cdot m^3}{mol^2}$$

Followed by the PR-EoS covolume, *b*:

$$b = \frac{0.07780RT_c}{P_c} = \frac{0.07780 \times 8.314 \times 304.1}{7380000} = 2.66532 \times 10^{-5} \frac{m^3}{mol}$$

Next the acentric factor for CO₂ is used to determine the PR-EoS kappa variable, κ :

$$\begin{aligned}\kappa &= 0.37464 + 1.54226\omega - 0.26992\omega^2 \\ &= 0.37464 + (1.54226 \times 0.239) - (0.26992 \times 0.239^2) \\ &= 0.72782204\end{aligned}$$

From this, the value of the temperature-dependent PR-EoS variable, α , is determined to be:

$$\alpha(T) = [1 + \kappa(1 - \sqrt{T_r})]^2 = \left[1 + 0.72782204 \left(1 - \sqrt{\frac{298.15}{304.10}}\right)\right]^2 = 1.014362064$$

Next, Microsoft Excel Solver™ is used to determine the initial and equilibrium state molar volumes $(V_m)_{1,ini}$ and $(V_m)_{1,eq}$. To do this, the equations are setup to minimize the difference between the value calculated for the right-hand side (RHS) of the PR-EoS and the value of the left-hand side (LHS) of the PR-EoS. The sample calculations are shown for the initial state molar volume calculation. The LHS of the PR-EoS is equal to the initial pressure reading observed for the experimental run, i.e. 102179 Pa. The RHS of the equation is expressed as follow:

$$\begin{aligned}RHS_{1,ini} &= \frac{RT}{(V_m)_{1,ini} - b} - \frac{a\alpha(T)}{(V_m)_{1,ini}^2 + 2b(V_m)_{1,ini} - b^2} \\ &= \frac{8.314 \times 298.15}{(V_m)_{1,ini} - 2.66532 \times 10^{-5}} \\ &\quad - \frac{0.396041535 \times 1.014362064}{(V_m)_{1,ini}^2 + [2 \times 2.66532 \times 10^{-5} \times (V_m)_{1,ini}] - (2.66532 \times 10^{-5})^2}\end{aligned}$$

Next, Microsoft Excel Solver™ was used to minimize the difference between the value calculated for $RHS_{1,ini}$ and the value specified for $LHS_{1,ini}$. From this the initial molar volume, $(V_m)_{1,ini}$, was determined to be $0.02412379 \text{ m}^3/\text{mol}$. Similarly, the equilibrium state molar volume, $(V_m)_{1,eq}$, was determined to be $0.089820182 \text{ m}^3/\text{mol}$ for an equilibrium pressure of 27556 Pa. From this, the excess number of moles of CO_2 gas present in the cell initially is determined to be:

$$(n_{exc})_{1,ini} = \frac{V_{cell}}{(V_m)_{1,ini}} = \frac{2.587 \times 10^{-5}}{0.02412379} = 0.001072385 \text{ moles}$$

Similarly, the excess number of moles of CO_2 gas present in the cell at equilibrium is determined to be:

$$(n_{exc})_{1,eq} = \frac{V_{void,1}}{(V_m)_{1,eq}} = \frac{2.087 \times 10^{-5}}{0.089820182} = 0.000232353 \text{ moles}$$

From this, the amount of moles of CO_2 absorbed by the solvent is determined to be:

$$n_{abs,1} = |n_{ini,1} - n_{eqi,1}| = |0.001072385 - 0.000232353| = 0.000840032 \text{ moles}$$

Next, the number of moles of solvent injected must be determined. For the purpose of this study, the weighted averages were used to determine the solvent density and molecular weight. For the 30wt% MEA (aq) solvent, these values were found to be 1.0036 g/cm^3 and 30.938 g/mol respectively. From this, the number of moles of solvent injected was calculated to be 0.162195358 moles. Based on this, the solvent rich loading is determined to be:

$$l_{rich,1} = \frac{n_{abs,1}}{n_{sample,1}} = \frac{0.000840032}{0.162195358} = 0.005179139 \text{ mol } \text{CO}_2/\text{mol solvent}$$


Thus the solvent loading, rounded to four significant figures, is 0.0052 mol CO₂/mol solvent. This step-by-step procedure was used to determine the loading of each solvent formulation tested.

Appendix G: Equipment Calibration Data




G.1. Pressure Transmitter Calibration Data

CIKA INSTRUMENTS (PTY) LTD
 Reg. No. 79/00475/07
 Manufactures and Distributors of
 Pressures and Temperature Measuring Instrumentation

Auckland Park, Cr. Section & Auckland str,
 Paarden Eiland, 7420
 P O Box 475
 Millerton
 7435
 Tel: 021-511-9228
 Telefax: 021-511-5866



Certificate of Calibration No. 078

| | | |
|---|--|---|
| Date of Issue: | Calibration of: | Manufacturer: |
| 01/04/2011 | Pressure Transmitter | WIKA |
| Date of Expiry: | Serial No: 2612JYT | Model No: S10 |
| 31/03/2012 | | |
| Range: 0-1,6BAR ABS | Excitation voltage: | Ambient Temp: |
| BAR | DC 10..30 V | 20.9 deg C |
| Calibrated For: University Of Stellenbosch Process Engineering | Calibrated by: C. BARNES  | Checked by: K. SOLOMON   |

Procedure

The pressure transmitter was calibrated by applying know pressure to it using reference standards. The output current was then measured using a precision calibrator. The accuracy of the reference standards used is traceable to a SANAS accredited laboratory.



| | | |
|---------------------------|---------------|-----------------|
| Reference Standards Used: | Serial No: | Certificate No: |
| Unomat Calibrator | 04290 | 146-18061011 |
| Mensor CPC2500 | 730223 CH - C | A 3344 |

Result:

| APPLIED PRESSURE IN BAR | EQUIVALENT CURRENT OUTPUT IN mA | MEASURED PRESSURE OUTPUT IN BAR |
|----------------------------|------------------------------------|------------------------------------|
| 0 | 4.00 | 0 |
| 0,40 | 6.70 | 0,40 |
| 0,80 | 9.30 | 0,80 |
| 1,00 | 12.00 | 1.00 |
| 1,20 | 14.70 | 1.20 |
| 1,40 | 17.40 | 1.40 |
| 1,60 | 20.00 | 1.60 |

The Uncertainty of measurement is 0.01 %

- The values in this certificate were correct at the time of calibration. Subsequently the accuracy will depend on such factors as operation temperature, the care exercised in handling, frequency of use and its use under conditions other than that specified by the manufacture. Recertification should be performed after a period, which has been chosen to ensure that the equipment's accuracy remains within the desired limits required.
- In the event of a mistake being made by WIKAL INSTRUMENTS in calibration work performed for the application, any legal liability arising therefore shall be limited to the cost of recalibration, but the application indemnifies WIKAL INSTRUMENTS against any consequential or other loss.

Directors: Alexander Wiegand* • Rainer Holz* (Managing) • Franz Schamm* (Financial)* *German

Figure G.1 – Calibration certificate for the pressure transmitter.

The pressure transmitter was sent to Cika Instruments (Pty) Ltd for calibration. The calibration certificate is shown in Figure G.1. The data logger readings for the calibrated pressure transmitter are correlated with the actual pressure at three points, i.e. absolute zero, atmospheric pressure, and maximum transmitter pressure (Table G.1).

Table G.1 – Calibration data entered into the DMS for the pressure transmitter.

| Data Logger Reading [mV] | Actual Pressure [bar] |
|---------------------------------|------------------------------|
| 0.0 | 0.0 |
| 1487.87 | 1.01325 |
| 2444.00 | 1.60 |

G.2. Temperature Transmitter Calibration Data

Calibration data for the data monitoring system temperature controller and recorder are shown in Table G.2.

Table G.2 – Calibration data entered into the DMS for the temperature controller and recorder.

| Data Logger Reading [mV] | Actual Temperature [°C] |
|---------------------------------|--------------------------------|
| 923.7 | 14.0 |
| 928.4 | 16.0 |
| 933.1 | 18.0 |
| 938.3 | 20.0 |
| 943.8 | 22.0 |
| 949.5 | 24.0 |
| 955.6 | 26.0 |
| 962.3 | 28.0 |
| 968.5 | 30.0 |
| 974.6 | 32.0 |
| 980.9 | 34.0 |
| 987.1 | 36.0 |
| 993.1 | 38.0 |
| 999.2 | 40.0 |

G.3. System Pressure Test Data

A series of six pressure test runs were conducted to investigate the possibility of leaks in the system. The first three runs were conducted for a positive force exerted on the system, and the remaining three runs were conducted for a negative (vacuum) force exerted on the system. The P-v-t data obtained for the first three runs are shown in Figures G.2 to G.4. The P-v-t data for the last three runs are presented in Figures G.5 to G.7.

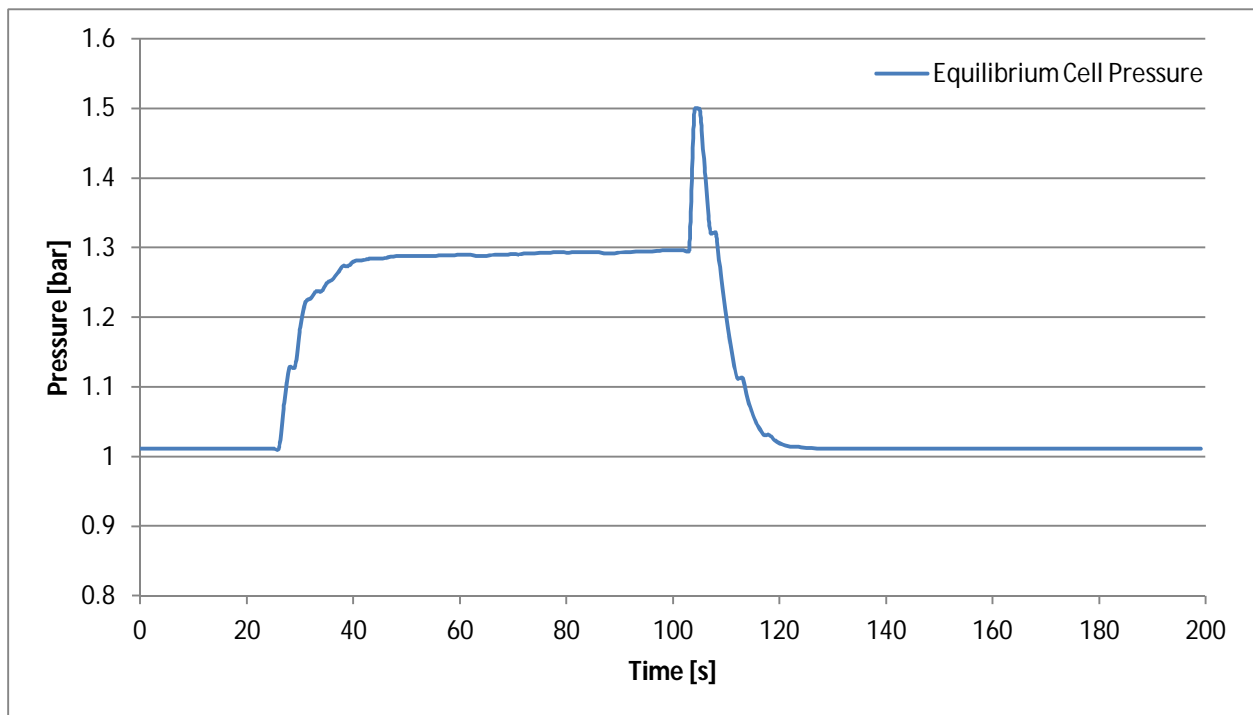


Figure G.2 – P-v-t graph for Pressure Test Run 1 (Positive Force Exerted).

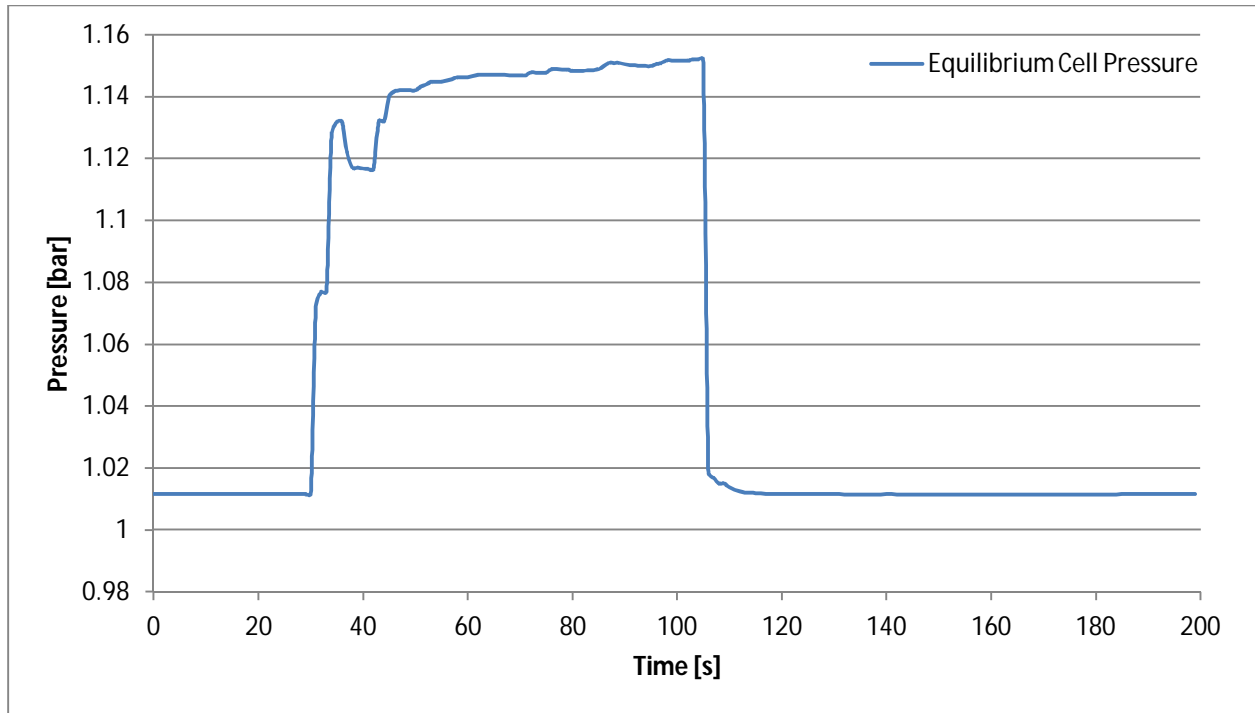


Figure G.3 – P-v-t graph for Pressure Test Run 2 (Positive Force Exerted).

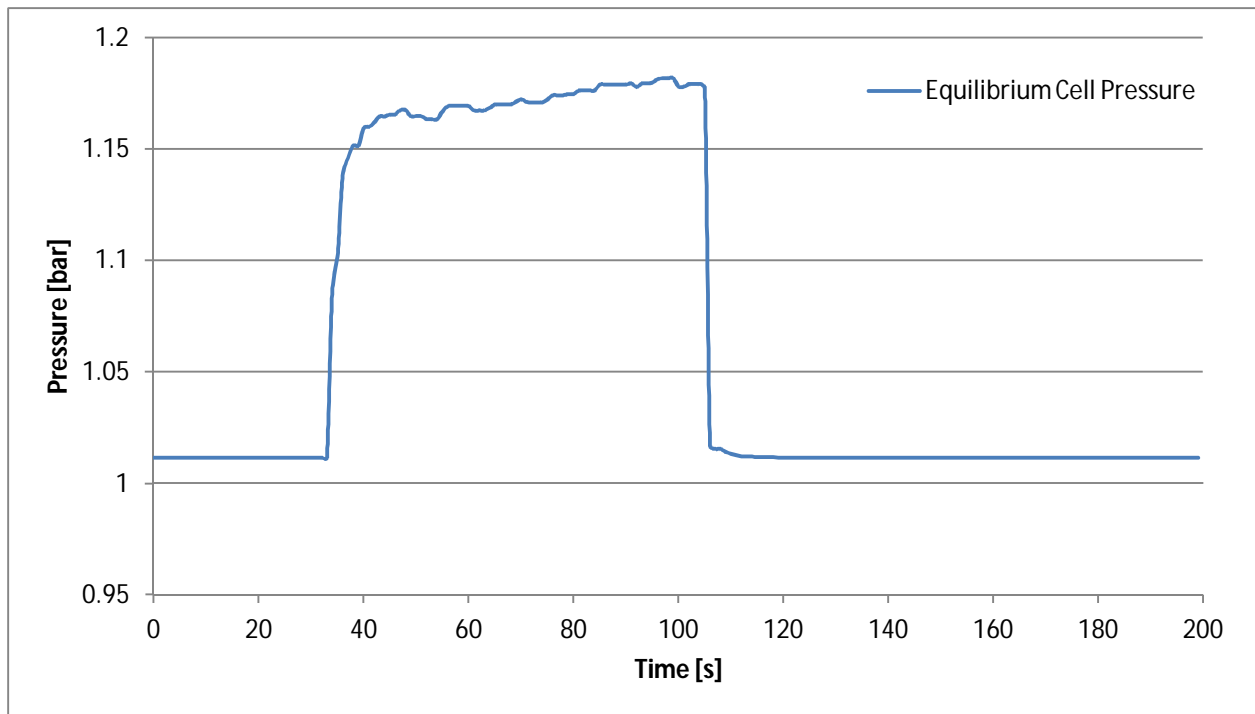


Figure G.4 – P-v-t graph for Pressure Test Run 3 (Positive Force Exerted).

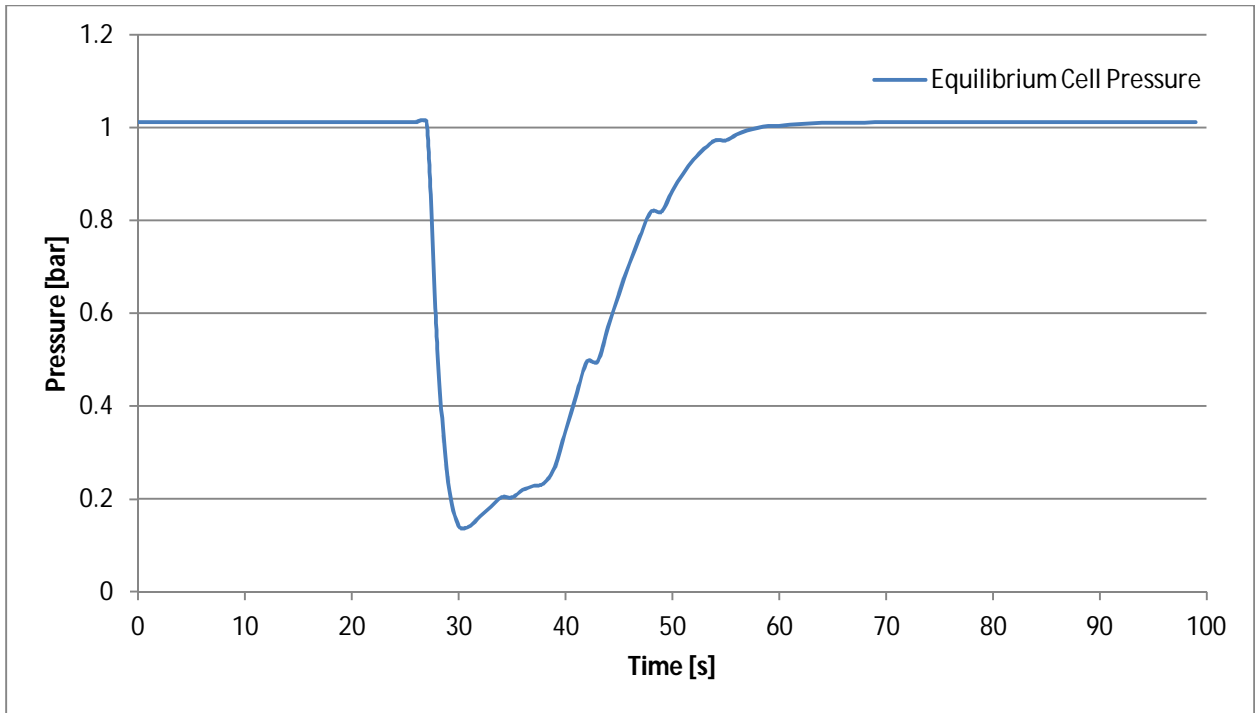


Figure G.5 – P-v-t graph for Pressure Test Run 4 (Negative Force Exerted).

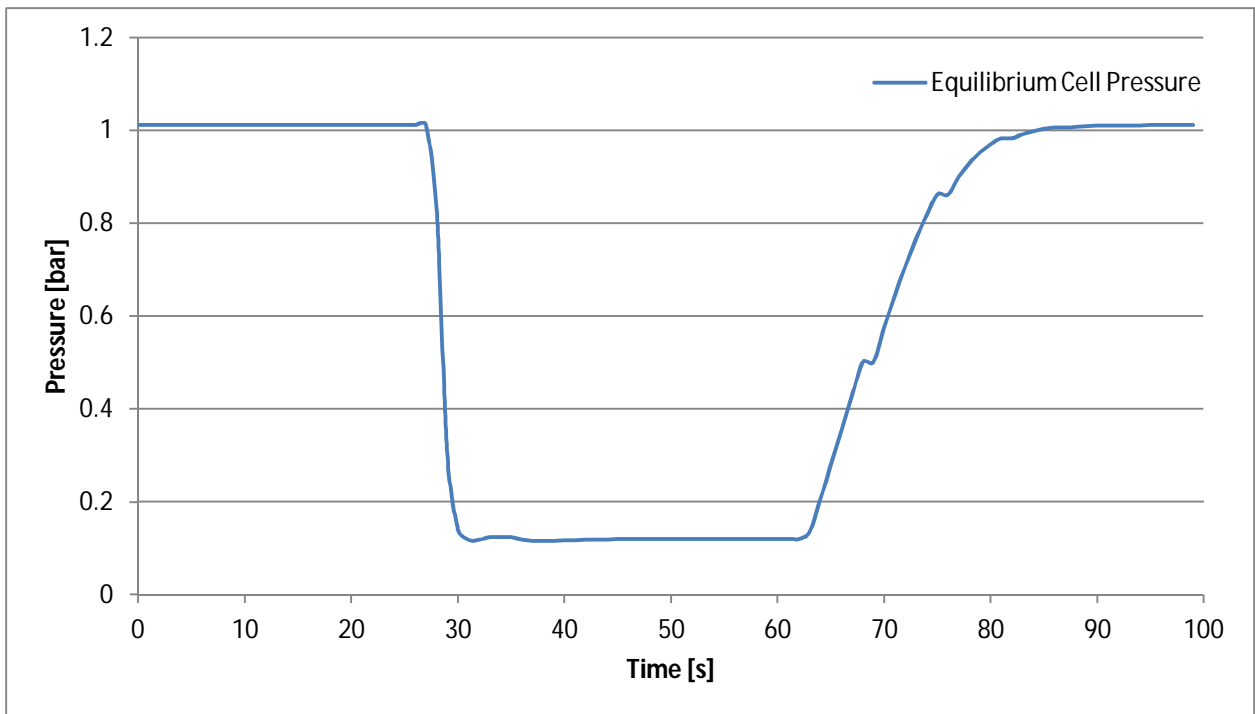


Figure G.6 – P-v-t graph for Pressure Test Run 5 (Negative Force Exerted).

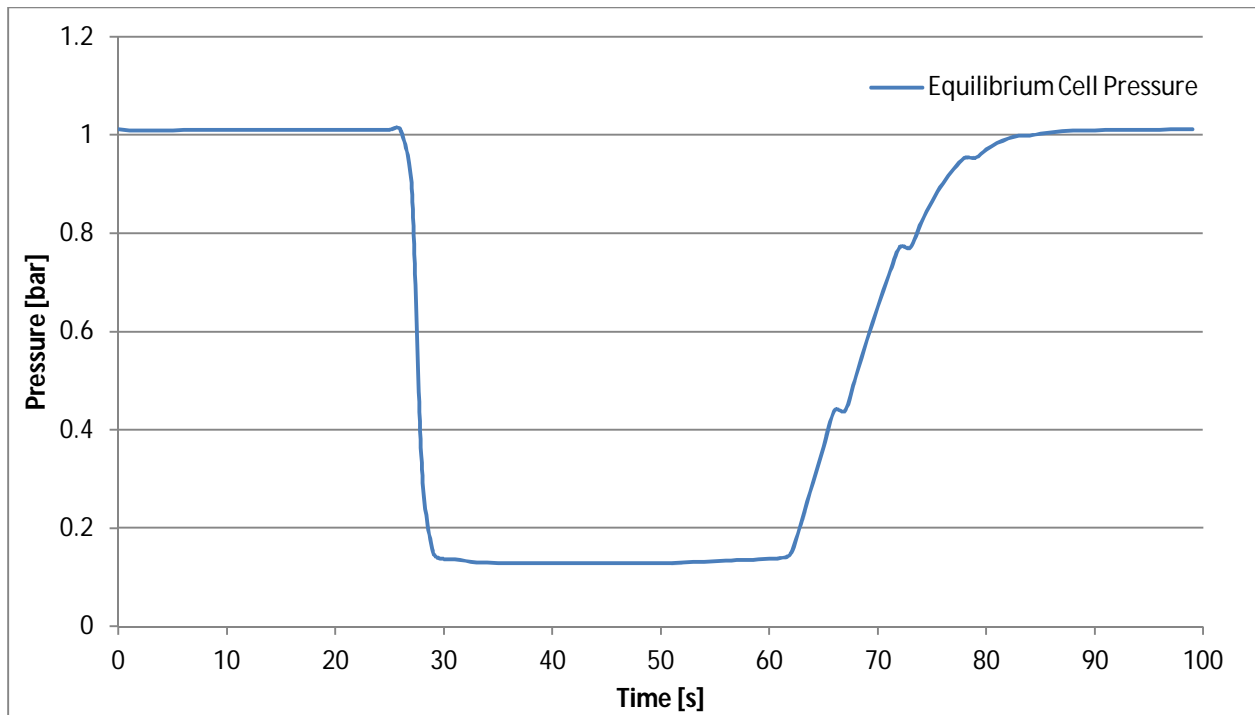


Figure G.7 – P-v-t graph for Pressure Test Run 6 (Negative Force Exerted).

The P-v-t data obtained for both the positive and negative pressure force tests clearly indicate the presence of leakages in the system. The GC septum sampling points are expected to be the source of the leaks. The data analysis of each solvent's absorption performance however was structured such the effect of leaks in the system on the calculated solvent loading is negligible.

Appendix H: EquiSolv User Manual

H.1. Getting Started

The first step in getting started with the EquiSolv package is to copy the files supplied on the CD to a folder on the computer. Create a new folder on the desktop of the computer and rename it to "EquiSolv". Copy the complete set of files supplied from the CD to this folder. Next, open the EquiSolv program by selecting the "EquiSolv.exe" file. A logon screen will be displayed (Figure H.1). The default username and password is "sun" and "chemeng" respectively (all lowercase characters). Enter the username and password and click "OK" to proceed.

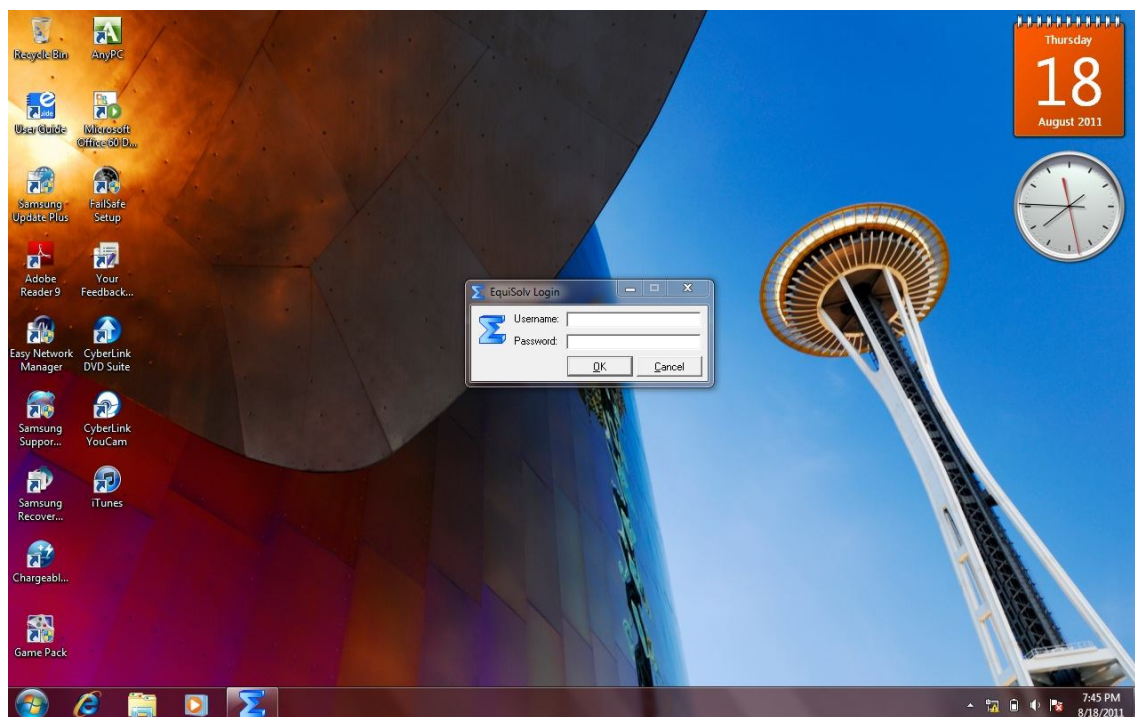


Figure H.1 – Screenshot of the EquiSolv logon screen.

Once the username and password has been accepted, the main screen will be displayed (Figure H.2). This is the control center of the EquiSolv package from where all operations originate. The software is now set up and ready to be used.

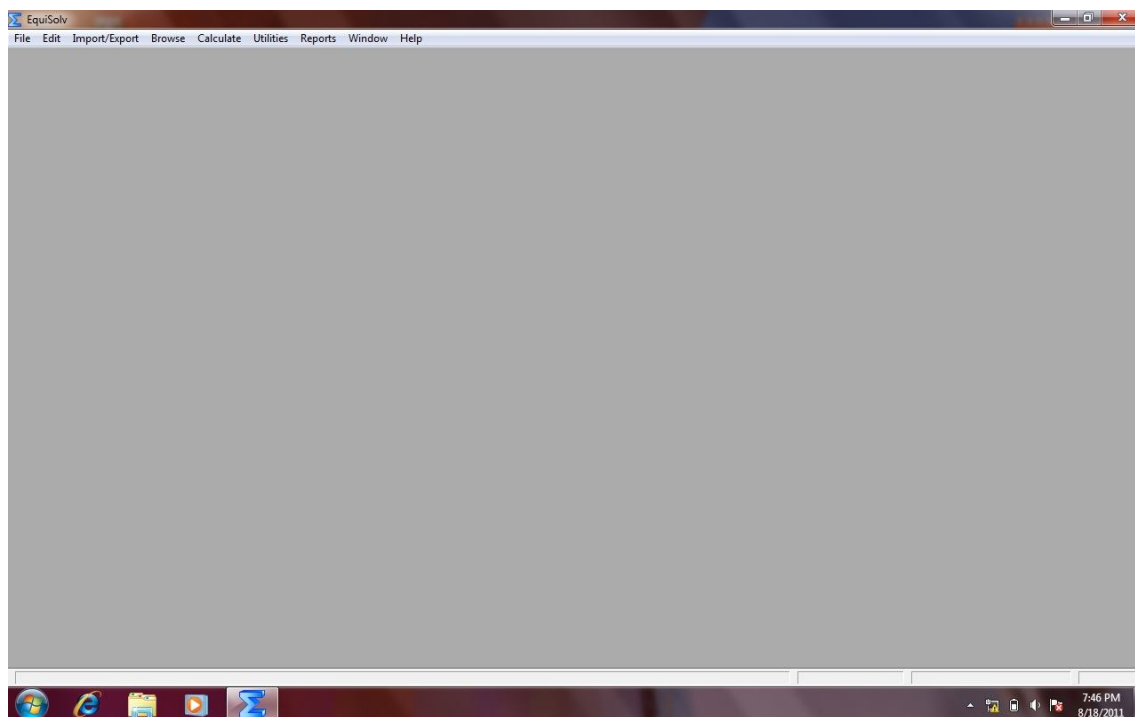


Figure H.2 – Screenshot of the EquiSolv main screen.

H.2. Importing and Exporting Solvent Data

Some solvent and solute data are required before any calculations can be done. The data can be imported into the EquiSolv database via use of a .csv (comma separated value) file. This makes it easy for the user to organize and prepare all solvent data in Microsoft Excel before importing the data into the EquiSolv database. The structure of the CSV import file must adhere to the column order specified in Table H.1. If, for a given solvent, there are no data available for one (or more) of the last four parameters (i.e. the solvent Ra, RED, CAP and CAPID values), they will be defaulted to a value of zero.

Table H.1 – Description of the CSV file column layout required for importing solvent data into the EquiSolv database.

| Column Number | Column Description | Units |
|---------------|--|-----------------------|
| 1 | Solvent number | - |
| 2 | Solvent name | - |
| 3 | Solvent dispersion bond energy HSP value | cal/cm ³ |
| 4 | Solvent polar bond energy HSP value | cal/cm ³ |
| 5 | Solvent hydrogen bond energy HSP value | cal/cm ³ |
| 6 | Solvent ionic bond energy HSP value | cal/cm ³ |
| 7 | Solvent molar volume | cm ³ /mol |
| 8 | Solvent Ra value (default value = 0) | cal/cm ³ |
| 9 | Solvent RED value (default value = 0) | Dimensionless |
| 10 | Solvent CAP value (default value = 0) | Price/cm ³ |
| 11 | Solvent CAPID value (default value = 0) | Price/cm ³ |

Table H.2 – Description of the CSV file column layout required for importing solute data into the EquiSolv database.

| Column Number | Column Description | Units |
|---------------|---|----------------------|
| 1 | Solute number | - |
| 2 | Solute name | - |
| 3 | Solute dispersion bond energy HSP value | cal/cm ³ |
| 4 | Solute polar bond energy HSP value | cal/cm ³ |
| 5 | Solute hydrogen bond energy HSP value | cal/cm ³ |
| 6 | Solute ionic bond energy HSP value | cal/cm ³ |
| 7 | Solute molar volume | cm ³ /mol |
| 8 | Solute radius | cal/cm ³ |

The procedure for importing solvent and/or solute data is as follow:

1. From the EquiSolv main screen, go to the "Import/Export" menu option;
2. Select the "Import the Solvents/Solutes CSV files" option;
3. A screen will be displayed with the various options for importing solvent and/or solute data (Figure H.4). The screen offers the option to import up to five separate lists of solvents and one list of solutes. Each list is imported separately;
4. To import solvent data into "Solvent List 1", click on the small square button with three dots on it (from here on called the "file lookup button") located in-line with the "Solvent List 1" label;
5. A lookup window will be displayed (Figure H.5). Use this window to navigate to the desired solvent CSV file located on the computer;
6. Once the solvent CSV file has been located, highlight it by clicking once on it. Then click the "Open" button at the bottom right-hand corner of the lookup window;

7. The solvent file will be preloaded into the EquiSolv import screen, i.e. the file path and name will be shown in the display field located directly adjacent the “Solvent List 1” option. The file is now ready for importing;
8. Click the “Import List 1” button to import the solvent data into the EquiSolv database;
9. A progress bar will indicate the progress of the import at the bottom of the import screen. Also indicated is the number of solvents imported;
10. Once the data has been imported, the program is ready for the next import;
11. Repeat steps 4 to 11 for each additional list (solvent or solute) to be imported.
12. Once the imports have been completed, click on the “OK” button to close the window. The imported data will now be available for viewing in the corresponding browse files (see Section H.3).

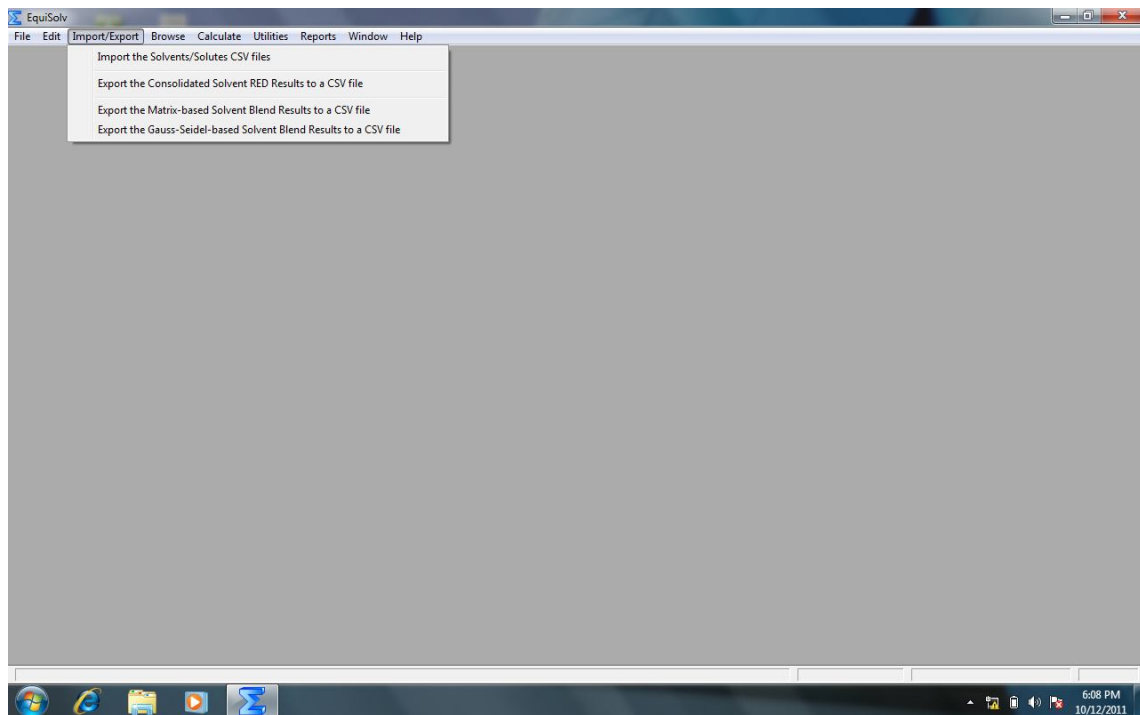


Figure H.3 – A screenshot of the Import/Export dropdown menu option.

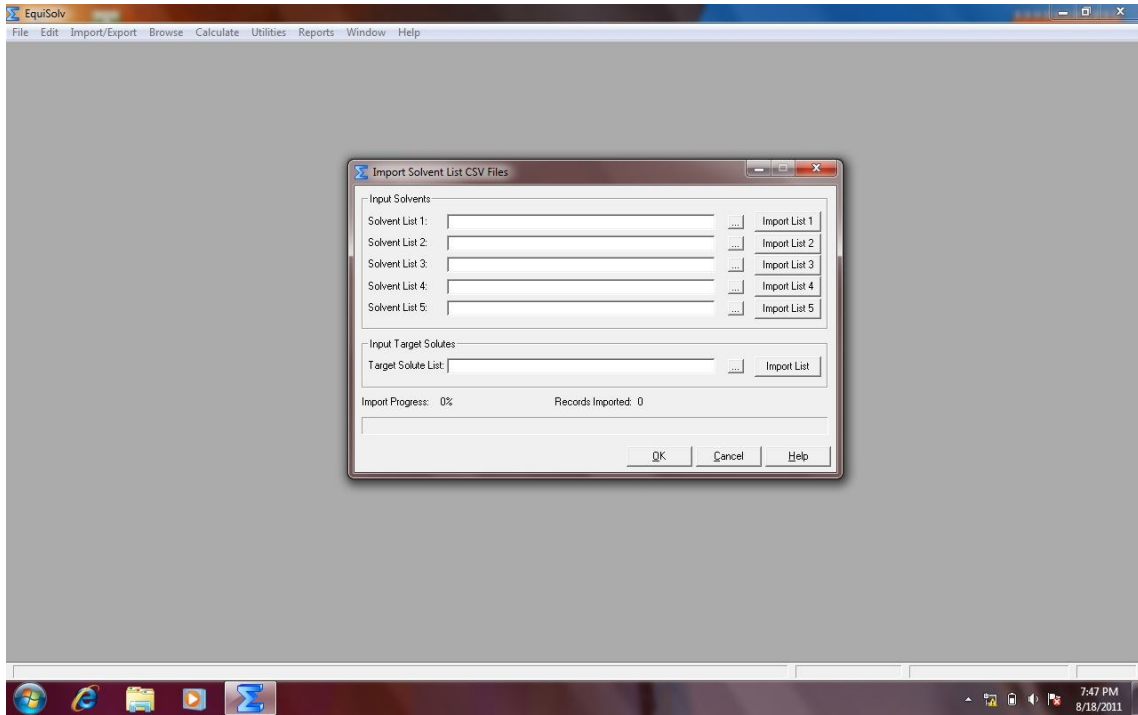


Figure H.4 – Screenshot of the solvent data import screen.

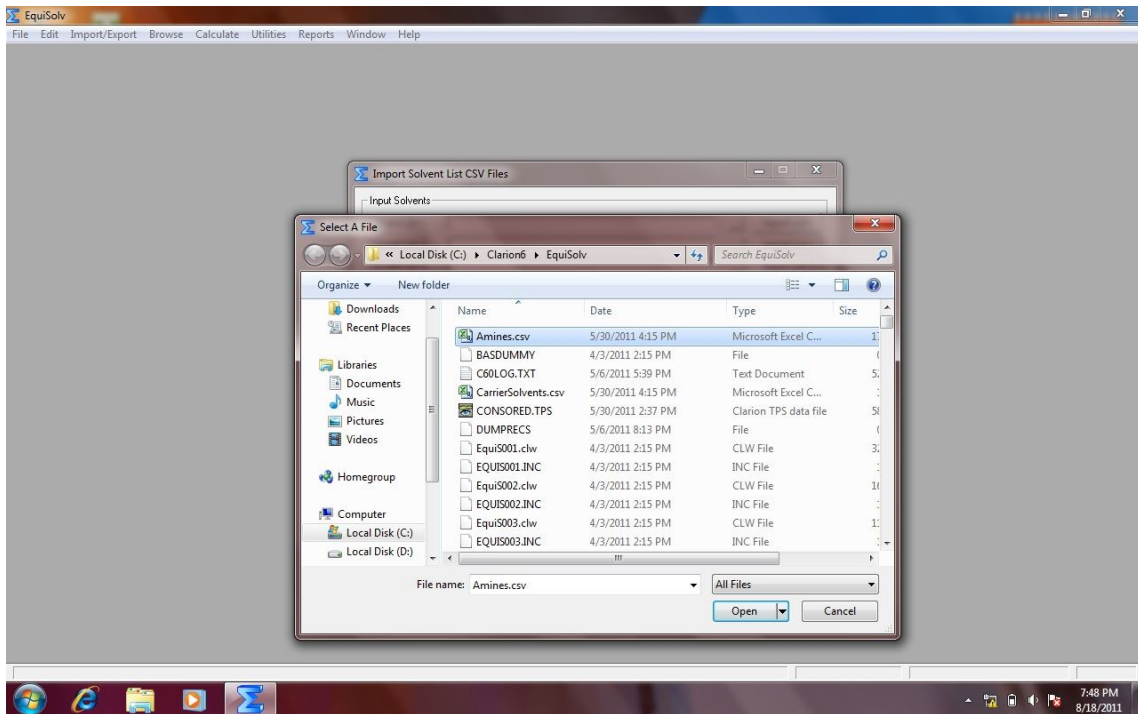


Figure H.5 – Screenshot of the import file lookup and selection screen.

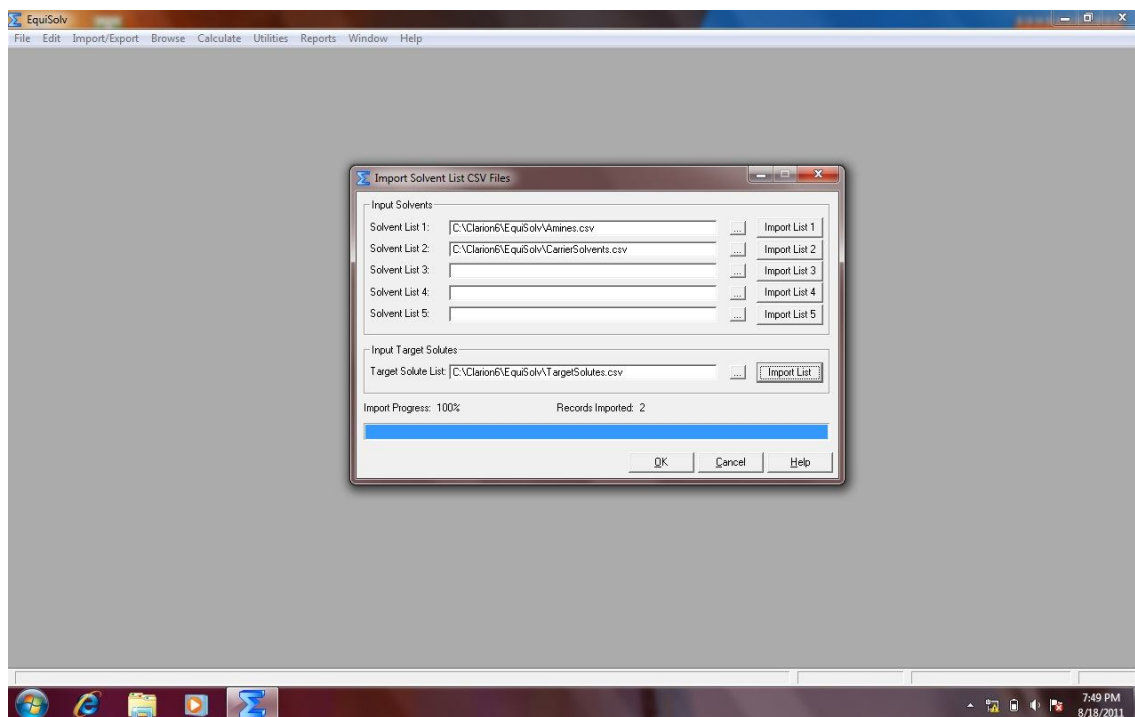


Figure H.6 – Screenshot of the import screen upon completion of a successful solvent (and solute) data import run.

Results from the solvent blend calculations (see Section H.4.3) as well as the solvent RED calculations (see Section H.4.2) can be exported from the EquiSolv database to a CSV file for further analysis and statistical calculations in Microsoft Excel. The procedure for exporting data to a CSV file is as follow:

1. From the main screen, go to the “Import/Export” menu option;
2. To export results from solvent blend calculations, select either the “Export the Matrix-based Solvent Blend Results to a CSV file” or “Export the Gauss-Seidel-based Solvent Blend Results to a CSV file” option depending on whether the data originated from matrix-based or Gauss-Seidel based calculations;
3. A screen will be displayed indicating the options available for exporting data (Figure H.7);
4. Indicated on the screen will be the default export CSV file path and name. This path and name can be changed to any path or name desired by the user;
5. Once the file path and name have been specified, click the “Export” button;
6. A progress bar will indicate the progress of the export process at the bottom of the screen. Also indicated is the number of records exported to the file;
7. Repeat steps 1 to 6 to export results from solvent RED calculations;

- Once the file has been successfully exported, click the “OK” button to close the window. The file can be found at the specified path and name for further analysis in Microsoft Excel.

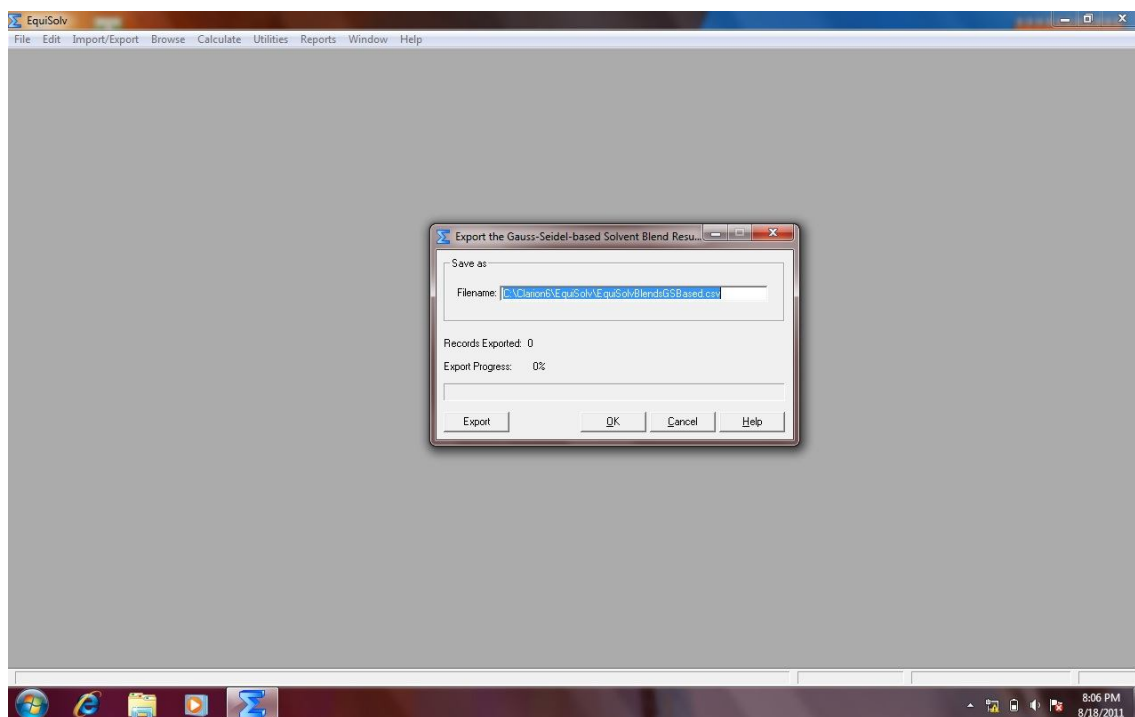


Figure H.7 – Screenshot of the data export screen.

H.3. Browsing and Querying Data

The solvent and solute data imported into the EquiSolv database (Section H.2) as well as results from EquiSolv calculations (Section H.4) can easily be viewed and/or queried using one of the “Browse” functions. The procedure will be described for browsing the data contained in “Solvent List 1”:

- From the EquiSolv main screen, go to the “Browse” menu option;
- Select the “Browse the Solvent List 1 file”;
- A browse window will be displayed showing all of the solvents imported for “Solvent List 1” (Figure H.9);
- To view any of the solvents individually, highlight the desired solvent by clicking once on it and then click the “View” button at the bottom left-hand corner of the screen;

5. A screen will be displayed showing the data for the selected solvent (Figure H.10). To dismiss this screen simply click the "OK" or "Cancel" button;
6. The browse window also offers the option to "Change" or "Delete" any of the existing solvent data;
7. Solvent data can be added to the list by clicking the "Insert" button at the bottom left-hand corner of the browse window;
8. The screen layout for the "Change", "Delete" and "Insert" functions are similar to that of the "View" screen shown earlier;
9. Additionally a "Query" button is provided at the bottom left-hand corner of the browse window. Click on this button to open the query functions (Figure H.11). The query function can be used to search for specific solvent records;
10. To use the query function, simply enter the query requirement value in the corresponding query field. The query operator (i.e. <, >, =, etc.) can be specified by clicking on the small square button located to the right of the query value field;
11. To apply the specified query, click the "OK" button. The solvent records that adhere to the query specifications will be shown in the browse window;
12. To clear the query, open the "Query" window again and click the "Clear" button. The browse window will be restored to its original state;
13. To close the browse window, simply click the "OK" or "Cancel" button at the bottom right-hand corner of the browse window.

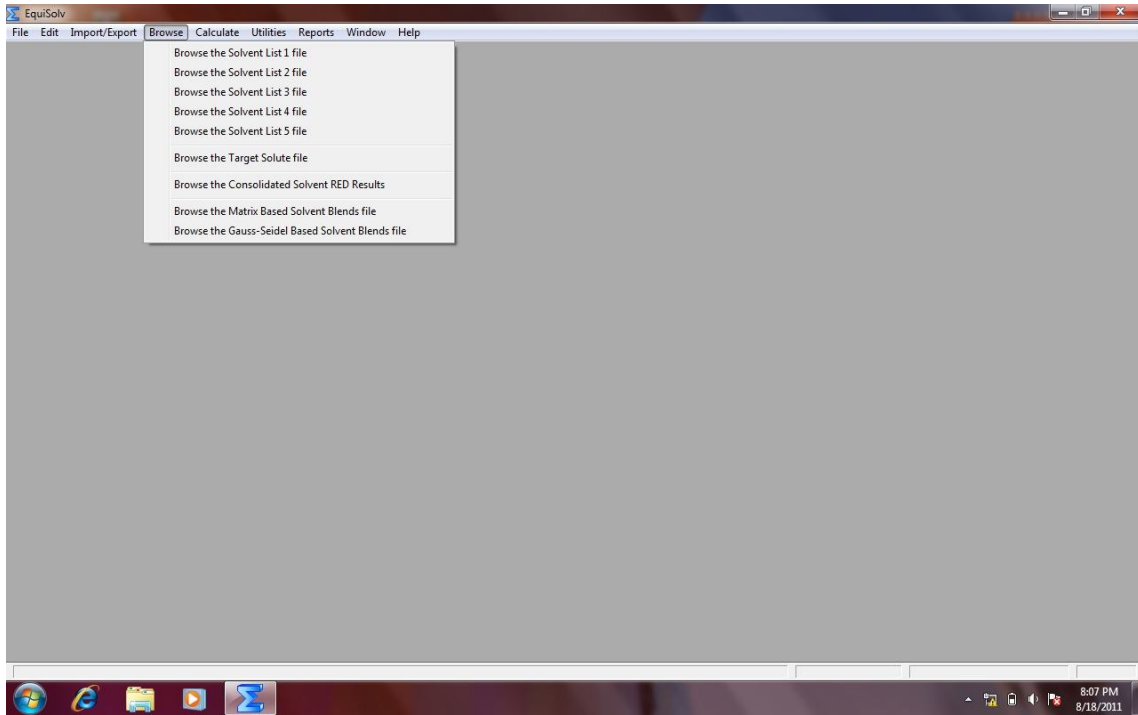


Figure H.8 – Screenshot of the Browse dropdown menu option.

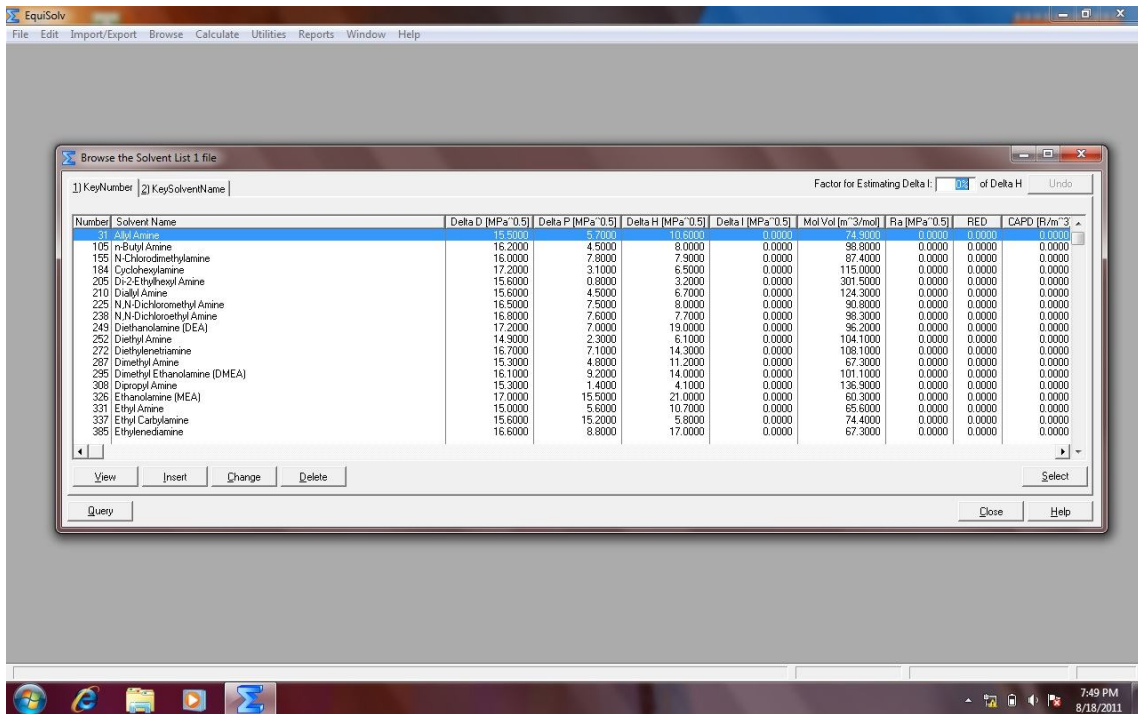


Figure H.9 – Screenshot of a browse window for a selected set of solvent data.

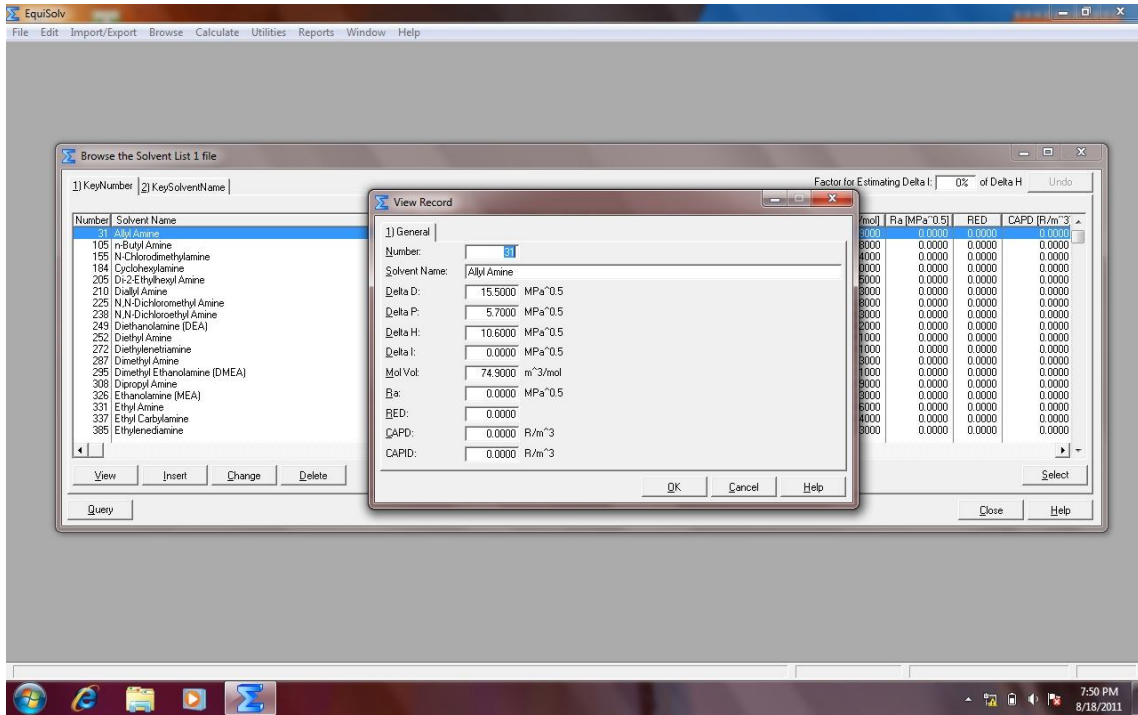


Figure H.10 – Screenshot of the individual record browse window for a selected solvent.

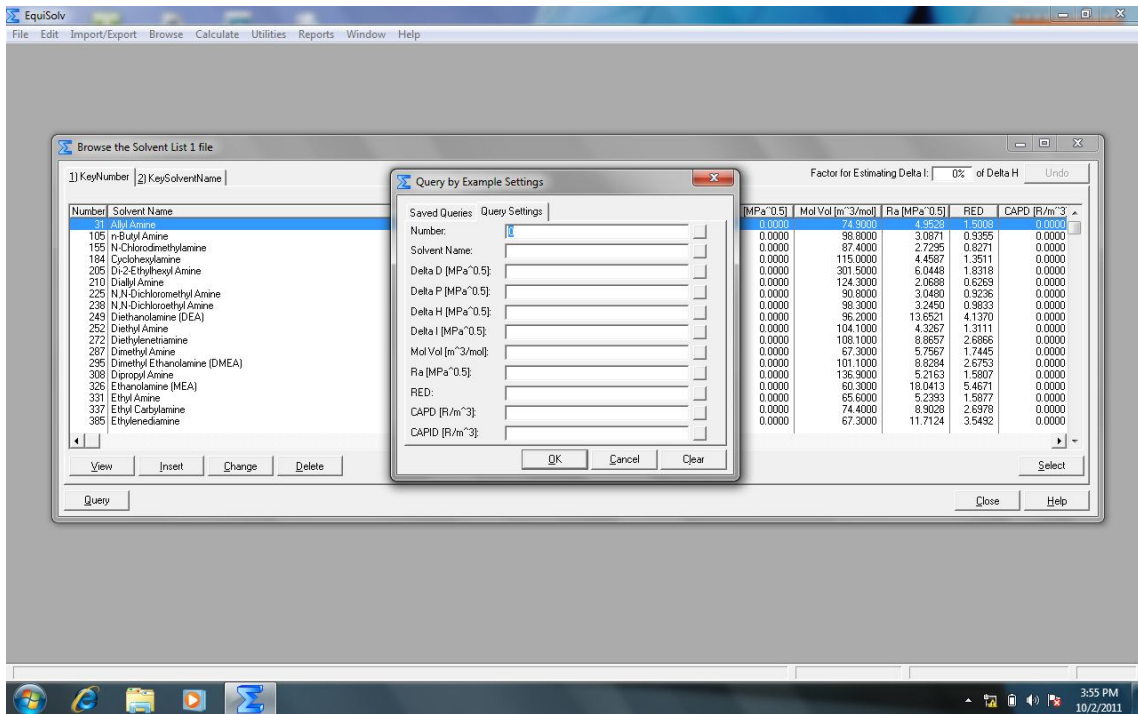


Figure H.11 – Screenshot of the query function provided from the browse window.

H.4. Performing Calculations

The EquiSolv package offers a number of calculation options, including: estimating solvent ionic bond energy HSP values, calculating solvent relative energy differences (REDs), analyzing combinations of solvents for alternative solvent blends, and a quick blend calculator for task specific blend calculations. The calculation options can be accessed from the “Calculate” menu option in the EquiSolv main screen (Figure H.12).

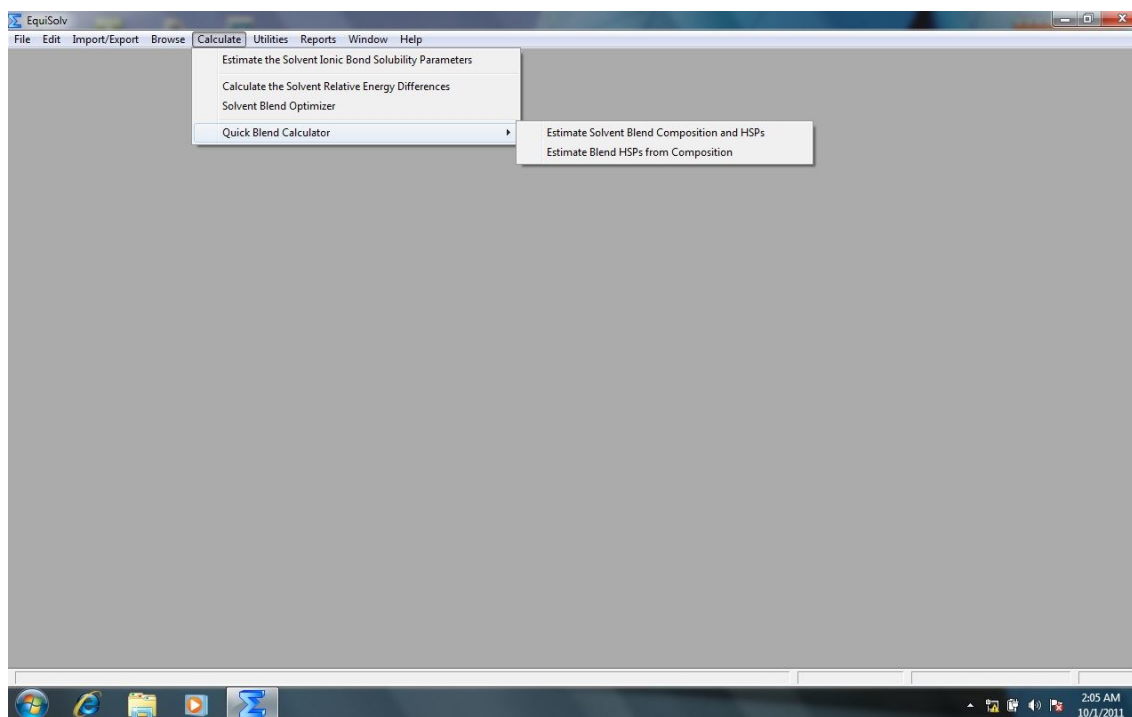


Figure H.12 – Screenshot of the Calculate dropdown menu option.

H.4.1. Estimating Solvent Ionic Bond Energies

The EquiSolv package has the capability to estimate solvent ionic bond energy HSP values based on their hydrogen bond energy HSP values. The ionic bond energy HSP values are estimated as a percentage factor of the original hydrogen bond energy HSP values. The procedure for estimating the ionic bond energy HSPs is as follow:

1. Select the “Estimate the Solvent Ionic Bond Solubility Parameters”;
2. The setup screen for estimating the parameters will be displayed (Figure H.13);

3. Set the percentage factor by which the hydrogen bond energy HSP values will be reduced using the spin box in the "Solvent Control Parameter" box. The factor can be set to any value in the range 0-100%;
4. The "Solvent Lists" box indicates the solvent lists that were imported and are available for factoring. Similarly, the "Target Solute" box indicates the solute list imported;
5. Each list can be factored separately by clicking the corresponding "Factor List" button located on the right-hand side of each solvent (and solute) list field;
6. A progress bar will indicate the progress of the factoring process at the bottom of the screen. Also indicated is the number of records factored for each list calculation (Figure H.14);
7. Once the ionic bond energy HSPs have been estimated, click the "OK" button to close the setup screen.

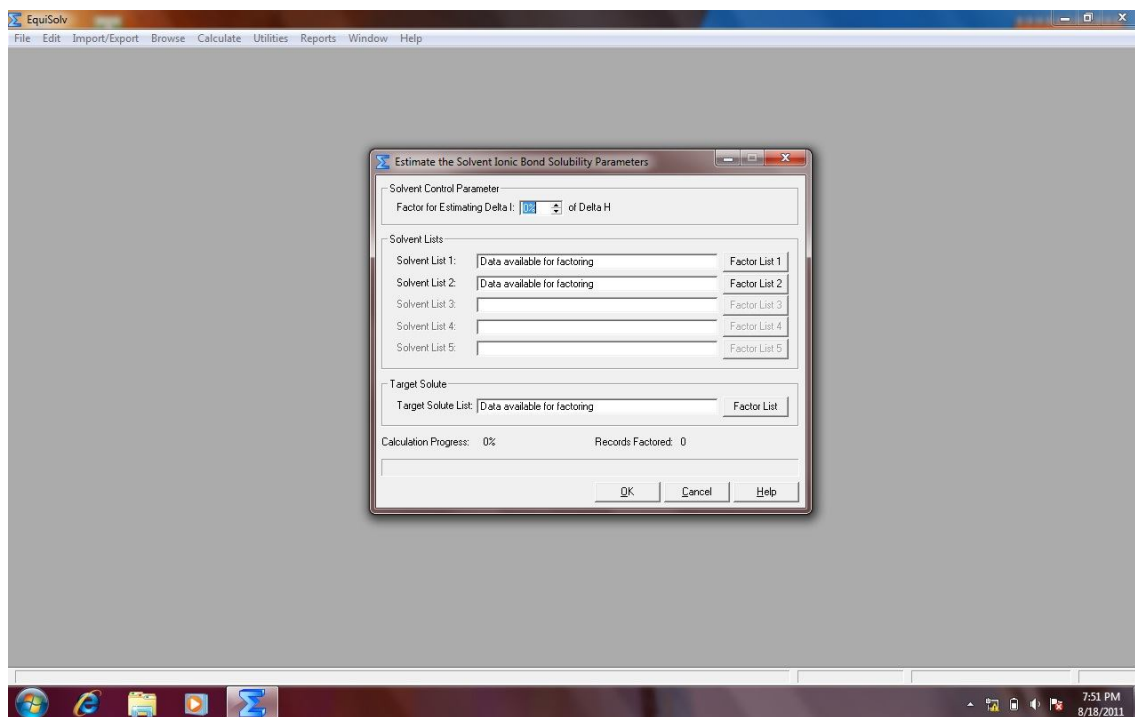


Figure H.13 – Screenshot of the setup window used for estimating the ionic bond energy parameters (δ_I) of selected solvents.

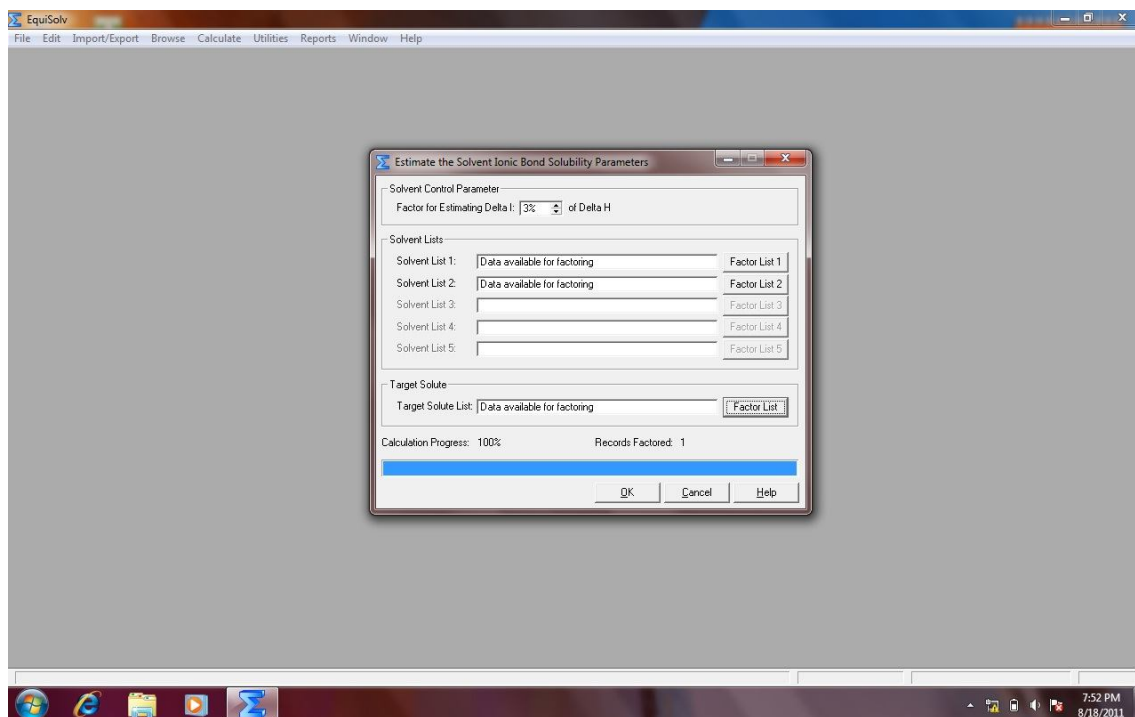


Figure H.14 – Screenshot of the setup window for estimating the ionic bond energies upon completion of a successful calculation run.

The results for the estimated ionic bond energy HSPs can be viewed for each solvent (and solute) list in their respective browse window (Figure H.15). The percentage factor by which the original hydrogen bond energy HSPs were reduced is indicated at the top right-hand corner of the browse window. An “Undo” option is provided to reverse the ionic bond energy HSP estimations for the specific list. This process will restore the solvent (or solute) list data to its original import state (Figure H.16).

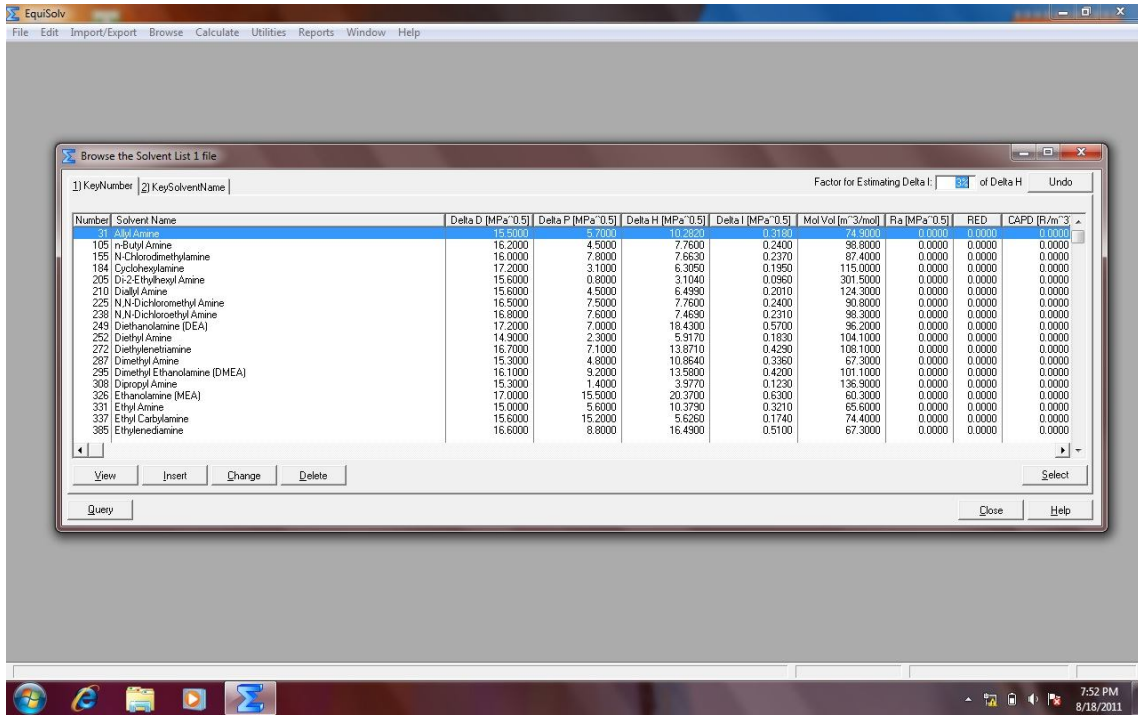


Figure H.15 – Screenshot of a browse window for a set of solvents selected for estimating the ionic bond energies.

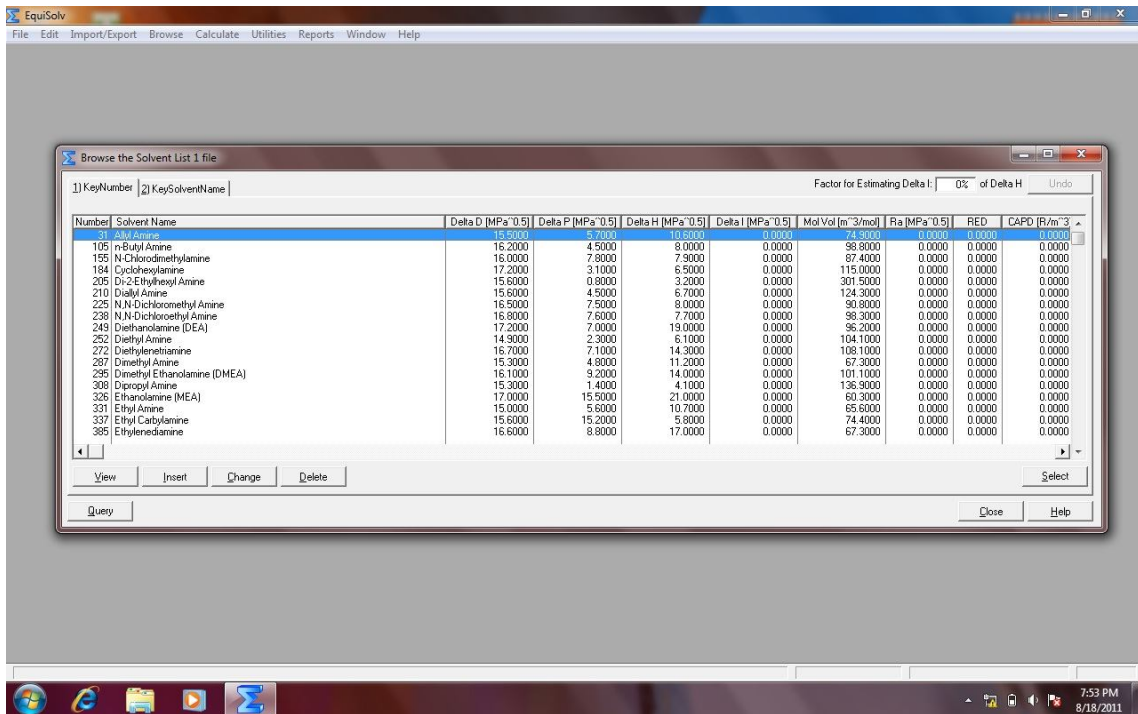


Figure H.16 – Screenshot of a browse window indicating that the ionic bond energy estimation have been reversed.

H.4.2. Calculating the Relative Energy Differences (REDs)

The relative energy differences (REDs) are calculated for the entire set of solvents imported (i.e. all solvent lists) with respect to a particular solute. The procedure for calculating the solvent REDs is as follow:

1. Select the "Calculate the Solvent Relative Energy Differences" option from the "Calculate" menu;
2. The setup screen calculating the RED values will be displayed (Figure H.17);
3. The calculated RED values are updated for each solvent in their respective browse lists. Select the "Consolidate Results" option if a separate consolidated RED results file must be created. The consolidated file has the advantage that the complete set of solvents can be sorted in order of descending solvent RED value (i.e. by "KeyRED") (Figure H.21);
4. Select the "Include Delta I in Analysis" option to include the proposed ionic bond energy HSP in the RED calculations;
5. Next, specify the target solute by clicking the file lookup button located in the "Calculation Setup" box;
6. A lookup window will be displayed, indicating the target solutes that were imported (Figure H.18);
7. Scroll through the list to the desired target solute;
8. Highlight the desired target solute by clicking on it once, and then preload it into the RED calculation setup by clicking the "Select" button at the bottom of the lookup window. The target solute properties will be displayed in the corresponding fields in the "Calculation Setup" box (Figure H.19);
9. Click the "Calculate" button to start the RED calculation process;
10. A progress bar will indicate the progress of the calculation process at the bottom of the setup screen. Also indicated is the number of solvents for which the RED calculation was done;
11. The results for the solvent REDs can be viewed for each solvent list in its respective browse window. If the "Consolidate Results" option was selected, a separate consolidated results list can be viewed by selecting the "Browse the Consolidated Solvent RED Results" option from the "Browse" menu (Figure H.21).

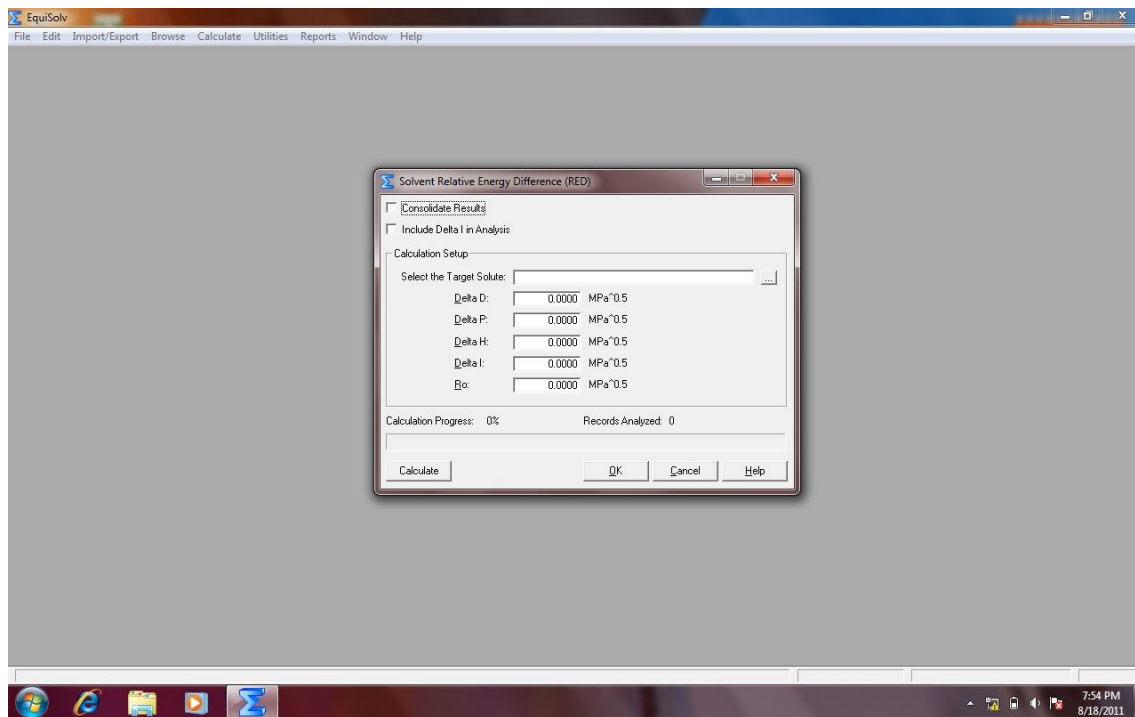


Figure H.17 – Screenshot of the setup window for calculating the solvent relative energy differences (REDs).

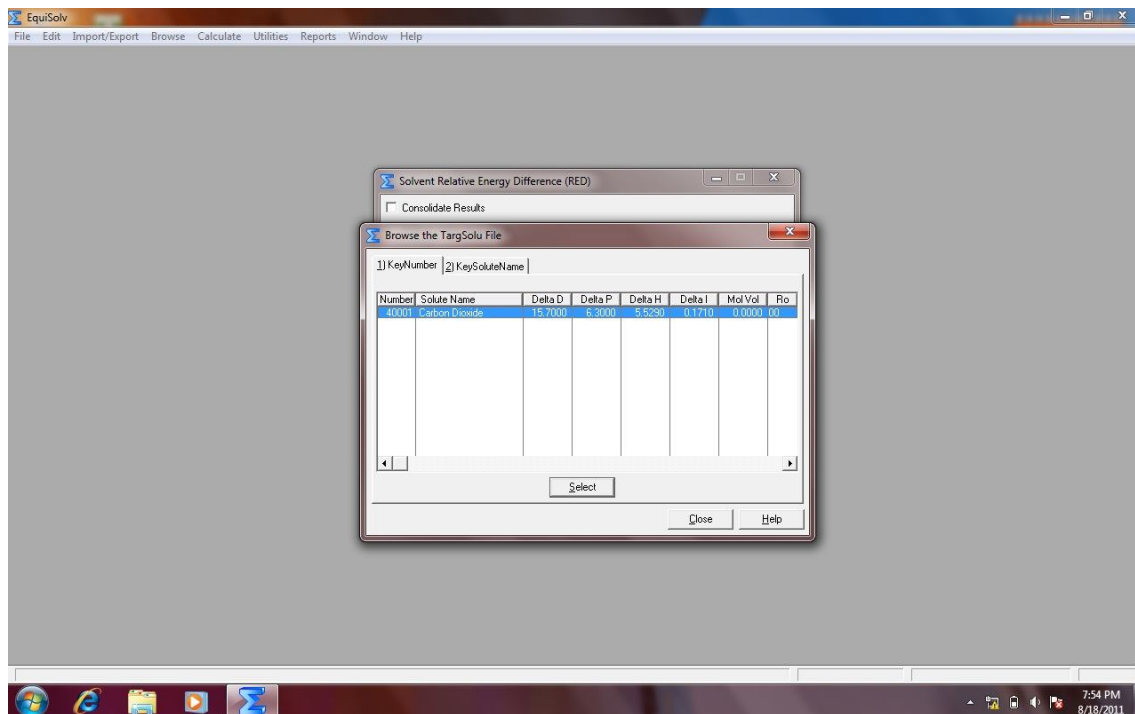


Figure H.18 – Screenshot of the solute lookup and selection window for the RED calculations.

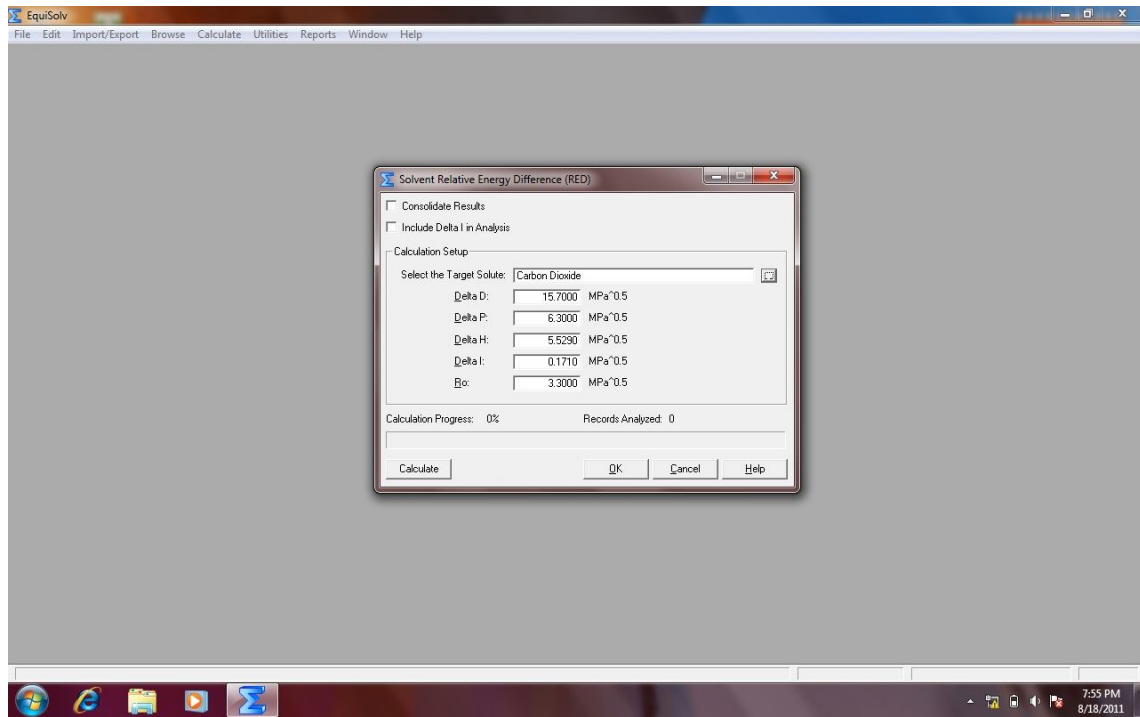


Figure H.19 – Screenshot of the RED calculation setup window with the target solute selected and ready for calculation.

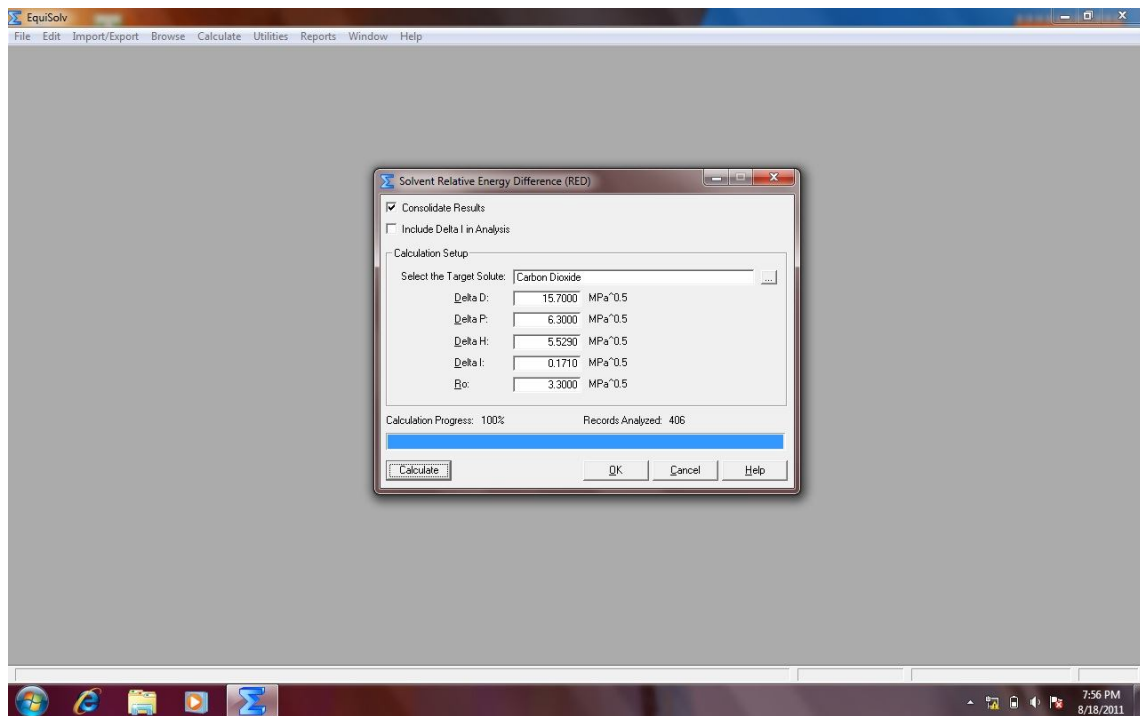


Figure H.20 – Screenshot of the setup window for calculation the solvent REDs upon completion of a successful calculation run.

| Number | Solvent Name | Delta D [MPa ^{0.5}] | Delta P [MPa ^{0.5}] | Delta H [MPa ^{0.5}] | Delta I [MPa ^{0.5}] | Mol Vol [m ³ /mol] | Ra [MPa ^{0.5}] | RED | CAPD [R/m ³] |
|--------|------------------------------|-------------------------------|-------------------------------|-------------------------------|-------------------------------|-------------------------------|--------------------------|--------|--------------------------|
| 31 | Allyl Amine | 15.5000 | 5.7000 | 10.6000 | 0.0000 | 74.9000 | 5.1220 | 1.5521 | 0.0000 |
| 105 | n-Butyl Amine | 16.2000 | 4.5000 | 8.0000 | 0.0000 | 98.8000 | 3.2165 | 0.9747 | 0.0000 |
| 155 | N-Chlorodimethylamine | 16.0000 | 7.8000 | 7.9000 | 0.0000 | 87.4000 | 2.8591 | 0.8694 | 0.0000 |
| 184 | Cyclohexylamine | 17.2000 | 3.1000 | 6.5000 | 0.0000 | 115.0000 | 4.4325 | 1.3514 | 0.0000 |
| 205 | Di-2-Ethylhexyl Amine | 15.6000 | 0.8000 | 3.2000 | 0.0000 | 301.5000 | 5.9761 | 1.8103 | 0.0000 |
| 210 | Diallyl Amine | 15.6000 | 4.5000 | 6.7000 | 0.0000 | 124.3000 | 2.1567 | 0.6535 | 0.0000 |
| 225 | N,N-Dichloromethyl Amine | 16.5000 | 7.9000 | 8.0000 | 0.0000 | 90.8000 | 3.1750 | 0.9633 | 0.0000 |
| 238 | N,N-Dichloroethyl Amine | 16.8000 | 7.6000 | 7.7000 | 0.0000 | 95.3000 | 3.3531 | 1.0161 | 0.0000 |
| 249 | Diethanolamine (DEA) | 17.2000 | 7.0000 | 19.0000 | 0.0000 | 96.2000 | 13.8187 | 4.1875 | 0.0000 |
| 252 | Diethyl Amine | 14.9000 | 2.3000 | 6.1000 | 0.0000 | 104.1000 | 4.3458 | 1.3169 | 0.0000 |
| 272 | Diethyltetramine | 16.7000 | 7.1000 | 14.3000 | 0.0000 | 105.1000 | 3.0316 | 2.7368 | 0.0000 |
| 287 | Dimethyl Amine | 15.3000 | 4.8000 | 11.2000 | 0.0000 | 87.2000 | 5.9203 | 1.7940 | 0.0000 |
| 295 | Dimethyl Ethanolamine (DMEA) | 16.1000 | 9.2000 | 14.0000 | 0.0000 | 101.1000 | 8.9893 | 2.7240 | 0.0000 |
| 308 | Dipropyl Amine | 15.3000 | 1.4000 | 4.1000 | 0.0000 | 136.9000 | 5.1664 | 1.5656 | 0.0000 |
| 326 | Ethanolamine (MEA) | 17.0000 | 15.5000 | 21.0000 | 0.0000 | 80.3000 | 18.1866 | 5.5111 | 0.0000 |
| 331 | Ethyl Amine | 15.0000 | 5.6000 | 10.7000 | 0.0000 | 65.6000 | 5.4027 | 1.6372 | 0.0000 |
| 337 | Ethyl Carbylanine | 15.6000 | 15.2000 | 5.8000 | 0.0000 | 74.4000 | 8.9064 | 2.6989 | 0.0000 |

Figure H.21 – Screenshot of a browse window for the consolidated solvent RED results.

H.4.3. Using the Solvent Blend Optimizer

The Solvent Blend Optimizer is the primary calculation module of the EquiSolv package. The procedure for using the solvent blend optimizer is as follow:

1. Select the “Solvent Blend Optimizer” option from the “Calculate” menu;
2. The setup screen for analyzing solvent blend formulations will be displayed (Figure H.22);
3. The setup procedure is structured in four easy-to-use steps. In Step 1, specify the basis for the calculation (i.e. Gauss-Seidel-based or matrix-based);
4. If Gauss-Seidel iteration is selected as the basis of calculation, it is necessary to specify the iteration and convergence limits as well (max. 50000 and 100% respectively);
5. Next, select the method for calculation (i.e. linear or square optimizing);
6. Select the number of solvent blend constituents (i.e. the number of solvent lists to be analyzed);
7. Specify if the proposed ionic bond energy HSP must be included in the blend analysis;
8. Proceeding to Step 2, specify if convergence should be accelerated by focusing on finding exact blend HSP matches to the target solute (i.e. “Include Exact Solutions”);

9. Specify if the blend constituent inter-miscibility (solubility) should be analyzed (i.e. "Test Blend Inter-miscibility");
10. If the inter-miscibility test is selected, the probable solubility confidence level must be specified as well (i.e. "Miscibility Confidence Level"). The confidence level can be set to any value in the range 0-100%;
11. Next specify the "Variance from Ideality" (0-100%), i.e. the acceptable deviation in HSP values from the specified target solute HSP values;
12. Also specify the amount of significant numbers (1-8) to be used in the calculation process;
13. On to Step 3, the solvent lists to be analyzed must be specified. For "Constituent List 1", select the corresponding file lookup button;
14. A lookup window will be displayed, indicating the solvent lists that were imported and are available for analysis (Figure H.23);
15. To select a solvent list, highlight it by clicking once on it and then click the "Select" button at the bottom of the lookup screen. The name of the selected list will be preloaded into the "Constituent List 1" display field (Figure H.24);
16. Repeat steps 13 to 15 for each additional constituent list to be specified;
17. For Step 4, specify the desired target solute. The procedure for selecting a target solute is similar to that described for selecting the target solute for solvent RED calculations;
18. Once Step 1 to 4 has been setup up, click the "Calculate" button to initiate the blend analysis process;
19. A progress bar will indicate the progress of the analysis at the bottom of the setup screen. Also indicated is the total number of blend formulations analyzed as well as the blend formulations found within specification;
20. To view the calculation error report, click the "View Calculation Report" button. A blank screen will be displayed if no errors were found (Figure H.26). Click the "Cancel" button to dismiss the error report window;
21. Once the analysis is complete, click on the "OK" button to close the window;
22. To view the analysis results, select either the "Browse the Matrix based Solvent Blends file" or "Browse the Gauss-Seidel based Solvent Blends file" option from the "Browse" menu, depending on the basis of calculation specified for the analysis (Figure H.27).

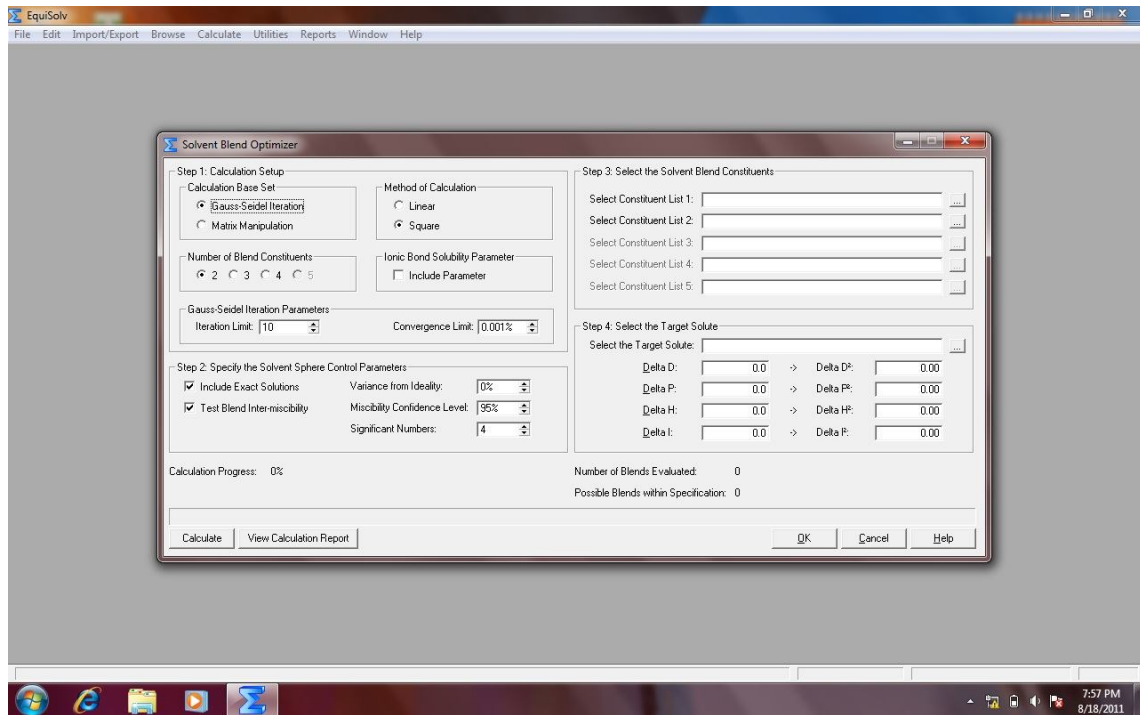


Figure H.22 – Screenshot of the setup window for analyzing alternative solvent blends.

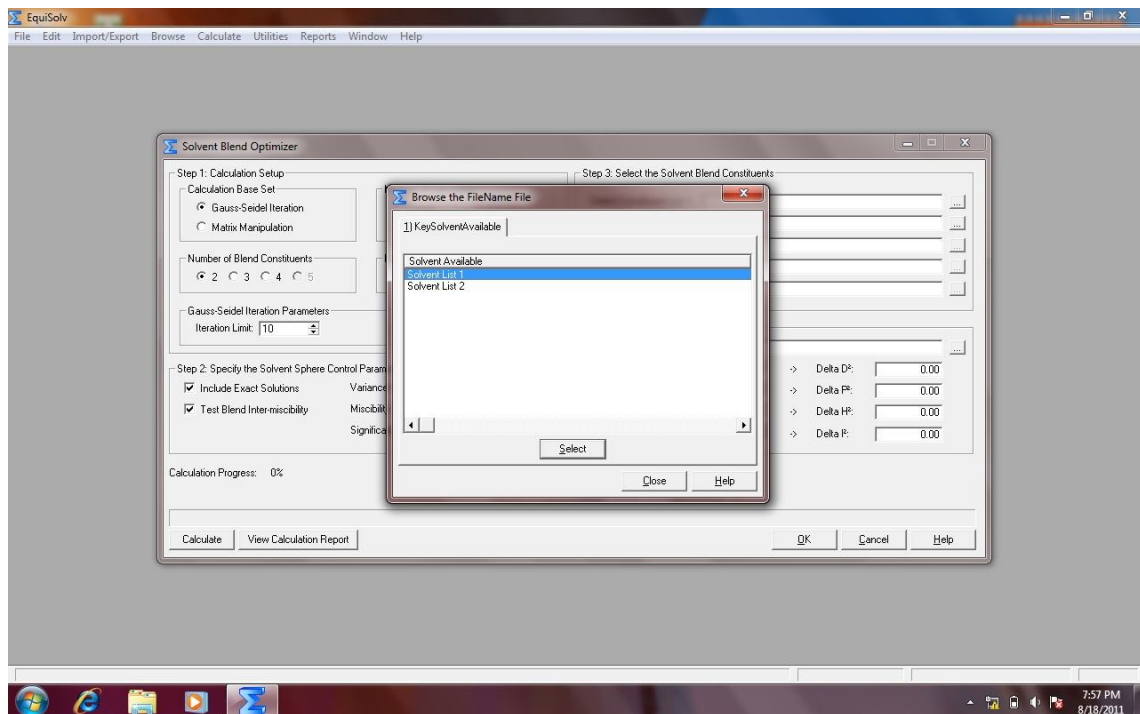


Figure H.23 – Screenshot of the solvent list lookup and selection window.

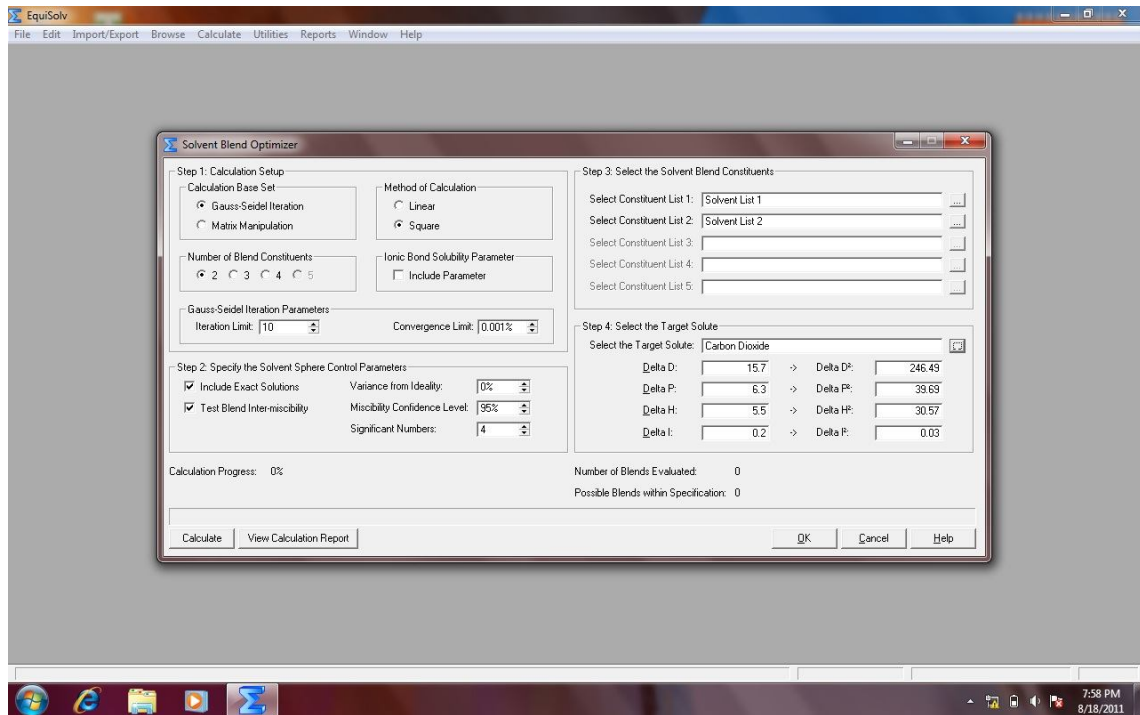


Figure H.24 – Screenshot of the solvent optimizer window set up and prepared for a calculation run.

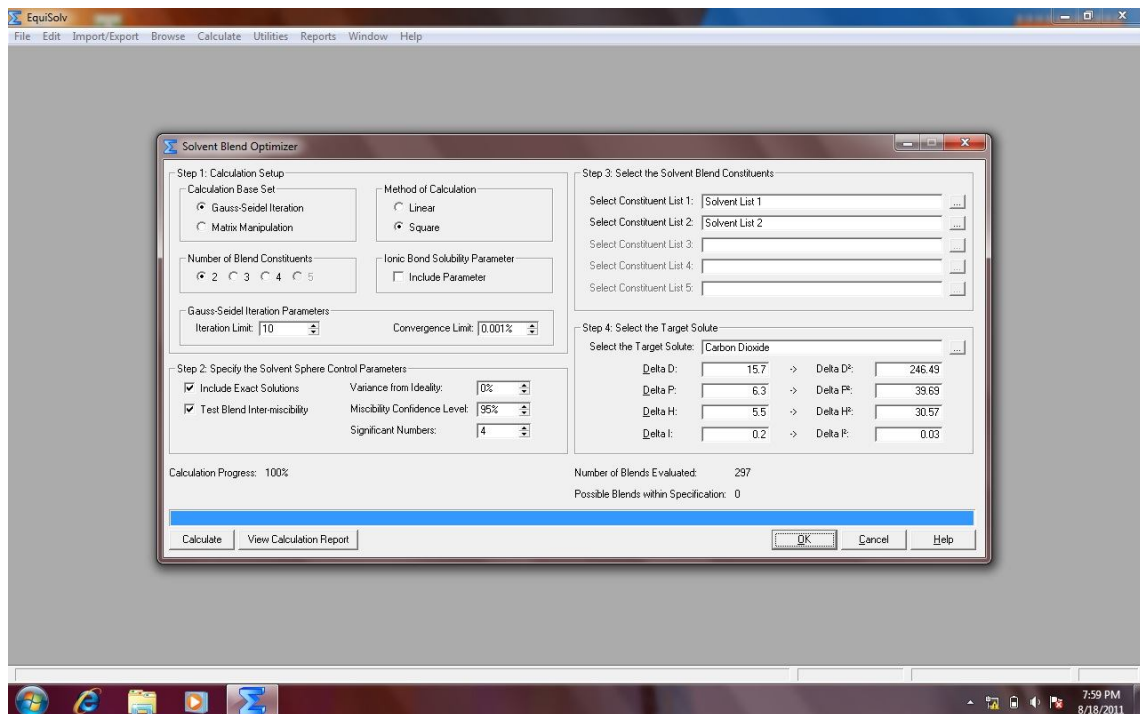


Figure H.25 – Screenshot of the solvent optimizer setup window upon completion of a successful calculation run.

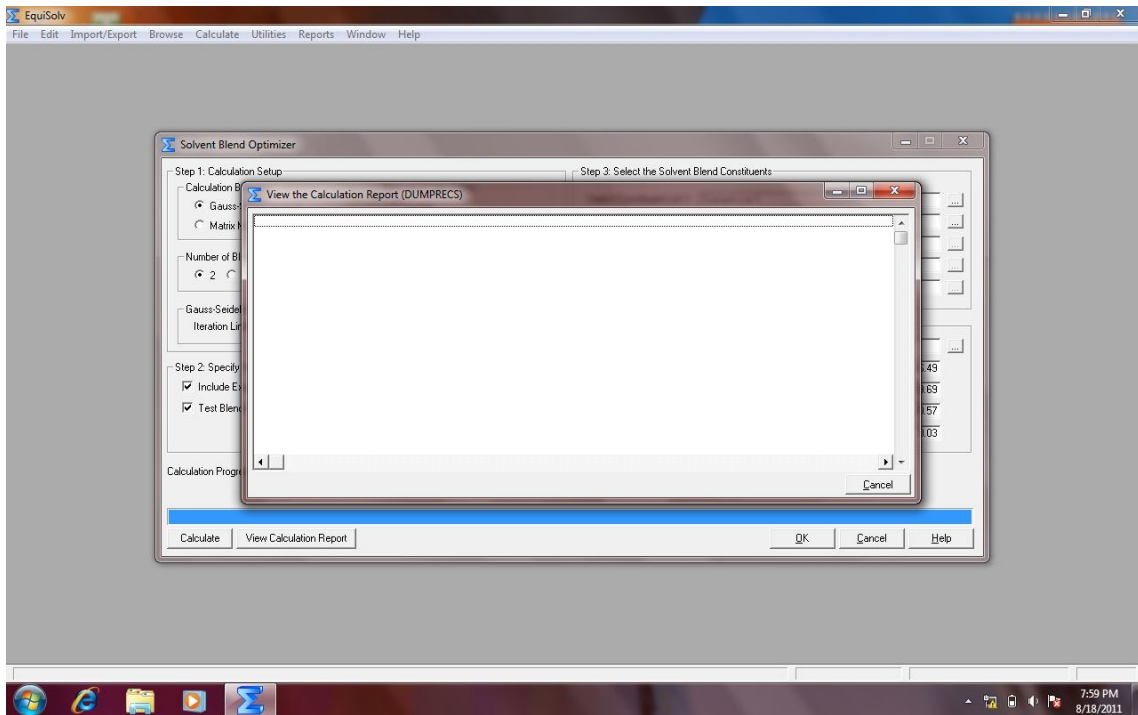


Figure H.26 – Screenshot of the blend analysis error report window.

Browse the Gauss-Seidel-based Solvent Blends file

1) KeyNumber | 2) KeyRED | 3) KeyCAPD | 4) KeyCAPID | Number of Possible Solvent Blends: 9

| Number | Solvent 1 | Solvent 2 | Solvent 3 | Solvent 4 | Solvent 5 | X1 [vol%] | X2 [vol%] | X3 [vol%] | X4 [vol%] | X5 [vol%] | Xtot [vol%] | X1* [vol%] | X2* [vol%] |
|--------|--------------------------------|-----------|-----------|-----------|-----------|-----------|-----------|-----------|-----------|-----------|-------------|------------|------------|
| 53 | Ethylamine, N,N-Diethyl | Water | n/a | n/a | n/a | 1.0903 | 0.0060 | 0.0000 | 0.0000 | 0.0000 | 1.0963 | 0.9945 | 0.0055 |
| 56 | Bis-(2,2,2-Trifluoro-Ethyl)- | Water | n/a | n/a | n/a | 1.2265 | 0.0199 | 0.0000 | 0.0000 | 0.0000 | 1.2465 | 0.9840 | 0.0160 |
| 57 | Methyl-(2,2,3,3,3-Pentafluoro- | Water | n/a | n/a | n/a | 0.7462 | 0.0020 | 0.0000 | 0.0000 | 0.0000 | 0.7482 | 0.9973 | 0.0027 |
| 224 | 4,4-Dinitrodiphenylamine | Water | n/a | n/a | n/a | 0.7364 | 0.0159 | 0.0000 | 0.0000 | 0.0000 | 0.7523 | 0.9769 | 0.0231 |
| 226 | p-Nitrodiphenylamine | Water | n/a | n/a | n/a | 0.7343 | 0.0239 | 0.0000 | 0.0000 | 0.0000 | 0.7582 | 0.9685 | 0.0315 |
| 231 | o-Nitrodiphenylamine | Water | n/a | n/a | n/a | 0.8212 | 0.0056 | 0.0000 | 0.0000 | 0.0000 | 0.8278 | 0.9920 | 0.0080 |
| 280 | Tryptamine | Water | n/a | n/a | n/a | 0.7765 | 0.0236 | 0.0000 | 0.0000 | 0.0000 | 0.8002 | 0.9634 | 0.0366 |
| 285 | Auramine | Water | n/a | n/a | n/a | 0.7765 | 0.0236 | 0.0000 | 0.0000 | 0.0000 | 0.8002 | 0.9634 | 0.0366 |
| 291 | 3,5-Bis-(Trifluoromethyl)Benz- | Water | n/a | n/a | n/a | 0.8042 | 0.1073 | 0.0000 | 0.0000 | 0.0000 | 0.9115 | 0.8923 | 0.1177 |

View | Insert | Change | Delete

Query | Close | Help

Figure H.27 – Screenshot of the calculated alternative blends browse window.

H.4.4. Using the Quick Blend Calculator

Included in the EquiSolv package is a Quick Blend Calculator. Rather than analyzing the entire set of solvents imported for blend formulations, the quick blend calculator can be used to perform specific blend calculations. Two versions of the quick blend calculator are available depending on the basis of calculation. The first option is a calculator capable of estimating both the blend composition and HSP values with respect to the desired target solute. The second option however, offers the option to specify the blend composition and will then calculate the blend HSP values for that composition with respect to the desired target solute.

H.4.4.1. Estimating the Solvent Blend Composition and HSPs

The procedure for using the Quick Blend Calculator to estimate both the solvent blend composition and HSP values is as follow:

1. Go to the "Quick Blend Calculator" option on the "Calculate" menu;
2. Select the "Estimate Solvent Blend Composition and HSPs" option from the "Quick Blend Calculator" sub-menu;
3. A setup screen for the quick blend calculation will be displayed (Figure H.28);
4. The setup procedure for the quick blend calculation is comprised of a four-step process similar to that of the Solvent Blend Optimizer. The setup for Step 1 is similar to that described for Step 1 of the Solvent Blend Optimizer setup (see Section H.4.3);
5. Proceeding to Step 2, specify the desired solvent blend constituents. For "Constituent 1", click on the corresponding file lookup button;
6. A lookup window will be displayed, indicating the solvents lists that were imported and from which a specific solvent can be selected (Figure H.29). To select a list, highlight it by clicking once on it and then click on the "Select" button;
7. A second lookup window will be displayed, showing the solvents available for selection from the specified solvent list (Figure H.30);
8. To select a specific solvent, highlight it by clicking on it once and then click the "Select" button at the bottom right-hand corner of the lookup window. The solvent name and properties will be preloaded in the calculation setup screen (Figure H.31);
9. Repeat steps 5 to 8 for each additional solvent blend constituent;

10. The procedure for selecting a target solute (Step 3) is similar to that described for selecting a target solute for solvent RED calculations (see Section H.4.2);
11. Once steps 1 to 3 have been setup, click the “Calculate” button;
12. The results for the blend composition and HSP values will be shown in the corresponding fields in the “Step 4: Calculation Results” box (Figure H.32);
13. The blend composition and RED is normalized to a unity sum of the constituent volume fractions and the results displayed next to the original results;
14. To close the window, simply click on the “OK” button.

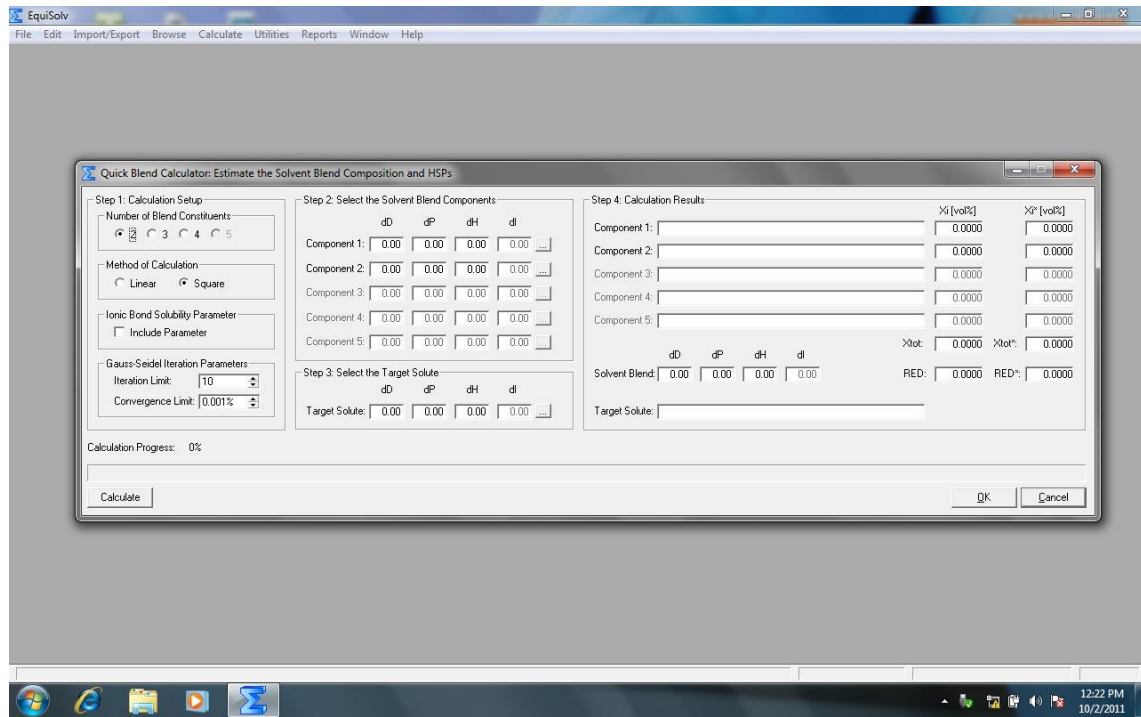


Figure H.28 – Screenshot of the setup window for quick blend calculations (estimating both the blend composition and HSPs).

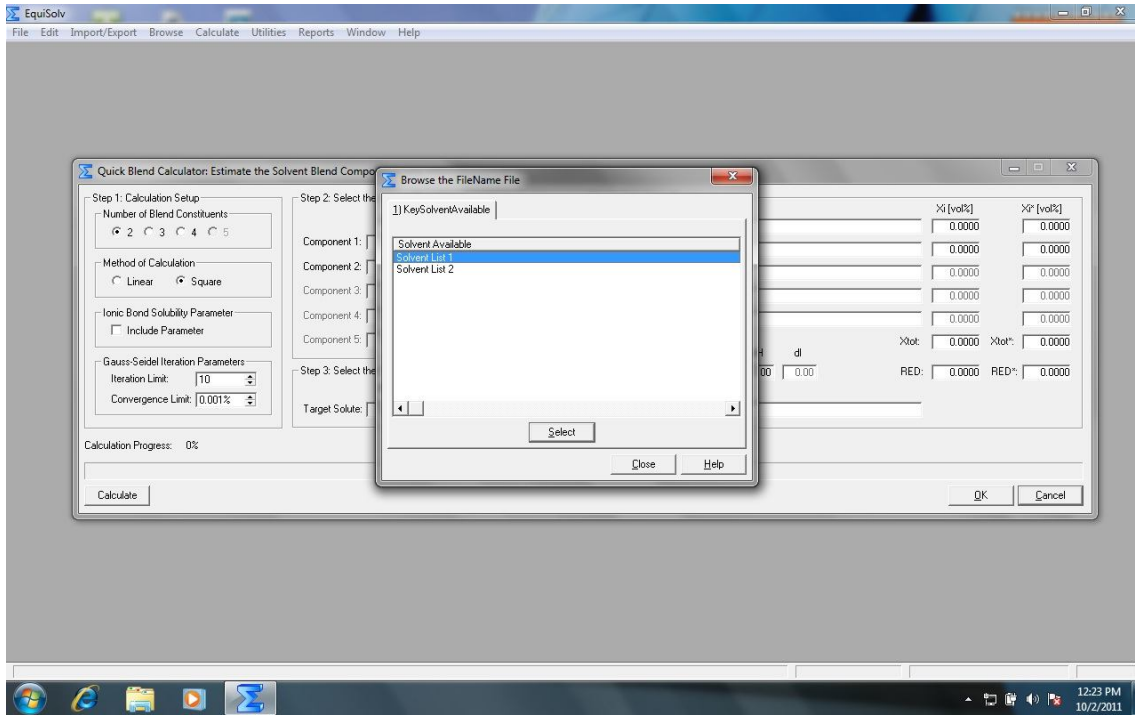


Figure H.29 – Screenshot of the solvent list lookup and selection window.

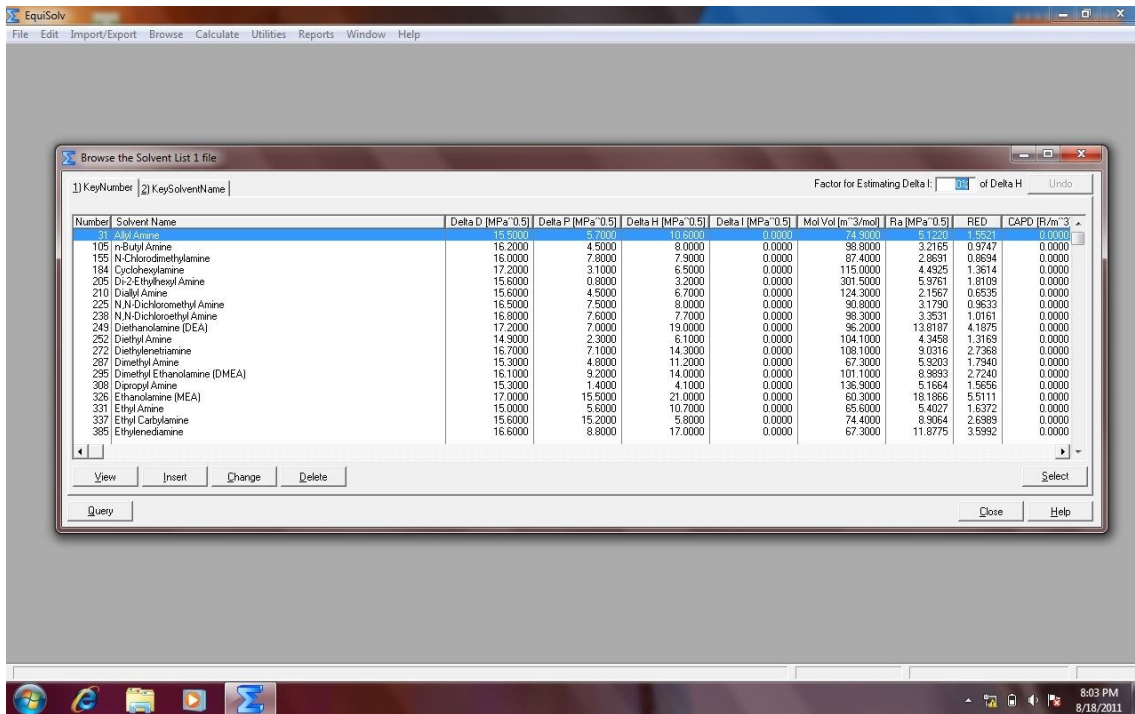


Figure H.30 – Screenshot of the solvent lookup and selection window.

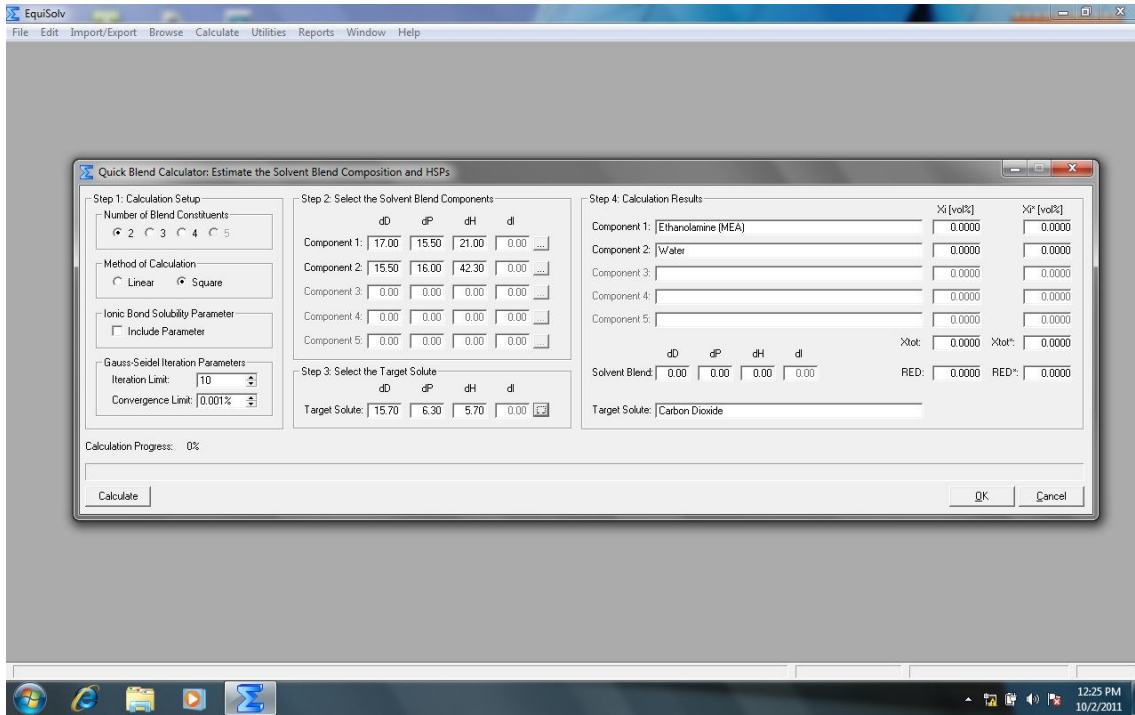


Figure H.31 – Screenshot of the quick blend calculator setup window prepared and ready for a calculation run.

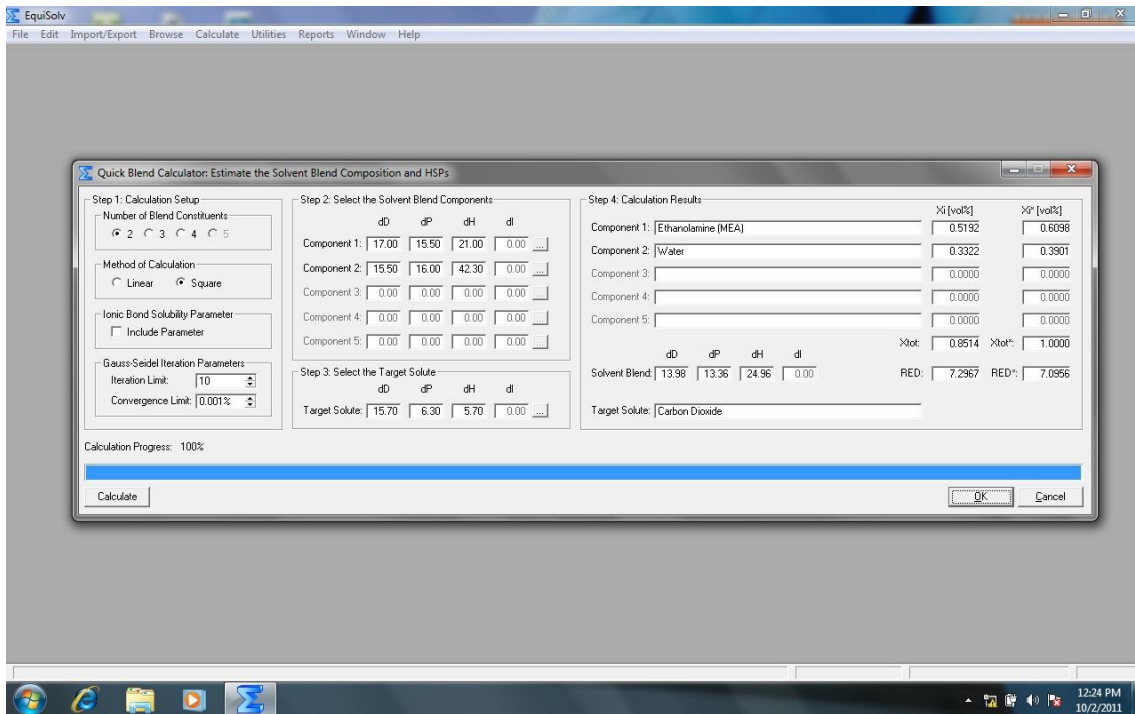


Figure H.32 – Screenshot of the quick blend calculator setup window upon completion of a successful calculation run.

H.4.4.2. Estimating the Solvent Blend HSPs for a Specified Composition

The procedure for using the quick blend calculator to calculate the blend HSP values for a specified composition is as follow:

1. Select the “Estimate Blend HSPs from Composition” option from the “Quick Blend Calculator” sub-menu;
2. A setup screen similar to that of the first version of the quick blend calculator will be displayed (Figure H.33);
3. The setup procedure for the second version of the quick blend calculator is similar to that described for the first version (H.4.4.1) with the exception that the blend composition must be specified in “Step 4: Calculation Results”;
4. Click the “Calculate” button to obtain the blend HSP values;
5. Click the “OK” button to close the window once the calculation is completed.

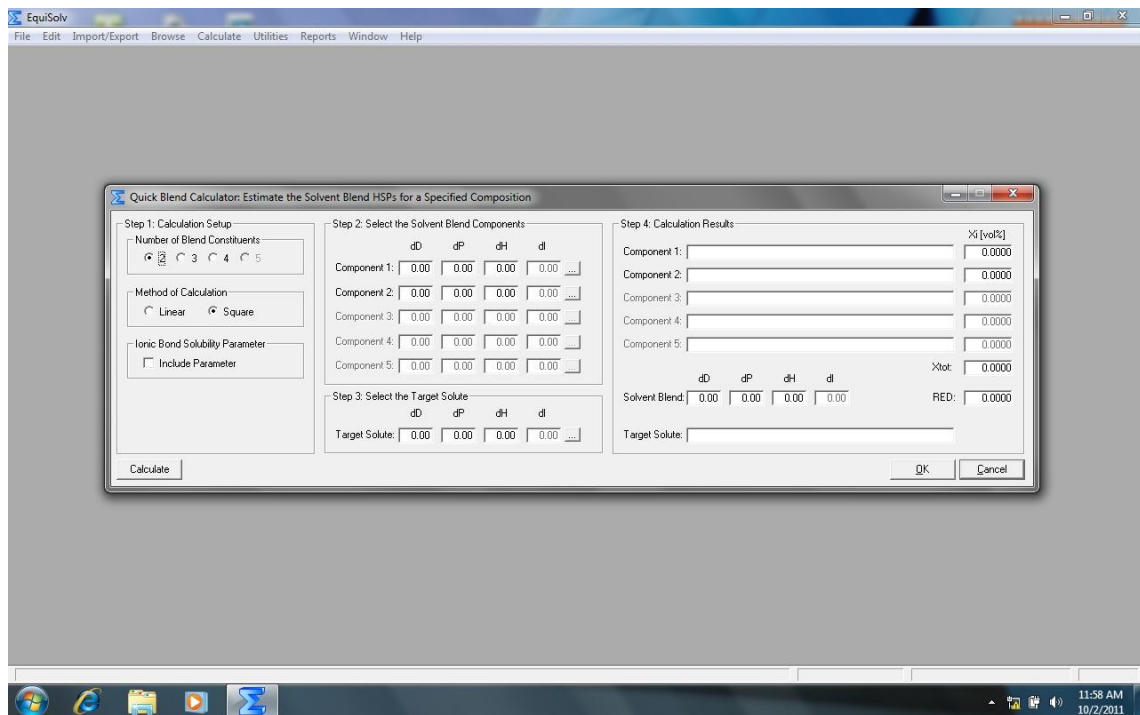


Figure H.33 – Screenshot of the setup window for quick blend calculations (estimating the blend HSPs for a specified composition).

H.5. Pulling Solvent Data and Calculation Reports

The EquiSolv package has the capability to print numerous solvent data and calculation result reports. These reports can be accessed by selecting any one of the options in the “Reports” menu on the EquiSolv main screen (Figure H.34). The reports can easily be printed to PDF files or to text depending on the requirements.

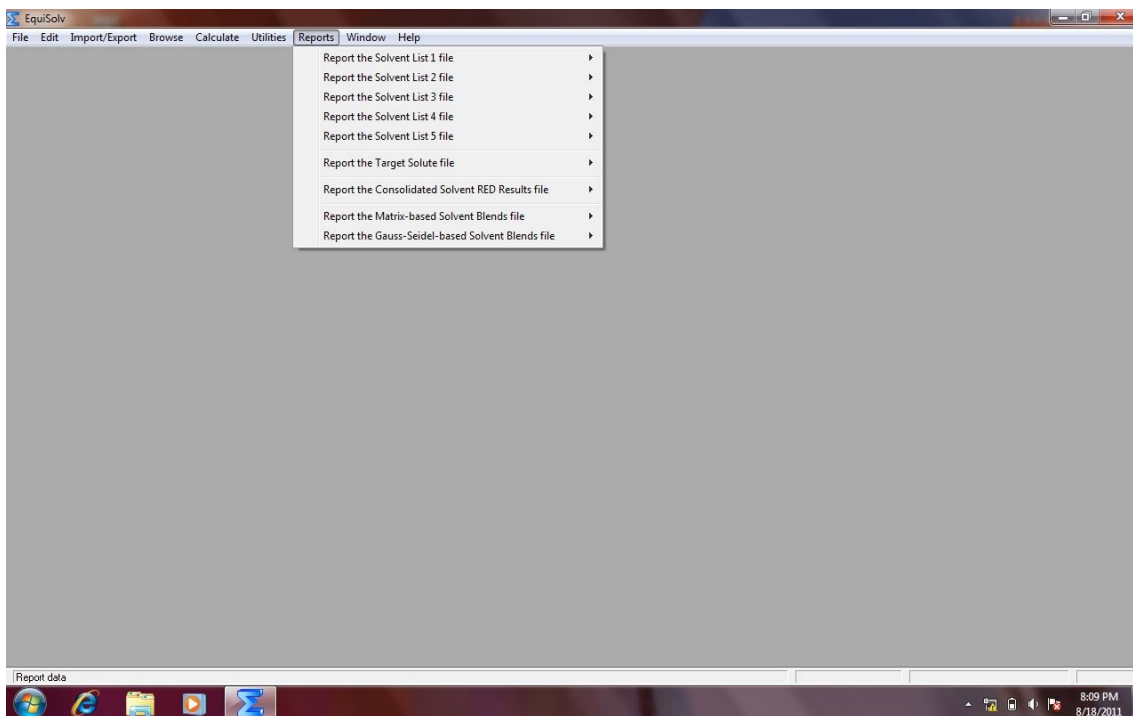


Figure H.34 – Screenshot of the Reports drop down menu option.

H.6. Clearing Solvent Data

The EquiSolv package offers the option to clear any or all of the data contained in the EquiSolv database. This includes both data imported as well as results calculated in the calculation modules. There are a number of clearing options offered. To access these options, go to the “Utilities” dropdown menu option on the main screen and select the “Clear Records” option. The various clearing options will be displayed (Figure H.35).

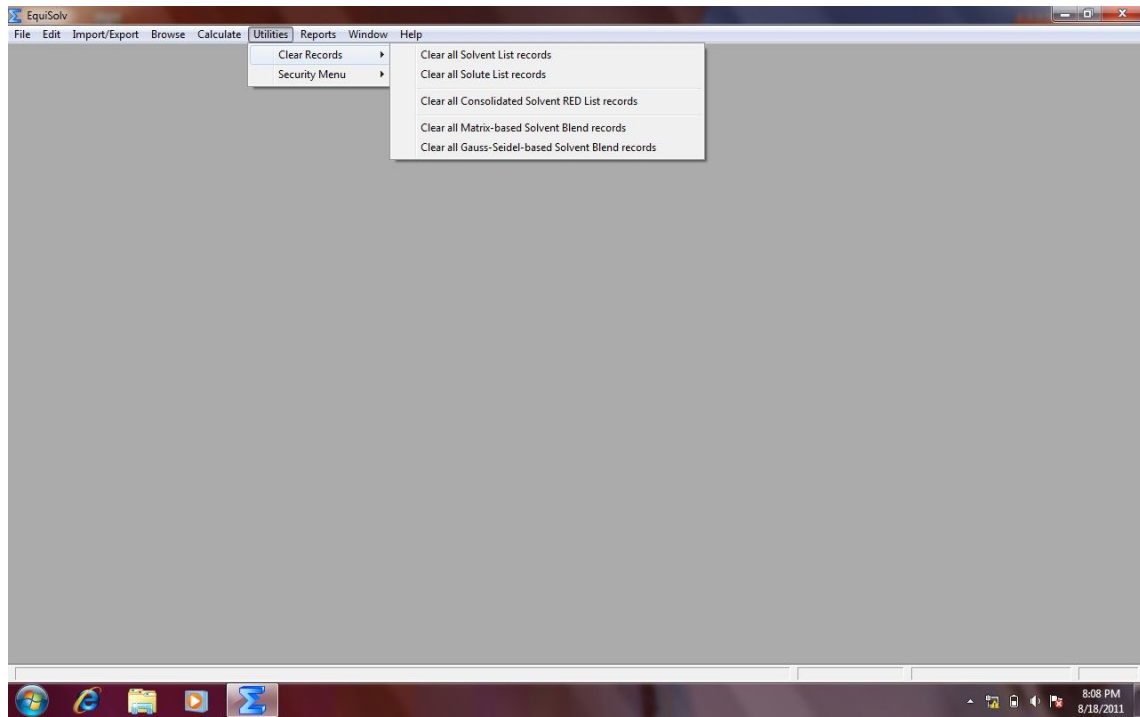


Figure H.35 – Screenshot of the Utilities/Clear Records drop down menu option.

Appendix I: MATLAB Code for Statistic Tests

The code presented here was developed by Dr. Lidia Auret of the Department of Process Engineering of the University of Stellenbosch.

```
function stats = kendalls_w_permutation(data)
% Kendall's W coefficient of concordance
% With permutation tests for significance
%
% Wikipedia reference:
% > http://en.wikipedia.org/wiki/Kendall%27s\_W
% Legendre reference:
% > Legendre, 2005, 'Species associations: the Kendall coefficient of
% concordance revisited', Journal of Agricultural, Biological and
% Environmental Statistics, 10(2), pp. 226-245.
%
% Description:
% m judges (columns) ranking n objects (rows)
% Kendall's W gives agreement between judge rankings
% 0 for no agreement, 1 for absolute agreement
% Permutation tests of W to give indication of significance
%
% Null hypothesis:
% Rankings produced by judges are independent
% Alternative hypothesis:
% At least one of the judges is concordant with one, or with some of the
% other judges
%
% Inputs:
% data = matrix of rankings, where rows are objects and columns are judges
% (note: one-sided test, since W summarizes agreement between rankings)
%
% Output:
% stats = structure with statistics
%
% (c) Stellenbosch University, L Auret, 2011

%% Data characteristics
% Number of judges and objects
[n,m] = size(data);
stats.n = n;
stats.m = m;

%% Reference statistics
% Calculate Kendall's W using Spearman's pairwise rank correlations
rcorr = corr(data, 'type', 'spearman', 'rows', 'pairwise');
rS = tril(rcorr,-1);
rS(rS==0) = [];
rbar = mean(rS);
Wref = ((m-1)*rbar+1)/m;
stats.Wref = Wref;
```

```

% Transform to Friedman's chi squared statistic
chi2ref = m*(n-1)*Wref;
stats.chi2ref = chi2ref;

%% Permutation tests
% Number of permutations
N = 999;
Wperm = zeros(N+1,1);
chi2perm = zeros(N+1,1);
for permInd = 1:N
    dataPerm = data;
    % Permute rankings from judges independently
    for judgeInd = 1:m
        dataPerm(:,judgeInd) = randperm(n);
    end % for-loop judgeInd in 1:m
    % Calculate Kendall's W using Spearman's pairwise rank correlations
    rcorrPerm = corr(dataPerm,'type','spearman','rows','pairwise');
    rSPerm = tril(rcorrPerm,-1);
    rSPerm(rSPerm==0) = [];
    rbarPerm = mean(rSPerm);
    Wperm(permInd) = ((m-1)*rbarPerm+1)/m;
    % Transform to Friedman's chi squared statistic
    chi2perm(permInd) = m*(n-1)*Wperm(permInd);
end % for-loop permInd = 1:N
% Add reference values to permutation distribution
Wperm(end) = Wref;
chi2perm(end) = chi2ref;
stats.Wperm = Wperm;
stats.chi2perm = chi2perm;

% One-tailed probability P of data under null hypothesis:
% Proportion of values of chi2perm in the distribution that are larger or
% equal to chi2ref
% Test indicates that the set contains concorant (agreeing) judges if P is
% equal to or smaller than a selected significance level, e.g. alpha = 0.05
P = mean(chi2perm>=chi2ref);
stats.P = P;

end

% Example data from Legendre (2005):
% data = [5 6 3 5; 10 4 8 2; 7 8 5 4; 8 10 9 2; ...
%        6 5 7 6; 9 7 10 7; 3 3 2 8; 1.5 2 4 9; ...
%        1.5 1 1 2; 4 9 6 10];

```